REVIEW

Check for updates

In situ polymerization process: an essential design tool for lithium polymer batteries†

Vidyanand Vijayakumar, [abc] Bihag Anothumakkool, [ad] Sreekumar Kurungot, [c] Martin Winter*[aef] and Jijeesh Ravi Nair *[a]

Polymer electrolytes (PEs), a type of solid-state electrolytes (SSEs), have been in contention for nearly half a century to replace organic liquid electrolytes (LEs) that are used in state-of-the-art lithium-ion batteries (LIBs). They are envisaged to accelerate the industrial-scale production of safe, energy-dense, flexible, and thin lithium polymer batteries (LPBs). LPBs are expected to be widely employed for electric propulsion and other futuristic applications, such as flexible electronics and the Internet of Things (IoT). Even though several polymer architectures and chemistries have been attempted so far, PEs that can outperform LEs remain a real challenge. Apart from inadequate Li$^+$-ion transport properties, challenges concerning the integration of PEs and the engineering of compatible, robust, and durable interfaces and interphases at both the electrodes of LPBs must be appropriately addressed. Recently, the *in situ* polymerization process has been widely employed as a robust fabrication tool for surpassing the intricacies related to the integration of PEs in LPBs. Hence, in this review, we focus on the *in situ* polymerization processes that employ various polymerization methods (*e.g.*, free-radical polymerization, ionic polymerization, electropolymerization, condensation polymerization, *etc.*), functional monomers and oligomers (*e.g.*, acrylate, methacrylate, allyl and vinyl ethers, epoxides, *etc.*), and PE integration strategies for the fabrication of lithium (ion and metal) polymer batteries (LIPBs and LMPBs). Additionally, this review also evaluates the approaches that have been developed until now to implement the *in situ* processing of LPBs from large-sized pouch cells to flexible-/printable-batteries and even microbatteries.

Broader context

Electrochemistry and polymer chemistry are two independent fields of science that have grown significantly over the last two centuries. Indeed, energy storage devices, in particular rechargeable lithium polymer batteries (LPBs), demand these two strong fields of science to be indispensable and mutually constructive to one another. An affordable polymer electrolyte (PE) with a suitable solvent-free fabrication method would revolutionize the secondary energy storage sector by bringing in thin architecture, low cost, high energy density, eco-friendliness, safety, and durability. Even if the raw material availability is expanded and a competitive synthesis procedure is established, transcending lithium ion batteries (LIBs) by superior LPBs is only possible through adaptive, integrated, economic, sustainable, and upscalable processing techniques. Indeed, *in situ* polymerization processes will empower the engineering of competent PEs and conformal interfaces and interphases in solid-state energy storage and conversion devices. In this review, we emphasize state-of-the-art LPB fabrication techniques (*in situ* and *ex situ* processes), the history of polymer-based rechargeable batteries (literature from the 1830s to the 2020s), numerous classes of monomers and oligomers, and various other innovative and modern PE processing approaches. In addition to conventional LPBs, the prospects of various *in situ* and *ex situ* approaches that are embraced for flexible and printable batteries (screen-printing, 3D-printing, *etc.*) and microbatteries are also envisaged.

[a] *Helmholtz Institute Münster, IEK-12, Forschungszentrum Jülich GmbH, Corrensstraße 46, 48149 Münster, Germany. E-mail: m.winter@fz-juelich.de, j.nair@fz-juelich.de*

[b] *Academy of Scientific and Innovative Research (AcSIR), Sector 19, Kamla Nehru Nagar, Ghaziabad, Uttar Pradesh, 201002, India*

[c] *Physical and Materials Chemistry Division, CSIR-National Chemical Laboratory, Pune, 411008, India*

[d] *TNO-Holst Centre, Dutch National Institute for Applied Scientific Research, High Tech Campus 31, 5656 AE Eindhoven, The Netherlands*

[e] *MEET Battery Research Center, Corrensstraße 46, 48149, Münster, Germany*

[f] *Institute of Physical Chemistry, University of Münster, Corrensstraße 28/30, 48149, Münster, Germany. E-mail: Martin.Winter@uni-muenster.de*

† Electronic supplementary information (ESI) available. See DOI: 10.1039/d0ee03527k

2708 | *Energy Environ. Sci.*, 2021, **14**, 2708–2788

This journal is © The Royal Society of Chemistry 2021

1. Introduction

Among the rechargeable battery technologies available today, lithium-ion batteries (LIBs) are unanimously considered as the most capable electrochemical energy storage (EES) technology due to their high gravimetric energy density of ≈ 260 W h kg^{-1} and possible energy density expansion above 500 W h kg^{-1}.[1-7] Since the commercialization in 1991 by SONY, LIBs have been extensively used in portable electronics. Indeed, LIBs are the frontrunner technology fueling the transition of the mode of transportation from non-renewable fossil fuel-based internal

Vidyanand Vijayakumar

Vidyanand Vijayakumar completed his PhD at CSIR-National Chemical Laboratory, Pune (CSIR-NCL), India (research supervisor: Dr Sreekumar Kurungot). His research mainly involves the synthesis, characterization, and application of novel polymer electrolytes and electrode materials for electrochemical energy storage and conversion devices such as lithium batteries, supercapacitors, and fuel cells. He spent one year as a research associate at Helmholtz Institute Muenster, Germany, in the group of Prof. Dr Martin Winter, on the development of lithium-metal polymer batteries. His research interests also include the design of multivalent ion conducting electrolytes and artificial polymeric interphases for lithium and post-lithium battery technologies.

Bihag Anothumakkool

Bihag Anothumakkool graduated from Madurai Kamaraj University, India, and obtained his PhD in Chemical Science from CSIR-National Chemical Laboratory in 2015 under the guidance of Dr Sreekumar Kurungot. After a Post Doc in lithium-ion capacitors at the University of Nantes, France, with Prof. Thierry Brousse, he joined a second Post Doc with Prof. Martin Winter in 2017 to research lithium-ion batteries at MEET, University of Muenster, Germany. After completion, he joined as a research scientist at TNO-Holst Centre, Eindhoven, in 2018 where he carries out research development on next-generation lithium-ion batteries.

Sreekumar Kurungot

Sreekumar Kurungot is working as a Principal Scientist at CSIR-National Chemical Laboratory, India. He received his PhD (2000) from Cochin University of Science & Technology, India. Subsequently, Dr Kurungot worked as a Post-Doctoral Fellow at Korea Institute of Science & Technology, S. Korea (2000–2001), and the University of Tokyo, Japan (2001–2003). During 2003–2007, Dr Kurungot worked as a scientist with the fuel cell development team of Toyota Motor Corporation, Japan. His current areas of research primarily include fabrication of systems for electrochemical energy applications, including polymer electrolyte membrane fuel cells (PEMFCs), solid-state charge storage systems and other energy conversion devices. He is also working on the development of multifunctional nanostructured electrode materials for various applications, including energy storage, conversion, and hydrogen generation. His other research interests include the development of solid-state polymeric electrolytes for battery applications, flexible devices and hierarchical materials for specific targeted applications. He has more than 190 publications and 20 patent applications to his credit. Dr Kurungot is also serving as an Associate Editor for RSC Advances from 2015 onwards.

Martin Winter

Martin Winter currently holds a professorship for "Materials Science, Energy and Electrochemistry" at the Institute of Physical Chemistry at Muenster University, Germany. The full professorship developed from an endowed professorship funded by the companies Volkswagen, Evonik Industries and Chemetall (today: Albemarle). He is a Director of the MEET Battery Research Center at Muenster University and the Helmholtz-Institute Muenster (HI MS) "Ionics in Energy Storage", a branch of Forschungszentrum Jülich. Martin Winter is the spokesperson of German Battery Research, and present speaker of the National Project Alliance "Batterie2020". Currently, he holds several president and chairman positions in scientific societies and is the recipient of 50 awards and recognitions.
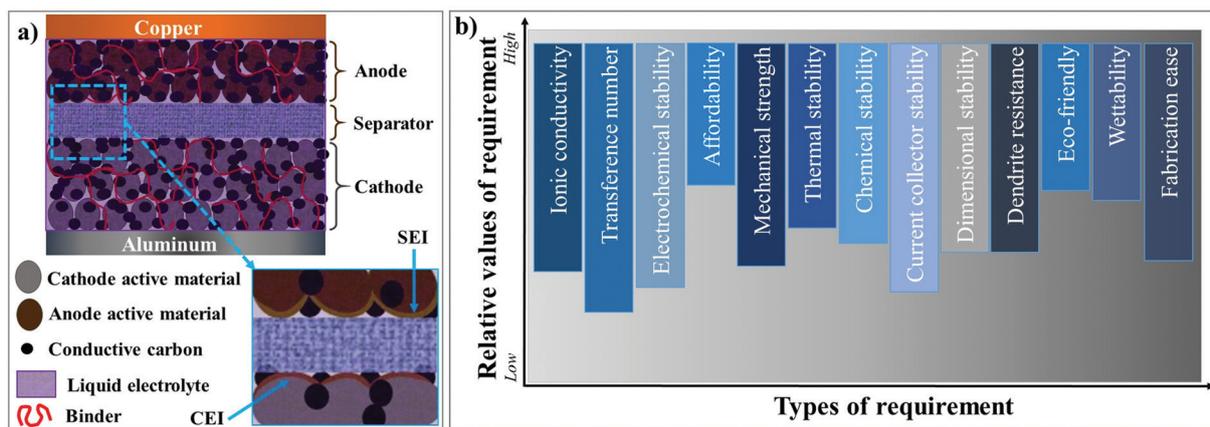
This journal is © The Royal Society of Chemistry 2021

Energy Environ. Sci., 2021, **14**, 2708–2788 | **2709**

Fig. 1 Schematic illustration of the components of the (a) state-of-the-art LIB cell and (b) fundamental requirements of an ideal electrolyte system.

combustion engines (ICEs) to the prospects of electromobility.[8,9] For example, a standard ICE burns an average of ≈ 5.5 L of gasoline for 100 km distance, and the same amount of fuel corresponds to ≈ 50 kW h of energy.[10] From the equal amount of energy stored in an LIB, an electric vehicle (EV) travels ≈ 312 km, which means that, in practical terms for 100 km, an EV consumes only 16 kW h of energy.[11] This indicates that an LIB with an electric motor is at least three times more efficient than a gasoline-powered ICE. Besides, the "lost" part of the energy (~ 34 kW h) from gasoline results in unproductive work, mostly heat. Therefore, LIBs are envisaged to contribute immensely towards the flourishment of sustainable means of transportation in the form of EVs and lower environmental hazards. Moreover,

Jijeesh Ravi Nair received his PhD, a European Doctorate (2010), in Materials Science and Technology from Politecnico di Torino, Italy. After the PhD, until 2017 he worked as a senior postdoctoral researcher at Politecnico di Torino. Since 2017, he is a research associate at the Helmholtz Institute Münster (HI MS) 'Ionics in Energy Storage', a division of Forschungszentrum Jülich GmbH. His research activities focus on the development of cross-linked SPEs

Jijeesh Ravi Nair

for LBs. Previously (2005–2006), he worked in the R&D department of Asian Paints Ltd., Mumbai (India), on emulsion polymerization process. In 2010, he won the Oronzio and Niccolo' De Nora Foundation Prize of the Italian Chemical Society (SCI) for the best PhD thesis. In 2012, he won the researcher under 30 years of age category award (Italy), 'ENI AWARD 2012–debut in research'. He has published 75 scientific articles and co-authored five book chapters. He has been awarded one international patent, and four of his other patent applications are under evaluation.

the efforts to implement LIBs for smart/green grid (stationary) energy storage systems assure effective intermittent and reliable energy generation, transmission, and distribution, through intermediate storage, thus further improving the goals of a sustainable lifestyle. In 2019, considering the development of LIBs and its impeccable impact on modern society, John B Goodenough, M Stanley Whittingham, and Akira Yoshino were conferred with the Nobel Prize in Chemistry.[12]

A typical LIB is composed of an anode (negative electrode), cathode (positive electrode), organic liquid electrolyte (LE), and separator, as demonstrated in Fig. 1a. Li^+-ion intercalating compounds (*e.g.*, graphite),[13,14] alloying materials (*e.g.*, Si and Sn),[15,16] and (nanoscale) metal oxides (*e.g.*, $Li_4Ti_5O_{12}$, TiO_2, and Fe_2O_3)[17] are often employed as the anode. Lithiated layered transition metal oxides [*e.g.*, $LiNi_xMn_yCo_zO_2$ (NMC), $LiCoO_2$ (LCO), and $LiNi_xCo_yAl_zO_2$ (NCA)] in several compositions, olivine-type metal phosphates [*e.g.*, $LiFePO_4$ (LFP) and $LiMnPO_4$], spinel oxides [*e.g.*, $LiMn_2O_4$ (LMO) and $LiMn_xNi_yO_4$ (LNMO)], *etc.*, are popular amongst the available cathodes.[18,19] Linear (*e.g.*, dimethyl carbonate, DMC) and cyclic (*e.g.*, ethylene carbonate, EC) carbonates in numerous compositions are exploited as electrolyte solvents, which in conjunction with lithium salts of perchlorate (*e.g.*, $LiClO_4$), fluoroborate (*e.g.*, $LiBF_4$), fluorophosphate (*e.g.*, $LiPF_6$), sulfonylimide (*e.g.*, LiFSI and LiTFSI), *etc.*, form the typical organic LEs. 1 M $LiPF_6$ in EC:DMC is a classic example of a widely used organic LE.[20] Porous single- or multi-layer polyolefin sheets (*e.g.*, Celgard™) or glass-fiber mats are often used as the separator.[21,22] Further, LIB electrodes contain binders,[23] conducting additives,[24–26] and current-collectors.[27,28] The main feature of a binder is its ability to hold together the electrode particles containing the active material and conductive additives such as carbon black (*e.g.*, Super P® and Super C®). Also, binders enhance the adhesion of electrode components to the respective current-collectors (Cu for the anode and Al for the cathode).[6] Indeed, poly(vinylidene difluoride) (PVdF) and its copolymer poly(vinylidene difluoride-*co*-hexafluoropropylene) (PVdF–HFP) are the most widely used binder materials.[29]

Organic LEs are an integral part of LIBs, playing the fundamental role of Li^+-ion conduction between the electrodes.[30–32]

Additionally, the LEs facilitate the formation of stable surface protection layers, *e.g.*, the solid electrolyte interphase (SEI)[33] and cathode electrolyte interphase (CEI)[34] on the respective electrode surfaces (see Fig. 1a), paving the way for reversible Li$^+$-ion shuttle.[31,35–40] The most relevant requisites for an ideal electrolyte are depicted in Fig. 1b, where every requirement is graded according to its relevance in delivering optimum performance in LIB cells. Nevertheless, LEs hold several inherent limitations, including the possibility of electrolyte leakage, a narrow range of operation temperature (5 to 45 °C), and a probable fire hazard during cell-failure through overcharging or dendrites [also called High Surface Area Lithium (HSAL) mediated cell short-circuit].[41–44] Besides, from a technological perspective, the electrochemical stability issues associated with the LEs combined with high-voltage nickel-rich cathodes are a significant concern to be resolved from a technical standpoint.[45] The recent developments in aqueous electrolytes made of a high concentration of lithium salt (also called 'water-in-salt') are envisaged to emulate the success of LIB technology of the 1990s.[46,47] Furthermore, aqueous electrolytes can address the environmental and safety concerns about the use of inflammable organic solvents. However, the research is in the early stage and yet to flourish beyond the lab-scale.

Affording the future energy demands for high energy applications like long-range EVs and grid-storage, the energy density of state-of-the-art LIBs should be increased beyond a value of > 500 W h kg^{-1}. Theoretically, the energy density of an LIB cell can be increased by 57% by doubling the capacity of a positive electrode. However, achieving high capacity beyond existing state-of-the-art materials at the cathode level is a monumental task. Indeed, high-voltage cathodes with high capacity require compatible electrolytes with high oxidative stability. Interestingly, a ten-fold increment in the capacity of a negative electrode can also result in a large increase ($\sim$47%) in energy density.[48–50] Therefore, the replacement of graphite (theoretical capacity of 372 mA h g^{-1}) by a Li-metal anode (theoretical capacity of 3860 mA h g^{-1})[51] can elevate the energy density of the resulting battery with the existing cathode materials and chemistries. In this aspect, LIBs that use Li-metal as the anode are receiving popular attention and are called lithium metal batteries (LMBs).

The complications arising from the currently pursued organic carbonate-based LEs against the Li-metal anode owing to HSAL growth are a grave concern, which is preventing the commercialization of LE-based rechargeable LMBs (LE-LMBs).[52–54] Even tailor-made LEs (highly concentrated solutions, fluorinated solvents, specialty additives that form a fluorine-rich SEI layer, *etc.*), which can control and modify the Li-metal surface by the formation of artificial SEIs, cannot fully avoid HSAL-related cell failure during long-term cycling. Such efforts require further optimizations and validations. In realistic conditions, where the LE amount is restricted below 3 g A h^{-1} and the areal capacity to be achieved is in the range of 2–5 mA h cm^{-2}, HSAL related issues become severe.[5] By a simple calculation, one can understand that 2.0 mA h cm^{-2} equivalent Li deposition corresponds to $\sim$10 μm thick layer of Li, whereas an equivalent of 5 mA h cm^{-2} leads to $\sim$25 μm thick layer at the Li-metal anode. Additionally, porosity or

voids formed during the Li plating/stripping processes will increase many fold the actual volume of the Li-metal anode in an LE-LMB. Hence, the continuously evolving Li-metal surface, volume expansion arising from Li deposition, short circuits induced by HSAL formation, and thin separator layer complicate the adaptation of LE-LMBs to commercial applications. Besides, the *in situ* formation of artificial SEI layers to protect the Li-metal surface within the cell housing by using a lower amount (<3 g A h^{-1}) of LE may induce excessive consumption and decomposition of solvents. Hence, the harmful side products formed, such as gases or even small organic molecules, may further catalyze the exothermic decomposition of the electrolyte components, resulting in increased cell impedance, short-circuits, and fire hazards. For example, HSAL growth induced failure of an LE-LMB cell during repeated charge–discharge cycling is schematically represented in Fig. 2, where a needle-like HSAL deposition piercing through the separator to induce a short-circuit is depicted.[55]

The ongoing intricacies associated with LEs have propelled the concept of solid-state electrolytes (SSEs) for LIBs and LMBs, resulting in the development of two major classes of solid-state systems, namely, polymer electrolytes (PEs) and inorganic solid-state electrolytes (ISEs). The primary objective of invoking SSEs for LIBs and LMBs is to address the safety concerns associated with organic LEs. Besides, the use of SSEs in place of LEs will facilitate the design of safer, flexible, durable, thinner, lightweight, leak-free, and easy to fabricate solid-state
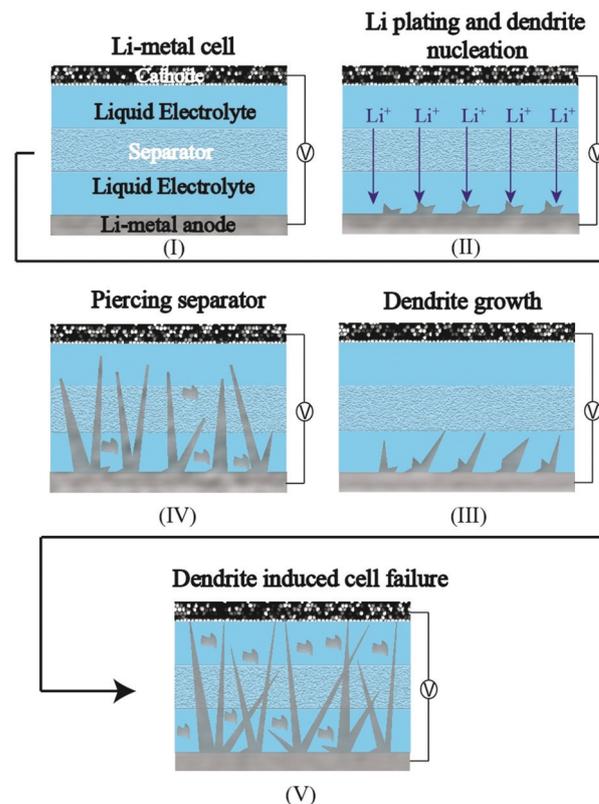

Fig. 2 The HSAL (needle-like)-incited failure of an LE-LMB cell during repeated charge–discharge cycling.

This journal is © The Royal Society of Chemistry 2021

Energy Environ. Sci., 2021, **14**, 2708–2788 | **2711**

LMBs and LIBs. It is anticipated/hypothesized that Li$^+$-ion conducting SSEs with shear modulus values higher than Li-metal ($G' > 3.4$ GPa) can hinder HSAL growth during repeated charge–discharge steps in solid-state LMBs.[56–61] Therefore, SSEs combined with thin Li-metal anodes (thickness <20 μm) can potentially fuel successful commercialization and widespread implementation of rechargeable solid-state LMBs. Fig. 3a–c depict the overall transformation of an earlier model of an Li-metal anode|LE-based primary LMB (pLMB) and LE-based rechargeable LMB (LE-LMB) (1st generation) to the state-of-the-art Li-metal-free anode (e.g., intercalation)|LE-based LIBs (2nd generation), and lastly to the most recent Li-metal anode|SSE-based rechargeable LMBs (3rd generation). In the context of this review, for simplicity, the term 'lithium battery (LB)' is used to represent all types of battery cells that make use of Li-based electrochemistry. When a PE is used as the SSE in the LMB configuration as shown in Fig. 3c, such solid-state LMBs are called lithium metal polymer batteries (LMPBs). Similarly, LIBs with a PE replacing the conventional LE are called lithium-ion polymer batteries (LIPBs). Besides, the term 'lithium polymer battery (LPB)' is used to generalize all PE-based LIBs and LMBs. The innate components such as SEI and CEI layers that are formed during the initial cycles of an LIB (Fig. 1a) apply to LPBs as well.

The synthesis and upscalability of PEs will be of paramount importance when LIPBs and LMPBs are considered for large scale production and commercialization. PEs for LPBs have been extensively reviewed in the past.[62–68] Indeed, excellent reviews are available discussing the different types of PEs such as gel polymer electrolytes (GPEs), polymer composite electrolytes (PCEs), and solid polymer electrolytes (SPEs).[69–71] Thorough overviews of the types of polymer hosts (such as PEO and PEO-free hosts) used in the preparation of PEs are also available.[72–74]
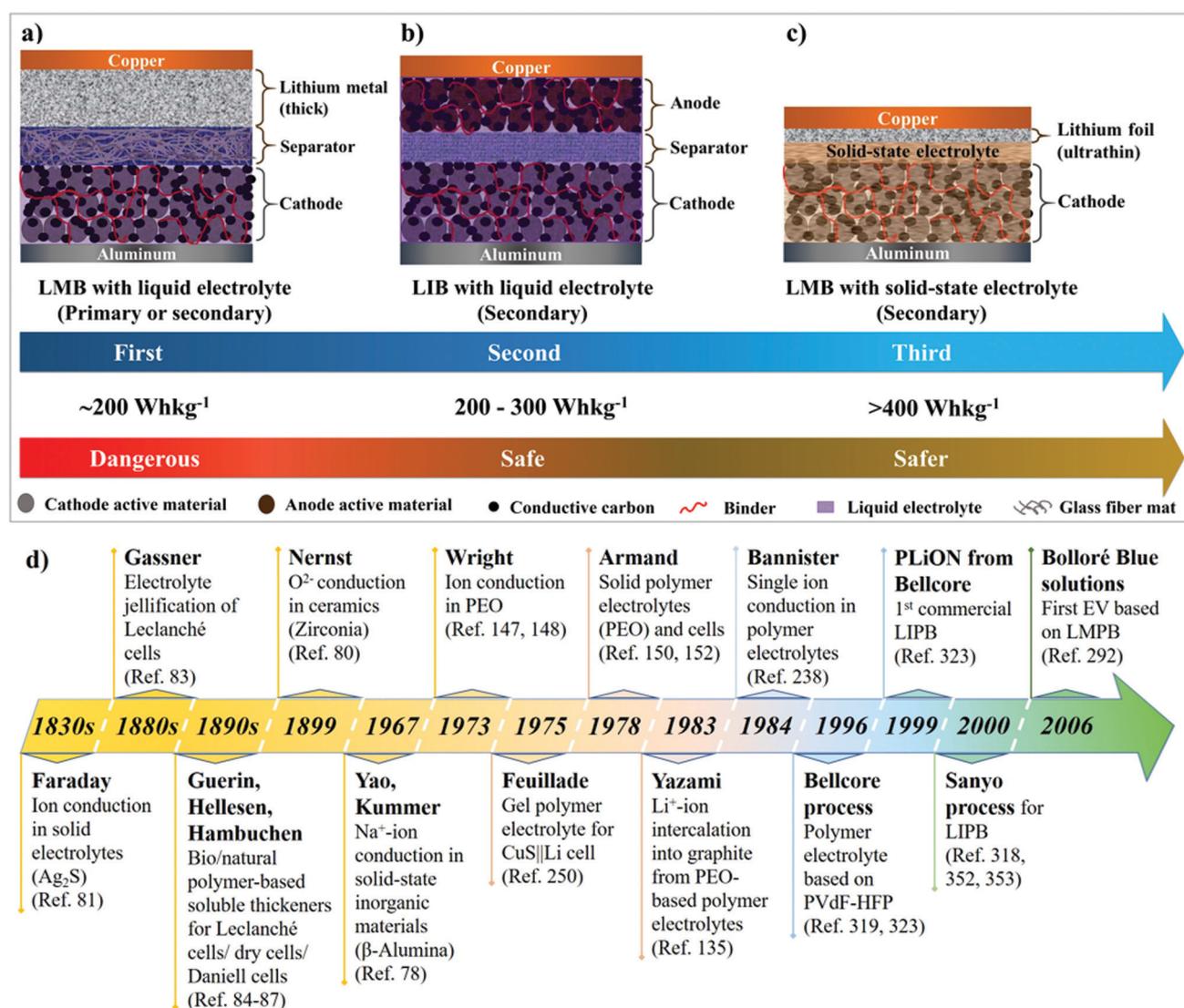

Fig. 3 Different generations of LBs and their features: (a) early generation LE-based primary and secondary (rechargeable) LMBs (pLMBs and LE-LMBs); (b) state-of-the-art LE-based rechargeable LIBs; (c) rechargeable LMBs with an SSE (ISE/PE) (when the SSE used is a PE, such LMBs are called LMPBs); and (d) schematic representation of key milestones in the evolution of PE-based energy storage devices.

2712 | Energy Environ. Sci., 2021, 14, 2708–2788

This journal is © The Royal Society of Chemistry 2021

Besides, a few available reviews address the fundamental aspects of order and disorder, and ion transport models of PEs.[75,76] These attempts mainly covered various types of PEs, their synthetic methods, and fundamental aspects in detail. However, reviews addressing the fabrication of LIPBs and LMPBs emphasizing the importance of processing methods, which significantly influence the electrode|electrolyte interfaces, interphases, and electrochemical performance, are scarce. Hence, understanding and segregating the bits and pieces of PE research from the LPB cell fabrication/processing point of view is vital, and, through this review, we are narrowing down this knowledge gap.

The primary objective of this review is to comprehensively discuss the reports on LIPB and LMPB cell fabrication methods focused on improving the electrode|electrolyte interface and interphase using the *in situ* polymerization process (explained in Section 4.2). A concise understanding of the enormous amount of scientific research activities carried out in the past four decades on the *in situ* processing of LBs can leverage their prospects of practical implementation and industrial-scale production. Hence, many of the available reports are comprehensively compiled, considering the type of *in situ* processing approach adopted and the polymer hosts used. The potential of the *in situ* process in futuristic microbatteries, and printable- (*e.g.*, 3D-printed), and flexible-LPBs is also discussed at the end.

2. History of LBs: liquid electrolytes to polymer electrolytes

The significant milestones in the evolution of solid-state electrolytes for various EES devices through history are presented in Fig. 3d.[77–80] Solidification of electrolytes for improving portability and preventing leakage of liquid components has been known since the 19th century. Michael Faraday, in the 1830s, discovered ionic conduction in solids for the first time.[81,82] Carl Gassner, in the 1880s, improved Leclanché cells by introducing the concept of 'electrolyte jellification' using plaster of Paris as the solid-state host.[83] Several other inventors later improvised the concept by employing jellified semi-solid electrolytes made of cellulosic materials (*e.g.*, sawdust), bio/natural polymer-based soluble thickeners (*e.g.*, starch, agar paste, *etc.*), simple cloth or starch-coated paper as the separator, *etc.*, in various Leclanché cells/dry cells/Daniell cells.[84–87] These reports dating back to the 19th century indicate the momentous importance of solidification/immobilization of the electrolyte in EES devices.

During the 1950s, there have been observations regarding the formation of a passivation layer on the surface of highly reactive Li-metal when immersed in organic solvents.[88–90] This surface passivation layer was later investigated in detail by Peled *et al.* and later named the SEI.[91–95] This SEI layer could prevent the continuous oxidation of Li-metal in the organic LE. Further research paved the path towards the conceptualization and commercialization of 1st generation LMBs (Fig. 3a) during the period of 1960–1970s, which comprised a thick Li-metal foil as the anode, an organic LE, and a cathode amongst transition metal halides (*e.g.*, CuCl$_2$), oxides (*e.g.*, MnO$_2$ and MoS$_2$),

SOCl$_2$, SO$_2$, *etc.*[77,96–100] However, the commercialized LMBs were LE-based pLMBs (Fig. 3a). When attempts were made to convert these pLMBs into rechargeable configurations, the morphological instability of Li-metal during the repeated charge–discharge cycling prevented the realization of safe, reliable, and rechargeable LE-LMBs. Nevertheless, these early models opened several new opportunities and challenges that led to modern-day rechargeable LIBs and LMBs.

Ever since the commercialization of pLMBs, enormous efforts were dedicated to transforming the model into a rechargeable one. The major part of the research was focused on tuning LEs and cathode materials, through which efficient 1st generation LE-LMBs (Fig. 3a) were expected to be realized (during the 1960s to 1980s).[101–104] Several breakthrough discoveries leading to state-of-the-art electrode materials and electrolytes used in contemporary LIB cells were the result of continuous research focused on developing safe LE-LMBs. For instance, the introduction of intercalation cathodes by Whittingham *et al.*[105,106] and the development of LiCoO$_2$ (LCO) by Goodenough *et al.*[107] were achieved during the period of the mid-1970s to the beginning of the 1980s (for details about the history of electrolytes, salts and cathode materials used in LBs, follow the referenced articles[31,108–118]). However, the inferior cycling life and unsafe operation of the then-designed LE-LMB models remained as the primary bottleneck, mainly due to the fire hazards and cell-failure arising from the HSAL growth at the anode side.[104,119–122] In fact, several manufacturers (*e.g.*, Moli Energy) recalled some of their commercialized LE-LMBs from the market due to fire hazards and malfunctioning of the associated devices, which ended the general curiosity on the same.[96,123] However, it should be noted that, even today, many of the pLMBs developed during the 1970s and 1980s, such as MnO$_2$|LE|Li and C|LiAlCl$_4$ in SOCl$_2$|Li, still have their market-share for niche applications.[77]

The quest towards developing safe anodes other than Li-metal led to the 2nd generation of LBs, currently known as LIBs, which were commercialized by SONY in 1991 (Fig. 1 and 3b). The state-of-the-art LIBs use a graphite-based intercalation anode. Unlike the reactive Li-metal, graphite can facilitate a stable SEI with the organic LE, hence preventing HSAL growth and cell-failure under normal service conditions. During the mid-1970s, Besenhard *et al.* proposed, for the first time, the concept of reversible electrochemical intercalation of alkali metal ions into graphite from organic LEs.[124–126] Several reports followed this discovery and developed different types of carbon-based materials that are capable of reversible Li-intercalation.[127–135] In 1977, Basu *et al.* put forward the preparation of stage 1 Li-intercalated graphite (LIG)[136,137] with a high-temperature physical method that paved the path towards the development of LiC$_6$ anode as an alternative to Li-metal at Bell Labs.[138,139] Later, Rachid Yazami in 1983 demonstrated the simple but groundbreaking phenomenon of electrochemical intercalation of Li$^+$-ions into a graphite host from a poly(ethylene oxide) (PEO)-based dry polymer electrolyte (DPE), for which he is often considered as the inventor of the graphite anode for LIBs.[135,140,141] Ultimately, Akira Yoshino from Asahi Kasei Corporation is credited

This journal is © The Royal Society of Chemistry 2021

Energy Environ. Sci., 2021, **14**, 2708–2788 | **2713**

as the inventor of the modern-day LIB, as he engineered the first practical prototype that operates through a dual-intercalation mechanism in LEs followed by commercialization in 1991.[142] Compared to 1st generation LMBs (pLMBs and LE-LMBs), LIBs are safe and long-lasting despite their lower energy density, which is compromised due to the replacement of Li-metal with a graphite analog.[143,144] Conversely, the new developments in LIBs include alternative materials such as alloying (*e.g.*, silicon and tin) and conversion anodes [*e.g.*, transition metal oxides (TMOs)] as close competitors to graphite for enhancing the energy density.[145,146] From a practical perspective, since commercialization in 1991, the configuration of state-of-the-art LIBs has not undergone major changes. Although several new materials (high-energy anodes and cathodes, better lithium salts, solvents, separators, *etc.*) have emerged, the basic configuration of LIBs remains the same. With the inception of SSEs (PEs and ISEs), the possibility of realizing safer, thinner, durable, and energy-dense solid-state LMBs possessing rechargeability has sprouted again (Fig. 3c, 3rd generation).

Ion conduction through polymer hosts has been known for nearly half a century.[88] The first example was PEO-based alkali metal (Li or K) ion conducting PEs (historically called DPEs), which were first introduced by P. V. Wright *et al.* in the 1970s, and later this research field flourished and was independently recognized with the critical contributions from Armand *et al.*[147–152] In the case of PEO, the polar heteroatoms (oxygen) of ethylene oxide (–EO–) chains facilitate the solubility of electrolyte salts, and the transport of these dissociated ions occurs through ion hopping and polymer chain segmental motion. Generally, the ion mobility induced by polymer chain segmental motion occurs above the glass transition temperature (T_g) of the constituent polymer host.[153–155]

Ideally, PEs are envisaged to be superior compared to ISEs (glass electrolytes, ceramic electrolytes, *etc.*) due to their low cost, ease of synthesis and processing, and excellent mechanical properties.[82,156–158] Indeed, many available fast and single-ion conducting ISEs are known for their instability against Li-metal.[71,159–161] Further, high grain boundary resistance and

processability are the immediate challenges that impede the application of ISEs in solid-state LIBs and LMBs.[162,163] Nonetheless, ISEs based on sulfides (*e.g.*, $Li_7P_3S_{11}$) are an exception as they display excellent ionic conductivity >1 mS cm^{-1} at RT[164,165] and a low activation energy of 12 kJ mol^{-1} for Li$^+$-ion transport.[166] Unfortunately, the narrow electrochemical stability window of sulfide electrolytes is a drawback, which demands artificial SEIs or separate polymer layers in practical applications.[165] Additionally, the sensitivity to air and moisture requires careful and precise processing conditions and stringent safety regulations (mainly due to sulfur). Moreover, the molar concentration (mol L^{-1}) of lithium required in ISEs is at least one to several orders of magnitude higher than organic LEs or PEs (see Table 1).[87] Thus, the overall research towards improving ISEs is in its early stages, and detailed overviews are available elsewhere.[167,168] Ultimately, the flexibility, low cost, and ease of processability of PEs enable them to be one of the suitable choices for futuristic solid-state LPBs. It is also reported that the flexible nature of PEs has another advantage of tolerating the volume changes occurring in the electrodes and minimizing HSAL growth and related SEI layer rupture during the charge–discharge cycles.[169–174] Indeed, such characteristics can reduce the risks/hazards related to short-circuits to an extent.

3. Polymer electrolytes

PEs can be broadly classified into dry polymer electrolytes (DPEs) and gel polymer electrolytes (GPEs), as shown in Fig. 4.[190,191] However, the classification of PEs is not straightforward. Indeed, different terminologies have been interchangeably used for addressing similar PEs. For example, the term DPE is not so popular despite being used in several earlier reports since its inception by Wright *et al.* and Armand *et al.* in the 1970s. In recent times, the popular terminology of solid polymer electrolyte (SPE) has almost replaced the term DPE, which covers all the PEs that are free from any additional liquid/liquid-like plasticizer components. In PEs, if the ionic conduction is predominantly

Table 1 Lithium concentration (mol L^{-1}) and ionic conductivity (at room temperature) comparison of LEs and SPEs against generally used ISEs (reproduced/adapted from ref. 87 with permission from IOP Publishing, Copyright 2019)[87]

Name	Formula	Li concentration, mol L^{-1}	Ionic conductivity, mS cm^{-1}
LE			
LP30	1 M LiPF$_6$ in EC:DMC (1:1)	1.0	*Ca.* 11.2 (25 °C)[175]
Solid polymer electrolyte			
PEO	P(EO)$_{20}$LiTFSI	1.1	*Ca.* 0.36 (60 °C)[176]
Inorganic solid electrolytes			
Oxide			
LLTO	Li$_{3.3}$La$_{0.56}$TiO$_3$	81.3	*Ca.* 1–0.01 (27 °C)[177]
LLZO	Li$_7$La$_3$Zr$_2$O$_{12}$	41.3	*Ca.* 0.2 (25 °C)[178,179]
LISICON-family	Li$_{14}$ZnGe$_4$O$_{16}$	66.7	*Ca.* 10^{-3}–10^{-4} (25 °C)[158,180,181]
Phosphate			
LATP	Li$_{1.3}$Al$_{0.3}$Ti$_{1.7}$(PO$_4$)$_3$	10.0	*Ca.* 3–0.7 (25 °C)[182,183]
Sulfide			
Agyrodite	Li$_6$PS$_5$Br	40.1	*Ca.* 1–10 (25 °C)[184–186]
Li$_2$S–P$_2$S$_5$ polyhedra	Li$_7$P$_3$S$_{11}$	28.0	*Ca.* 17 (25 °C)[187]
Li$_2$S–P$_2$S$_5$ crystalline	Li$_2$P$_2$S$_6$	14.9	*Ca.* 7.8 × 10^{-8} (25 °C)[188]
LGPS	Li$_{10}$GeP$_2$S$_{12}$	34.7	*Ca.* 12 (27 °C)[189]

2714 | *Energy Environ. Sci.*, 2021, **14**, 2708–2788

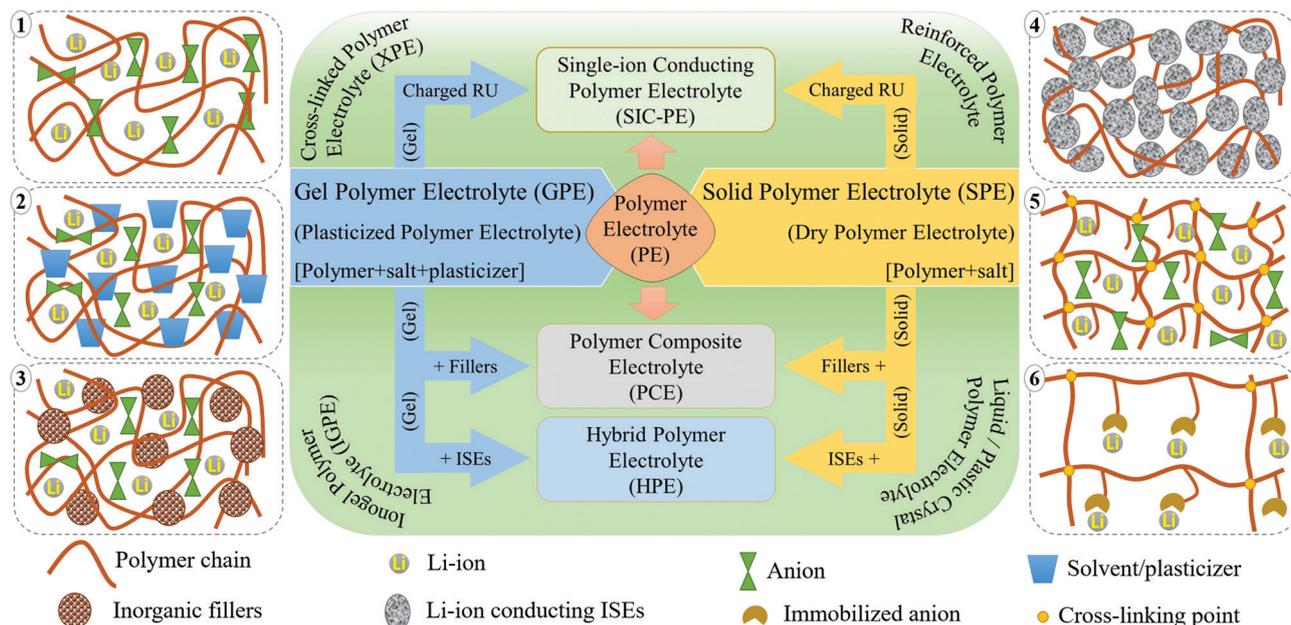This journal is © The Royal Society of Chemistry 2021

Fig. 4 Simplified classification of various PEs and conventional terminologies from a historical perspective (RU is the repeating unit of a polymer chain). A schematic illustration of major classes of PEs is also presented. (1) Classical DPEs/SPEs consisting of a polymer host and salt, (2) GPE/quasi-solid-state/ plasticized PEs, (3) PCEs/PNCEs, (4) HPEs, (5) cross-linked PEs, and (6) SIC-PEs.

occurring in the liquid phase and is partially decoupled from the segmental motion of the polymer chains, they are called GPEs. The terminology of GPE is often used to represent plasticized and quasi-solid-state PEs as well. However, the distinction is not well-defined in the literature. If the liquid content in a PE is very low so that the ionic conduction mechanism is majorly coupled with the polymer chain segmental motion and hopping, such PEs are often called plasticized PEs. In such systems, the added liquid is acting mainly as the polymer host softener, which may not necessarily involve directly in ion conduction. In the case of quasi-solid-state PEs, the liquid content is in between GPEs and plasticized PEs, where the ionic conduction is significantly contributed by both the polymer host and the added liquid moiety. In any case, the liquid components (*e.g.*, commonly used carbonate solvents in LEs) added into the polymer matrix are generally considered as plasticizers irrespective of their amount as they influence the polymer processing and their physical properties (Fig. 4(1)). Other than these conventional liquid plasticizers, molecules such as plastic crystals, liquid crystals, and oligomers of PEO and glymes with a low melting point [they are in a viscous/waxy state at RT and can be called liquid-like components] are also employed as plasticizers in PEs. Hence, the obtained PEs can also be included in the category of plasticized or quasi-solid-state electrolytes. PEs with plastic crystals and liquid crystals are often specifically called plastic crystal PEs (PCPEs) and liquid crystal PEs (LCPEs), respectively. In the context of this review, quasi-solid-state electrolytes and plasticized PEs are also considered in the category of GPEs as it is the most popular term used in literature reports. The terminology of plasticizer is not exclusively restricted to liquid/liquid-like components. Solid-plasticizers such as inorganic

nanofillers (*e.g.*, ceramic, glasses, *etc.*) are also used for tuning the properties of PEs. Even internal plasticization from side chains/functional groups of the polymer host is also possible. Such PEs with solid plasticizers/internal plasticizers are considered in the category of SPEs as the criterion of the absence of a liquid/liquid-like plasticizer component in the final PE is satisfied. However, even these SPEs can be easily transformed into GPEs by an activation process such as swelling/soaking or pre-incorporation by LEs. Ultimately, a variety of PEs such as polymer composite electrolytes (PCEs), hybrid polymer electrolyte (HPEs), single-ion conducting polymer electrolytes (SIC-PEs), reinforced polymer electrolytes, cross-linked polymer electrolytes, and so forth and so on are possible to be realized, which can be either SPEs or GPEs depending on the processing steps and components involved (Fig. 4).[192–195] Detailed classification of PEs and further discussion on their properties are available elsewhere.[65,66,172,196–199]

SPEs/DPEs

In a typical DPE, the salt is dissolved solely by the host polymer matrix without any external liquid/liquid-like plasticizers (Fig. 4(1)). The ion conduction occurs within the polymer host either by segmental motion or hopping, or both.[73] PEO and several other commonly available polymer hosts such as poly(methyl methacrylate) (PMMA), poly(vinyl acetate) (PVAc), poly(carbonates), PVdF, PVdF–HFP, poly(acrylonitrile) (PAN), and so on are used for the preparation of DPEs.[74] However, the ionic conductivity remains very low ($<10^{-5}$ S cm^{-1} at RT) due to the inferior ion transport characteristics of these predominantly crystalline polymer hosts at ambient temperatures (PEs with nearly 100% crystallinity are also called crystalline PEs).[200,201] Possessing a

lower T_g value and improved polymer segmental mobility can facilitate ionic conduction in DPEs.[202] This relationship between T_g and the amorphous nature of the polymer host fueled research on tweaking the polymer host's amorphous nature to enhance the ion mobility[75,203,204] so that DPEs possessing ionic conductivity par with LEs are expected to be achieved.[205,206] The amorphous character of a polymer host in a DPE can be tuned by adding solid-plasticizers, by introducing cross-links and interpenetrated polymer networks, or by constructing block copolymer architectures. Indeed, every approach reduces the crystallinity leading to the development of various sub-classes of PEs (shown in Fig. 4). Fig. 4 also schematically illustrates various types of PEs commonly discussed in the literature reports. As already discussed, this review opts for the term SPE to represent DPEs and all other related PEs devoid of liquid/liquid-like components in line with the modern-day literature reports.

Innovation in SPEs can be achieved by adopting various interdisciplinary approaches. For instance, as the polymer host architecture can influence the electrolyte chemistry, especially the segmental motion of the polymer chains, creating novel polymer hosts such as block copolymers and polymer brushes, blending of two or more polymers, and preparation of semi- or fully-interpenetrated polymer networks, covalent organic frameworks (COFs), cross-linked polymers (Fig. 4(5)), and organic–inorganic hybrid copolymer systems are all of prime importance.[207–212] An array of targeted, precise, and innovative polymer hosts and architectures can be synthesized using controlled polymerization techniques such as Reversible Addition Fragmentation Chain Transfer (RAFT) polymerization and Atom Transfer Radical Polymerization (ATRP) or simple anionic, cationic, and free-radical polymerization techniques.[212–218] Besides, SPEs can be polymer-in-salt (rubbery electrolytes) and salt-in-polymer systems (a rarely used terminology). In the former, the weight percentage of the Li-salt exceeds 50 wt% of the polymer host, whereas it is *vice versa* in the latter.[219–221]

Preparation of SPEs as polymer nanocomposites (PNCs) with suitable inorganic nanofillers [*e.g.*, SiO_2, $LiAlO_2$, MgO, $MgAlO_2$, CeO_2, TiO_2, metal–organic frameworks (MOFs), MXenes, BN, clay minerals, *etc.*] has also been attempted, and such classes of electrolyte systems are known as polymer composite electrolytes (PCEs) or polymer nanocomposite electrolytes (PNCEs) (Fig. 4(3)).[69,176,222–230] These nanofillers in the right proportions enhance the thermal properties, interfacial adhesion, and electrochemical and ion conduction characteristics. In PCEs, the nanofillers aid the Li^+-ion transport through the functionalities (such as hydroxyl groups) and net charge present at the surface. These nanofillers also interact with polymer chains and modify their physical characteristics such as crystallinity, modulus, and flexibility. Thus, these nanofillers used in PCEs can also be considered solid-plasticizers as already discussed when used in low concentrations. Another family of PCEs, which has an individual identity and is gaining recent importance, is hybrid polymer electrolytes (HPEs). HPEs are produced by the interdisciplinary combination of organic and inorganic chemistry, where ISEs (*e.g.*, LAGP, LLZO, LATP, *etc.*) are used as fillers so that they can also take part in ion conduction (Fig. 4(4)).[230–235]

The latest addition to the SPE family is polymeric lithium salts in which the mobility of anions is restricted by incorporating negative charge into the repeating units of either the polymer backbone or the pendant chain. They are mostly adopted for the preparation of single-ion conducting PEs (SIC-PEs) (Fig. 4(6)).[236–238] In such systems, a high Li^+-ion transference number ($0.8 \leq T_{Li^+} \leq 1$) can be achieved due to the presence of immobilized anions as the only mobile species is the cation. Additionally, the salt concentration gradient (concentration polarization effect) is minimized at high charge–discharge rates due to the presence of only one type of charged species at the electrode|electrolyte interface. A similar effect can also be achieved by trapping the anions using anionic trapping agents such as boron-based Lewis-acids, macromolecules (*e.g.*, calix[4]arene and calix[*n*]pyrroles), and anion-grafted/co-grafted inorganic particles, which can be incorporated into the polymer matrix as an additive to improve T_{Li^+}.[64,239–245] Polymerized ionic liquid-based block copolymer hosts exhibiting a polyelectrolyte nature are also popular among SPEs.[246–248] However, bringing the ionic conductivity of SPEs to the order of LEs is yet to be achieved. Still, all the aforementioned efforts have resulted in a pool of new polymers that can surpass the classical PEO as the primary host.

GPEs

The practical complexities related to the low ionic conductivity of SPEs are overcome by introducing the concept of GPEs. In a GPE,[70] along with a polymer matrix and a conducting salt, a liquid solvent/liquid-like plasticizer is also used, which in turn increases the amorphous regions in the polymer matrix and enhances the ion transport (Fig. 4(2)).[75,249] In other words, GPEs combine the advantages of both SPEs and LEs with high ionic conductivity and solid-like mechanical stability. This concept was first coined in 1975 by Feuillade *et al.*[250] In contrast to SPEs, in GPEs (including plasticized and quasi-solid-state PEs), the ion conduction occurs through the synergistic contribution from both the plasticizer and the polymer phase. However, provided that the GPE is made from a surplus quantity of liquid solvent, the assistance from the polymer host towards ion conduction and mechanical property enhancement will be minimal. Nevertheless, the scope of GPEs is broad compared to SPEs, as many other electrochemical devices such as supercapacitors and solar cells prefer GPEs due to the possibility of achieving improved interfacial contact arising from the presence of a certain degree of LE-like character.[251–253] The use of cross-linked, interpenetrated, and block copolymer hosts is explored to improve the LE or solvent retention capability in GPEs. However, the non-realistic addition of a liquid component to boost the electrochemical performance will compromise the safety aspects targeted for GPEs due to the decreased mechanical properties (*e.g.*, low tensile strength, shear modulus, Young's modulus, *etc.*). Thus, the weight percentage of the liquid phase in GPEs is an important parameter to be taken into consideration. Indeed, an ideal GPE for LPBs is expected to possess high ionic conductivity with the least amount of liquid component incorporated in it. Similar to composite SPEs, composite GPEs (gel-PCEs) are also popular, which can to an extent compensate the disadvantages imposed by the presence of extra solvents.[254–256]

In many cases, the polymer hosts used in SPEs are also used for the preparation of GPEs.[63,257–259] Carbonate solvents, glymes,

2716 | *Energy Environ. Sci.*, 2021, **14**, 2708–2788

This journal is © The Royal Society of Chemistry 2021

low molecular weight poly(ethylene glycol), *etc.*, are used for the activation/plasticization of the polymer matrix.[260–262] Besides, room-temperature ionic liquids (RTILs) are used as a safe alternative to low boiling point plasticizers, and several studies have been carried out in this direction.[263–267] RTILs as a plasticizer are an interesting case for several reasons. Firstly, these organic salts are liquid at RT, whereas a conventional salt like LiTFSI is solid. Secondly, RTILs can act as a liquid plasticizer to reduce T_g of the polymer host and, at the same time, can facilitate ion transport. Finally, these are high boiling solvents with negligible vapor pressure; hence, even after being employed as an organic liquid plasticizer, fire hazards can be avoided. The addition of RTILs into a polymer matrix and the classification of the resulting PE is an unresolved debate yet. In many literature reports, it is considered as a quasi-solid-state PE, but several others referred it as an SPE since RTIL by itself is a salt. The term ionogel PE (IGPE) is also often used to consider it as a separate class of PE.[268,269] The major issues with IGPE systems are their high cost, low purity, and low T_{Li^+} value, and such problems must be addressed to implement these systems for commercial applications. Even polymeric ionic liquids (PILs) acting as a host and salt in GPEs and SPEs are also finding attraction among researchers.[270–272] Other solvents like H_2O, acetonitrile (ACN), dimethylformamide (DMF), *N,N*-dimethylacetamide (DMAC), and *N*-methyl pyrrolidone (NMP) are also used in GPEs for specific applications.[273–277]

The advantages of SPEs over GPEs include their high mechanical stability and enhanced compatibility with the Li-metal anode owing to the absence of a liquid phase. Although the liquid phase in GPEs may often undergo unwanted parasitic reactions over the Li-metal anode and destabilize the interface and interphase, the liquid-like ionic conductivity of GPEs is the utmost advantage due to the enhanced ion transport characteristics. Despite the trade-off between GPEs and SPEs in many aspects, both systems are promising to be used for the commercial production of LPBs. Recently, PEs have found applications in microbatteries, and flexible- and printable-LBs.[278–281] Additionally, other metal-ion (Na$^+$, Zn^{2+}, Mg^{2+}, *etc.*) conducting PEs are also being noticed with the surge in interest towards batteries beyond lithium chemistry.[282–289] This underlines that the concomitant development of both SPEs and GPEs is indeed crucial for pushing the further development of LPBs and other EES technologies. It is worth mentioning that LPBs are already under commercialization by companies like IONIC MATERIALS INC,[290] A-123 Systems, DNK Power,[291] Panasonic, LG Chem, and Bolloré.[292] In the next few years, widespread interest in LMPBs with SPEs is expected to grow many folds also for EV application.[293,294]

4. Intricacies of interfaces and interphases, and related challenges in PEs

The electrode|electrolyte interfaces and interphases are two critical components influencing the electrochemical performance of any LB cells. Interfaces are the regions in an LB cell where the electrode and electrolyte are in direct contact with each other. On the other hand, the interphase refers to a desirable passivation layer, which is formed over the electrode surface by electrochemical processes taking place at the interface. Interphases have a definite chemical composition that prevents direct contact between the electrode and electrolyte components, but, at the same time, ensures facile Li$^+$-ion transport. The interface qualitatively indicates the extent of contact between the electrode and electrolyte species inside an LB cell. Electrode|electrolyte interfaces in LBs are of two types: the (i) anode|electrolyte interface and (ii) cathode|electrolyte interface.[295] Accordingly, the two types of electrode|electrolyte interphases formed over the anode and cathode are known as the SEI and CEI, respectively. An ideal electrode|electrolyte interface indicates the complete wetting of the electrode particles present at the surface and bulk regimes of the composite electrode film irrespective of the coating thickness. Ideally, achieving maximum interfacial contact and active material utilization within an LB cell requires electrolyte impregnation into pores distributed in the sub-micron regimes, those including nanopores, mesopores, and micropores of the electrode particles, which is indeed challenging. Indeed, the interface and interphase are two interrelated features since the interphase can only be formed at the interface between the electrode and electrolyte. Therefore, in any battery cell, the first step is attaining a conformal electrode|electrolyte interface (simply, good wetting). Later, the electrochemical processes occurring at the interface lead to the formation of conformal interphase layers (SEI and CEI), hence impeding both the electrode and electrolyte components from further degradation or decomposition. However, all interphases are not equally useful in avoiding parasitic reactions between the electrode and electrolyte or providing interfacial stability within the LB cell. Attaining a conformal interface can ensure an equally conformal interphase. However, the nature and the quality of the interphase is ultimately decided by the electrode and electrolyte components, and the cell operating conditions.

Generally, the SEI and CEI are considered desirable interphases and very important for the functioning of LBs. However, undesirable interphases formed by parasitic reactions between the electrode and electrolyte do not lead to ideal SEI- and CEI-like characteristics. The favorable features of SEI and CEI are: (i) ionically conducting, (ii) thin and uniform, (iii) chemically and thermally stable, (iv) capable of absorbing the stress from the volume change occurring during the cycling process, (v) capable of avoiding leaching of active electrode materials, (vi) electronically non-conducting, and so forth and so on. As one of the authors of this review emphasized earlier in one of his influential perspective articles on interphases, 'the SEI and CEI formed at the electrode surfaces are thin solid electrolytes, but the fact is often ignored.[174] Indeed, interphases are one of the most important but least understood components of a battery cell. In most of the literature, the interphases in an LB cell are depicted as a superficial layer formed on the surface of the composite electrode film. However, it is not representing real-world conditions since the interphase covers not only the

This journal is © The Royal Society of Chemistry 2021

Energy Environ. Sci., 2021, **14**, 2708–2788 | **2717**

surface of the composite electrode film but also the surface of individual electrode particles (Fig. 5a).

The physical interaction between a hypothetical PE and a thick and porous LB electrode (anode/cathode) can be considered as a model system for understanding the electrode|electrolyte interface and interphase, as presented in Fig. 5a. Here, the regions accessed by the PE are denoted as retaining a conformal electrode|electrolyte interface, whereas the regions inaccessible
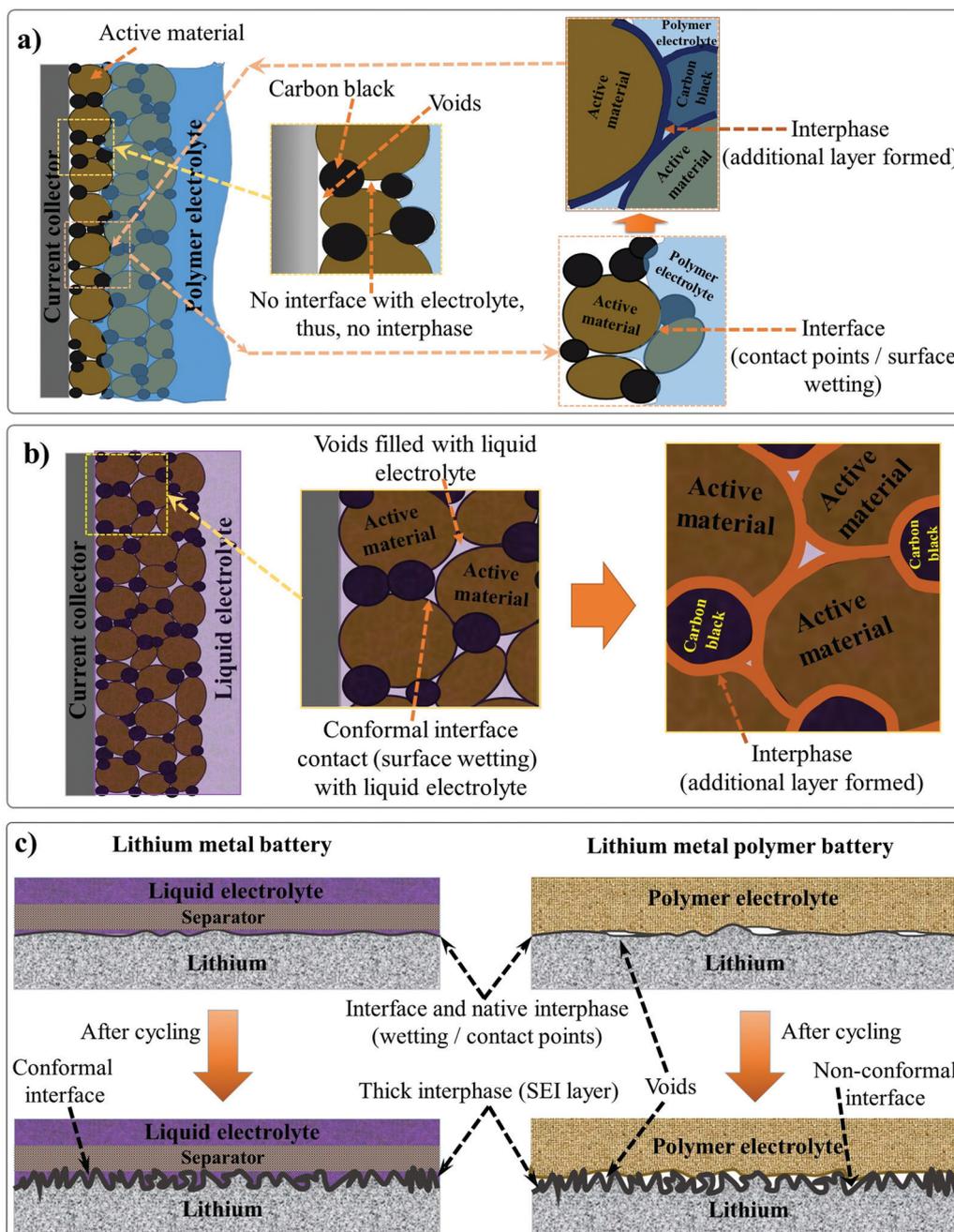
Fig. 5 (a) The electrode|electrolyte interface and interphase formed inside the LPB cell with a PE (film) placed over the porous composite electrode (anode/cathode) (binder molecules are not shown for simplicity). Due to the solid-like character of the PE, the conformal interface or contact points between the electrode and PE is mainly confined to the electrode particles present at the surface, whereas the bulk-particles do not meet the PE, hence resulting in low active material utilization. The points at which the PE is not in contact with the electrode particles are indicated as voids. In these voids, the quintessential SEI/CEI layers are not formed, and these particles cannot take part directly or efficiently in the charge-storage process. (b) The electrode|electrolyte interface and interphase of a LIB cell with LE: unlike the case with PE, the free-flowing character of the LE allows the wetting of electrode particles present both at the surface and underneath. Therefore, the electrode|electrolyte interface and interphase coverage in an LE are conformal and ideal. Ultimately, the challenge with PEs is the inability to emulate the electrode|electrolyte interface like that of an LE. (c) The electrode|electrolyte interface in a relatively flat Li-metal anode surface in contact with a PE (in LMPB) and LE (in LE-LMB) before and after cycling.

2718 | Energy Environ. Sci., 2021, 14, 2708–2788

This journal is © The Royal Society of Chemistry 2021

to the electrolyte are indicated as possessing non-conformal electrode|electrolyte interfaces. A non-conformal electrode|electrolyte interface within the electrode reduces the overall active material utilization and maximum achievable energy density. The formed interphase in the interface regions, at which the PE is holding excellent contact with the electrode material, is also highlighted. Fig. 5a concludes that in a typical scenario, a PE cannot offer an ideal electrode|electrolyte interface or interphase, especially in cases when used as a film sandwiched between the electrodes. However, in LEs, the free-flowing nature and low viscosity help in the adequate wetting of the electrode particles at the surface and those buried beneath the composite electrode film (Fig. 5b). The LE can easily impregnate into the bulk-regimes of the porous electrode matrix, providing an extended conformal electrode|electrolyte interface and interphase, in turn ensuring inter-particle Li$^+$-ion transport and maximum active material utilization. Therefore, during the transition from LEs to PEs, achieving an electrode|electrolyte interface and interphase similar to LE is challenging, especially with typical porous and thick electrodes. The inferior electrode|electrolyte interface is one of the most fundamental challenges to be solved in LIPBs, which leads to inferior electrochemical performance when compared to conventional LIBs.

In the case of LMPBs with a flat Li-metal anode of relatively low surface area and porosity compared to graphite, achieving a conformal anode|electrolyte interface, which is more or less similar to conventional LEs, is often not challenging with a PE (still, an externally prepared PE film cannot precisely mimic the Li-metal|LE interface as illustrated in Fig. 5c, where voids would still exist at the Li-metal|PE interface). However, it should be noted that the high reactivity of Li-metal can decompose the PE components during cycling. Additionally, the stress arising from the volume changes on the Li-metal surface during the continuous lithium plating/stripping process will destabilize the interface and interphase (Fig. 5c), a similar scenario to the case of an LE-LMB (Fig. 2 and 5c). During continuous cycling, it is possible that the relatively smooth Li-metal surface eventually turns rough and uneven due to HSAL growth, and the continuous electrolyte decomposition leads to the formation of a thick interphase. HSAL nucleation and the thick interphase can lead to cell failure with time, which is more severe in LE-LMBs but can be present in LMPBs also with an otherwise inefficient PE. Hence, LMPBs demand PEs that can provide a stable interface without compromising the Li-metal|electrolyte interphase. As already discussed in Section 3, a PE with a high Young's modulus value may be suitable to stabilize the Li-metal|PE interface and interphase. However, the chemical composition of the PE and its compatibility with Li-metal are also equally important to avoid any detrimental parasitic reactions, which can lead to the formation of undesirable interphases without typical SEI features. Even for those PE films providing a good interface and interphase at the Li-metal anode, the challenges of maintaining the ideal interface still persist with the porous and thick cathode. In conclusion, novel cell fabrication strategies and polymerization techniques should be considered and implemented for LIPBs and LMPBs with smart PEs that can

offer LE-like (or close to LE-like) interfaces and interphases for the flourishing of LPBs in general.

4.1 The *ex situ* process and device fabrication thereof

The conventional approach for the fabrication of LPBs involves multiple steps in which a PE is externally prepared as a self-standing film,[296–298] followed by sandwiching between the electrodes.[299–303] For example, the preparation of a PE film by heat-/light-induced polymerization and the subsequent assembly of an LMPB cell are presented in Fig. 6. Here, the primary requirement is a precursor solution (also called reactive mixture, reactive solution, or merely precursor) containing polymerizable monomers (also including oligomers: they are polymerizable molecules made of a few monomer units, examples include dimers, trimers, tetramers, *etc.*), a conducting salt and a suitable polymerization initiator (molecules that initiate the polymerization process when provided with the right conditions). The presence of an electrolyte solvent/plasticizer (solid/liquid/liquid-like) is optional, depending on whether an SPE or GPE is of interest. Later, the precursor is cast on a flat surface, and, following the polymerization process, a PE film with the desired thickness is obtained. In many cases, a polymer film is prepared from the precursor in the absence of electrolyte components (salt and plasticizer) and later subjected to activation by a swelling (soaking) process in an LE to produce an ionically conducting GPE.[304] In any case, the prepared PE film is used in the sandwich configuration, where it plays the additional role of the separator as well. Such a strategy of LPB cell fabrication using an externally prepared PE film is often given by the term: 'the *ex situ* fabrication of LPB cells' (simply, the *ex situ* (polymerization) process).

The preparation of PE films, as depicted in Fig. 6, can be called a *bottom-up* approach since the polymer host is evolved from a precursor consisting of basic constituent units of reactive monomers/oligomers. Polymerization methods such as free-radical polymerization, ionic polymerization, condensation reactions, click chemistry, and so on are finding immense attraction among researchers for the preparation of PE films by such a *bottom-up* approach.[300,304–307] Indeed, these polymerization reactions can be triggered by energy sources such as heat, ultraviolet (UV)/visible light irradiation, and microwave/infrared/γ-ray exposure. *Bottom-up* polymerization methods are suitable to prepare and tune the properties of homo-polymers, copolymers, and cross-linked or even reinforced SPEs and GPEs. In fact, this *bottom-up* approach by radiation-induced polymerization came into the limelight with the work of Abraham *et al.* in 1995, where a reinforced GPE film was prepared using a Celgard separator soaked with a PE precursor made of a tetraethylene glycol diacrylate cross-linker, a carbonate-based LE, and a photo-initiator.[308] This work inspired several successive studies that later employed UV-polymerization for the production of various types of PEs.[309,310] The advantage of the *bottom-up* approach is that any additional solvents other than those required for the plasticization of the PE can be avoided as most of the monomers/oligomers are inherently capable of dissolving the Li-salt, hence minimizing the wastage of solvent. However, if required, a small amount of solvent can be used
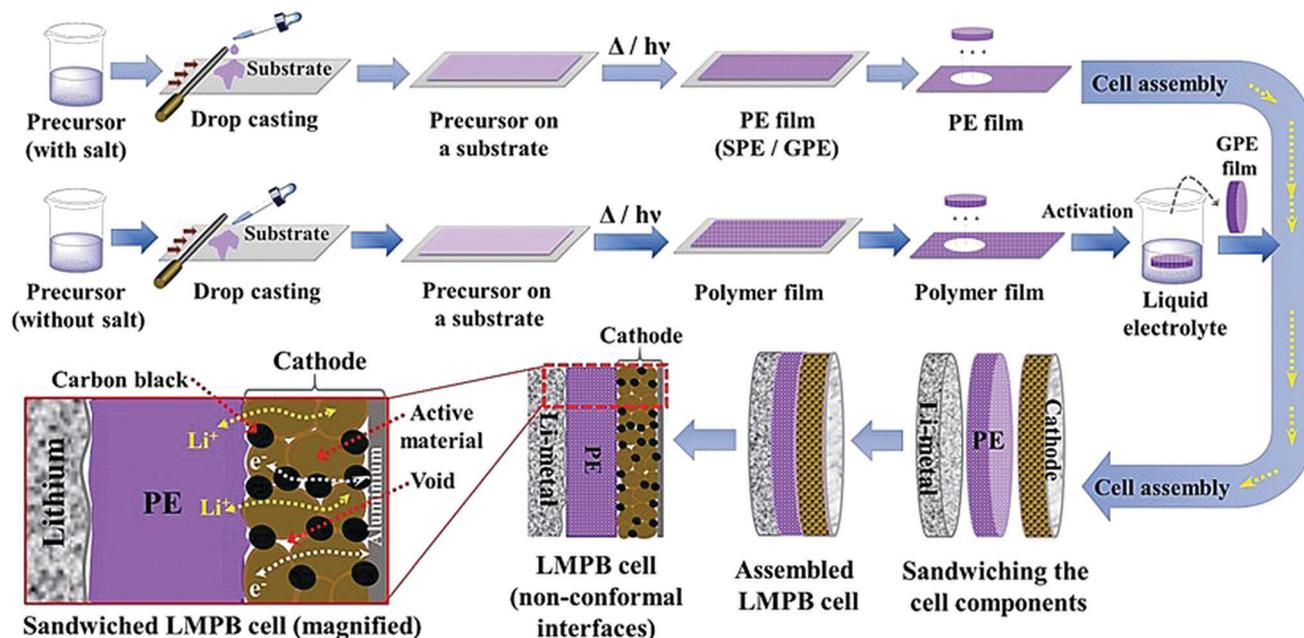
This journal is © The Royal Society of Chemistry 2021

Energy Environ. Sci., 2021, **14**, 2708–2788 | **2719**

Fig. 6 Schematic representation of the *ex situ* process in which the PE is prepared separately as a film by free-radical or any other polymerization methods (*e.g.*, ionic polymerization) and then assembled by sandwiching it between the anode and cathode to obtain an LMPB (or LIPB) cell (an LMPB is illustrated for simplicity). In this case, the externally prepared PE can even be activated in an LE, using a swelling process to improve the ionic conductivity. The electrolyte-inaccessible regions in the Li-metal anode and cathode are shown as voids, which represent the dead-volume in the electrode, not contributing to charge-storage (for simplicity, only the *ex situ* processing of LMPBs is illustrated, but all the processes mentioned in this figure are applicable to LIPBs as well).

during the PE processing, which can be evaporated off in the subsequent steps depending on the requirement that a plasticized PE or SPE is required. Ultimately, the *bottom-up* approach of PE film preparation is applicable in both solvent-supported (*wet*) and solvent-free (*dry*) conditions.

In conventional dry/solvent-free processing of PE film preparation by the *ex situ* process, a polymer is melted above the melting point (T_{m}), and then electrolyte components are added to the melt.[311] Depending on the type of components added, and the involvement of the activation step, an SPE or GPE film can be prepared. Thus, this melting-induced dry processing can be considered a *top-down* approach as the polymer host is directly used to prepare the PE film, unlike the on-site conversion of monomer/ oligomer units to PEs by the *bottom-up* approach. One of the disadvantages of this process is that the desired mixing can be achieved only at high temperatures under high mechanical shear. Also, the salt or even polymer decomposes at such high temperatures and mechanical stress conditions, and expected results are often not achieved. A modified version of this method called melt-pressing is also popular.[197,312] In this process, the polymer host and other solid-components such as salts and fillers (preferably in the powdered form) are mixed and ground well until a homogenous blend is obtained. Later, the mixture is hot-pressed close to the melting point (T_{m}) of the polymer matrix by keeping it between two Teflon (PTFE) sheets (or stainless-steel plates or other substrates) so that a PE film or pellet can be prepared. However, in this method as well, the temperature-induced decomposition of the electrolyte components is mostly unavoidable.

There are several conventional wet (solvent-supported) processes used for the preparation of PE films.[72,197,313] In a typical wet process, the polymer is dissolved in a suitable solvent with or without the presence of a salt and other solid-additives (since a polymer is directly employed, these methods can also be considered in the category of the *top-down* approach). The cast membrane, following vacuum drying and evaporation of the solvent, can be either directly used as an SPE (if a salt is present) or activated by an LE. This activation process induces plasticization of the polymer chains due to the interaction with the salt and the plasticizer components. Therefore, T_{g} is reduced, while the flexibility of the overall PE is increased. The swelling time or rate is controlled to obtain mechanically stable GPE or plasticized/ quasi-solid-state PE films. The swelling also determines the amount of plasticizer and salt components present in the PE, which decides the overall electrochemical properties.[314–316] For example, the ionic conductivity is increased with an increase in the LE content; at the same time, swelling of the polymer film induces volume expansion due to the uncoiling or unpacking of the polymer chains from the ordered phases (crystalline) of the polymer matrix. This phenomenon decreases the mechanical properties; nevertheless, the solvent uptake increases the mobile phase within the polymer electrolyte. The method developed by Sony Co. in the year 1999 for the preparation of PVdF–HFP-based GPE films activated by carbonate-based LEs is popularly known as the Sony process for GPE preparation.[317,318]

Extraction–activation methods for the preparation of GPE films are a commercially important wet process (*top-down*)

2720 | *Energy Environ. Sci.*, 2021, **14**, 2708–2788

This journal is © The Royal Society of Chemistry 2021

developed by Bellcore.[319,320] In this method, the polymer is mixed with a slurry of electrode material in the presence of a plasticizer and coated over the current-collectors. Then the plasticizer is extracted, followed by wetting the electrodes by an LE during cell assembly. However, this method is tedious and dangerous, owing to the use of the toxic dibutyl phthalate (DBP) plasticizer. The approach is further improvised in such a way that the extraction step is avoided and this is popularly known as the phase-inversion method.[320–322] Bellcore is also credited with the early models of LIPBs, which were commercialized in 1999 under the name PLiON (plastic lithium-ion battery).[319,323] In several reports, viscous GPE solutions are also used, which are often directly cast over the electrode surface for electrochemical device fabrication (e.g., PMMA dissolved in LiClO$_4$/PC solution).[251,324] This method is found to improve the electrode|electrolyte interface compared to the case when PE membranes are otherwise used as films. However, even this approach fails with thick electrodes due to the size-mismatch of the pores in the electrode material and the high molecular weight of the polymer chains.[325,326] Moreover, this method intensively compromises the ultimate aim of achieving a high performance and mechanically stable GPE, which does not lure the research community beyond the lab-scale.

Although PE films that are *ex situ* processed are essential and significant in LPBs (even commercialized to an extent), absolute improvement in terms of the electrode|electrolyte interface/interphase to match with that of an LE (Fig. 5b) can be envisaged when looking towards the future. For example, when a PE film is used in the *ex situ* process, the electrode|electrolyte interaction is primarily confined to the surface but not to the bulk of the electrode (see Fig. 5a and 6). The *ex situ* process leads to low active material utilization in LPBs, resulting in a reduction in the maximum achievable energy density. In a battery electrode, it is vital to maintain an excellent electronic and ionic flow within the composite electrode (Fig. 6 magnified cell) so that the redox reactions leading to the charge–discharge process can occur with the lowest overpotential or activation energy. Recent modeling studies also emphasize the significant role of Li$^+$-ion transport within the composite electrode matrix, which largely influences the overall performance of LBs, especially at higher current rates (power density) and with thick electrodes (energy density).[327] The low rate capability in the case of LPB cells fabricated by the *ex situ* process, especially in thick electrodes, is due to the non-accessibility of the PE components to the electrode particles buried beneath the surface of the composite electrode film and the electrode pores. In Fig. 5a and 6, the regions in which the electrolyte accessibility is minimal are represented as void spaces. Such void spaces indicate that *ex situ* processed PE films are incapable of emulating the efficient electrode|electrolyte interface/interphase similar to conventional LEs.[295,328] Thus, inter-particle Li$^+$-ion transport in LPBs with thick electrodes can only be achieved with the help of an ion conducting (e.g., PE) medium present within the electrode bulk.

4.2 The *in situ* process and device fabrication thereof

To overcome the limitations associated with electrode|electrolyte interfaces and interphases in LPB cells using the *ex situ* process,

ample modifications are proposed that can be implemented from the PE synthesis step itself. One such strategy is called 'the *in situ* fabrication of LPB cells,' or simply, the '*in situ* (polymerization) process,' which has received considerable attention in recent years.[329–334] The *in situ* process involves the single-step generation of a PE ensuring an effective electrode|electrolyte interface and interphase extended to both the surface and bulk particles of the composite electrode. The *in situ* processing of LPB cells is often carried out in three different ways (Fig. 7a):

(i) separator assisted approach (Fig. 7b and 8a)
(ii) direct deposition approach (Fig. 7c and 8b)
(iii) sacrificial and artificial protection approach (Fig. 7d).

The 1st and 2nd approach directly address the fabrication of LIPBs and LMPBs. The 3rd approach is mainly used for the production of conformal protective interphase layers over the active material and conductive carbon of the composite electrode so that the performance of LE-based LIB and LE-LMB cells can be improved. Also, this protection approach can be improvised for the fabrication of LMPB and LIPB cells through an emerging process called a multi-layer approach, as explained in Section 4.2.3.
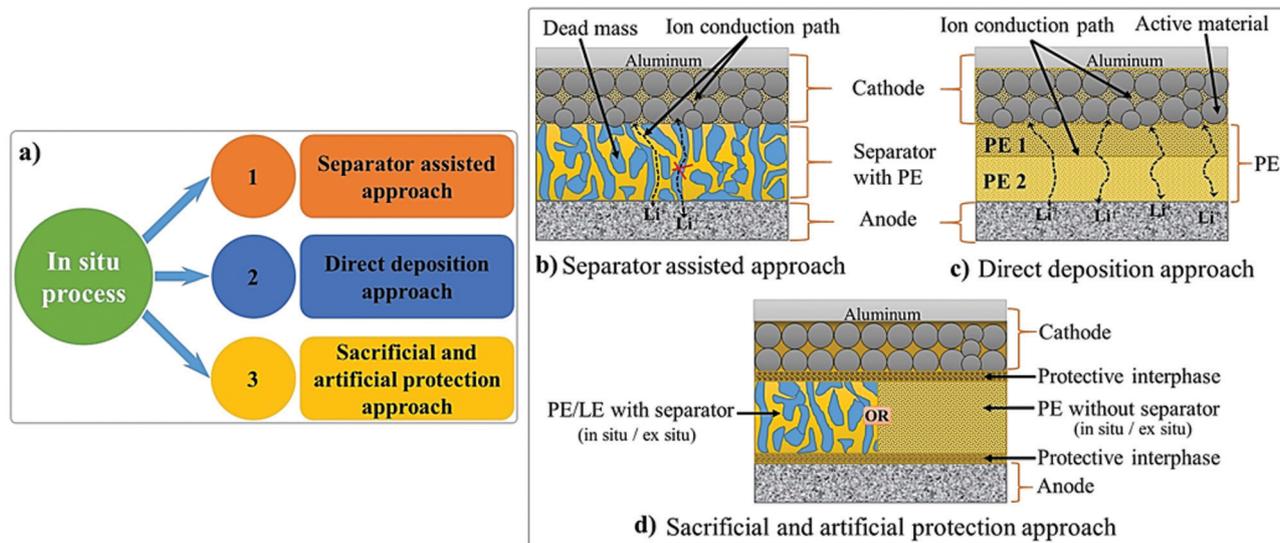
The first step of the *in situ* process is the preparation of a precursor similar to that of the *ex situ* process, as shown in Fig. 6, consisting of polymerizable monomers/oligomers and a conducting salt in the presence of a suitable initiator. Solid- or liquid- plasticizers and additives can also be introduced into the precursor to fine-tune the physicochemical and electrochemical properties, including interphase formation. The *in situ* process is usually carried out by impregnating the coated composite electrode with the precursor, which is later polymerized using an external energy source (e.g., heat or light) so that the PE generation takes place internally within the pores and voids of the electrode coating. The infusion of the electrode by a less viscous precursor in the liquid state, which is similar to an LE, helps in (nearly) saturating the sub-micron pores with low molecular weight monomers, Li salt, solvent, and soluble additives. The impregnation of the precursor followed by the polymerization step ensures an intimate and compelling electrode|electrolyte interface/interphase in the final battery cell close to that offered by an LE (Fig. 5b).[325,326,335] It is highly desirable that the size of the molecular species present in the precursor is comparable to the pore-size/volume of the electrode materials for allowing maximum impregnation and a suitable electrode|electrolyte interface as well as conformal and uniform interphase formation.

The factors, challenges, and advantages pertaining to the interface and interphase formation in the context of the *in situ* process and LPBs, in general, are summarized below.

(a) PE impregnation depends on the viscosity and surface energy of the precursor, bulk porosity and thickness of the composite electrode film, inherent porosity of the electrode materials, continuity of pores/voids, and processing conditions such as temperature and vacuum. The greater the electrolyte impregnation, the higher the active material utilization.

(b) The surface characteristics of electrode materials also determine the interface and interphase. Factors such as the native layers, surface area, surface chemistry, and surface energy of

This journal is © The Royal Society of Chemistry 2021
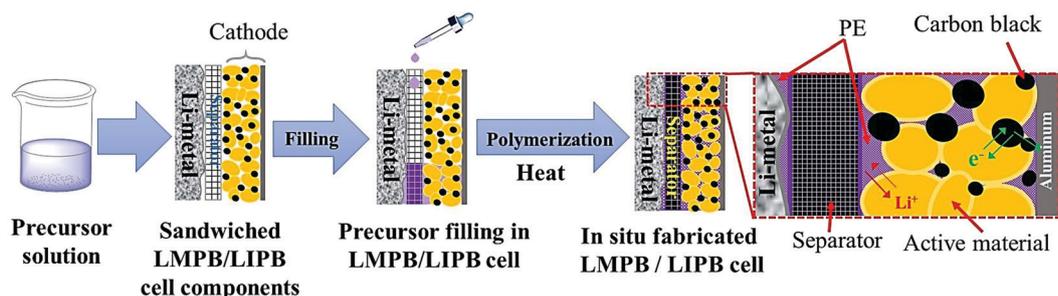
Energy Environ. Sci., 2021, **14**, 2708–2788 | **2721**

Fig. 7 (a) Various types of *in situ* processing approaches. (b) In the case of the separator assisted approach, the inert separator contributes to the dead weight, which does not take part in the ion conduction process but blocks the ion transport pathways. (c) In the case of the direct deposition approach, the PE layer deposited over the individual electrode films itself is acting as both an ion conducting medium and a physical partition between the two electrodes. PE 1 and PE 2 represent individual PE layers formed over the cathode and anode, respectively (direct deposition approach 2). In most of the literature reports related to LMPBs, direct deposition is usually carried out only on the cathode (direct deposition approach 1) since achieving a suitable electrode|electrolyte interface is more critical for a somewhat porous cathode than the relatively flat Li-metal anode. Herein, the whole PE is active towards ion conduction without any dead weight from the separator, unlike the case with the separator assisted approach. (d) In the case of the sacrificial and artificial protection approach, the protective interphase layers are first prepared over the electrode films. Later the LB is fabricated using an inert separator soaked with an LE or an *in situ* or *ex situ* processed PE. The fabrication of LPBs by such a method is known as the multi-layer approach as the subsequent layer over the protective interphases is an *in situ* or *ex situ* processed PE (for simplicity, only the *in situ* processing of LMPBs is illustrated; however, all the processes are applicable to LIPBs as well). (e) Summary of the main advantages (⊕) and disadvantages (⊖) of the three types of *in situ* processing approaches discussed in (a)–(d).

individual electrode components are essential. Comparable surface energy of the electrode and electrolyte precursor ensures effective impregnation and a nearly liquid-like interface throughout the electrode (at the surface and the bulk).

(c) The purity of electrode and electrolyte materials influences the control and stabilization of the interphase. Additive chemistry that is already established for LEs can be used for interphase tuning. The effectiveness of interface formation (improved wetting),

2722 | *Energy Environ. Sci.*, 2021, **14**, 2708–2788

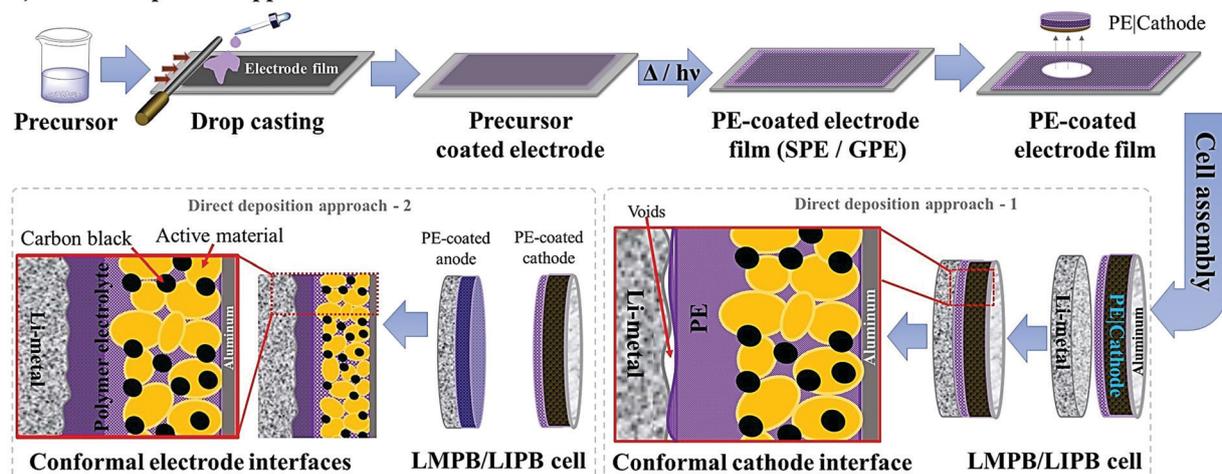This journal is © The Royal Society of Chemistry 2021

Fig. 8 (a) Separator assisted approach of the *in situ* processing of LMPB/LIPB cells. The precursor is filled and subjected to polymerization in a pre-assembled battery cell with the anode, cathode, and separator. Often, a precursor-soaked separator can also be used. (b) Direct deposition approach for the *in situ* processing of LMPB/LIPB cells, which involves the deposition of the precursor over the electrode film followed by free-radical or ionic polymerization methods, and subsequent cell fabrication. If the cathode alone is *in situ* processed (direct deposition approach 1), there is a chance that the electrode|electrolyte interface at the anode can be inferior. However, the inferior interface that may arise at one of the electrodes can be overcome by the *in situ* processing of both anode and cathode electrodes (direct deposition approach 2) followed by cell fabrication (for simplicity, only the *in situ* processing of LMPBs is illustrated, all the processes are applicable to LIPBs as well).

compounds formed due to the decomposition/consumption of the electrolyte (*e.g.*, additives, monomers, salt, and plasticizer) components, nature of byproducts formed (*e.g.*, gaseous or non-gaseous, corrosive or non-corrosive, and catalytic or noncatalytic), reactivity of monomers and oligomers with the electrode components, *etc.*, also affect the stability of the interphase. Interphase characteristics such as the uniformity, thickness, mechanical properties, grain boundary characteristics (especially for inorganic SEI/CEI layer), and related ion transport properties affect the overall cell performance.

(d) Changes to which the electrodes are subjected during electrochemical cycling (*e.g.*, surface area and volume changes of the cathode/anode active materials, continuously evolving surface morphology of the lithium-metal anode, changes in the chemical composition of the electrode material and electrolyte, *etc.*) may affect the quality of the interface/interphase. The physical changes associated with the electrodes may be accompanied by the rupture/delamination of the interphase and a loss of contact (interface) between the electrode and electrolyte. *In situ* processed self-healing PEs may be envisaged

to recover/maintain suitable electrode|electrolyte interfaces and interphases.

(e) The ionic and electronic transport within the composite electrode between individual electrode particles, or, in other words, the inter-particle ion diffusion, is essential to achieve high energy and high-power batteries. However, the PE must not hamper the electronic transport between the electrode particles.

(f) Visualizing the processes taking place at the electrode|electrolyte interfaces and characterization of the formed interphase are indeed essential to help advance existing LBs with the rational development of tailor-made electrode and electrolyte formulations. The characterization of the solid|liquid interfaces in state-of-the-art LIBs is relatively well-established with post-mortem analysis of cycled cells using techniques such as NMR, XPS, Raman analysis, XRD, microscopy, *etc.*, in *ex situ* experimental conditions. However, it is crucial to investigate the interfacial processes under operando and *in situ* conditions in a non-destructive fashion. For this purpose, the existing *in situ* and operando characterization methods

(XPS, Raman analysis, NMR, microscopy, *etc.*), which are designed mostly for the characterization of LE-based LBs, should be modified to make them compatible for thorough analysis of the more challenging solid|solid interfaces in solid-state batteries (PE- and ISE-based LBs). Advanced X-ray tomography techniques are also potential candidates for non-destructive investigation of solid|solid interfaces.

The *in situ* processes using free-radical polymerization by means of thermal- and photo-curing methods are extensively explored for the fabrication of both LMPBs and LIPBs on the lab-scale.[336–340] Free-radical photo-polymerization is usually carried out in a UV-chamber under inert atmospheric (preferably) conditions, whereas ordinary laboratory ovens can be used for the thermal polymerization process.[307,341–343] However, other energy sources such as gamma (γ)-rays,[331] visible light, and lasers[344] are also used for initiating various types of polymerization reactions, but are not as popular as the former heat- or UV-induced polymerization methods. Apart from the free-radical induced *in situ* polymerization process, other methods such as ionic polymerization,[345–347] condensation polymerization,[348,349] and electropolymerization are also receiving attention nowadays.

The number of polymerizable functionalities (*n*) (*e.g.*, polymerizable reactive moieties such as a double bond, epoxide units, and thiol) of monomer or oligomer molecules incorporated in the precursor significantly influences the ion transport and mechanical properties of the formed PE. Depending on the '*n*' value, the polymer hosts in the PE can be either cross-linked or non-cross-linked. Indeed, the physicochemical characteristics of PEs are ultimately dependent on the type of polymer host. A non-cross-linked polymer host is formed from a precursor employing polymerizable species (monomer/oligomer) with an '*n*' value of 1 (mono-functional). If a single type of mono-functional monomer/oligomer molecule is used in the precursor, the obtained polymer host can be called a non-cross-linked homo-polymer (linear or branched). On the other hand, a combination of two or more different types of mono-functional monomer/oligomer molecules produces a non-cross-linked copolymer (linear or branched). The polymer chains in a non-cross-linked polymer host are flexible and dynamic, facilitating ion conduction in a PE. The non-cross-linked character may also lower the physical properties such as softening, melting, and flow-temperature points. Thus, a non-cross-linked PE may not retain the mechanical properties in a wide temperature range. In most cases, when a non-cross-linked homo-polymer or copolymer host is used in a PE, a thicker PE sample is preferred to avoid internal short-circuit. When the value of '*n*' is ≥ 2 (multi-functional), cross-linked polymer hosts are formed. Here, a single type of multi-functional or a combination of different kinds of multi-functional monomer/oligomer molecules can be employed to prepare cross-linked polymers. If the cross-linking density (a measure of cross-linked points per unit volume, unit: mol cm^{-3})[350,351] is very high, it can affect the polymer chain dynamics and reduce the ionic conductivity of the associated PEs. However, a high cross-linking density beyond a certain limit will enhance mechanical properties such as toughness and brittleness and, in turn, reduce flexibility. Thus, a certain degree of flexibility is always desirable for the polymer host to

facilitate ion conduction. Besides, if the polymer host interacts with other electrolyte components such as a salt, plasticizer, *etc.*, the physical properties may vary.

Another approach of preparing relatively flexible cross-linked PEs is by employing a precursor made by combining judiciously selected mono- and multi-functional monomer/oligomer molecules. Such systems consist of a polymer backbone with cross-links inducing a connection between several individual linear/branched long polymer chains derived from the mono-functional molecule present in the precursor. They can often display better flexibility than tightly cross-linked polymer hosts due to the reduced cross-linking density. If internal plasticization from the pendant chains of monomer/oligomer molecules is present, the dynamics of the polymer chains can be further enhanced, favoring ion transport. Depending on the concentration of multi-functional monomer/oligomer molecules present in the precursor, the cross-linking density of polymer hosts can be fine-tuned to achieve the desired flexibility and toughness, optimizing the ion conduction, electrode wetting behavior, and mechanical stability. Considering the mechanical flexibility that long-chain oligomer molecules [*e.g.*, acrylate, methacrylate, and allyl and vinyl ether derivatives of poly(ethylene glycol), *etc.*] can provide to the polymer hosts, they are more prevalent in the preparation of PEs over small-sized monomers [*e.g.*, methyl methacrylate (MMA)].

A detailed explanation of the various types of *in situ* processing approaches is discussed in the following sub-sections.

4.2.1 Separator assisted approach. The most common *in situ* process employed for the fabrication of LPBs is the separator assisted approach depicted in Fig. 8a. In this method, typically, a precursor is filled into a pre-assembled battery pouch containing an anode, a cathode, and a separator in the sandwich configuration. Later, the precursor is polymerized inside the sealed pouch cell. The separator helps provide dimensional stability to an otherwise dimensionally and mechanically unstable (mostly due to the high plasticizer/liquid electrolyte content) PE, and effective partition between the anode and cathode, avoiding short-circuit within the cell. This single-step method also guarantees improved electrode|electrolyte interfacial contact at the anode and cathode during battery cell fabrication. It is like the present-day LIB fabrication process using LEs, except for the additional polymerization step involved. As the polymerization is happening inside a closed environment, UV-light cannot be used for polymerization initiation. Hence, heat-induced free-radical or ionic polymerization methods are best suited. It is important to use suitable monomers/oligomers and initiators that do not produce any gases or other side products inciting bubble formation, pressure build-up, or undesirable reactions with the cell components during the fabrication or functioning of the cell. Besides, the lithium salt, additives, plasticizers, and monomers/oligomers should be thermally stable at the polymerization temperature and should not significantly dampen the polymerization process. One of the other drawbacks of the separator assisted *in situ* process is the dead weight and the inactive ion conduction areas imposed by the supporting separators. In general, cellulose, glass fiber, polyolefin (Celgard), and PVdF or similar polymers are used as separators. These separators

2724 | *Energy Environ. Sci.*, 2021, **14**, 2708–2788

This journal is © The Royal Society of Chemistry 2021

are inert and often do not participate in the ion conduction process, as shown in Fig. 7b.

The separator assisted approach is not always useful in the context of an LMPB since certain types of monomers/oligomers (*e.g.*, acrylates and methacrylates) present in the precursor may undergo undesirable parasitic reactions over the reactive Li-metal surface, hence producing unwanted and unsuitable passivation layers. Therefore, the chemical aspect of the monomers/oligomers such as compatibility with the electrode components also should be considered while selecting the PE components and the polymerization method. However, if monomers/oligomers that are compatible with Li-metal or a precursor with SEI forming additives are used, the separator assisted *in situ* approach can find immediate applications in LMPB fabrication as well. As of now, this method is generally considered to be handy and extensively used in the fabrication of LIPBs. Indeed, the separator assisted approach is primarily used to evade leakage of the LE from the battery pouch so that smart, lightweight, and thinner packaging can be used for battery construction. For instance, the separator assisted *in situ* process was adopted by Sanyo in 2002 for the industrial production of LIPBs, as displayed in Fig. 9.[352,353] The *in situ* process implemented by Sanyo is known as the Sanyo process (see the Fig. 9 caption for details). In the preparation of most laboratory-grade LPB cells, separator pre-soaking in the precursor is used instead of filling in a pre-assembled pouch- or coin-cell. Ultimately, the separator assisted approach is not useful in customized LPB cell designs such as microbatteries as the use of an additional separator is not feasible since it may add to the overall size of the microdevice.

4.2.2 Direct deposition approach. The second type of *in situ* process is a separator-free direct deposition approach, as illustrated in Fig. 8b. In this approach, the precursor is cast over the composite electrode film and allowed to undergo polymerization. Later, the obtained PE-integrated electrodes are used for LMPB and LIPB fabrication. In the case of LMPBs, usually the PE is *in situ* polymerized over the cathode and later assembled against the Li-metal anode (direct deposition approach 1). However, the PE can also be generated over both the anode and cathode in separate steps followed by these PE-integrated electrodes being integrated together to obtain an LIPB/LMPB cell (direct deposition approach 2). In the direct deposition approach 1, the disadvantage (side reactions) of a separator assisted approach can be avoided as the pristine monomer or oligomer species do not come in direct contact with the Li-metal. Additionally, in the direct deposition method, the inactive or deadweight of the reinforcing separator can be avoided entirely (Fig. 7c). It is indeed essential that the formed PE must be mechanically stable enough to withstand the pressure suffered by the electrodes, thereby preventing internal contact between the electrodes and the resulting short-circuit. Interestingly, if a PE with appropriate mechanical characteristics is selected,
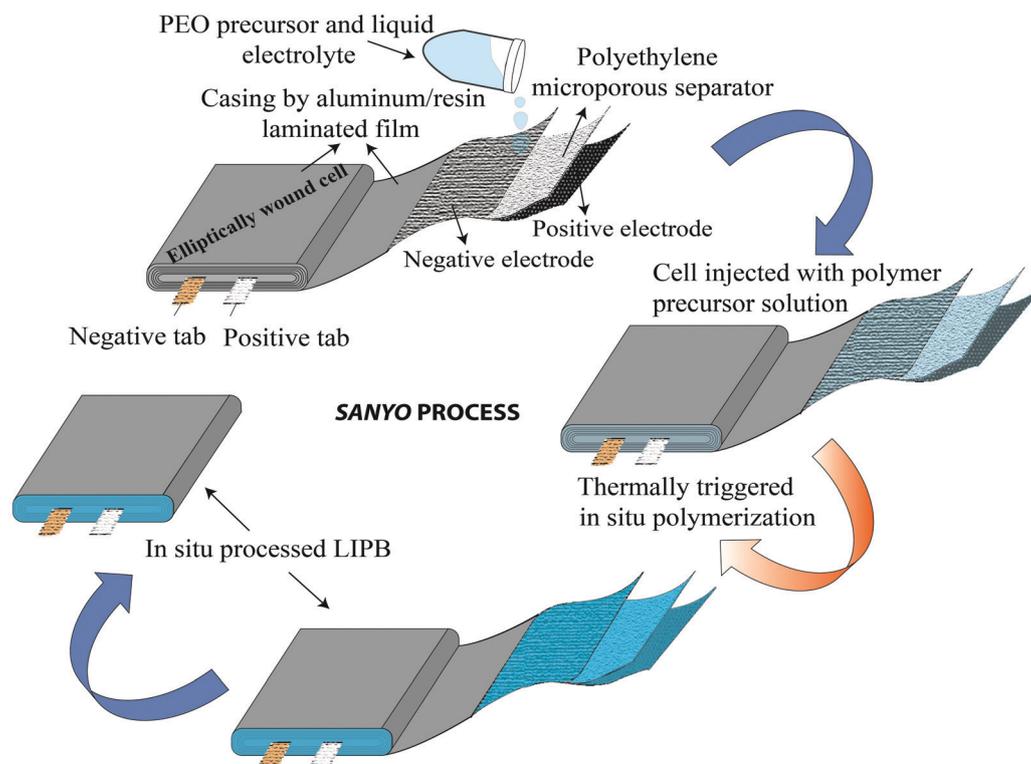
Fig. 9 Sanyo process (ref. 352 and 353) for the fabrication of an LIPB cell by the separator assisted approach. In this method, typically, a positive electrode using LCO, a negative electrode using graphite, and a polyethylene microporous separator are wound together in an elliptical fashion. This cell element is enclosed in a casing, and a precursor containing an LE [lithium bis(pentafluoroethanesulfonyl) amide [(LiN(SO$_2$C$_2$F$_5$)$_2$, LiBETI] dissolved in a carbonate-based solvent] and an ethylene oxide-based precursor are injected. Then, the cell is heated to induce the polymerization of the precursor.

This journal is © The Royal Society of Chemistry 2021

Energy Environ. Sci., 2021, **14**, 2708–2788 | **2725**

the pulverization of the active materials can be avoided entirely or considerably reduced.[354] It is also worth noting that, due to the separator-free configuration, the direct deposition approach is also suitable for microbattery fabrication.

4.2.3 Sacrificial and artificial protection approaches

For LE-based LBs (LIBs and LE-LMBs). For understanding the concept of the sacrificial and artificial surface protection approaches based on the *in situ* polymerization process, it is essential to define a new term called 'polymeric ionic-skin (PIS)'. An ionic-skin can be considered as a conformal and thin coating of an ion conducting layer (nanometre to few micrometer thick) formed over the anode/cathode active materials as well as other electrode components (conducting additives such as carbon). Such a layer is formed on the surface and the bulk of the electrode particles of an LIB/LE-LMB/LPB cell during electrochemical cycling. Also, these layers can be artificially prepared before cell fabrication. In a broader perspective, all SEIs and CEIs can be considered in the category of inorganic, organic, or composite ionic-skins that are capable of protecting the electrode as well as electrolyte components from several undesirable electrochemical events. Provided that these SEIs/CEIs also include polymeric components that are formed from the chemical/electrochemical reactions of LE solvent molecules or additives, they can be called PIS-interphases. In the same perception, the classical SEI and CEI layers formed from the decomposition/polymerization of carbonate solvents/additives [PC, EC, fluoroethylene carbonate (FEC), vinylene carbonate (VC), and so on] at the electrodes of an LB cell include materials that are polymeric and can be called PIS-SEIs and PIS-CEIs, respectively.[88,355–357] Indeed, the term PIS is a metaphor for the SEI/CEI formed over the electrode, which is polymeric in character. Such polymer formation due to the uncontrolled decomposition of the electrolyte solvents can be called sacrificial polymerization due to the destruction of the structure of these solvent molecules, which even produces unwanted side products. These polymeric components may have variable molecular weight and not well-defined physicochemical characteristics. However, when appropriate molecules are added as additives and targeted polymeric materials are conformally formed at the surface of the electrode components, such a process can be called the artificial polymerization process, which is rather precise and target specific compared to sacrificial polymerization. In other words, surface protection by the PIS-interphase formed by the sacrificial polymerization of the LE solvent molecules is a universal phenomenon occurring inside all organic LE-based LBs and other alternative Li-free battery cells. Indeed, these polymerizations are truly electrochemical in origin. Therefore, the generation of a PIS-SEI or PIS-CEI during the formation cycles of LIB cells can be considered the simplest example of sacrificial surface protection induced by the *in situ* (electrochemical) polymerization process. In the cases mentioned above, the formation of a PIS-interphase occurs within the assembled cell, and features such as thickness and composition cannot be often controlled. The controlled deposition of PIS-interphases can be achieved from a precursor-based LE in a standard three-electrode or two-electrode electrochemical cell by polymerization initiated by electrochemical oxidation or reduction processes on the electrode of interest.

In addition to the electrochemically assisted *in situ* processing of artificial PIS-interphases, other polymerization methods (free-radical, ionic, and condensation polymerization) are also employed to generate artificial polymeric surface protection layers. Here, the first step involves the coating of a precursor containing suitable monomers/oligomers over the composite electrode film, like that of the direct deposition approach. Later, the polymerization reaction is initiated by light, heat, or other means depending on the type of monomer/oligomer used. The motive of the *in situ* polymerization process in this approach is not the formation of a thick PE layer that can separate the two electrodes but a conformal PIS-based ultra-thin protection layer. Even if a precursor in the absence of electrolyte salt is used, the formed non-conducting polymer layer on contact with the LE eventually converts to a PIS by an activation (swelling) step within the LE-based cell.

Mostly, the *in situ* processing of artificially formed PIS-SEIs/PIS-CEIs as surface protection layers is very useful in LE-based LIB/LMB cells to prevent the direct attack of LE components that may degrade the electrode during cycling (*e.g.*, transition metal dissolution, electrode particle cracking, *etc.*). Besides, these layers can reduce or even altogether avoid the continuous decomposition of an electrolyte by the electrode components. In other words, an artificial PIS-SEI/PIS-CEI is mutually beneficial for both the electrode and electrolyte. Once this conformal coating by the PIS is achieved over the electrode, the full cell can be fabricated by using a conventional LE. Hence manufactured LB cells cannot be included in the category of LPBs due to the use of traditional LEs except for the presence of a thin PIS-interphase coating. However, by this method, stable electrochemical cycling with Li-metal has been even realized in state-of-the-art LE-based LMBs (LE-LMBs), unlike the case with an unprotected Li-metal anode. As part of this review, the reports in the context of surface protection of LBs using an *in situ* processed PIS-interphase are also thoroughly discussed as this has never been reviewed elsewhere.

For LMPBs and LIPBs (multi-layer approach). The artificial/sacrificial protection approach can be extended to LIPB/LMPB fabrication by an emerging process called the multi-layer approach. In the multi-layer processing of LPBs, the first step involves the individual electrodes being protected by an *in situ* processed PIS-interphase. A relatively thick subsequent PE layer (over the PIS) can be prepared either by the direct deposition approach or as an *ex situ* processed PE layer/film (Fig. 7d).[361,362] Here, the electrode|electrolyte interphase is taken care by the PIS, whereas the thick PE layer effectively separates the two electrodes facilitating ion transport. The multi-layer approach is, in fact, a combined strategy, where the surface protection approach is in conjunction with the direct deposition or the *ex situ* process. Due to the presence of multiple electrolyte layers (first layer of a PIS-interphase and a subsequent layer of a PE), this approach is also called layer-by-layer fabrication of an LIPB/LMPB. Various types of polymer, monomer/oligomer, salt, plasticizer, or additive chemistry can be used for individual layers; hence, tailor-made LPBs can be prepared. Research in

2726 | *Energy Environ. Sci.*, 2021, **14**, 2708–2788

This journal is © The Royal Society of Chemistry 2021

this direction is indeed rare. However, multi-layer processed LPBs are strong candidates for the industrial-scale production of the next generation of LMPBs or LIPBs. The advantages and disadvantages of the three different types of *in situ* processing approaches are summarized in Fig. 7e.

The following sections will explain the individual cases of the *in situ* processing of LPBs and the role of each study in further improving the field.

5. *In situ* process by photo-/thermal-induced free-radical polymerization

In this section, relevant reports in which the *in situ* processing of LB cells is carried out by a free-radical polymerization reaction using photo- or thermal-curing are comprehensively analyzed and summarized according to the type of monomers as well as the type of *in situ* processing approach adopted. Separator assisted, direct deposition, sacrificial and artificial protection, and multi-layer processing approaches are discussed in detail.

Free-radical polymerization is usually carried out using energy sources such as heat, UV light, visible light, gamma rays, microwaves, infrared (IR) rays, and so on.[344,371] Using these techniques, various types of linear and branched homopolymers, copolymers, and cross-linked systems can be produced within a few seconds to a few hours. A typical free-radical thermal/ photopolymerization reaction needs monomers or oligomers

having an unsaturated functional group (vinyl or allyl) and an initiator. In general, free-radical photo-initiators are of two types, namely *Norrish Type I* and *Norrish Type II*.[372] The photo-initiator 2-hydroxy-2-methylpropiophenone (HMPP) is a type I system that, on UV exposure, decomposes into radicals by the homolytic cleavage of the excited (high energy state) α-carbon bond and produces two radical fragments (initiating free-radical, I•). These radicals react with other reactive mono-mers/oligomers to form an initiating radical chain. Indeed, the free-radical initiator attacks the loosely bound pi-electron cloud of the double bond of the monomer/oligomer so that the initiating radical chain is formed. Later, the initiating radical chain further continuously reacts with the other monomer/ oligomer molecules present in the reaction mixture. This step is called the propagating reaction. Finally, this propagating chain is terminated either by removing the energy source, by side reactions, or by the exhaustion of the reactive monomer/ oligomer species. A similar reaction pathway involving the direct cleavage of initiator species to free-radical fragments and subsequent propagation is followed in thermally initiated free-radical polymerization as well, where peroxide (*e.g.*, benzoyl peroxide, BPO) and azo compounds (*e.g.*, azobisisobutyronitrile, AIBN) are the most popularly employed free-radical initiators. The mechanism of a typical free-radical thermal-/photo-polymerization reaction involving the aforementioned steps is displayed in Fig. 10a.[358] It is not always necessary that the initiator molecule on excitation by an external stimulus such as
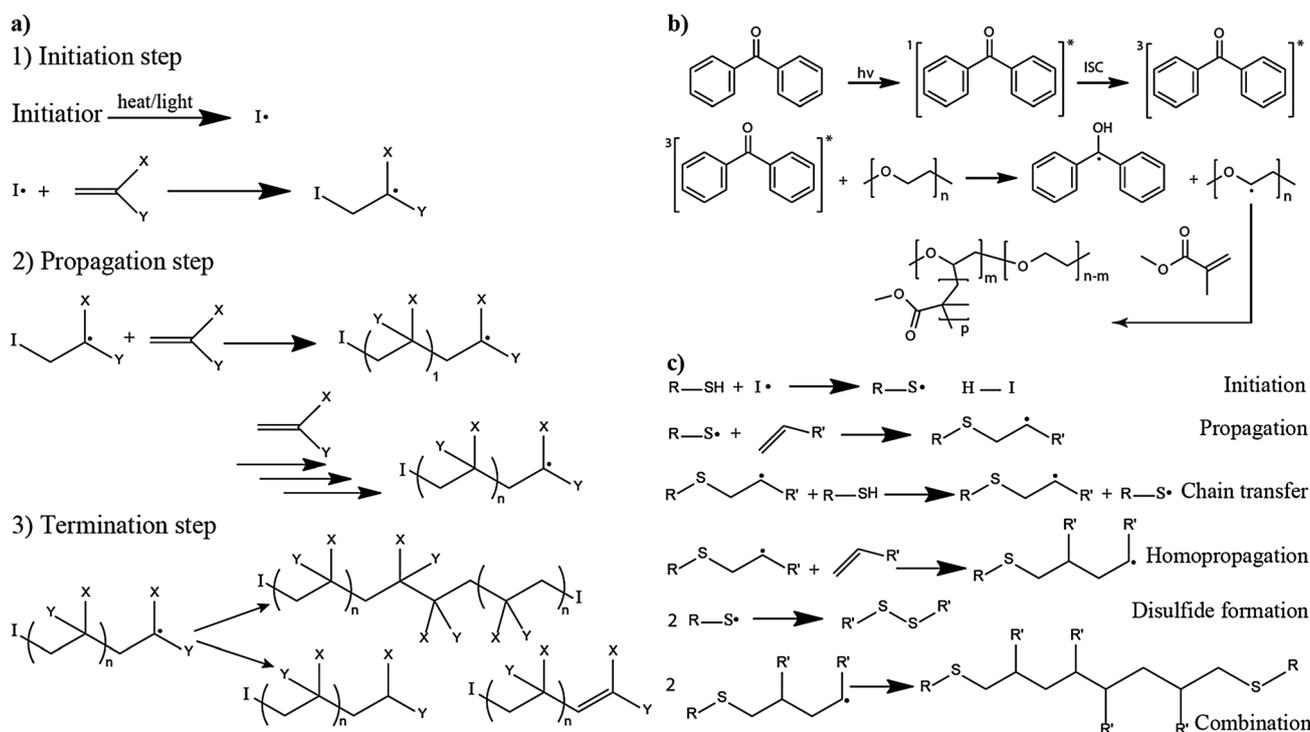
Fig. 10 (a) Mechanism of a typical free-radical polymerization reaction initiated by light/heat (reproduced/adapted from ref. 358 with permission from The Royal Society of Chemistry[358]); (b) an example of the polymerization reaction involving hydrogen abstraction from PEO by the initiator and subsequent copolymerization with the MMA monomer (reproduced/adapted from ref. 359 with permission from Springer Nature, Copyright 2009[359]); and (c) the possible reaction pathways for the generated free-radicals during the thiol–ene click reaction (reproduced/adapted from ref. 360 with permission from John Wiley and Sons, Copyright 2010[360]).

This journal is © The Royal Society of Chemistry 2021

Energy Environ. Sci., 2021, **14**, 2708–2788 | **2727**

light should undergo direct cleavage to fragment into free-radicals and then attack the pi-electron cloud of a double bond to propagate the polymerization reaction as shown in Fig. 10a. For example, specific free-radical initiators (*e.g.*, benzophenone) can be sensitized[372] by photo-irradiation and abstract an active hydrogen atom from the sp[3] hybridized carbon of a suitable molecule such as PEO (namely, a donor molecule) to generate a carbon free-radical that can take part in the polymer chain propagation/cross-linking reaction,[359,373,374] and these are called Norrish type II initiators. Such hydrogen abstraction induced generation of free-radicals is useful for introducing cross-links in otherwise linear PEO chains.[362,375] An example of hydrogen abstraction from PEO by the Norrish type II initiator benzo-phenone and the subsequent copolymerization with MMA is presented in Fig. 10b.[359] In many cases, such a technique is used to modify a polymer chain by a functionalization or grafting reaction, and such techniques can also be used on already prepared membranes (post-polymerization). Unlike photo-initiated hydrogen abstraction, thermally initiated counterparts are indeed rare.

Another example of free-radical polymerization is by the $S^{\bullet}$ free-radical (thiyl radical) from the thiol moiety (–SH), which can further attack the pi-electron cloud of the 'ene' moiety to propagate the polymerization reaction, which is also called the thiol–ene reaction.[376–379] Indeed, the thiol–ene reaction can proceed even in the absence of any external initiator by simple UV or thermal irradiation.[380,381] However, an initiator's addition is reported to improve the efficiency of initiation, where both type 1 and type 2 photo-initiators or even thermal initiators can be employed.[372,382,383] The thiol–ene reaction facilitates the facile formation of –C–S–C– (thioether) linkages in a polymer host (Fig. 10c).[360] Considering their high efficiency and relatively mild reaction conditions, photo-initiated thiol–ene reactions are more prevalent in the context of PEs. Interestingly, the thiol–ene reaction falls under the category of a click reaction as it satisfies conditions such as (i) high yield, (ii) stereospecificity, (iii) formation of safe byproducts if any, (iv) no stringent reaction conditions required, (v) readily available starting materials, and (vi) use of environmentally benign solvents or solvent-free reaction conditions.[376] Other than the 'ene' group, epoxy groups are also suitable for thiyl radicals to carry out the click-reaction. Such reactions are called thiol–epoxy reactions.[384] They are also useful in the preparation of PEs.

Although the typical free-radical polymerization method, as presented in Fig. 10a, is the most explored in the context of the *in situ* processing of LBs, the hydrogen abstraction and thiol–ene click reactions are also addressed in a few reports. Many mono- and bi-functional acrylate and methacrylate monomers/oligomers that are commonly used in the free-radical initiated *in situ* processing of PEs and LBs are presented in Fig. 11 and 12, respectively. Many of the important literature reports related to the *in situ* process involving free-radical polymerization are covered in Sections 5.1–5.3.

5.1 Separator assisted *in situ* process

One of the first reports on the *in situ* process for the fabrication of a GPE-based LIPB (LCO|GPE|carbon) was published by Sun
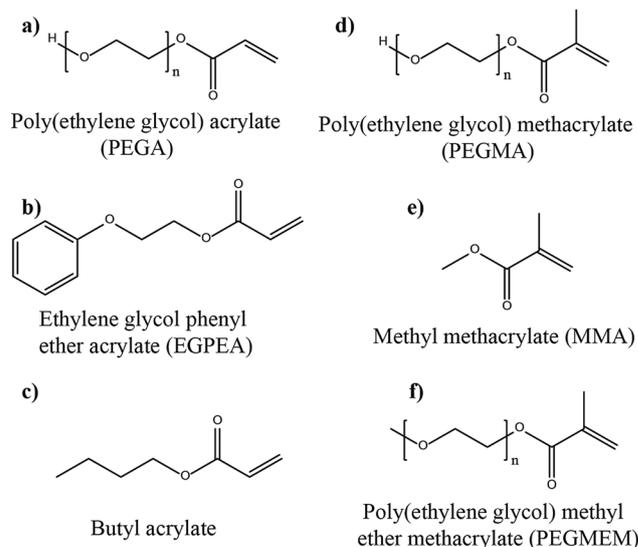
Fig. 11 The chemical structures of mono-functionalized acrylate and methacrylate monomers and oligomers used to prepare PEs and *in situ* processing of LBs by the free-radical polymerization process. (a) Ref. 363 (b) ref. 364 (c) ref. 365 (d) ref. 366 (e) ref. 331, 333, 347, 367 and 368 and (f) ref. 329, 369 and 370.

a) Poly(ethylene glycol) acrylate (PEGA)

b) Ethylene glycol phenyl ether acrylate (EGPEA)

c) Butyl acrylate

d) Poly(ethylene glycol) methacrylate (PEGMA)

e) Methyl methacrylate (MMA)

f) Poly(ethylene glycol) methyl ether methacrylate (PEGMEM)

et al. in 1997.[397] This work introduced the concept of "*mono-mers are reacted in place, either on a piece of thin supporting fabric or directly onto one electrode surface, just prior to cell assembly,*" by a thermally-induced free-radical polymerization reaction. In other words, this work put forward the concept of both the separator assisted and direct deposition approaches. Herein, the *in situ* processing of the LIPB is carried out in the presence of a synthetic fabric separator considering the ease of handling, although a detailed account of the exact procedure used is not discussed. Also, the possibility of using acrylate, allyl, and vinyl ether monomers/oligomers as potential candidates to carry out the *in situ* process is also proposed in the same work. The prepared GPE is claimed to possess a high ionic conductivity in the order of 1 mS cm^{-1} at room temperature (RT), and the LIPB cell retained 80% of its initial specific capacity even after 500 cycles. Later, in the early 2000s, Kim *et al.* fabricated an LIPB pouch cell based on a cross-linked GPE starting from a precursor made of the oligomer named triethylene glycol dimethacrylate (TEGDMA), a plasticizer (LiPF$_6$ in EC:DEC as the LE), and a thermal initiator (BPO), which is injected into the LCO|GPE|graphite cell assembly containing a Celgard separator followed by a heating step (80 °C for 40 min).[343] The GPE exhibited high ionic conductivity (6.34 mS cm^{-1} at 20 °C) with an oxidative stability of 4.5 V *vs.* Li|Li$^+$. The flow chart of the pouch cell fabrication by the *in situ* process is displayed in Fig. 13a. The cell at a current density of 0.5C showed a capacity of ≈675 mA h at 20 °C, with 100% retention over 20 charge–discharge cycles.

A few of the other monomers and oligomers appearing in subsequent reports on the *in situ* processing of LIPBs during the first decade of the 21st century include MMA, tetraethylene glycol diacrylate, 1,3-butanediol diacrylate (BDDA),
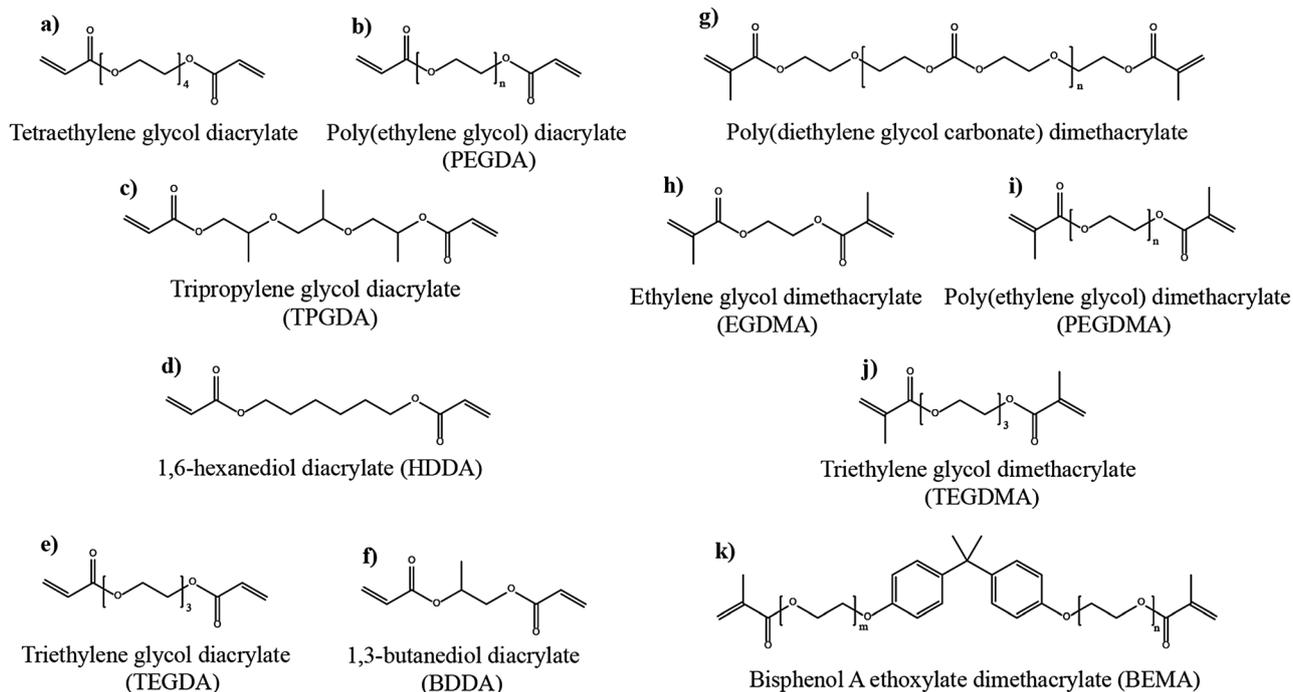
2728 | *Energy Environ. Sci.*, 2021, **14**, 2708–2788

This journal is © The Royal Society of Chemistry 2021

Fig. 12 The chemical structures of mono-functionalized acrylate and methacrylate monomers and oligomers used for the preparation of PEs and *in situ* processing of LBs by the free-radical polymerization process. (a) Ref. 308 and 385 (b) ref. 361 and 386–389 (c) ref. 390 (d) ref. 269 and 391 (e) ref. 365 (f) ref. 392 (g) ref. 393 (h) ref. 368 (i) ref. 370, 394 and 395 (j) ref. 343 and (k) ref. 329, 342, 354 and 396.

and poly(ethylene glycol) acrylate (PEGA).[363,367,385,392] These reports also employed heat-induced *in situ* processing using organic carbonate-based solvents as plasticizers and LiPF$_6$ salt as the Li$^+$-ion source.[392] However, it is important to note that Li-salts such as LiPF$_6$ (thermal stability of 107 °C in a dry and inert atmosphere) have very low thermal stability and therefore require special attention.[398–400] The presence of even a few ppm of water in the electrolyte can induce the conversion of PF$_5$ (PF$_5$ is formed by the decomposition of LiPF$_6$ salt) to toxic gaseous products such as HF and POF$_3$ even at RT, and the same reaction will be accelerated at elevated temperatures. These side-reaction byproducts can catalyze several other reactions such as the decomposition of other organic solvents or monomers/oligomers and even the leaching of transition metals from the electrode active materials. However, within the first few years of the 21st century, the separator assisted approach of the *in situ* process by thermal curing was commercialized for the production of LIPBs as already demonstrated in the case of the Sanyo process, but with a thermally stable sulfonylimide-based (LiBETI) salt (see Fig. 9).[352,353,401]

With the rejuvenated interest in LMPBs during the same period, in several reports, the electrochemical performance of LMPBs is often found to be inferior compared to the related LIPBs when acrylate/methacrylate functional monomers are used. For instance, the NMC111|GPE|Li cell constructed using a PEGA oligomer-based GPE displayed inferior rate-capability compared to the NMC111|GPE|graphite counterpart.[363] Similarly, when MMA is used as the monomer and the performance is compared in LIPBs and LMPBs, the inferior electrochemical performance associated with LMPBs is addressed.[331,367] In both

LPB cells based on MMA, LiNi$_{0.8}$Co$_{0.2}$O$_2$ (LNC) is used as the cathode. Here, in the case of the Li-metal anode, a large voltage-drop is observed in the first charging cycle compared to the cell with a graphite-based anode. This voltage-drop is attributed to the non-conducting polymer layer (*e.g.*, PMMA layer) formed at the Li-metal anode during the polymerization process. This PMMA layer is claimed to disintegrate during the charging process, which can affect the Li plating/stripping process leading to the uneven deposition of Li (HSAL growth) in the subsequent cycles. Also, in the same report,[367] the reduction of the ester groups from the unreacted acrylate monomers over the Li-metal surface leading to the formation of undesirable ketol products (Fig. 13b) is explained. This reduction reaction can take place even before the electrochemical cycling and can lead to capacity loss even in the first cycle itself. Interestingly, when the complete monomer to polymer conversion reaction is achieved using high energy γ-ray irradiation,[331,403–405] the formation of ketol products is found to be reduced. It should also be noted that, when MMA is polymerized by thermal irradiation, an oxidative stability window of 4.2 V *vs.* Li|Li$^+$ is observed, whereas it is increased to 4.5 *vs.* Li|Li$^+$ in the case of more effective γ-ray irradiation. This indicates that the presence of residual (unreacted) monomers not only affects the cathodic but also the anodic processes. Even though high energy γ-ray irradiation is costly, unsafe, and uncontrolled (highly random in nature during polymerization), the above-mentioned work provides significant insights on the importance of avoiding undesirable parasitic reactions imposed by pristine monomers/oligomers on the Li-metal surface, which

Fig. 13 (a) Flow-chart representing the various steps involved in the *in situ* processing of LIPBs in a pouch cell configuration by the separator assisted approach. The two electrodes and the separator are assembled in an aluminum laminated pouch. Later, the precursor solution is filled into the assembled cell and vacuum-sealed. Thermal curing at 80 °C for 40 min results in an LIPB (reproduced/adapted from ref. 343 with permission from Elsevier, Copyright 2002[343]). (b) A plausible mechanism for the reduction of ester groups from methacrylate monomers leading to the formation of a ketol layer over Li-metal (reproduced/adapted from ref. 331 with permission from Springer Nature, Copyright 2004[331]). (c) The plausible mechanism for the decomposition of molecules containing ester groups in the proximity of Li-metal (reproduced/adapted from ref. 402 with permission from American Chemical Society, Copyright 2019[402]).

are often detrimental to the battery performance. Additionally, they also highlighted the importance of selecting suitable monomers/oligomers and achieving complete polymerization during the *in situ* process. Indeed, it is worth mentioning that the polymerization time is an important factor, as it determines the duration for which the MMA monomer molecules remain close to the reactive Li-metal surface. In the case of thermal polymerization, the time required is very long compared to γ-ray irradiation. Even though the article does not specifically mention this factor, the polymerization time could be an important parameter in controlling the surface reactions.

In recent reports, Grünbaum *et al.* suggest that the presence of trace impurities such as water and alcohol is the primary reason for the decomposition of the ester group in proximity with Li-metal. Also, it is demonstrated that the formation of LiOH or lithium alcoholates (LiOR) can hydrolyze ester bonds in a continuous process (ester saponification or Claisen condensation), which, as a side product, can generate more alcohol molecules as shown in Fig. 13c.[402] Additionally, the native impurities such as

LiOH formed on the surface of Li-metal, which is solubilized by the moisture present in the monomer, can also induce several of these side reactions. Therefore, it is crucial to make sure that ester-based monomers and oligomers are dry and extra pure when used in LMPBs to achieve the best performance. Provided that additives that can guarantee the formation of a stable SEI over Li-metal anodes or Li-metal compatible acrylate/methacrylate molecules are used in the precursor, the separator assisted approach can be much effectively revisited for LMPB fabrication,[395] but preferably with a precursor free from impurities (ultra pure/battery grade). Despite the aforementioned drawbacks, PEs that are derived from acrylate and methacrylate monomer/oligomer molecules remain the most explored and popular for executing the *in situ* processing of LPBs due to their ease of polymerization and low cost.

The transition from non-cross-linked to cross-linked acrylate/ methacrylate hosts has been found to improve the interfacial properties of PEs against the Li-metal anode. Unlike the PEs based on linear polymer hosts such as PMMA, cross-linked PEs

2730 | *Energy Environ. Sci.*, 2021, **14**, 2708–2788

This journal is © The Royal Society of Chemistry 2021

minimize HSAL-growth. An illustration in the context of a cross-linked PE formed from the oligomer called poly(ethylene glycol) dimethacrylate (PEGDMA) is presented in Fig. 14a.[394] In a multi-functional cross-linker molecule bearing acrylate/methacrylate functional groups, the spacer molecule between the terminal functional groups can be of different chemical nature. For example, the spacer group can be ethylene oxide (–EO–), polycarbonate, polyurethane, polysiloxane, *etc.* The spacer molecule/chain part can largely influence the physicochemical, interfacial, and electrochemical characteristics of the final cross-linked polymer network. Additionally, these spacer chains can have many or a few repeating units (RU); hence, the properties of the cross-linked polymer network can be tailor-made according

to the application. For example, methacrylate oligomers having the spacer molecule poly(diethylene glycol carbonate) are used for the preparation of GPEs and SPEs for LMPB cells by employing the *in situ* process [Fig. 14b–d].[393] A precursor made of poly-(diethylene glycol carbonate) dimethacrylate (PDEC-DMA), which is a bi-functional cross-linker, other hydroxyl and ethyl terminated mono-functional methacrylic derivatives, a plasticizer (EC/DMC), a thermal initiator (AIBN), and LiTFSI salt are used for producing cross-linked GPEs. At the same time, a precursor for the SPE is prepared in the absence of a plasticizer. A cellulose separator pre-soaked in the precursor is used for the *in situ* processing of the LMPB cell. The GPE exhibited an ionic conductivity of 0.17 mS cm^{-1} (25 °C) and a T_{Li^+} value of 0.47, which is higher
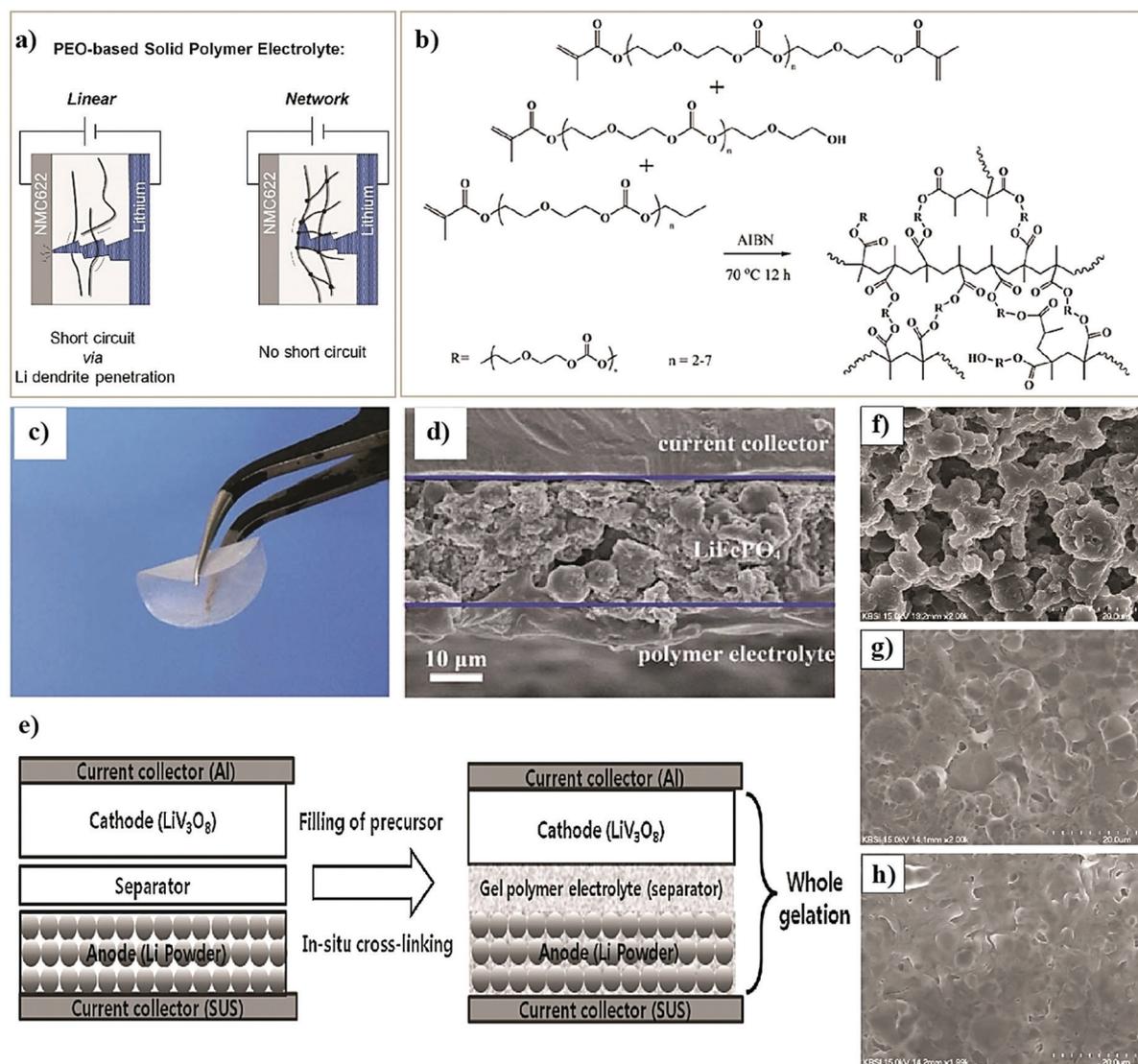
Fig. 14 (a) Schematic representation of the mechanism by which HSAL-growth induced cell failure is prevented in a cross-linked PEO (depicted as a network)-based SPE compared to that of a linear PEO-based SPE (reproduced/adapted from ref. 394 with permission from Elsevier, Copyright 2020[394]). (b) Synthesis scheme for the preparation of the SPE based on methacrylate monomers derived from poly(diethylene glycol carbonate) molecules. (c) Photograph of the cellulose reinforced PE. (d) Cross-sectional view of the electrode|electrolyte interface in the LFP cathode retrieved from the LMPB cell (reproduced/adapted from ref. 393 with permission from The Royal Society of Chemistry[393]). (e) The *in situ* processing of an LMPB with a Li-powder anode and LVO cathode by the separator assisted approach. (f and g) The SEM images of the pristine (f) and cycled Li-metal anodes with a low (g) and high (h) degree of cross-links in the GPE (reproduced/adapted from ref. 395 with permission from Elsevier, Copyright 2014[395]).

than several LEs (T_{Li^+} value of 0.2–0.3).[167] The improvement in the T_{Li^+} value is also attributed to the presence of spacers based on carbonate moieties.[406] GPE- and SPE-based LMPB (LFP∥Li) cells delivered cycling stability over several hundred cycles at both 25 and 100 °C. Indeed, the good cycling stability can be attributed to the cross-linking and the cellulose reinforcing nature of these PE systems.

A GPE-based LMPB cell is fabricated using a heat-assisted *in situ* process in which a LiV$_3$O$_8$ (LVO) cathode is assembled with (Fig. 14e) a Li-powder-based anode.[395] The cross-linked GPE is produced from a precursor containing a dimethacrylate-based oligomeric cross-linker, which bears spacer chains based on –EO– molecules (poly(ethylene glycol) dimethacrylate, PEGDMA), a plasticizer (1 M LiPF$_6$ EC:DEC as an LE), and a thermal initiator (*t*-amyl peroxypivalate, TAPP). In this work, the potential of additive chemistry is explored for enhancing the overall electrochemical performance, for which a small amount of (1 wt%) vinylene carbonate (VC) is added into the precursor. In LEs, the primary role of VC is to act as an artificial SEI layer forming agent over the anode surface; in this case, it is Li-metal.[407–409] Here, as the polymerization rate of methacrylate is very high and the concentration of VC in the precursor is very low, it is not expected that the VC molecule will become a part of the main chain of the polymer network. Although not explicitly mentioned, the presence of VC in this work is expected to mitigate/minimize any undesirable passivation (by dimethacrylate) over the Li-metal anode. A typical artificial PIS-SEI formed due to the presence of VC may also include species such as poly(vinylene carbonate) (poly-VC), Li$_2$CO$_3$, and lithium alkyl carbonates. Again, this work further emphasizes the significant relationship between the impact of cross-links and reduction in dendritic HSAL growth (as explained in Fig. 14a). Unfortunately, the powdered Li-metal anode is very reactive due to its high surface area available for reactions with the electrolyte components. The HSAL growth in the powdered Li-anode is a big challenge, and it is found to be suppressed when the cross-linking density in the GPE is further increased with a higher PEGDMA concentration in the precursor [Fig. 14f–h].[57,395,410] Indeed, at higher current rates (2C), the GPE-based cell retained 85% of the discharge capacity (187 mA h g^{-1}) compared to the value at 0.2C (220 mA h g^{-1}). This work indicates that fine-tuning of the cross-linking density or, in other words, the toughness of the PE is crucial for achieving improved interfacial properties, hence preventing HSAL growth and ensuring good cycling performance in LMPBs.

The *in situ* processing of an LNMO|GPE|Li cell using a precursor consisting of a combination of a low molecular weight diacrylate cross-linker (triethylene glycol diacrylate, TEGDA), a co-monomer (butyl acrylate, BA), a plasticizer LE (1 M LiPF$_6$ in a mixture of carbonate solvents), and a thermal initiator (2,2′-azobis-(2,4-dimethylvaleronitrile), ABVN) was reported by Fan *et al.*[365] Here, the amount of BA (monoacrylate) used is almost double that of TEGDA in the precursor, which reduces the overall cross-linking density, rendering the finally produced cross-linked PE with enough flexibility and ease of processibility. The GPE was claimed to possess ionic conductivity

(5.5 mS cm^{-1}, 25 °C) close to that of an LE, and oxidative stability up to 5 V *vs.* Li|Li$^+$. Finally, the fabricated LNMO|GPE|Li cell delivered a discharge capacity of 226 mA h g^{-1} between 2 V and 4.8 V (0.1C, 25 °C). Recently, a hierarchical gel-PCE, as shown in Fig. 15a, was produced by using only a bi-functional cross-linker (tri propylene glycol diacrylate, TPGDA). The resulting gel-PCE in which SiO$_2$ hollow nanospheres are used as nanofillers is analyzed in LMPBs.[390] Due to the high porosity of the nano SiO$_2$ spheres, during the activation process, these PCEs act as an electrolyte reservoir, hence absorbing a considerable amount of LE (1 M LiPF$_6$ in organic liquid carbonates).[420] The LMPB fabrication is carried out by the *in situ* process; the researchers incorporated the LE (1 M LiPF$_6$ in organic carbonates) and AIBN into the precursor followed by thermal curing at 60 °C for 12 h. The resulting SiO$_2$-integrated gel-PCE (called SiSE) exhibited high mechanical stability owing to the cross-linked polymer host derived from TPGDA, and a good ionic conductivity value of 1.7 mS cm^{-1} at RT. Interestingly, the SiSE displayed dramatically low flammability due to the presence of SiO$_2$, along with improved interfacial resistance and HSAL growth suppression at the Li-metal anode (Fig. 15b). High oxidative stability (4.9 V *vs.* Li|Li$^+$) and good cycling stability in LFP|SiSE|Li cells (discharge capacity = 160 mA h g^{-1} at 0.2C, 200 cycles, Fig. 15c) are also achieved.

Several studies use multi-functional acrylate/methacrylate monomer/oligomer molecules with '*n*' (number of functionalities) value > 2 (called poly-functional to distinguish from bi-functional molecules) that can result in cross-linked PEs [Fig. 16a–d]. Zhou *et al.* used a tri-acrylate cross-linker (trimethylolpropane trimethyl-acrylate, TMPTMA) and a thermal initiator (lauryl peroxide, LPO) in the presence of an LE (1 M LiPF$_6$ in a mixture of carbonate solvents).[412] The resulting cross-linked GPE film exhibited a high ionic conductivity (1 mS cm^{-1}) and oxidative stability value (5.0 V *vs.* Li|Li$^+$). The LIPB (fabricated by the separator assisted process) cell (LCO|GPE|graphite) exhibited an initial discharge capacity of 129 mA h g^{-1} at 0.2C over 100 cycles with a specific capacity retention of 83%, which underlines the potential of poly-functional monomers for the *in situ* processing of LPBs. Jeong *et al.* used a slightly different cross-linker (trimethylolpropane triacrylate, TMPTA), a non-volatile plasticizer (PEGDME, M_n = 250 Da), a thermal initiator (AIBN), and an LE (LiTFSI in PC).[411] The precursor is used for LFP|GPE|Li cell fabrication using the separator assisted *in situ* approach. Even though the increase in cross-linking density due to the increased amount of TMPTA (15 wt%) reduced the ionic conductivity and high rate capability, the onset potential of oxidative decomposition of the GPE is increased up to 5.3 V *vs.* Li|Li$^+$. In line with the studies using multi-functional cross-linker monomers/oligomers, Li *et al.* reported a GPE based on a tetra-acrylate cross-linker (pentaerythritol tetraacrylate, PETEA) and the final LIPB is fabricated by combining a high voltage LiNiCoAlO$_2$ (NCA) cathode, and the separator assisted *in situ* process.[417] The free-radical polymerization mechanism of PETEA is presented in Fig. 17a.[418] The work also demonstrates the capability of the separator-supported GPE in providing enhanced safety to the LIPB cell over LEs by the nail penetration test [Fig. 17b–d]. During the safety test, the surface temperature of the LE-based
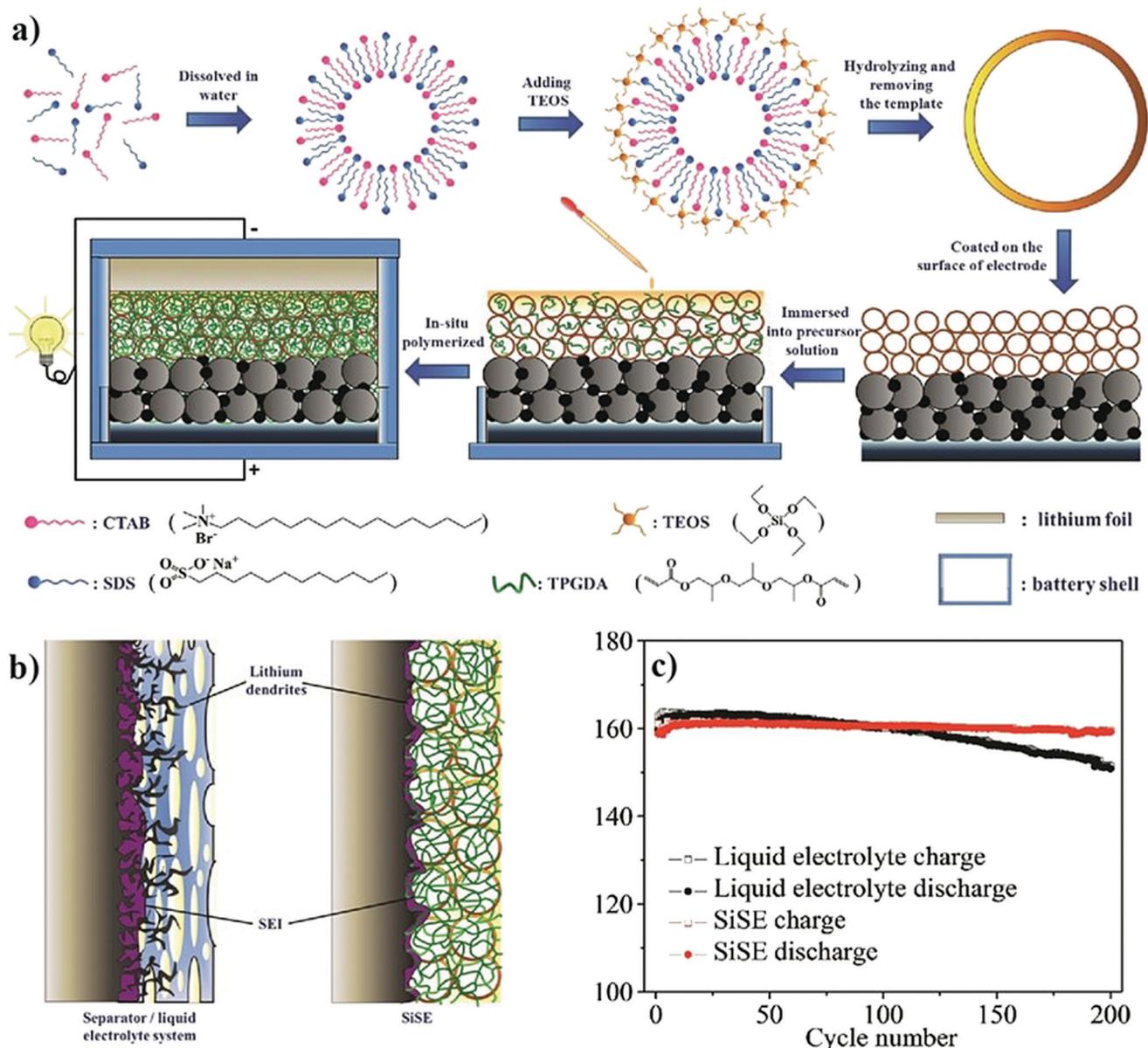
2732 | *Energy Environ. Sci.*, 2021, **14**, 2708–2788

This journal is © The Royal Society of Chemistry 2021

Fig. 15 (a) Schematic illustration of the steps involved in the SiO$_2$ templated *in situ* processing of LFP|SiSE|Li cells; (b) stable SEI over Li-metal in the presence of SiSE preventing HSAL growth compared to that of the poor SEI formed in the case of LEs; and (c) comparison of the cycling stability of SiSE- and LE-based LFP‖Li cells (reproduced/adapted from ref. 390 with permission from John Wiley and Sons, Copyright 2016[390]).

LIB cell increases beyond 200 °C, whereas only to 105 °C in the LIPB, in turn resisting the hazardous combustion reaction [Fig. 17c and d]. Indeed, in the same work, it has been convincingly demonstrated by the same authors that the elastic nature of the cross-linked GPEs can suppress the volume changes occurring in Si-electrodes during repeated electrochemical cycling (in a NCA|GPE|Si cell). A general scheme representing the elastic nature of the PEs controlling the volume expansion of the Si anode is illustrated in Fig. 18a and b.[421] In another study of a similar kind by Bok *et al.*, the cross-linked homo-polymer-based GPE derived from the cross-linker ethoxylated trimethylolpropane triacrylate (ETPTA) is found to be effective in controlling the volume change of Si anodes in LIPBs.[413] Here, it is claimed that the precursor

blends with the silicon anode *via* synergistic coupling (Fig. 18c). The discharge capacity, rate capability, and cycling stability of the Si|GPE|Li half-cell with GPEs are found to be far superior to the LE-based cells. Scanning electron microscope (SEM) images evidencing the suppressed volume changes in different types of silicon anodes in the *in situ* processed LIPB cells are also presented in Fig. 18d–l.

Poly-functional acrylate-based PEs also find application in the *in situ* processing of advanced LMBs, in particular lithium–sulfur (S|PE|Li) batteries.[418,422] In S|PE|Li battery cells, it has been proposed that cross-linked PEs can trap the polysulfides (Fig. 19a) and help in suppressing their migration to the metallic Li-anode, which in turn improves the cycling stability
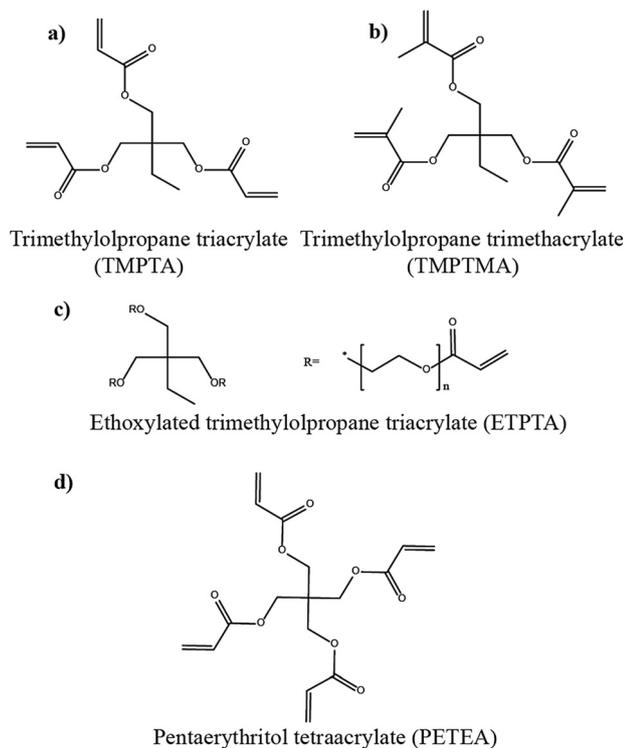
a) Trimethylolpropane triacrylate (TMPTA)

b) Trimethylolpropane trimethacrylate (TMPTMA)

c) Ethoxylated trimethylolpropane triacrylate (ETPTA)

R=

d) Pentaerythritol tetraacrylate (PETEA)

Fig. 16 The chemical structures of poly-functional acrylate and methacrylate monomers used for the generation of PEs and fabrication of LBs by the *in situ* process. (a) Ref. 411 (b) ref. 412 (c) ref. 269 and 413–416 and (d) ref. 417–419.

and Coulombic efficiency.[423–425] For this purpose, a PETEA-based precursor was thermally cured to obtain cross-linked GPEs by Kang *et al.*[418,419] During the LMPB cell preparation process, the precursor is injected into a PMMA-based electro-spun fiber network, which isolates the Li-metal anode and S-cathode. The resulting GPE exhibits a high ionic conductivity of 1 mS cm^{-1}. The S|GPE|Li cell is operated between 1.7 and 2.8 V showing a discharge capacity of 486 mA h g^{-1} at 5C. Indeed, the excellent cycling stability (83% capacity retention after 500 cycles at 0.3C) of the S|GPE|Li cell is attributed to the largely reduced polysulfide diffusion/shuttling imparted by the cross-linked polymer host (similar to the representation in Fig. 19a). The same group further demonstrated the use of cross-linked GPEs for the fabrication of polysulfide|GPE|Li and S|GPE|SnO$_2$ battery cells, and improved performance due to the cross-linked nature of the PE system is confirmed.[422,426]

Polymerizable ionic liquids[427] (1-methyl-3-(2-acryloyloxyhexyl) imidazolium tetrafluoroborate, MIT, Fig. 19b) with acrylate groups have been used as long-chain monomers for the preparation of GPEs, and their evaluation in *in situ* processed high voltage LMPB cells (LCO|GPE|Li) is carried out.[428] The polymeric ionic liquid host in the GPE is realized by the separator assisted thermal polymerization of the MIT monomer. In a typical procedure, the MIT monomer is dissolved in an LE (1 M LiBF$_4$ in EC:DEC) in the presence of a thermal initiator (TAPP) and thermally cured (90 °C for 20 min) with the support of a separator. A small amount of fluoroethylene carbonate (FEC) is also added to the precursor as a

PIS-interphase forming additive. The ionic conductivity of the GPE decreases with an increase in the percentage of the MIT monomer; however, an ionic conductivity of 1 mS cm^{-1} is easily achieved at RT. The *in situ* processed LMPB cell by the separator assisted approach displayed a discharge capacity of ≈ 134 mA h g^{-1} (25 °C) with good specific capacity retention (90%, 50 cycles, 0.2C). In a similar approach, however, using a novel PE matrix architecture such as an interpenetrated network (IPN), Huang *et al.* demonstrated a polymeric ionic liquid-based GPE for the separator assisted processing of LMPBs. Indeed, a porous PVdF–HFP electro-spun membrane is used as a separator for the *in situ* fabrication of an LMPB (LFP|IPN–GPE|Li) cell by the thermal curing process (70 °C, 12 h).[429] An IPN polymer is a mixture of two or more polymer networks that are not covalently linked to each other but entangled (interlaced) in such a way that the individual polymer networks cannot be pulled apart unless chemical bonds are broken.[389] In this work, along with a mono-functional ionic liquid-based long-chain acrylate monomer (1-butyl-3-(2-methacryloyloxyhexyl)imidazolium bis(trifluoro-methane sulphonyl) imide, MHBIm-TFSI), a diacrylate oligomer (poly(ethylene glycol) diacrylate, PEGDA) is also used as a cross-linker to enhance the cross-linking density, which improves the overall mechanical stability of the resulting IPN–GPE. The resulting highly cross-linked IPN–GPE delivered a high ionic conductivity (1.3 mS cm^{-1}) and a wide oxidative stability value (5 V *vs.* Li|Li$^+$). The *in situ* processed (separator assisted) LMPB coin-cell is galvanostatically cycled at 40 °C, which displays a high specific capacity value (152 mA h g^{-1}, 0.1C) along with good retention (94%, 100 cycles). Interestingly, a flexible LMPB pouch cell fabricated using the same approach also delivered a similar overall cycling performance.

Hetero functionalities often facilitate the fine-tuning of the chemical resistance,[430] interfacial and transport properties (*e.g.*, ionic conductivity, T_{Li^+}), and thermal properties (*e.g.*, non-flammability and high-temperature stability) of PEs.[431–436] For this purpose, *in situ* processable organic–inorganic hybrid monomers/oligomers are explored. In line with this, functional moieties such as siloxane, boranes, and phosphate groups are introduced into the monomer/oligomer structure.[299,366,437] For example, Kim *et al.* used a star-shaped siloxane acrylate cross-linker for the preparation of LIPBs (LCO|GPE|graphite) by the separator assisted *in situ* process (Fig. 20a).[437] The precursor made of siloxane acrylate, an LE (1 M LiClO$_4$ in EC:DMC), and a thermal initiator (*t*-butyl peroxypivalate, TBPP) is supported on a microporous polyethylene substrate between the electrodes and subjected to thermal curing (80 °C, 20 min). The GPE with a cross-linker content of 5.0 wt% displayed a high ionic conductivity (1.3 mS cm^{-1}) at ambient temperature along with wide oxidative stability (4.5 V *vs.* Li|Li$^+$). The *in situ* processed LIPB cell delivered a discharge capacity of 137 mA h g^{-1} (0.5C) with 84% capacity retention over 100 cycles. Later, the same group used a tri-acrylate cross-linker (tris(2-(acryloyloxy) ethyl) phosphate, TAEP, Fig. 20b) to prepare a PE.[438] The device fabrication followed a similar procedure except for using a phosphate-based cross-linker in place of siloxane acrylate, which demonstrated a comparatively average performing cell. Moreover, when they
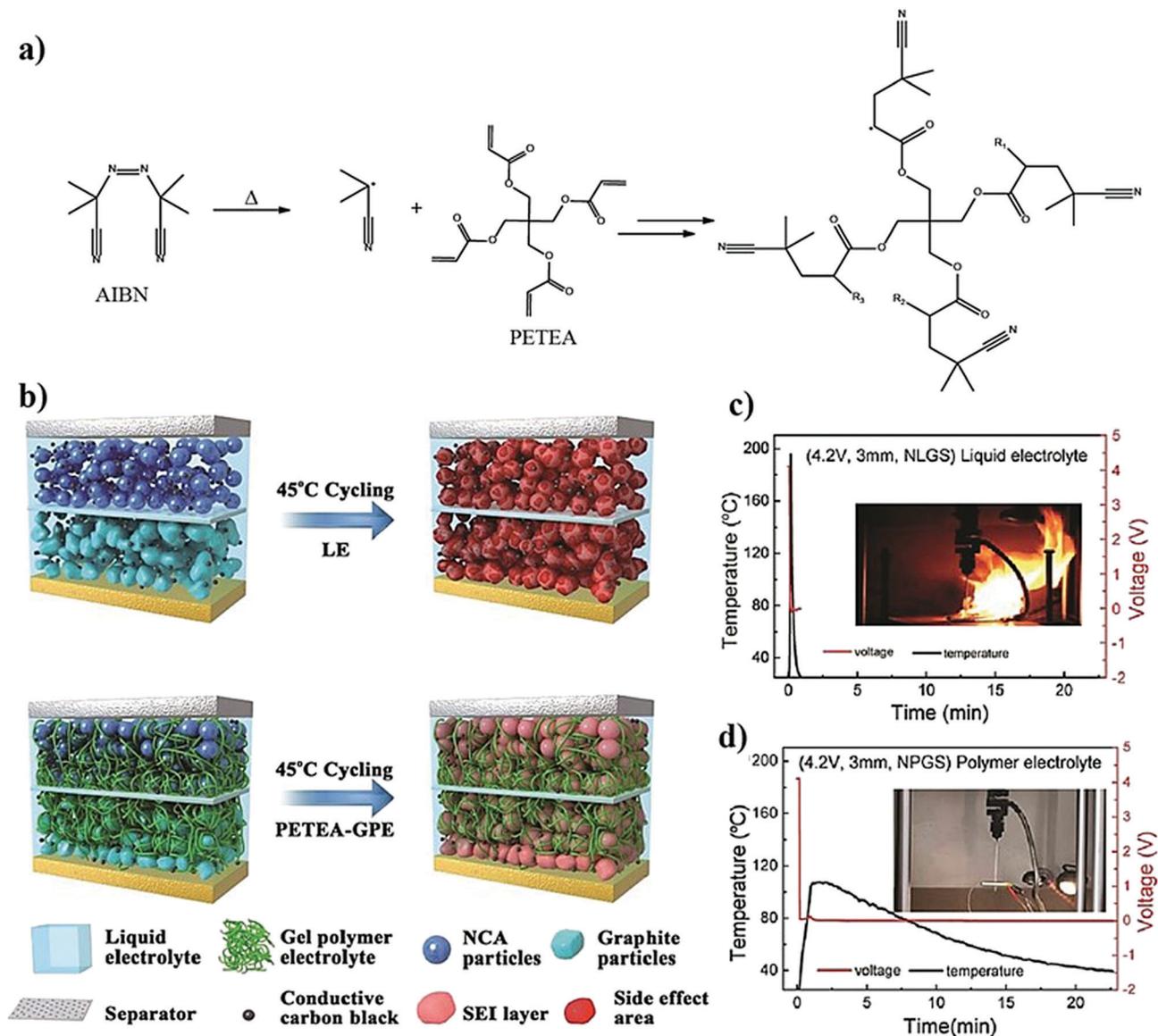
2734 | *Energy Environ. Sci.*, 2021, **14**, 2708–2788

This journal is © The Royal Society of Chemistry 2021

Fig. 17 (a) The mechanism for the free-radical polymerization of PETEA to poly-PETEA (R_1, R_2, and R_3 represent molecular chains (reproduced/adapted from ref. 418 with permission from Elsevier, Copyright 2016[418]). (b) The illustration of changes occurring inside the LE- and GPE-based cells (denoted as NLGS and NPGS, respectively) during cycling. In the case of LE-based cells, the interphases at the electrodes are not uniform and not effective. This leads to side reactions between the electrode and LE components, leading to early failure of the cell. However, in the case of the *in situ* processed GPE-based cell, the efficient interphases inhibit the side reactions and improve the cycling stability. (c) The nail penetration test results of the LE-based cell leading to inflation and violent combustion (the surface temperature increased to 200 °C). (d) The GPE-based cell exhibited no obvious changes, and the highest surface temperature reached after the nail penetration test is only 105 °C (reproduced/adapted from ref. 417 with permission from The Royal Society of Chemistry[417]).

moved to a GPE based on a fluorinated phosphorous-based cross-linking agent named 2-(2-(1,1-difluoro-2-hydroxy ethoxy)-1,1,2,2-tetrafluoroethoxy)-2,2 difluoroethylacrylate (FTGA) (Fig. 20c), superior ionic conductivity (0.49 mS cm^{-1} for the TAEP-based GPE and 0.56 mS cm^{-1} for the FTGA-based GPE) is exhibited by the FTGA-based GPE.[439] Indeed, both GPE systems exhibited a lower oxidative stability value of 4.2 V *vs.* Li|Li$^+$. Thus, it can be learned that the selection of the hetero-functionality is critical for achieving improved electrochemical performances, and even though fluoro- and phosphate-based polymers deliver improved safety, their electrochemical performance needs to be further enhanced.

In contrast to the earlier-mentioned reports in which a single hetero-atom functionalized cross-linker is used alone, boron-based cross-linked copolymer hosts derived from a combination of linear and branched acrylate cross-linkers have been proposed for LMPBs.[366] Here, boron-containing acrylate cross-linkers are prepared by a reaction involving trimethyl borate (TMB). For instance, the bi-functional linear borate cross-linker (LBC) is synthesized from glycerol monomethacrylate (GMMA) and TMB in the presence of poly(ethylene glycol) (PEG) (Fig. 21a). On the other hand, the tri-functional branched borate cross-linker (TBC) is prepared by the reaction between poly(ethylene glycol)
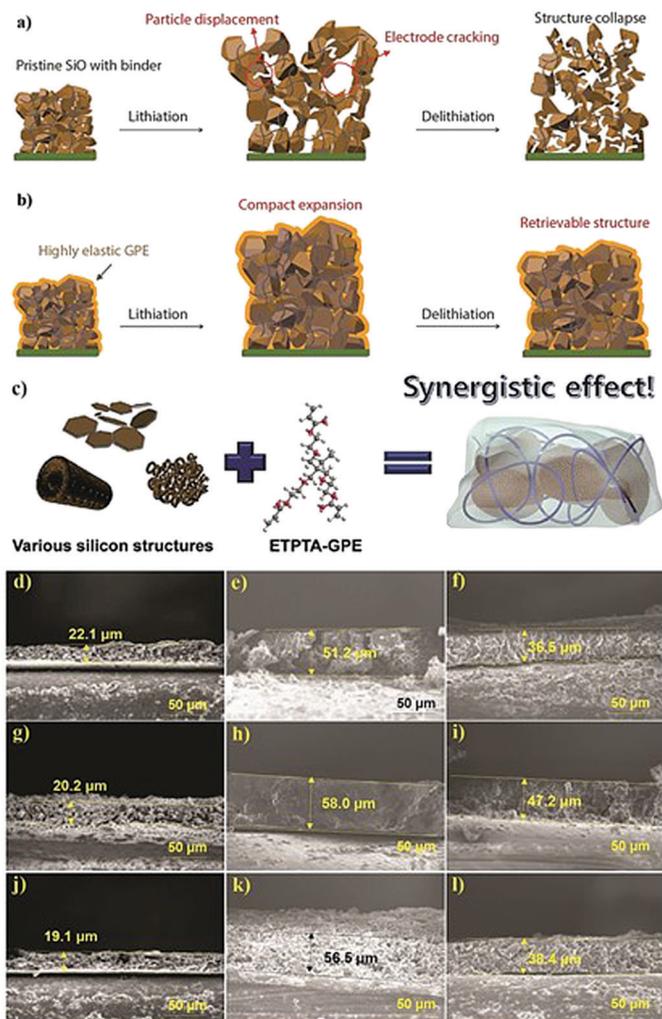
This journal is © The Royal Society of Chemistry 2021

Energy Environ. Sci., 2021, **14**, 2708–2788 | **2735**

Fig. 18 (a) Volume change, particle displacement, and cracking leading to the structural collapse of the silicon-anode during the repeated lithiation and de-lithiation process in the absence of an elastic GPE; and (b) the suppression of the afore-referenced structural collapse in the case of a silicon-anode integrated with an elastic GPE (reproduced/adapted from ref. 421 with permission from Springer Nature, Copyright 2019.[421] Distributed under a Creative Commons Attribution License International 4.0 (CC BY 4.0) (https://creativecommons.org/licenses/by/4.0/)). (c) Schematic illustration of various silicon structures used as anode materials and their synergistic coupling with an ETPTA-based GPE during the in situ process; and (d–l) cross-sectional SEM images depicting the extent of volume expansion of various Si-anodes. In the 1st column (d–j), pristine anodes are shown. The 2nd and 3rd column depict the volume expansion of Si-anodes retrieved from the LE (e–k) and GPE (f–l) based cells (after 100 cycles). (d–f) mesoporous Si; (g–i) micro-sized macroporous Si; and (j–l) Si sheet (reproduced/adapted from ref. 413 with permission from The Royal Society of Chemistry[413]).

methacrylate (PEGMA) and TMB (Fig. 21b). Considering the combination of di- and tri-functional methacrylate cross-linkers, the PE can be considered to possess a well-balanced 3D-structure with a cross-linked and mechanically stable polymer host. The authors have convincingly demonstrated that the thermally cross-linked and flexible GPE (3D-BGPE) with a high T_{Li^+} value of 0.76 inhibits HSAL growth compared to that of conventional LEs, as illustrated in Fig. 21c. In particular, the

high T_{Li^+} value is achieved due to the Lewis-acid character of the boron center, which interacts with the anions facilitating the free-movement of Li$^+$-ions within the polymer matrix. Besides, the boron-containing 3D-GPE with a high T_{Li^+} value can maintain uniform Li$^+$-ion flex at the Li-metal|electrolyte interface, favoring the smooth deposition of Li, which is not possible to achieve with a conventional LE.[440] It is worth mentioning that the 3D-BGPE exhibits a good ionic conductivity (0.084 mS cm^{-1}, 30 °C) and an overall oxidative stability (4.5 V vs. Li|Li$^+$). The LFP|3D-GPE|Li cell fabricated using the in situ process in the presence of a cellulose-based separator retains ≈90% of the initial capacity (118 mA h g^{-1}, 0.5C) over 400 cycles at 30 °C (Fig. 21d). Indeed, this work is an excellent example of using an inorganic polymer matrix having a boron atom, which plays the part of a copolymer chain and a Lewis acid center to deliver high T_{Li^+} values. However, such studies focusing on hetero-atoms are scarce in the literature and must be explored further.

In line with acrylate/methacrylate monomers and oligomers being explored for more than two decades, non-acrylate/metha-crylate molecules are recently receiving attention in the context of the in situ process. For example, the monomer vinylene carbonate (VC) is often used as a popular additive in LEs for improving the properties of the PIS-SEI formed on both graphite and Li-metal anodes.[441,442] Since VC contains an unsaturated double bond, it is possible to polymerize VC to poly-VC homo-polymer-based PEs by the free-radical polymerization process. One such approach was attempted by Chai et al. (Fig. 22a)[443] in which an SPE-based LMPB (LCO|SPE|Li) cell is in situ processed using a thermal polymerization process. A precursor containing 1.0 M lithium difluoro(oxalato) borate (LiDFOB) in VC and an AIBN initiator is injected into a 2032-coin cell with a cellulose separator and subjected to thermal curing (Fig. 22b). However, the complete conversion of the monomer to the polymer required about 24 h. The time taken for the polymerization is very high compared to acrylates and methacrylates, which undergo polymerization faster during the thermal and UV curing process. Indeed, the UV curing process may take a few seconds to minutes for acrylates and methacrylates, whereas thermal curing takes a few minutes to hours. The poly-VC-based SPE exhibits an ionic conductivity of 0.01 mS cm^{-1} at 25 °C. The SPE also showed a T_{Li^+} value of 0.57 and an oxidative stability value of 4.5 V vs. Li|Li$^+$. At 50 °C, the separator (cellulose paper) assisted in situ processed LCO|SPE|Li cell displayed a discharge capacity of 146 mA h g^{-1} (0.1C), and after 150 cycles, 84% of the total initial capacity is retained. The photograph of the post-cycled PE-integrated cathode is displayed in Fig. 22c along with the cross-sectional SEM image of the cathode|electrolyte interface (Fig. 22d) of the PE-covered surface of the LCO electrode and a pristine LCO surface (Fig. 22e). The results obtained by Chai et al. are promising for VC to be further explored for PE applications as a PEO-free alternative for LMPBs.

Another study by the same group extended the poly-VC-based PE for the in situ processing of LIPBs as well, in which, along with the precursor solution containing VC and AIBN, an LE (1 M LiDFOB in EC:DEC) is also introduced to obtain a GPE.[444] Compared to the SPE, the GPE exhibited a high ionic

2736 | Energy Environ. Sci., 2021, **14**, 2708–2788

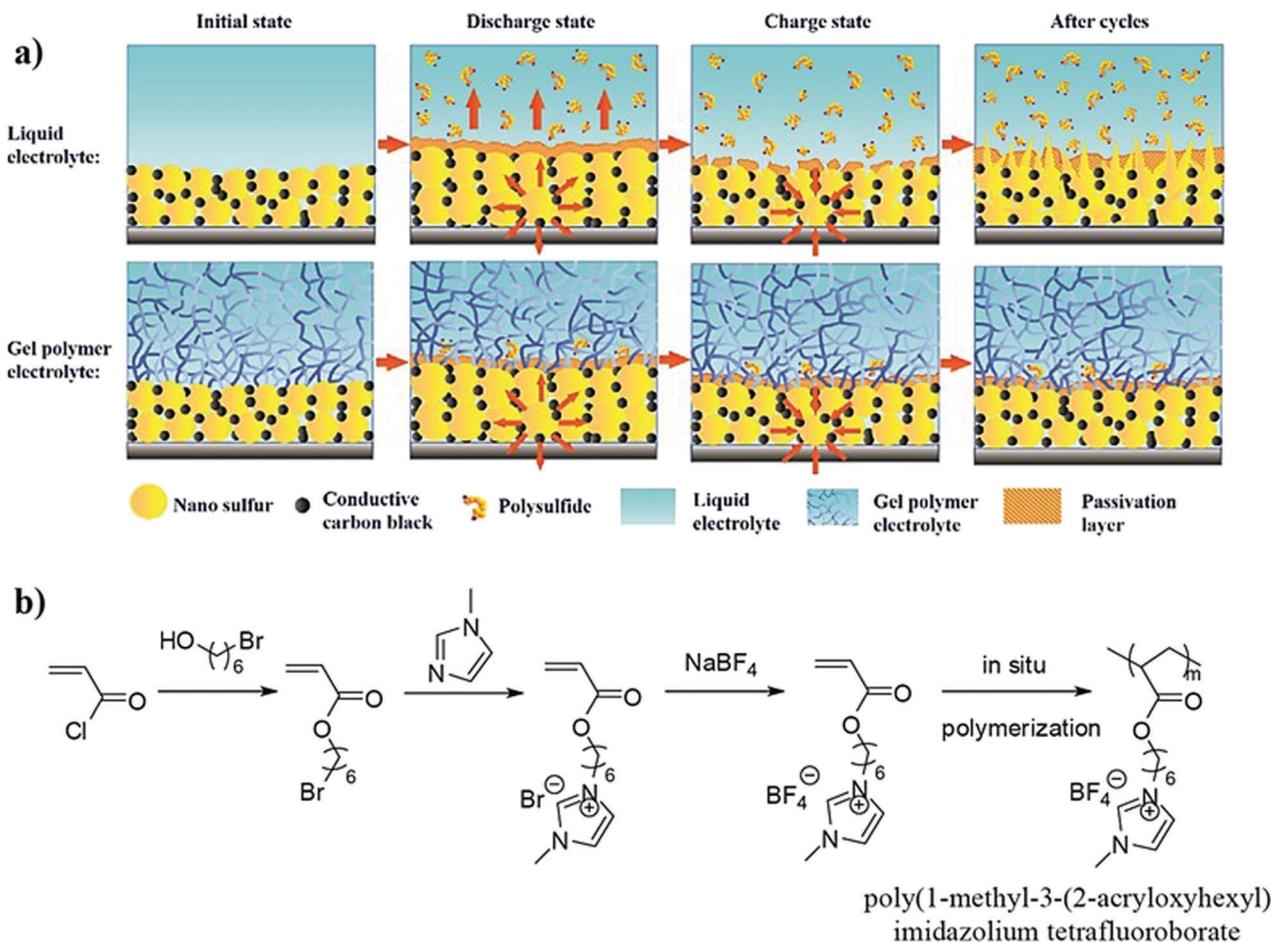This journal is © The Royal Society of Chemistry 2021

Fig. 19 (a) The mechanism of trapping of polysulfides in a PETEA-based GPE. In the LE-based S|LE|Li battery cell, the breakdown and reconstruction of the passivation layer (CEI) due to the volume changes in the S cathode during the charge/discharge cycles lead to the dissolution of polysulfides. However, the *in situ* processing helps the tightly cross-linked PETEA-based GPE to cover the S electrode effectively by providing flexibility to the passivation layer against volume changes of sulfur particles. The PETEA-based GPE, in combination with a flexible passivating layer, effectively suppresses polysulfide dissolution and the gradual evolution of interfacial resistance (reproduced/adapted from ref. 418 with permission from Elsevier, Copyright 2016[418]). (b) Synthesis of the polymerizable ionic liquid monomer called MIT (reproduced/adapted from ref. 428 with permission from Elsevier, Copyright 2013[428]).

conductivity of 0.56 mS cm^{-1} and an overall oxidative stability of 4.8 V *vs.* Li|Li$^+$ despite the low T_{Li^+} of 0.34. Indeed, from a mechanical characteristic point of view, even though it is a GPE, the rigid cyclic carbonate moieties in the polymer backbone provide excellent mechanical stability. The GPE is used for the fabrication of LiFe$_{0.2}$Mn$_{0.8}$PO$_4$ (LFMP)|GPE|graphite cells by the separator assisted *in situ* process in both the 2032-coin and pouch cell configurations. At 1C, the coin-cell delivered a discharge capacity of 120 mA h g^{-1} with a capacity retention of 88.7% even after 1000 cycles with a Coulombic efficiency of 100%. Ultimately, these unconventional polymer hosts other than the classical PEO or acrylates/methacrylates are also promising for PE applications concerning high T_{Li^+}, oxidative stability, and mechanical properties. Therefore, such PEs must be investigated further.
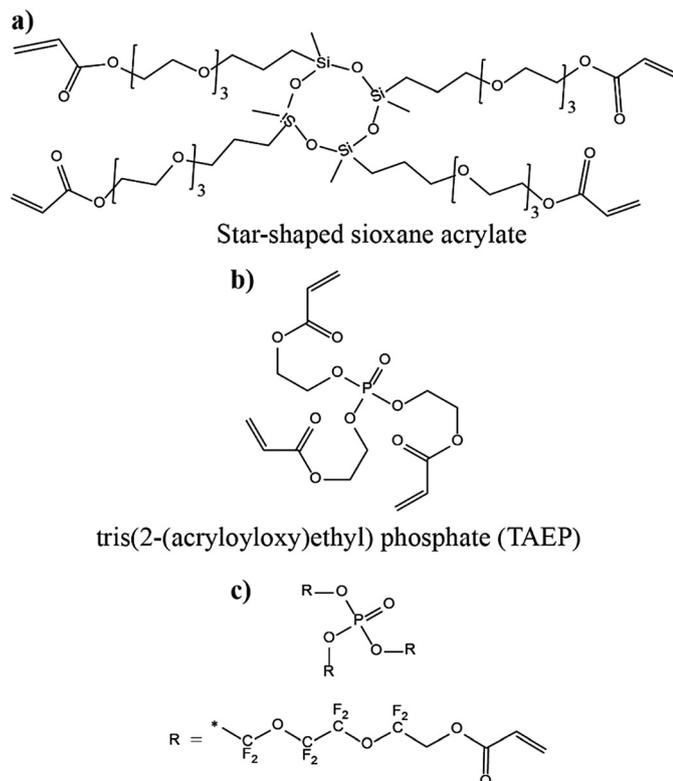
5.2 *In situ* processing by the direct deposition approach

In this section, the reports on the *in situ* processing of LPB cells using the direct deposition approach are emphasized. In this approach, cross-linked polymer hosts are considered as

the most promising candidates due to their excellent mechanical properties compared to linear polymer hosts. Many of the cross-linked PEs discussed in the context of the separator assisted *in situ* process may be useful for the direct deposition approach as well. The transition from the separator assisted approach to direct deposition is helpful in the context of LMPBs since those precursors contain Li-metal incompatible acrylate/methacrylate or any other reactive molecules. These precursors do not come in direct contact with Li-metal, since the PE deposition is often carried out at the cathode side as shown in the direct deposition approach 1 (Fig. 8b). Hence, the unwanted side-reactions (if any) between the reactive Li-metal surface and the pristine monomers/oligomers can be avoided (Section 5.1, Fig. 13b and c).

One report in which the direct deposition approach is employed for the *in situ* processing of LMPB cells by Niu *et al.* uses a mono-functional monomer called ethylene glycol phenyl ether acrylate (EGPEA).[364] This work is important as it overrules the two conventional schools of thought existing in the LB community based on the existing literature reports that

This journal is © The Royal Society of Chemistry 2021

Energy Environ. Sci., 2021, **14**, 2708–2788 | **2737**

Fig. 20 (a) Chemical structure of the siloxane functionalized acrylate monomer;[437] (b) tris(2-(acryloyloxy) ethyl) phosphate;[438] and (c) the fluorinated phosphorous-based cross-linking agent.[439]

(i) acrylate/methacrylate monomers are not suitable for LMPBs, and (ii) cross-linked PEs are indeed necessary to prevent HSAL growth, by convincingly proving that Li-metal compatible acrylate monomer-derived non-cross-linked homo-polymer hosts with high mechanical stability are also suitable for LMPBs. Interestingly, the non-cross-linked homo-polymer-based GPE derived from EGPEA exhibits good mechanical strength, which could be due to the bulky phenyl group present in the monomer structure. A similar acrylate monomer with a phenyl group in its chemical structure called 2-hydroxy-3-phenoxypropyl acrylate (HPA) was previously used for the *in situ* processing of non-aqueous GPE-based supercapacitors providing high mechanical stability compared to the phenyl-free MMA counterpart.[326] It is worth mentioning that the work by Niu *et al.* is one of those rare reports in which a non-cross-linked acrylate-based homo-polymer host is employed for the *in situ* processing of LMPBs by the direct deposition approach over the Li-metal anode. The work claims that, during the *in situ* polymerization process, the solvent molecules, the oligomeric EGPEA, and the PEGPEA fragment are firmly bound to the Li-metal surface to constitute the PIS-SEI layer. Indeed, the Li-metal body is protected against any volume changes by the synergistic combination of the PIS-SEI layer and the subsequent bulk GPE present above it. Moreover the PIS-SEI and GPE layers can suppress HSAL growth as compared to an LE or any other commonly used non-cross-linked PEs derived from monomers such as MMA. The EGPEA-based GPE exhibited an RT

ionic conductivity of 3.35 mS cm^{-1} with an oxidative stability value beyond 4.9 V *vs.* Li|Li$^+$. The as-fabricated LiNi$_{0.5}$Mn$_{0.3}$Co$_{0.2}$O$_2$ (NMC532)|GPE|Li cell can be operated between 2.8 and 4.6 V at RT. At 0.2C, the LMPB cell displayed a discharge capacity of 150 mA h g^{-1}, with 98% retention over 70 cycles.

Nair *et al.* reported a Li$^+$-ion conducting semi-interpenetrated (s-IPN) SPE and an innovative water-based spray deposition process of a PE coating over the cathode surface.[342] Unlike an IPN, an s-IPN is a polymer blend in which the constituent individual polymer networks may be separated without disrupting a chemical bond.[389] By using such a polymer matrix architecture, the benefits of multiple polymer hosts can be effectively utilized. For example, the *T*g value, mechanical properties, crystallinity, and chemical sensitivity can be fine-tuned. The s-IPN-SPE is produced from a precursor solution containing an oligomeric cross-linker, namely bisphenol A ethoxylate dimethacrylate (BEMA, denoted as BDM in this work), PEO, LiTFSI salt, AIBN, and acetonitrile solvent as a processing aid. The optimized SPE displayed an ionic conductivity in the order of 0.01 mS cm^{-1} at 20 °C which exceeded 1.0 mS cm^{-1} at 80 °C with an oxidative stability value of 4.5 V *vs.* Li|Li$^+$. For the fabrication of LMPBs (LFP|SPE|Li) in a pouch bag configuration by the *in situ* process, the precursor (water as a solvent and 2,2′-azo bis(2-methylpropionamidine) dihydrochloride (AAPH) as the initiator) is spray-coated over the cathode surface followed by a thermal curing process. The formed SPE-integrated composite electrode is then dried under a vacuum at 90 °C for the complete removal of water. At 70 °C, the LMPB cell delivered a discharge capacity of 160 mA h g^{-1} at 0.1C. Surprisingly, at 1C, a capacity value of 140 mA h g^{-1} is obtained, and 70% of it is retained even after prolonged 2000 cycles. In another report, a GPE based on BEMA combined with a high boiling point organic plasticizer, namely dimethyl polyethylene glycol (DPG) and LiTFSI salt, is reported (Fig. 23a).[396] This approach is a solvent-free *in situ* processing technique and carried out using a thermal curing process (AIBN, 80 °C for 1.0 h.) Compared to SPEs based on BEMA and PEO, the GPE system exhibited high ionic conductivity values of 0.10, 0.14, and 1.4 mS cm^{-1} at 0, 20, and 100 °C, respectively. This proves that better plasticization is induced by DPG as compared to long chain and high molecular weight PEO. Additionally, the T_{Li^+} values achieved for DPG-based GPEs are also superior to those of PEO-based SPEs. It is worth noting that this process is a solvent-free technique, less tedious, and faster than solvent-based processing. Finally, the GPE is stable beyond 4.7 V *vs.* Li|Li$^+$, and a T_{Li^+} of 0.45 at 25 °C is also obtained. The cathode–electrolyte composite electrode is then contacted with a Li-metal anode, and the LMPB cell is fabricated. The *in situ* processed LFP|GPE|Li (LFP modified with PEDOT:PSS) cell displayed a discharge capacity of 130 and 140 mA h g^{-1} (at 0.1C) when cycled at 25 and 70 °C, respectively. In both cases, it is also cycled for more than 300 cycles without any failure. These two reports are engaging in the context of a direct deposition approach as they use a single bi-functional cross-linker BEMA in the precursor solution, and both solvent-induced and solvent-free processing approaches are proposed along with a spray deposition method and an s-IPN polymer host architecture.
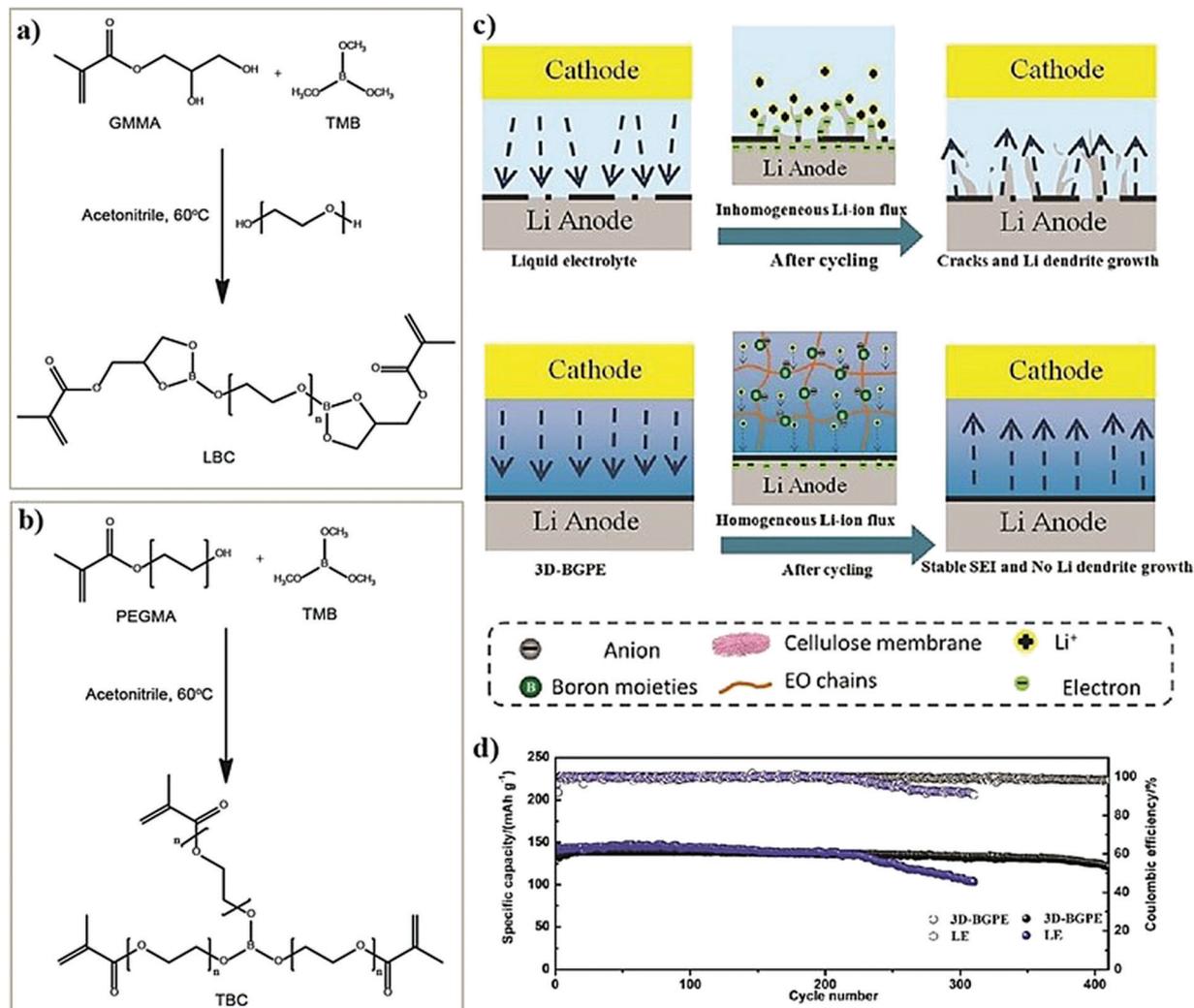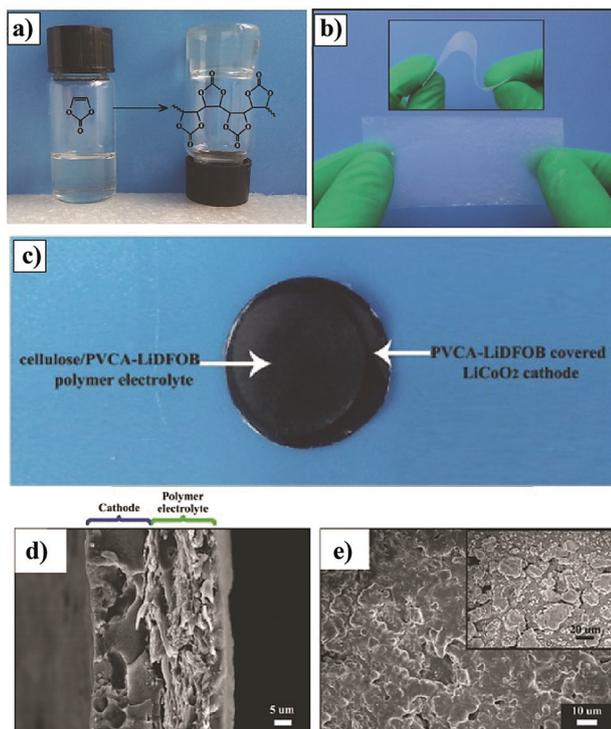
2738 | *Energy Environ. Sci.*, 2021, **14**, 2708–2788

This journal is © The Royal Society of Chemistry 2021

Fig. 21 Synthesis route to (a) di- and (b) tri-methacrylate cross-linker monomers containing boron; (c) the illustration of the homogenous Li$^+$-ion flux offered by boron-containing PEs with a high T_{Li^+} value facilitating HSAL-free cycling in Li-metal cells compared to conventional LEs; and (d) improved cycling stability of the LFP|3D-GPE|Li cell over the LE counterpart (reproduced/adapted from ref. 366 with permission from The Royal Society of Chemistry[366]).

Gerbaldi *et al.* reported an RTIL-based cross-linked IGPE by the UV irradiation process (10 min).[329,369] The precursor consists of di- and mono-methacrylate oligomers, namely BEMA and poly(ethylene glycol) methyl ether methacrylate (PEGMEM), respectively. HMPP is used as the UV initiator and the RTIL (*N*-methoxyethyl-*N*-methylpyrrolidinium bis(trifluoromethane-sulfonyl)imide, PY$_{1201}$-TFSI-RTIL) as the liquid plasticizer along with LiTFSI salt. The optimized IGPE exhibited an ionic conductivity of 0.80 and 5.5 mS cm^{-1} at 20 and 80 °C, respectively. Here, the copolymer host can be considered as a loosely cross-linked copolymer due to the combination of di- and mono-methacrylate oligomers present in the precursor, which results in a low cross-linking density. Additionally, the pendant chain of PEGMEM can act as an internal plasticizer to reduce T_g and increase the Li$^+$-ion transport. Due to the presence of the RTIL, which is thermally stable at high temperature, the overall thermal stability of the IGPE is beyond 300 °C, and a high

oxidative stability value of 5.2 V *vs.* Li|Li$^+$ is also achieved. High thermal stability is inherited from the high boiling point of the RTIL used, which cannot be achieved using conventional carbonate-based solvents. However, the T_{Li^+} value is found to be as low as 0.18 at 60 °C, which is a typical challenge concerning the use of RTILs, where the high concentration of mobile ions imparts a high total ionic conductivity (coming from the conductivity of the anion and cation), but limited Li$^+$-ion conductivity (σ_{Li^+}). Indeed, for application in LMPBs, in general, PEs should possess a very high σ_{Li^+} and the total conductivity is not quite sufficient. Still, the *in situ* processed LFP|IGPE|Li cell demonstrated a discharge capacity of 85 mA h g^{-1} (0.1C) at RT, good cycling stability, and capacity retention up to 30 cycles.

In another report from the same group, a similar precursor is used to fabricate LIPBs and LMPBs using a thin-film of V$_2$O$_5$ as the cathode.[354] This approach is close to the one used for silicon anodes, where the volume expansion is controlled by the

This journal is © The Royal Society of Chemistry 2021

Energy Environ. Sci., 2021, **14**, 2708–2788 | **2739**
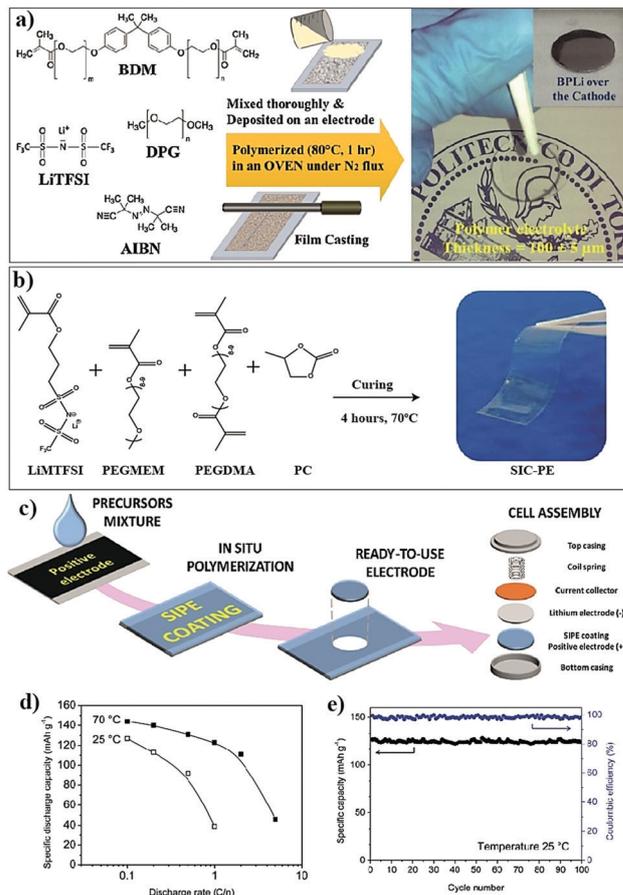
Fig. 22 (a) The photograph presenting the conversion of VC into poly-VC followed by heating at 60 °C for 24 h; (b) photograph of the cellulose reinforced poly-VC-based SPE (denoted as cellulose/PVCA–LiDFOB); (c) photograph of the SPE-deposited LCO cathode after electrochemical cycling; (d) cross-sectional SEM image presenting the cathode|electrolyte interface; and (e) SEM image of the LCO surface before (inset) and after SPE deposition (reproduced/adapted from ref. 443 with permission from John Wiley and Sons, Copyright 2016.[443] Distributed under a Creative Commons Attribution License International 4.0 (CC BY 4.0) (https://creativecommons.org/licenses/by/4.0/).

Fig. 23 (a) Materials and processes involved in synthesizing a BEMA-based GPE and the *in situ* processing of the PE over an LFP electrode. On the right-hand side, the physical appearance of the self-standing GPE film is given. The inset presents the ready-to-use PE deposited LFP electrode for LMPB fabrication (reproduced/adapted from ref. 396 with permission from Elsevier, Copyright 2016[396]). (b) Components in the precursor and scheme adopted for the synthesis of the SIC-PE film; (c) schematic representation of the *in situ* processing of LFP|SIC-PE|Li cells by the direct deposition approach; (d) specific capacity as a function of C-rate at 25 and 70 °C; and (e) plot of the cycling stability of the LFP|SIC-PE|Li cell at 25 °C (reproduced/adapted from ref. 370 with permission from American Chemical Society, Copyright 2016[370]).

use of a strong network forming polymer matrix [Fig. 18a and b]. Nanomaterials such as V_2O_5, when exposed to long-term cycling, undergo pulverization, where these particles break into smaller particles and eventually degrade the cell. Indeed, in this work, the authors demonstrated that the *in situ* polymerized GPE could hold the nanoparticles tight and avoid pulverization; hence long-term cycling can be achieved. The LMPB cell displayed a discharge capacity of 130 mA h g^{-1} at a current rate of 1.5C. After cycling for 500 cycles at various current rates, a 70 mA h g^{-1} specific capacity is still retained at 10C. Besides, in the LIPB cell (graphite anode), the specific capacity is found to be around 100 mA h g^{-1} (1C) and 75 mA h g^{-1} (5C) after 50 cycles.

In another study from a different group, using a similar approach, a cross-linked IGPE is prepared from a combination of tri- and di-acrylate cross-linkers, and an RTIL/lithium salt mixture (Pyr$_{13}$-TFSI/1 M LiTFSI) in the presence of HMPP.[269] It is observed that the RT ionic conductivity is a maximum for the IGPE derived from the short-chain cross-linkers ETPTA and 1,6-hexanediol diacrylate (HDDA) (1.1 mS cm^{-1}). The *in situ* processed LMPB cell (LFP|IGPE|Li) exhibited a specific capacity of 120 mA h g^{-1} (0.2C and 20 °C), and was stable over 50 cycles. Apart from the thermal stability offered to the PE by the RTIL,

this work also suggests the suitability of cross-linked IGPEs in offering better Li-plating morphologies than carbonate solvents in GPEs. Hence, it can be learned that RTILs combined with suitable cross-linked polymer hosts can convincingly reduce the pulverization of electrode materials, offer high thermal and oxidative stability, and improve the Li-deposition morphologies in LMPBs.

Single-ion conducting polymer electrolytes (SIC-PEs) are those in which the anion is covalently attached to a polymer chain so that the ion conduction occurs exclusively due to the mobility of cations (or *vice versa*). Such Li$^+$-ion conducting SIC-PEs can offer remarkably high T_{Li^+} values, which can help suppress HSAL growth by maintaining a uniform flux of Li$^+$-ions close to the Li-metal surface.[446–449] It is a challenging task to achieve a PE that simultaneously possesses high T_{Li^+} and

2740 | *Energy Environ. Sci.*, 2021, **14**, 2708–2788

This journal is © The Royal Society of Chemistry 2021

ionic conductivity values.[450] In a recent report, an SIC-PE possessing the aforementioned features was developed and used for LMPB fabrication by the *in situ* process (Fig. 23b).[370] The new SIC-PE is prepared by facile and single-step free-radical copolymerization of lithium 1-[3-(methacryloyloxy)-propyl sulfonyl]-1-(trifluoromethylsulfonyl) imide (LiMTFSI) with mono- and bi-functional methacrylate oligomers, namely PEGMEM and PEGDMA, respectively. Besides, PC is used as a plasticizer to enhance the ionic conductivity. The optimized SIC-PE exhibited a high ionic conductivity of 0.11 mS cm^{-1} along with a high oxidative stability value of 5.5 V *vs.* Li|Li$^+$ at 25 °C. The single-ion conduction in the PE is attributed to the anionic character of the loosely cross-linked copolymer-host due to the covalent tethering of the MTFSI$^-$ moieties in the polymer backbone. As a result, the only mobile species present in the PE are Li$^+$-ions, which eventually act as the predominant charge carrier. Hence, high T_{Li^+} values of 0.88 and 0.90 are achieved at 25 and 70 °C, respectively. Besides, in synergy with PC, the SIC-PE membranes also demonstrate excellent interface/interphase stability against the Li-metal anode. The fabrication of an LMPB cell (LFP|SIC-PE|Li) by the *in situ* direct deposition process is presented in Fig. 23c. A high LFP mass loading of 5 mg cm^{-2} is used for the cell assembly, which exhibited high cycling performance both under high (143 mA h g^{-1}, 0.1C, 70 °C) and low (126 mA h g^{-1}, 0.1C, 25 °C) temperature conditions (Fig. 23d). Indeed, the *in situ* processed LMPB cell at RT retained 98% of its initial capacity even after 100 cycles at 0.1C.

Apart from ester-containing acrylate and methacrylate vinyl monomers and oligomers, acrylate/methacrylate-free allyl species are also employed for the *in situ* processing of LPBs by the free-radical polymerization pathway. However, such reports are rare due to the relatively slow-polymerization of allyl monomers and oligomers.[451] The slow polymerization rate of allyl molecules is mainly arising from the high stability of allyl free-radicals, which results in the inhibition of the propagating chain. The stabilization of allyl radicals is known as 'degradative chain transfer,' which involves the abstraction of allylic hydrogen and resonance stabilization, as shown in Fig. 24a.[454] Consequently, allyl monomers and oligomers lead to the formation of low molecular weight polymers and often require large quantities of free-radical initiator species to achieve the complete conversion of the monomer to the polymer. Brandall *et al.* used allyl ether-terminated polycarbonate oligomers for the *in situ* fabrication of thin-film LMPB cells by the UV polymerization technique.[445] The mono-functional allyl ether monomer (2-allyloxymethyl-2-ethyltri-methylene carbonate, AEC) is prepared by the ring-closing reaction of trimethylolpropane mono-allyl ether in the presence of 1,1-carbonyldiimidazole (CDI) (Fig. 24b). The AEC monomer is then partially homo-polymerized using 1,8-diazabicyclo[5.4.0]-undec-7-ene (DBU) as an organocatalyst, and benzyl alcohol as a protic initiator. The low molecular weight PAEC oligomer formed is later mixed with LiTFSI and a photo-initiator (2,2-dimethoxy-2-phenylacetophenone, DMPA), and subjected to another round of UV irradiation to get a mechanically stable and self-standing SPE. The SPE films displayed ionic conductivities of 0.0004 mS cm^{-1} and 0.005 mS cm^{-1} at 25 °C and 60 °C, respectively, which are
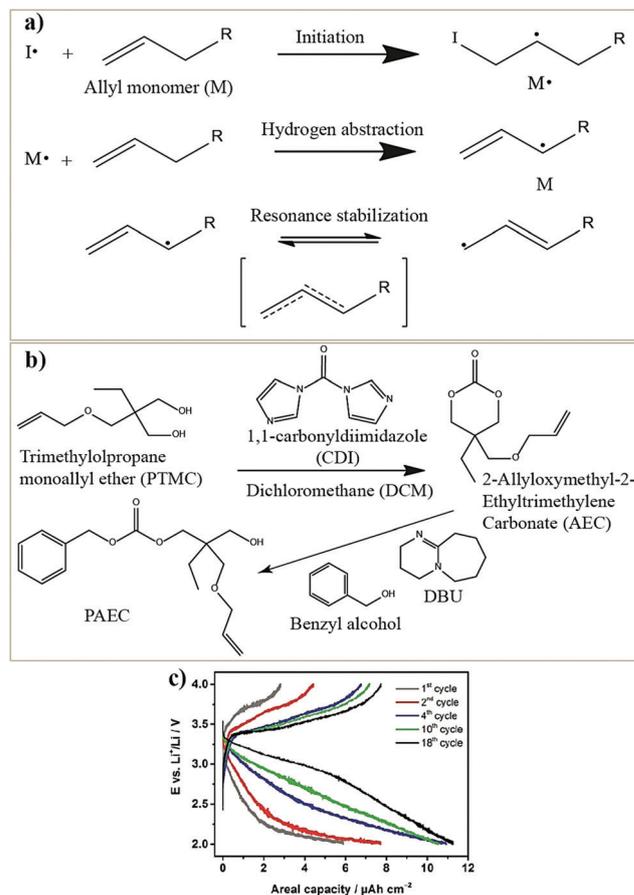

Fig. 24 (a) The process of allyl radical resonance stabilization by a degradative chain transfer mechanism.[454] (b) Synthesis of allyl ether monomer AEC and its conversion to PAEC. The PAEC is made into a precursor in the presence of a LiTFSI salt and DMPA initiator and is subjected to UV irradiation over a V$_2$O$_5$ cathode (direct deposition) for the *in situ* processing of LMPBs. (c) Galvanostatic charge–discharge profile of the V$_2$O$_5$|SPE|Li cell as a function of cycle number at 60 °C (reproduced/adapted from ref. 445 with permission from John Wiley and Sons, Copyright 2016[445]).

comparatively lower than the classical PEO–LiTFSI system. However, the SPE is directly prepared over the V$_2$O$_5$ electrode to obtain a V$_2$O$_5$|SPE|Li cell and galvanostatically cycled at 60 °C (Fig. 24c). Indeed, the cells are made from Li-metal and V$_2$O$_5$ thin films as the anode and cathode, respectively, which are mainly intended to be used in thin-film microbatteries. Hence, the lower conductivity may not be that detrimental as compared to a standard conventional LMPB cell.

As already explained in Fig. 10b, one way to achieve an ester-free cross-linked PE starting from linear homo-polymers such as PEO is by the generation of free-radicals by the hydrogen abstraction process. In such an approach, Porcarelli *et al.* used a precursor made using PEO, tetraglyme, LiTFSI, and a UV initiator (4-methyl benzophenone, MBP) (see Fig. 25a).[375] Indeed, the cross-linking process is initiated through the abstraction of hydrogen from PEO; in other words, it is a protic mechanism (Norrish type II) generating a free-radical.[455] This free-radical later reacts with another free-radical in the same or another –EO– chain. Tetraglyme can also be a part of the polymer chain since it also
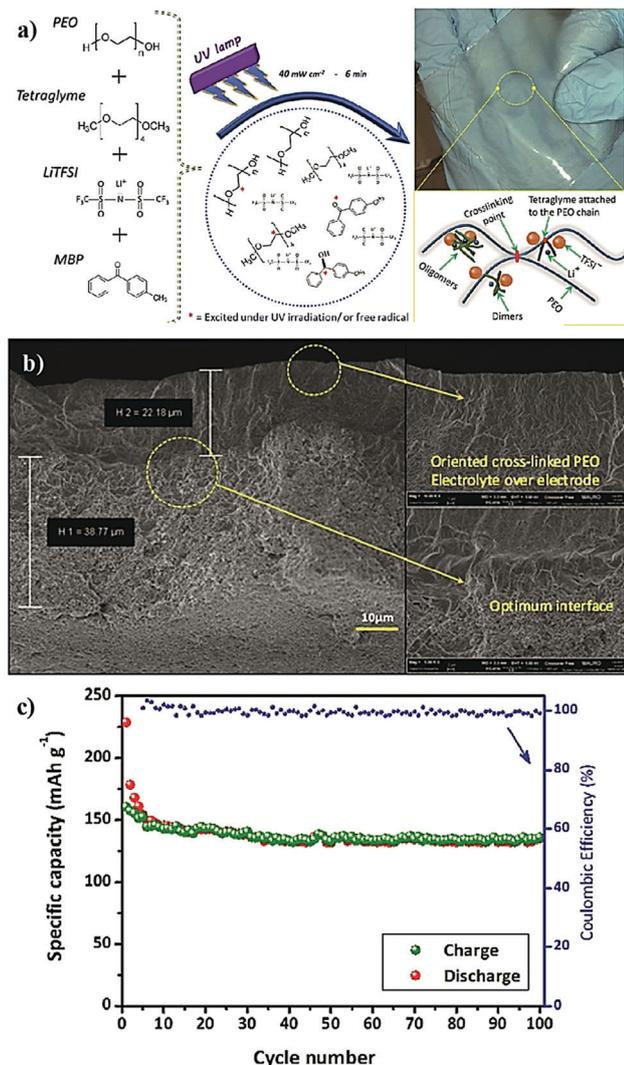
This journal is © The Royal Society of Chemistry 2021

Energy Environ. Sci., 2021, **14**, 2708–2788 | **2741**

Fig. 25 (a) Representation of the UV-light induced cross-linking process of PEO and tetraglyme by a Norrish type II pathway for the preparation of a PE. A plausible illustration of interconnected PEO chains is provided at the bottom, and the mechanically stable SPE film is shown at the top right-hand side. (b) SEM image of the electrode|electrolyte interface. (c) The complete cycling stability data of the *in situ* processed (direct deposition approach) TiO_2|SPE|Li cell (reproduced/adapted from ref. 375 with permission from Springer Nature, Copyright 2016.[375] Distributed under a Creative Commons Attribution License International 4.0 (CC BY 4.0) (https://creativecommons.org/licenses/by/4.0/)).
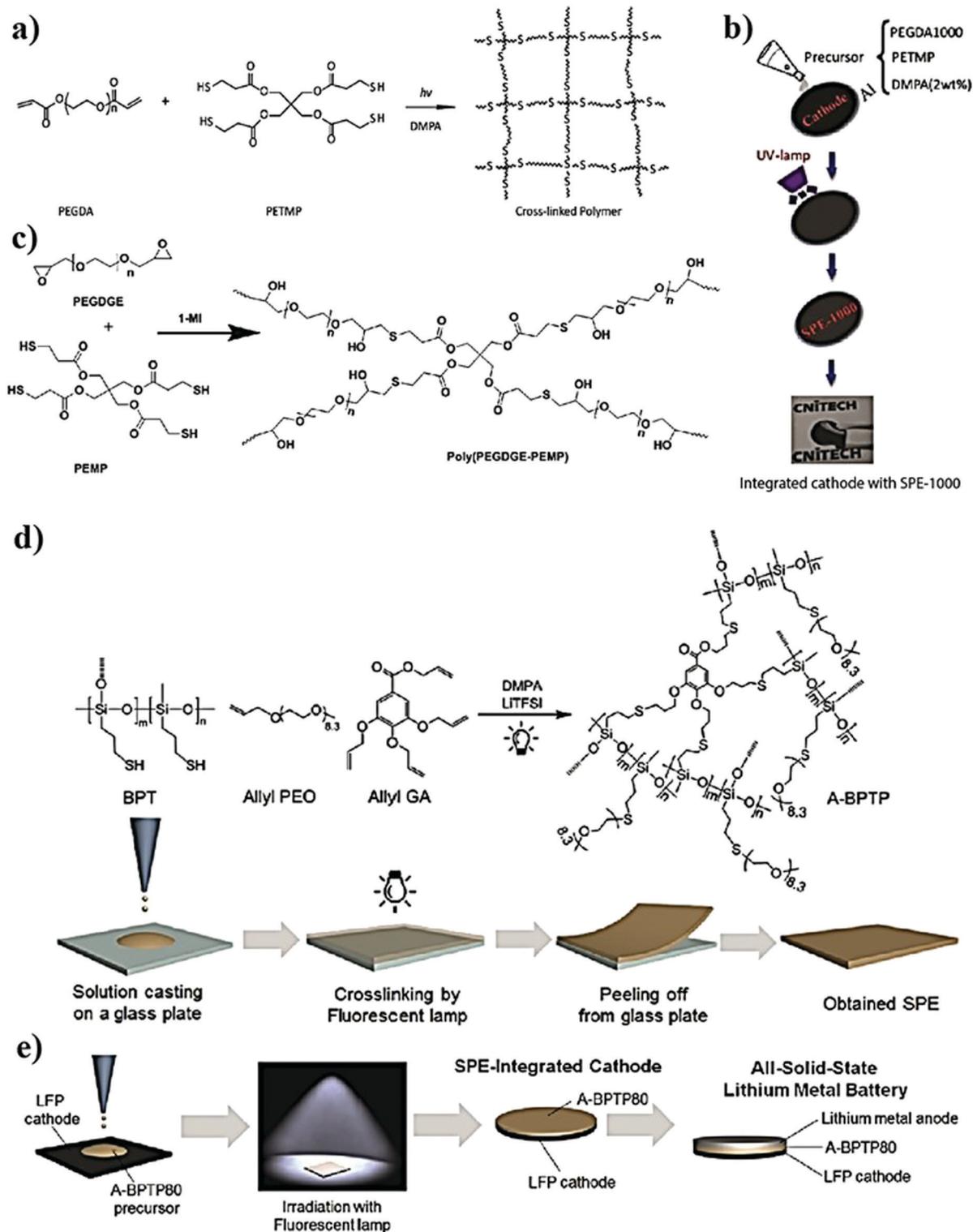
possesses hydrogen that can be abstracted like PEO. Additionally, it is reported that several oligomers of tetraglymes can be formed in cross-linked PEs, providing an additional plasticization effect. The structure of the polymer host can be considered as linear chains of PEO, cross-linked to each other, which are tethered with covalently linked tetraglyme units. One of the advantages of such an approach is that the physical properties of the polymer chain, such as crystallinity, can be controlled by the cross-linking process as the interlinking restricts the mobility of polymer chains to pack into their crystalline form. All the cross-linked PE samples exhibited ionic conductivities beyond 0.1 mS cm^{-1} at 25 °C. A maximum T_{Li^+} value of 0.55 is achieved for the optimized

sample along with a high oxidative stability value that goes beyond 5 V *vs.* Li|Li$^+$. In Fig. 25b, the SEM image of the cross-linked PE-integrated TiO_2 electrode is shown. The *in situ* processed TiO_2|PE|Li cell exhibited a discharge capacity of ≈ 140 mA h g^{-1} at 0.1 mA cm^{-2} over 100 continuous cycles (20 °C) [Fig. 25c]. In another study, a similar approach was attempted by the same group, but, instead of tetraglyme, an RTIL is used.[455] The mobile RTIL in the cross-linked PEO host can induce effective plasticization, which is also reflected in the improved ionic conductivity value of the IGPE (0.25 mS cm^{-1}, 20 °C). Additionally, the cross-linking process aids in reducing or even altogether avoiding the leakage of the RTIL from the PE along with improved elasticity. Indeed, the *in situ* processed LFP|IGPE|Li cell cycled at both 20 and 50 °C demonstrated a high rate capability and an excellent Coulombic efficiency.

Large size bipolar-stacked LMPBs are very important for high-voltage and high-energy applications. In line with improving the electrode|electrolyte interface in such designs, Wei *et al.*[388] adopted the *in situ* polymerization process for the preparation of an SPE and cell fabrication by a thiol–ene click reaction.[340,377,452,456,457] For this purpose, they employed materials such as the PEGDA oligomer, a multi-functional thiol (pentaerythritol tetra (3-mercaptopropionate), PETMP), DMPA initiator, and LiTFSI salt (Fig. 26a). The precursor prepared using the above materials is directly deposited over the LFP cathode and UV-cured to produce a PE integrated composite electrode, followed by LMPB fabrication (Fig. 26b). The molecular weight of the PEGDA and the EO:Li ratio are found to influence the ionic conductivity of the SPEs. The PEGDA ($M_w = 1000$ Da)-based SPE with EO:Li = 20:1 displayed the highest ionic conductivity (0.13 mS cm^{-1}, 60 °C). The high molecular weight of PEGDA can induce longer and more flexible chains between the chemical junctions in the SPE network, which provides better internal plasticization and chain mobility, thus facilitating ion conduction. Additionally, by using a long cross-linker, the cross-linking density can also be controlled. The oxidative stability value of SPE-1000 is ≈ 5.1 V *vs.* Li|Li$^+$ with excellent thermal stability. Another report by Grewal *et al.* also suggests the suitability of using click reactions as a tool for producing cross-linked SPEs.[452] Here, along with thiol–ene chemistry, a thiol–epoxy click reaction is also demonstrated as an efficient tool for SPE preparation (Fig. 26c). Although the *in situ* processing of the LPB cell is not attempted in this work, thiol–epoxy click chemistry is also expected to gain attention in the near future, which gives enough maneuverability to the production of various types of PEs.

Apart from the 'ene' group from acrylates/methacrylates, allyl ether monomers are also employed for thiol–ene click reactions. Shim *et al.* reported the synthesis of an SPE by a thiol–ene click reaction under fluorescent light irradiation (Fig. 26d).[453] An allyl-PEO oligomer, an allyl gallic acid ($n = 3$) monomer, and a branched polysiloxane oligomer having a thiol group (BPT) are used for the generation of a cross-linked polymer backbone. LiTFSI and DMPA are used as a conducting salt and photoinitiator, respectively. The optimized SPE (A-BPTP80) displayed an ionic conductivity of 0.4 mS cm^{-1} at 60 °C. The precursor is directly deposited on an LFP cathode followed by a cross-linking

2742 | *Energy Environ. Sci.*, 2021, **14**, 2708–2788

This journal is © The Royal Society of Chemistry 2021

Fig. 26   (a) The synthetic route towards the preparation of a cross-linked polymer network by a UV-light induced thiol–ene click reaction; (b) the schematic representation of the *in situ* processing of the LMPB cell by the direct deposition approach using an SPE prepared by a thiol–ene click reaction (reproduced/adapted from ref. 388 with permission from Elsevier, Copyright 2018[388]); (c) an example of a thiol–epoxy click reaction (reproduced/adapted from ref. 452 with permission from John Wiley and Sons, Copyright 2019[452]); (d) the formation of a cross-linked SPE by a fluorescent lamp irradiation-induced thiol–ene click reaction from allyl ether and thiol monomers (the SPE film preparation by the *ex situ* process is also displayed); and (e) the *in situ* processing of LMPBs by a thiol–ene click reaction-assisted direct deposition approach (reproduced/adapted from ref. 453 with permission from Elsevier, Copyright 2017[453]).

reaction induced by irradiation with a fluorescent lamp for the *in situ* processing of the LMPB (LFP|A-BPTP80|Li) cell (Fig. 26e). The disadvantage of the fluorescent lamp is that the intensity of photons in the UV range will be significantly less so that the polymerization rate will be low, which demands irradiation for a long duration (16 h) for SPE formation. However, the final *in situ* processed LMPB cell displayed a discharge capacity of 150 mA h g^{-1} (0.1C) with a capacity retention of 88% after 50 cycles.

5.3 *In situ* processing of the PIS-interphase layers

5.3.1 Artificial protection for LIBs and LE-LMBs. There are a few early reports in which the artificial protection of the Li-metal surface of LE-LMBs has been achieved by PIS-SEI production by free-radical polymerization methods. For instance, Park *et al.* prepared a thin (10 μm) conformal layer of a GPE as a PIS-SEI layer directly on the surface of a Li-metal anode by using the UV-polymerization technique. A precursor made of HDDA, 1 M LiClO$_4$ in organic carbonates as an LE, and methyl benzoylformate (MBF, a photo-initiator) is employed for the conformal PIS-SEI synthesis purpose.[391] The cross-linked GPE, as a self-standing film, exhibited an ionic conductivity of 0.58 mS cm^{-1} (RT). Electrochemical Impedance Spectroscopy (EIS) characterization validated that the surface coating of the Li-metal anode helped in stabilizing the cell impedance during long-term storage. Additionally, the PIS-SEI formed on the Li-metal anode using the *in situ* processed GPE layer is smoother than the cell with a bare Li-counterpart. Successive studies from the same group also explored the positive effects of additives in the same precursor to improve the overall ion-transport properties.[458] For example, an anion-receptor, namely oligoethylene glycol borate (OEGB), and a linear polymer PVdF are introduced into the precursor to improve T_{Li^+} of the GPE from 0.61 to 0.80.[459] Indeed, the PIS-SEI with an improved T_{Li^+} can maintain a uniform Li$^+$-ion flux on the anode surface. However, the surface protection of the Li-metal anode using acrylate/methacrylate monomers has not been explored much in LMPB fabrication, most probably due to the several subsequent reports emphasizing the parasitic reactions between the Li-metal anode and the monomers as explained in Section 5.1.

A phosphate-based tri-functional cross-linker TAEP is also used to prepare a cross-linked surface protection layer over NMC111 cathode particles.[460] The LE can plasticize the polymer film so that it can act as a PIS-CEI. In the LE-based LIB cell, such a protection layer can save the active cathode materials from the violent attacks of the LE. Here, the polymer-coated LIB cell retains 84% of the initial discharge capacity (180 mA h g^{-1} at 1C) over 50 cycles. However, the unprotected NMC111-based LIB cell retained only 74% of its initial specific capacity after the same number of cycles. In several other studies by various research groups, different polymers are used for the preparation of artificial PIS-interphases. The possibility of adopting a polyacrylate-based surface coating over a high-voltage LCO cathode was demonstrated by Lee *et al.* [see Fig. 27a and b].[386] In this report, the precursor containing ethylene glycol diacrylate (EGDA) and HMPP is deposited over the LCO cathode. On UV curing, the LCO surface is covered by a thin layer of a cross-linked PEGDA network (20 nm). This polymer

integrated electrode is then used for the fabrication of an LIB coin cell. During the cell assembly, the LE (1 M LiPF$_6$ in EC:DMC) activates the PEGDA surface coating so that it transforms into a PIS-CEI. The cycling performance of the cell is investigated (3–4.4 V), and the assembled LIB cell delivers a first-cycle specific capacity of 150 mA h g^{-1} (0.5C), which is equal to that of a pristine LCO cathode-based cell. However, the specific capacity retention after several cycles is found to be higher for the LIB cell with a PIS-CEI coating compared to the uncoated counterpart (Fig. 27c). Indeed, the EIS data of the cells confirmed that the ultrathin artificial PIS-CEI remarkably reduced the impedance of the cell during long-term galvanostatic cycling as compared to the PIS-CEI-free cell. It is worth mentioning that the direct contact of LEs with pristine LCO-based cathodes leads to the formation of a highly resistive interphase layer,[461] which during long-term cycling hinders the charge transfer between LCO and the LE, leading to inferior cycling characteristics (low capacity retention, low Coulombic efficiency, *etc.*). However, these intricacies are avoided by using the PIS-CEI layer so that this work can be considered as an excellent example of an artificially tailored PIS-CEI for LIBs.

5.3.2 Multi-layer approach for LPBs. Very recently, a novel phase diagram approach for optimizing the composition of an SPE for tuning the ionic conductivity was explored by Li *et al.* (Fig. 28a).[361] This work is important as it demonstrated the multi-layer approach for the processing of LMPBs (Section 4.2.3). Here, the precursor is carefully optimized, and the crystalline phase is eliminated so that a prominent isotropic phase is present in the resulting PE.

The isotropic phase imparts an amorphous character to the mixture, which is beneficial for increasing the ionic conductivity, and one such mechanically stable self-standing SPE film is displayed in Fig. 28b. The phase diagram approach is systematic as it can fine-tune the properties of the PE, unlike the conventional trial and error method. The precursor is made of a PEGDA oligomer, glutaronitrile (GN), LiTFSI, lithium bis(oxalato)borate (LiBOB), and a photo-initiator [bis(2,4,6-trimethylbenzoyl)-phenyl-phosphineoxide]. Using this formulation and process, a cross-linked PE is produced that exhibits a superior ionic conductivity of 1.0 mS cm^{-1} (30 °C). Here, GN is a plastic crystal, which can improve the ionic conductivity owing to its high polarity (dielectric constant, $\varepsilon = 37$).[462] Indeed, such PEs are often called plastic crystal PEs (PCPEs). Incorporation of plastic crystals into *ex situ* processed PE films has been reported in several studies; however, the application of these materials in the *in situ* process is scarce.[463–466] In this work, although the authors have termed the PCPE as an SPE, considering the plasticization induced by the GN plastic crystal with a low melting point (−29 °C), a more apt term would be calling it a plasticized or quasi-solid-state PE. The oxidative stability value of this binary-salt incorporated PE (LiTFSI + LiBOB) is 4.5 V *vs.* Li|Li$^+$, which is higher than a single-salt counterpart (only LiTFSI). For the *in situ* fabrication of the LMPB cell, the precursor is infiltrated into an LFP electrode film and UV-cured so that the PIS-CEI layer is formed over the electrode surface. Later, an additional layer of PE film is also placed over the *in situ* processed electrode to ensure perfect separation between the electrodes

2744 | *Energy Environ. Sci.*, 2021, **14**, 2708–2788

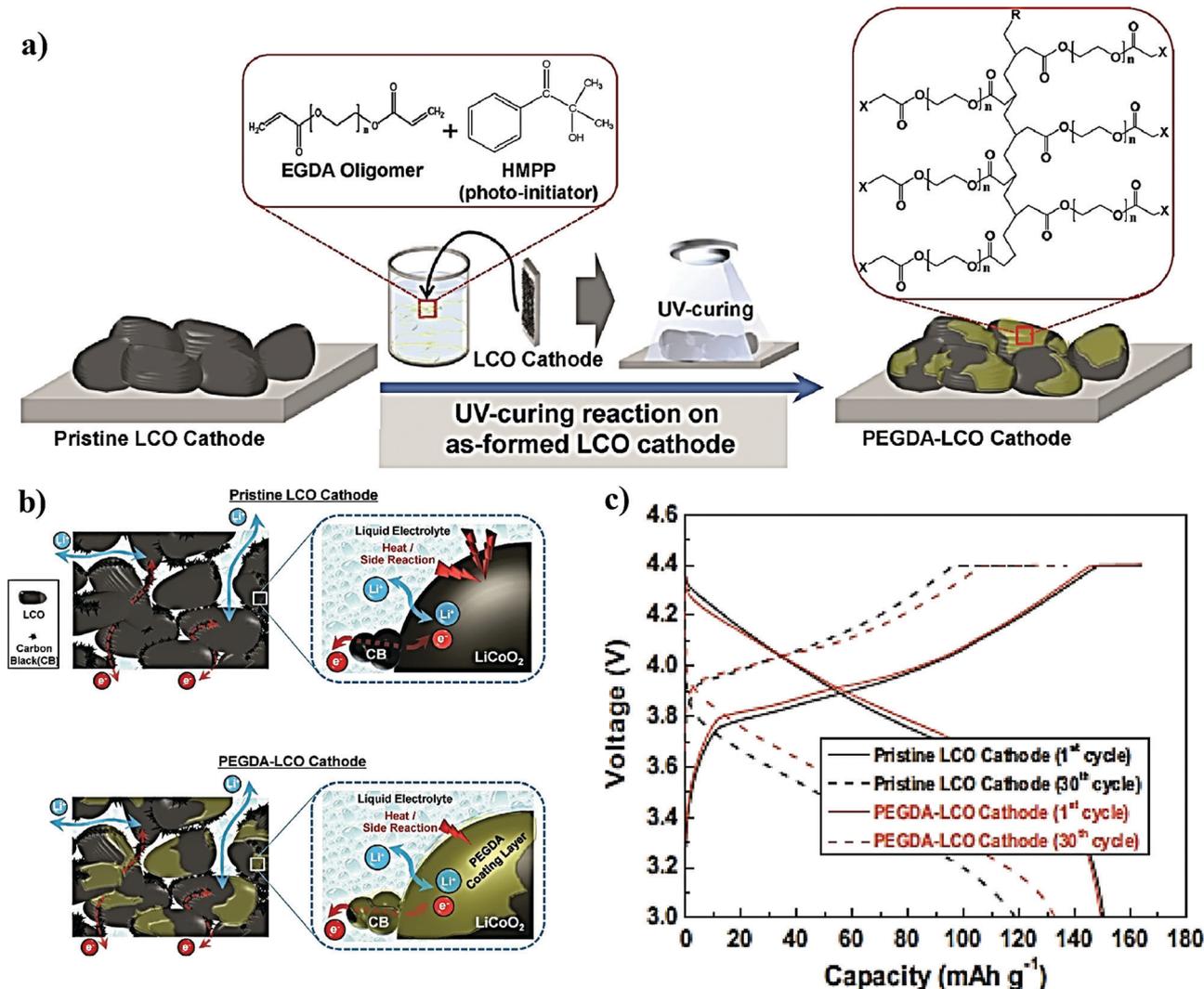This journal is © The Royal Society of Chemistry 2021

Fig. 27 (a) Schematic illustration of the production of a PEGDA-based PIS-CEI coating over an LCO cathode from the EGDA oligomer by the UV-light assisted *in situ* polymerization process; (b) schematic representation of the PIS-CEI layer over the LCO cathode reducing the heat generation and side-reactions compared to the pristine-LCO cathode in the LE-based LIB cell; and (c) voltage *vs.* capacity plot showing the performance of pristine-LCO and PIS-CEI coated LIB cells (reproduced/adapted from ref. 386 with permission from Elsevier, Copyright 2013[386]).

(hence considered as a multi-layer approach). The conformal coating of the PIS-CEI layer formed over the cathode for enhancing the interfacial properties is presented in Fig. 28c. When galvanostatically cycled, the assembled LMPB cell (LFP|PCPE|Li) exhibited an initial capacity of 138 mA h g^{-1} (30 °C, 0.2C) close to that of an LE-based cell with a specific capacity retention of 86% (370 cycles) and a Coulombic efficiency of 99.99% (Fig. 28d). The same phase diagram approach is extended to the formation of other PCPEs by replacing GN with another plastic crystal succinonitrile (SN), however, the *in situ* LPB processing is not demonstrated.[467,468]

In another example, multi-layer processing of a silicon–graphene composite anode (Si–FLG)-based LPB was reported by Falco *et al.*[362] Herein, the *in situ* processing of a thin layer of IGPE over Si–FLG is achieved by a hot-pressing step followed by UV-curing. The precursor made of an RTIL (Pyr$_{14}$TFSI), LiTFSI, PEO, and benzophenone is deposited over the silicon electrode

and subjected to hot-pressing (70 °C) between two polypropylene sheets. On UV-curing, the cross-linking of PEO chains will occur, resulting in an IGPE layer with a thickness of ≈60 μm, and this layer can be considered a PIS-SEI. The thin layer of IGPE is soft and can improve the interfacial contact between the PE and the electrode particles and the electrolyte materials can impregnate into the pores of the electrode. The cross-linking of PEO occurs through a hydrogen-abstraction mechanism, as already discussed in the previous sections (Fig. 10b and 25a). Once the soft IGPE-based PIS layer (soft-PIS) is achieved, a hard IGPE film is prepared by a similar hot-pressing and UV-curing method and placed over the soft-PIS coated Si–FLG. An additional UV-curing step ensures the contact between the soft and hard IGPE layers as well. Such a combination of the *in situ* processed soft-PIS and the *ex situ* processed hard IGPE film is termed as a bilayer PE (BLPE). The scheme and digital photographs illustrating the BLPE over the Si–FLG anode are presented in Fig. 29a. The BLPE exhibits ionic
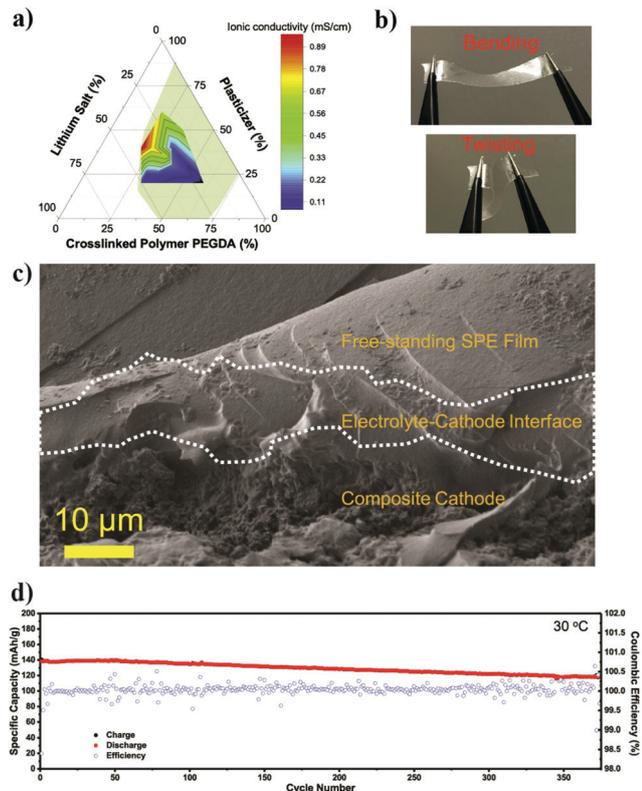
This journal is © The Royal Society of Chemistry 2021

Energy Environ. Sci., 2021, **14**, 2708–2788 | **2745**

Fig. 28 (a) Ternary phase diagram representing the ionic conductivity (measured at 20 °C) of the SPE (or PCPE) as a function of the contents of individual components in the precursor solution at 20 °C. The shadow area in the phase diagram represents the composition at which the prominent isotropic phase can be achieved in the SPE. (b) Illustration of the dimensional and mechanical stability of the optimized SPE film under bending and twisting conditions. (c) Cross-sectional SEM image of the multi-layer electrode–electrolyte assembly showing the individual layers of the cathode (composite cathode), *in situ* processed PIS (electrode–cathode interface), and SPE film (free-standing SPE film). (d) Cycling stability plot of the assembled LFP|SPE|Li cell at 30 °C and 0.2C (reproduced/adapted from ref. 361 with permission from Elsevier, Copyright 2018[361]).

conductivity values of 0.1 and 1.3 mS cm^{-1} (at 30 and 60 °C, respectively). The BLPE-based multi-layer processed Si–FLG|BLPE|Li cell (Fig. 29b) performs better compared to a conventional test-cell without the BLPE (Si–FLG|RTIL|Li, Fig. 29c). Compared to the RTIL–LiTFSI-based LE, the impregnated layer aids in holding the particles together and improves the specific capacity by increased active material utilization and a concomitant reduction in the capacity-loss after several cycles.

In summary, Section 5 provides an overview of the various types of *in situ* processing approaches used for the fabrication of LIPB and LMPB cells by employing free-radical polymerization techniques. Thermal curing and UV curing are the most used polymerization methods for the *in situ* process. The critical parameters that determine the properties of the *in situ* processed LPBs are the type of monomers, the number of functionalities, the type of spacer molecules in the oligomers, and the molecular weight of monomers/oligomers. All these characteristics will decide whether a PE that is formed is a tightly cross-linked or loosely cross-linked one. It is vital to find a balance between these

two characteristics of the PE because properties such as ionic conductivity, volume changes of nano-sized active materials (V$_2$O$_5$, Si, *etc.*), and HSAL growth mainly depend on it. Acrylates and methacrylates are used for the free-radical polymerization process even though they show reactivity towards the Li metal anode due to the presence of ester groups. However, there are other functionalities such as epoxides and ester-free vinyl- and allyl-molecules that are suitable against the Li-metal anode, which must be further explored. Additionally, cross-linked PEs find application in S‖Li cells owing to their capability to minimize polysulfide shuttling, which is one of the most notorious problems of such advanced battery systems. Apart from conventional free-radical polymerization reactions following Norrish type-I or a similar type of thermal polymerization mechanism, hydrogen abstraction by Norrish type-II initiators and click-chemistry (thiol–ene, thiol–epoxide, *etc.*) have also been increasingly employed recently for the *in situ* process. The *in situ* processing approach is highly advantageous from a futuristic and practical perspective as tailor-made components such as artificial PIS-SEIs or PIS-CEIs can be judiciously engineered. Such tailor-made interphases can also be important in futuristic and industry-friendly methods like the multi-layer processing of LPBs, where individual PE and artificial interphase layers can be designed according to the end application. Indeed, the free-radical polymerization reaction, which is well established and the *in situ* widely used in the coating industry, is highly suitable to realize the multi-layer processing of LPBs. In Tables 2–5, the key performance indicators of the important reports discussed in Sections 5.1–5.3 are all compiled and presented.

6. *In situ* polymerization by miscellaneous methods

In the thermal- and photo-assisted *in situ* polymerization process, an external free-radical initiator is inevitable to trigger the polymerization reaction unless hazardous high energy radiation such as γ-rays is used. Although present in tiny quantities, the residues of un-reacted free-radical initiators may incite undesirable effects on the cycling performance of the cell. Thus, there are attempts to carry out the *in situ* processing of PEs and related battery cells in the absence of additional substances such as initiators. Ionic polymerization methods such as cationic and anionic polymerization are the frontrunners in this respect.[470–473] Besides, *in situ* electropolymerization and condensation polymerization methods are also suitably employed to achieve similar results. One of the key advantages of these polymerization methods is that a variety of monomers such as epoxides, acrylates, methacrylates, allyl and vinyl ethers, azides, alcohols, carboxylates, and aldehydes can be used. Additionally, in many cases, these methods are also less sensitive to atmospheric conditions than free-radical polymerization. Besides, they are equally useful for producing artificial PIS-interphase-based surface protection as well. Recently, all these polymerization methods have gained a lot of attention and can be considered as potential competitors to the free-radical polymerization methods. In the following sections, the type of *in situ* process adopted (separator assisted, direct deposition, and surface
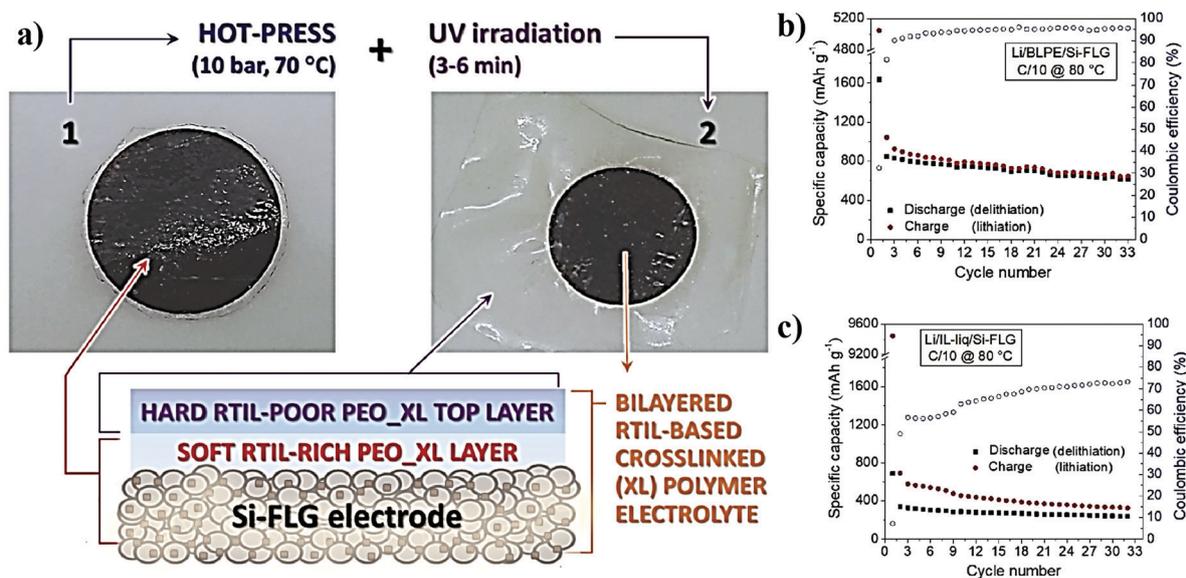
2746 | *Energy Environ. Sci.*, 2021, **14**, 2708–2788

This journal is © The Royal Society of Chemistry 2021

Fig. 29 (a) Digital images of the Si−FLG electode integrated with BLPE. A schematic illustration of the soft-PIS layer and the subsequent hard IGPE layer over the Si−FLG electrode is also shown. Electrochemical cycling performance of the (b) Si−FLG|BLPE|Li and (c) Si−FLG|RTIL|Li cell at 80 °C (reproduced/adapted from ref. 362 with permission from Elsevier, Copyright 2020.[362] Distributed under a Creative Commons Attribution-NonCommercial-NoDerivatives License International 4.0 (CC BY-NC-ND 4.0) (https://creativecommons.org/licenses/by-nc-nd/4.0/)).

protection approaches) is classified and highlighted wherever applicable.

6.1 Anionic polymerization

Anionic polymerization is one of the types of addition (chain-growth) polymerization in which the growing chain head that carries a negative charge is balanced by a counter cation.[475] Anionic polymerization is initiated by nucleophilic reagents (metal alkoxides, organolithium compounds, Grignard reagents, etc.).[476] A list of commonly used initiators for the anionic polymerization reaction is summarized in Fig. 30a.[469] Generally, the monomers employed in anionic addition polymerization are vinyl monomers with electron-withdrawing groups (e.g., MMA, acrylonitrile, 2-vinylpyridine, etc.) and conjugated monomers (styrene and 1,3-butadiene).[469] The types of monomers that can undergo the anionic polymerization reaction are also listed in Fig. 30b.[469] Anionic polymerization is often also called living polymerization as the propagation reaction continues without termination under suitable conditions.[477] Living polymerization facilitates the controlled construction of various polymer structures so that various types of well-defined copolymers such as block copolymers can be made by the sequential addition of different types of monomers. Anionic addition (co)polymerization is employed to produce industrially relevant polymers such as synthetic rubbers (styrene-butadiene rubbers, SBR), thermoplastic elastomers, and ABA triblock copolymers (e.g., polystyrene-b-polybutadiene-b-polystyrene, SBS). Additionally, the same technique can also be used for ring-opening polymerization (ROP) or popularly called anionic ROP (AROP) of cyclic monomers having high electrophilicity.[478] Heterocyclic compounds such as epoxides, episulfides and other cyclic compounds having carbonyl groups (lactones, cyclic carbonates, lactams, etc.) undergo a nucleophilic

attack by the initiators to undergo AROP. For example, the general mechanism of AROP of epoxides initiated by alkali metal alkoxides is presented in Fig. 31.[474] The reagents used and the initiating and propagating chains formed during the anionic polymerization reaction bear high basicity and nucleophilicity; thus, stringent experimental conditions are required. Hence, the presence of water and oxygen should be generally avoided, and an inert atmosphere (N_2, Ar, or a high vacuum) must be used to ensure high reproducibility depending on the type of initiators and monomers used. The types of monomers and their electrophilicity, initiators and their nucleophilicity or basicity, and reaction conditions (low temperature is preferred due to the high reactivity and stability issues of the initiators and propagating chains) influence the polymerization process. Besides, the stability, polarity, and melting point of the solvents are also crucial. The most commonly employed solvents for anionic polymerization include THF, diethyl ether, benzene, toluene, etc.[477,479,480]

The in situ processing of LBs has been carried out through the anionic polymerization strategy; however, research work in this direction is scarce. Hence, there is room for exploring the suitability of this technique for the in situ processing of PEs and PIS-interphase layers and related device fabrication. For example, cyanoacrylate monomers are one of the most studied for this purpose,[482–485] which provide several advantages such as the Lewis acid–base interaction of nitrile and acrylate groups with Li$^+$-ions leading to complete salt dissociation as well as increased ion transport.[486] In cyanoacrylates, the strong electron-withdrawing nitrile moiety is covalently linked to the unsaturated α-carbon atom of the acrylate group.[487] Therefore, the β-carbon becomes highly electrophilic, resulting in high-reactivity for cyanoacrylate monomers. Unlike the free-radical polymerization pathway in the presence of an external initiator and energy source, anionic

This journal is © The Royal Society of Chemistry 2021

Energy Environ. Sci., 2021, **14**, 2708–2788 | **2747**

Table 2 Summary of the in situ processing of LPBs using mono- and bi-functional acrylate/methacrylate and acrylate-free monomers/oligomers by the free-radical polymerization method

Acrylate/methacrylate	Plasticizer/salt/electrolyte/additive	Type of polymerization	Initiator	Ion transport properties (σ, T_{Li+}, etc.)	Cell	Operating voltage range	Capacity	Capacity retention	Ref.
Tetraethylene glycol diacrylate*	1.1 M LiPF$_6$/EC:PC:EMC:DEC	Thermal	BPO	6.34 mS cm^{-1} at 20 °C	LCO|GPE|graphite	3–4.2 V	57 mA h (0.5C, 20 °C)	90%, 40 cycles, 0.5C	385
PEGA*	1 M LiPF$_6$/EC:PC:EMC:DEC BBP	Thermal	BBP	6.2 mS cm^{-1} at RT	NMC|GPE|Li	2.8–4.4 V	164 mA h g^{-1} (0.2C, 20 °C)	—	363
PEGA*	1 M LiPF$_6$/EC:PC:EMC:DEC BBP	Thermal	BBP	6.2 mS cm^{-1} at RT	NMC|GPE|graphite	2.8–4.4 V	160 mA h g^{-1} (0.2C, 20 °C)	90%, 300 cycles, 0.5C	363
TEGDMA*	1 M LiPF$_6$/EC:DEC	Thermal	BPO	5.9 mS cm^{-1} at 20 °C	LCO|GPE|graphite (Pouch bag)	3–4.2 V	675 mA h (0.5C, 25 °C)	100%, 20 cycles, 0.5C	343
BDDA*	1 M LiPF$_6$/EC:EMC:DMC	Thermal	AIBN	3.2 mS cm^{-1} at 20 °C	LCO|GPE|MCMB (Pouch bag)	2.75–4.2 V	757 mA h, (0.5C, 20 °C)	85%, 300 cycles, 0.5C	392
MMA*	1 M LiPF$_6$/EC:DEC	γ-Irradiation	—	≈1 mS cm^{-1} at RT	LNC|GPE|graphite	3–4.2 V	145 mA h g^{-1} (0.2 mA cm^{-2}, RT)	85%, 20 cycles	331
PEGDMA*	1 M LiPF$_6$/EC:DEC, VC	Thermal	TAPP	≈1 mS cm^{-1} at 25 °C	LVO|GPE|Li	2–3.6 V	220 mA h g^{-1} (0.2C, RT)	>85%, 100 cycles	395
TPGDA supported on SiO$_2$,*	1 M LiPF$_6$/EC:EMC:DMC	Thermal	AIBN	1.74 mS cm^{-1} at RT	LFP|gel-PCE|Li	2.4–4.2 V	160 mA h g^{-1} (0.2C, 25 °C)	100%, 200 cycles, 0.2C	390
PMIT*	1 M LiBF$_4$/EC:DEC, FEC	Thermal	TAPP	1 mS cm^{-1} at RT	LCO|GPE|Li	3–4.2 V	134 mA h g^{-1} (0.2C, 25 °C)	90%, 50 cycles, 0.2C	428
MHBIm-TFSI, PEGDA*	0.5 M LiTFSI	Thermal	AIBN	1.3 mS cm^{-1} at 30 °C	LFP|IPN–GPE|Li	2.5–4 V	152 mA h g^{-1} (0.1C, 40 °C)	94%, 100 cycles, 0.1C	429
BEMA, PEGMEM$^\#$	LiTFSI/EC:DEC	UV	HMPP	—	V$_2$O$_5$|GPE|Li	2.5–3.8 V	130 mA h g^{-1} (1.5C, RT)	Stable over 500 cycles	354
BEMA, PEGMEM$^\#$	LiTFSI, PY$_{1201}$-TFSI, and PC	UV	HMPP	≈1 mS cm^{-1} at 25 °C	LFP|IGPE|Li	2.5–4 V	85 mA h g^{-1} (0.1C, RT)	Stable over 30 cycles	369
PEGMEM, PEGDMA$^\#$	LiMTFSI and PC	UV	HMPP	0.11 mS cm^{-1} and a T_{Li+} of 0.88 at 25 °C	LFP|SIC-PE|Li	2–4 V	126 mA h g^{-1} (0.1C, 25 °C)	98%, 100 cycles, 0.1C	370
BEMA with PEO$^\#$	LiTFSI	Thermal	AAPH	≈0.01 mS cm^{-1} at RT	LFP|SPE|Li	2.5–4 V	140 mA h g^{-1} (1C, 70 °C)	70%, 2000 cycles	342
BEMA$^\#$	LiTFSI and DPG	Thermal	AIBN	0.14 mS cm^{-1} at 20 °C and a T_{Li+} of 0.45	LFP|GPE|Li	2.4–4 V	130 mA h g^{-1} (0.1C, 25 °C)	36%, 300 cycles	396
EGPEA$^\#$	1 M LiPF$_6$/EC:PC:EMC	Thermal	AIBN	3.35 mS cm^{-1} at RT	NMC|GPE|Li	2.8–4.6 V	150 mA h g^{-1} (0.2C, 25 °C)	100%, 70 cycles	364
PEGDA, PETMP (thiol)$^\#$	LiTFSI	UV	DMPA	0.13 mS cm^{-1} at 60 °C	LFP|SPE|Li	2.8–3.8 V	139 mA h g^{-1} (0.1C, 60 °C)	81%, 200 cycles	388
PEGDA$^\$$	LiTFSI, LiBOB, and GN	UV	Irgacure 819	1 mS cm^{-1} at 30 °C	LFP|PCPE|Li	2.5–3.9 V	138 mA h g^{-1} (0.2C, 30 °C)	86%, 370 cycles	361

*Separator assisted. $^\#$Direct deposition. $^\$$Multi-layer approach.

2748 | Energy Environ. Sci., 2021, 14, 2708–2788

This journal is © The Royal Society of Chemistry 2021

Table 3 Summary of the *in situ* processing of LPBs using multi-functional acrylate/methacrylate monomers/oligomers by the free-radical polymerization method

Acrylate/ methacrylate	Electrolyte/ additive/ plasticizer	Initiator	Type of polymerization	Ionic conductivity	Cell	Operating voltage range	Capacity	Capacity retention	Ref.
TMPTMA*	1 M LiPF6 in EC:EMC:DMC	LPO	Thermal	>1 mS cm^{-1} at 25 °C	LCO|GPE| graphite	3–4.2 V	129 mA h g^{-1}, (0.2C, 25 °C)	≈100%, 100 cycles, 2C	412
TMPTA*	LiTFSI in PC, PEGDME	AIBN	Thermal	≈0.3 mS cm^{-1} at 25 °C	LFP|GPE|Li	2.5–4.2 V	≈150 mA h g^{-1} (1C, RT)	≈100%, 100 cycles, 2C	411
ETPTA, HDDA#	1 M LiTFSI in Pyr$_{13}$-TFSI	HMPP	UV	1.1 mS cm^{-1} at RT	LFP|IGPE|Li	2–4.2 V	≈100–120 mA h g^{-1} (0.2C, RT)	100%, 50 cycles, 0.2C	269
PETEA*	1 M LiPF$_6$ in EC:DEC:EMC	AIBN	Thermal	8.5 mS cm^{-1} at 25 °C	NCA|GPE| graphite	2.75–4.5 V	1.88 A h (5C, 25 °C)	92.5%, 200 cycles, 5C	417
PETEA*	1 M LiTFSI in 1,2-DOL:DME, LiNO$_3$	AIBN	Thermal	11 mS cm^{-1} at 25 °C	S|GPE|Li	1.7–2.8 V	601 mA h g^{-1} (1C, 25 °C)	82%, 400 cycles, 0.5C	418
PETEA*	1 M LiTFSI in 1,2-DOL:DME, LiNO$_3$	AIBN	Thermal	1 mS cm^{-1} at 25 °C	S|GPE|Li	1.7–2.8 V	486 mA h g^{-1} at 5C and 25 °C	83%, 500 cycles, 0.3C	419

* Separator assisted. # Direct deposition.

Table 4 Summary of the *in situ* processing of LPBs using hetero-functional acrylate/methacrylate monomers/oligomers by the free-radical polymerization method

Acrylate/ methacrylate	Electrolyte/ salt/additive	Initiator	Type of polymerization	Ion transport properties (σ, T_{Li^+} etc.)	Cell	Operating voltage range	Capacity	Capacity retention	Ref.
Siloxane acrylate*	1 M LiClO$_4$ in EC:DMC (1:1)	TBPP	Thermal	1.3 mS cm^{-1} at RT	LCO|GPE|MCMB	2.8–4.2 V	137 mA h g^{-1} (0.5C, RT)	84%, 100 cycles, 0.5C	437
TAEP*	1 M LiClO$_4$ in EC:DMC (1:1)	TBPP	Thermal	0.2–0.5 mS cm^{-1} at RT	LCO|GPE|MCMB	2.8–4.2 V	122 mA h g^{-1} (0.5C, RT)	95%, 250 cycles, 0.5C	438
FTGA*	1 M LiClO$_4$ in EC:DMC (1:1)	TBPP	Thermal	0.56 mS cm^{-1} at RT	LCO|GPE|MCMB	2.8–4.2 V	142 mA h g^{-1} (0.5C, RT)	89%, 200 cycles, 0.5C	439
Boron containing methacrylates*	1 M LiTFSI in EC:DMC (1:1)	AIBN	Thermal	0.084 mS cm^{-1} at 30 °C with a T_{Li^+} of 0.76	LFP|GPE|Li	2.5–4 V	118 mA h g^{-1} (0.5C, 30 °C)	90%, 400 cycles, 0.5C	366

* Separator assisted.

Table 5 Summary of the *in situ* processing of LPBs using acrylate/methacrylate-free monomers/oligomers by the free-radical polymerization method

Acrylate- or methacrylate-free molecule	Electrolyte/ salt	Initiator	Type of polymerization	Ionic conductivity	Cell	Operating voltage range	Capacity	Capacity retention	Ref.
PAEC#	LiTFSI	DMPA	UV	0.0004 mS cm^{-1} at 25 °C	V$_2$O$_5$|SPE|Li	2–4 V	—	—	445
Allyl PEO, allyl gallic acid, BPT (thiol)#	LiTFSI	BPO	UV	0.4 mS cm^{-1} at 60 °C	LFP|SPE|Li	2.5–4.2 V	150 mA h g^{-1} (0.1C, 60 °C)	88%, 50 cycles, 0.1C	453
Tetraglyme, PEO#	LiTFSI	MBP	UV	>0.1 mS cm^{-1} at 25 °C	TiO$_2$|SPE|Li	1–3 V	140 mA h g^{-1} (0.1 mA cm^{-2}, 20 °C)	Stable >100 cycles, 0.1 mA cm^{-2}	375
VC*	LiDFOB	AIBN	Thermal	0.022 mS cm^{-1} at 25 °C	LCO|SPE|Li	2.5–4.3 V	146 mA h g^{-1} (0.1C, 50 °C)	84%, 150 cycles, 0.1C	443
VC*	1 M LiDFOB in EC:DEC	AIBN	Thermal	0.56 mS cm^{-1} at 25 °C	LFMP|GPE| graphite	2.5–4.35 V	120 mA h g^{-1} (1C, 25 °C)	89%, 1000 cycles, 1C	444

* Separator assisted. # Direct deposition.

polymerization is energy efficient and can be carried out even at ambient temperature. Moreover, a lower polymerization activation energy and long-living active center are added advantages.

The anionic polymerization of the ethyl cyanoacrylate (ECA) monomer initiated by Li-metal (see Fig. 32a) is a novel approach for LMPB fabrication and also for Li-metal surface protection by the *in situ* process.[481] Transfer of electrons from the Li-metal to the unsaturated double bond results in the generation of anionic active species to initiate the polymerization reaction. For instance, a precursor composed of 1 mL ECA, 3 mL of 4 M LiClO$_4$ in

This journal is © The Royal Society of Chemistry 2021

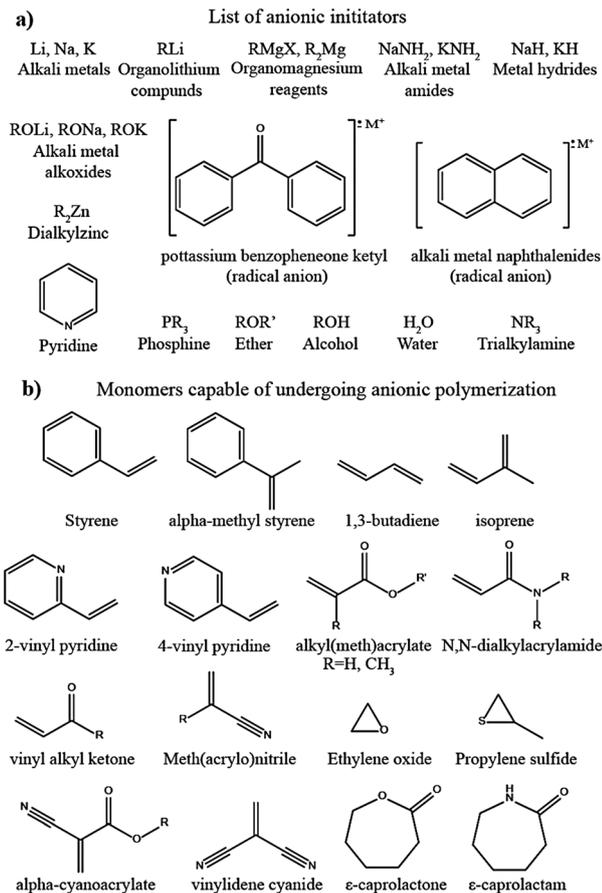Energy Environ. Sci., 2021, **14**, 2708–2788 | 2749

Fig. 30 (a) List of commonly used species that can initiate the anionic polymerization reaction; and (b) list of monomers capable of undergoing the anionic polymerization reaction.[469]
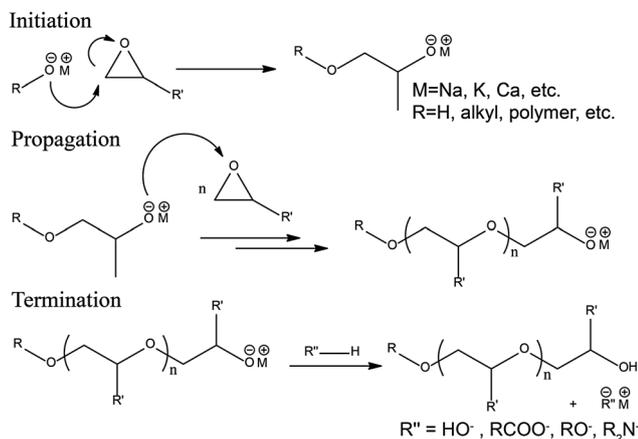

Fig. 31 Steps involved in the AROP reaction mechanism of epoxides initiated by alkali-metal alkoxides (reproduced/adapted from ref. 474 with permission from Elsevier, Copyright 2013[474]).

EC:DMC, and 100 ppm of Li-powder (acts as the initiator) was employed by Cui *et al.* for the preparation of a GPE. Most importantly, the GPE could be formed in 2 h in the absence of external catalysts, initiators, or energy sources such as light or heat, unlike the conventional free-radical polymerization methods.
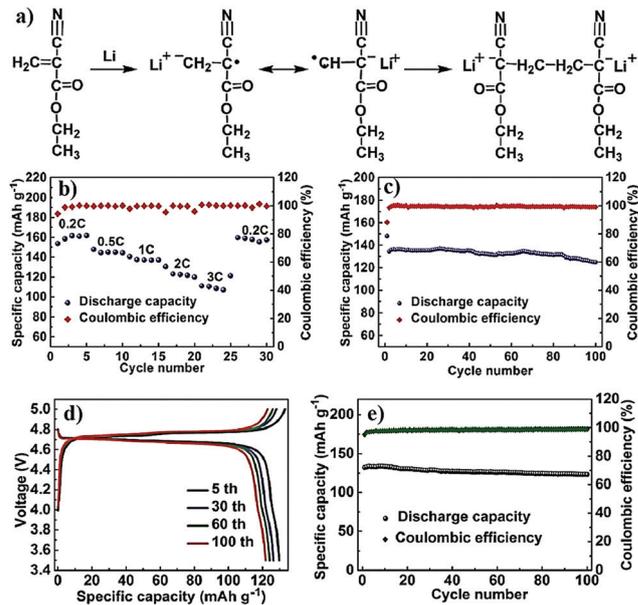

Fig. 32 (a) The anionic polymerization mechanism involved in the conversion of ECA to PECA is initiated by Li-metal. In the first step, the transfer of an electron from Li-metal to the unsaturated double bond in ECA occurs, resulting in the generation of an active anionic species. This anionic species further propagates the polymerization of ECA. (b) and (c) present the specific capacity values at different C-rates and the cycling stability profile of the LFP|PECA-GPE|Li cell, respectively, at RT. (d) and (e) present the galvanostatic charge–discharge and cycling stability profiles of the LNMO|PECA-GPE|Li cells, respectively, at RT (reproduced/adapted from ref. 481 with permission from American Chemical Society, Copyright 2017[481]).

It is worth noting that a nonfluorinated salt, such as $LiClO_4$, is used as the Li^+-ion source since the HF and PF_5 impurities from $LiPF_6$ can terminate the active anionic center. The GPE film, when prepared alone, could display an ionic conductivity of 2.7 mS cm^{-1} (RT), with a T_{Li^+} of 0.48, and an oxidative stability value of 4.8 V *vs.* Li|Li$^+$. Finally, an LMPB is *in situ* processed by the direct deposition approach over the composite cathode film. The low viscosity ECA can easily penetrate the deeper regions of the cathode composite, which is otherwise not possible with the *ex situ* processed GPE film. The *in situ* processed LFP|PECA–GPE|Li cell delivers a discharge capacity of 140 mA h g^{-1} (1C) with a retention of 90% (100 cycles) [Fig. 32b and c]. Additionally, a high voltage LNMO|PECA–GPE|Li cell is also assembled, which exhibits a discharge capacity of 122 mA h g^{-1} (1C) with a retention of 93% (100 cycles) [Fig. 32d and e]. In another report, the ECA monomer is explored to protect the surface of a high-voltage LNMO cathode by the formation of a PIS-CEI.[346] It is shown that the *in situ* polymerized conformal coating (10 nm) of the PECA-based PIS-CEI could reduce the dissolution of the multivalent cations owing to the strong interactions with the N and O atoms of the cyano-ester moieties present in the PECA (Fig. 33a). This is reflected in the high cycling stability of PECA-coated LNMO (92% retention after 100 cycles) as compared to that of the non-coated counterpart (72% retention after 100 cycles) [Fig. 33b and c].

Similarly, the *in situ* processed PECA-based artificial PIS-SEI layer on the Li-metal surface is found to inhibit the inhomogeneous
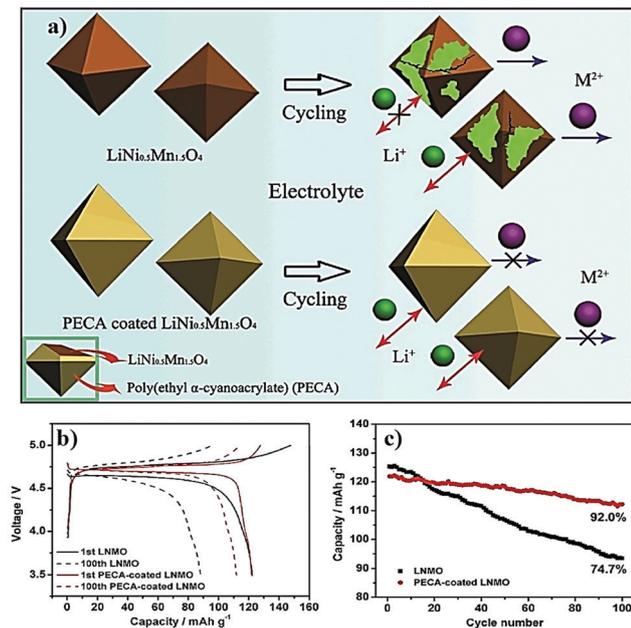
2750 | *Energy Environ. Sci.*, 2021, **14**, 2708–2788

This journal is © The Royal Society of Chemistry 2021

Fig. 33 (a) The influence of a conformal coating of a PECA-based PIS-CEI layer over the LNMO cathode preventing the multivalent ion leaching into the electrolyte; and (b) galvanostatic charge–discharge profile, and (c) cycling stability profiles of the pristine and artificial PIS-CEI coated LNMO cathode-based LB cell (LNMO|LE|Li) (reproduced/adapted from ref. 346 with permission from Elsevier, Copyright 2017[346]).

deposition/dissolution of Li-metal.[488] This tailor-made surface protection can also be employed for improving the electrochemical behavior of the Li-metal anode even in a conventional LE-based LMB (LE-LMB). In a typical procedure, the precursor is prepared in acetone with ECA (ECA/acetone = 1 : 5) and $LiNO_3$ salt (0.1 M relative to acetone). This solution is applied over Li-metal, where the anionic polymerization at RT is initiated by LiOH present on the Li-metal surface (Fig. 34a). Hence, such anionic polymerization reactions can also be considered as a scavenging process in which the polymerization process removes the unwanted LiOH from the surface of the lithium metal. LE-LMB (LFP|LE|Li) cells are fabricated, where the LE has a composition of 1 M $LiPF_6$ in EC:DMC. The LE-LMB cell delivers a specific capacity of 150 mA h g^{-1} (2C) with 100% capacity retention (500 cycles). The isolation effect by the PECA layer ensures a low polarizing voltage, a lower consumption of Li-metal through minimized side reactions, and a homogenous distribution of Li^+-ion flux that suppresses the corrosion/pitting of the anode. The cycling performance of the PECA-based cell is superior to the PECA-free counterpart. Moreover, the high mechanical stability of PECA (Young's modulus of 25 GPa) is an added advantage, which can accommodate even the volume changes in the electrode. The effect of the PECA coating for facilitating the suppression of dendrite growth is illustrated in Fig. 34b, and the superiority of such a layer over the Li-metal surface of an LFP|LE|Li cell is also evident in the electrochemical cycling profiles presented in Fig. 34c.

There are also attempts to make LMPBs smarter using the *in situ* anionic polymerization method. For instance, thermal
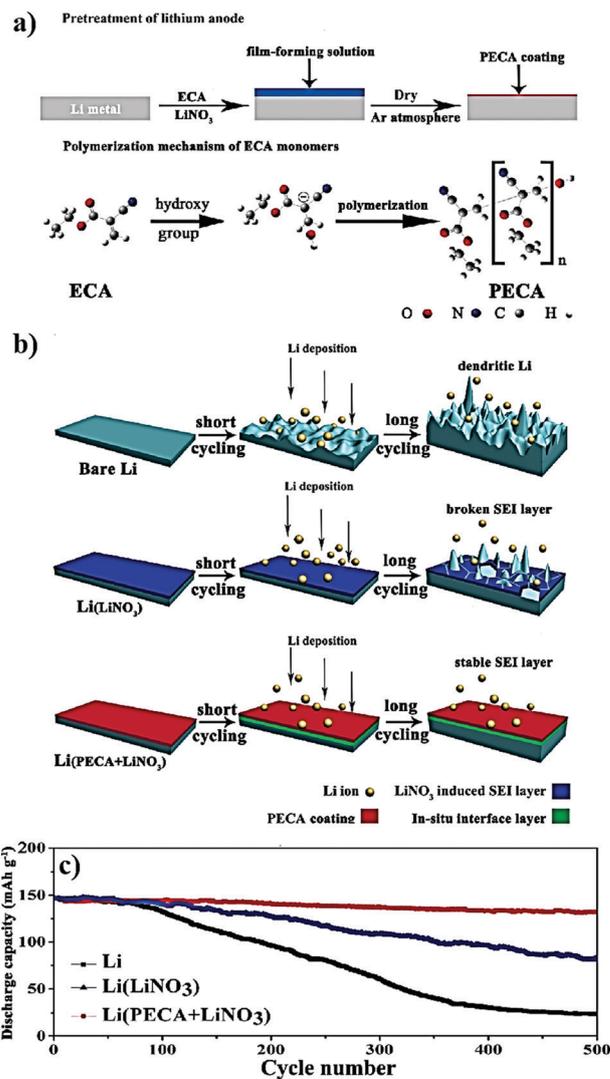

Fig. 34 (a) Schematic representation of the pre-treatment of Li-metal by the ECA monomer to form an artificial PIS-SEI layer-based surface coating. The polymerization mechanism of ECA over the Li-metal surface, which is assisted by hydroxyl groups over Li-metal, is also depicted. (b) The bare Li-metal undergoes side reactions with the electrolyte, and dendrite growth starts within a few cycles. In the case of the $LiNO_3$ coated Li-metal surface in the absence of a PECA coating, a non-polymeric SEI is formed, which is stable and prevents HSAL growth in the earlier cycles. However, the non-polymeric SEI breaks during prolonged cycling. Later, the *in situ* processed PECA-$LiNO_3$ (PIS-SEI) layer over the Li-metal surface effectively prevents HSAL growth even after a high number of charge–discharge cycles, imparting high cycling stability. (c) Cycling profiles depicting the advantage of the PECA coating imparting high stability over the PECA non-coated counterparts (reproduced/adapted from ref. 488 with permission from American Chemical Society, Copyright 2017[488]).

runaway is one of the failure mechanisms of LBs, where the temperature inside the cell is increased because of exothermic reactions. The heat generated inside the cell due to the thermal runaway reaction often leads to destructive developments such as explosion or fire. There can be several reasons for the thermal runaway reaction, which include short-circuit, overcharging, HSAL growth, damaged cell components, or even a

failure in the battery management system (BMS). In an LB stack, the thermal runaway can be catastrophic as the failure of even a single cell can propel a cascade of reactions, and the resulting exponential increase in temperature causes a complete loss of the battery system. The initiator-free polymerization approach of VC to poly-VC in the presence of LiI is used as a tool for triggering the thermal shutdown of the LMPB cell by sensing any potential failure due to thermal runaway (Fig. 35a).[489] This work can be considered as an example of the *in situ* process for injecting smartness into the battery, where the separator assisted approach is employed. Here, LiI plays multiple roles as a catalyst for the ring-opening polymerization of VC and a Li^+-ion source in the resulting GPE. Thermal curing at 80 °C for 1 h is required for the VC to poly-VC conversion. Indeed, the authors claim that the polymerization of VC occurs through the formation of lithium iodoalkoxide, which is a byproduct formed during the decarboxylation of VC by iodide (I^-) ions during the initiation step. The mechanism of the polymerization reaction, as claimed by the authors, is provided in Fig. 35b. Although the GPE displayed an ionic conductivity of 1.8 mS cm^{-1} (25 °C), the oxidative stability is limited by the presence of iodide ions in the electrolyte (3.5 V vs. Li|Li$^+$). Therefore, LiI induced anionic polymerization is not suitable for high-voltage applications; nevertheless, the functioning of an LTO|GPE|Li cell (LMPB cell) cycling (RT) between 1 and 2 V is demonstrated, which retains 50% of the initial specific capacity (75 mA h g^{-1}) after 700 cycles. It should be noted that the conversion of VC to poly-VC is not complete in the GPE so that further polymerization would still be possible during the operation of the cell. Consequently, when the operating temperature of the battery cell is increased to 80 °C, a drastic increase in the electrolyte resistance by a factor of 10^3 is observed, indicating complete polymerization, which converts the GPE to a highly resistive SPE (Fig. 35e). Hence, the cell undergoes a self-shutdown mode due to the extremely high internal resistance incited by the SPE in line with the concept of imparting smartness to batteries. The self-shut down is evident from the charge–discharge profile presented in Fig. 35c, where the increase in temperature from 25 to 80 °C leads to cell failure, and corresponding cycling data is provided in Fig. 35d. This work opens up new opportunities with the *in situ* polymerization processing strategies to realize safer batteries with inbuilt sensing and safety mechanisms.

6.2 Cationic polymerization

Cationic polymerization is also an addition (chain-growth) polymerization, in which the growing chain head is carrying a positive charge balanced by a counter anion.[490] Cationic addition polymerization (CAP) is usually applied for vinyl monomers with electron-donating groups in the presence of an electrophilic agent acting as the initiator (*e.g.*, Brønsted acids: $HClO_4$ and CF_3SO_3H, Lewis acids: BF_3 and $SnCl_4$, and carbenium ions: trityl and tropylium).[491] Lewis acids alone or along with another protonogen (water or alcohol) or a cationogen (alkyl halides) can also be used for the *in situ* formation of strong protonic acids (high pK_a value) and subsequent initiation of cationic
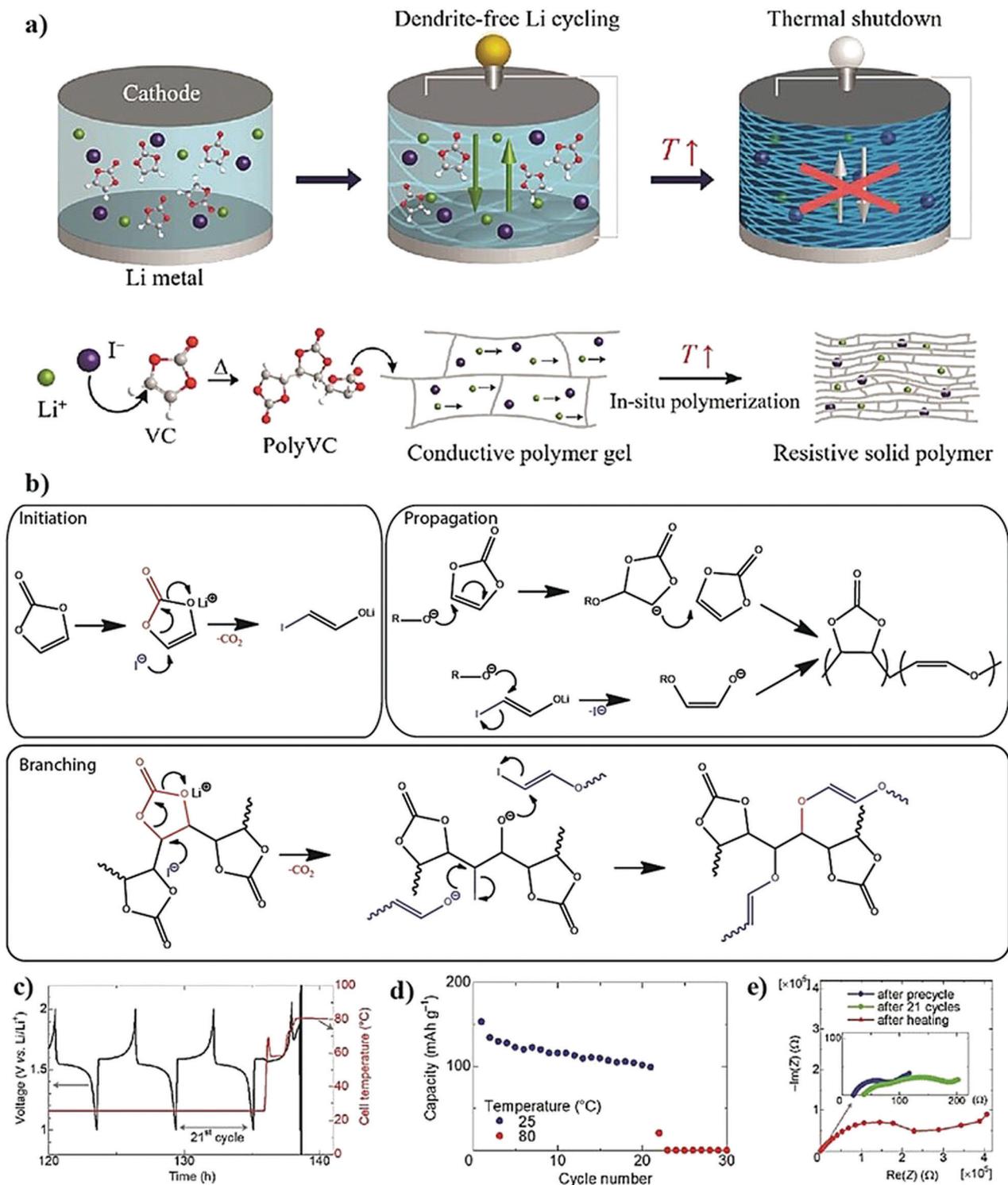
polymerization. In this case, the cation donor and the Lewis acid species are called the initiator and co-initiator, respectively.[492] For instance, a Lewis acid such as BF_3 with water forms an ideal initiating system such as $H^+(BF_3OH)^-$. A few of the typical vinyl monomers that are used for cationic polymerization are listed in Fig. 36a.[490] Cationic polymerization is often used to produce industrially important polymers such as polyisobutylene (PIB), butyl rubber, and poly(vinyl ethers) (PVEs).[491,493]

The cationic polymerization mechanism of a vinyl monomer initiated by a typical protic acid is presented in Fig. 36b (A in the chemical structure represents an H atom).[490] The reaction starts with an electrophilic addition of a proton onto the electron-rich alkene to produce a carbocation (sp^2-hybridized) with a counter anion balancing the charge. The initiating species undergoes further continuous addition of monomers (propagation reaction) to form a long polymeric chain. The propagating reaction follows a chain-growth mechanism. The stability of the carbocation is very important in cationic polymerization, which depends upon the type of initiator used or the anion formed during the initiation process. Besides, the choice of solvent is also very critical in CAP due to the tendency of the system to undergo side reactions such as termination and chain transfer. The polymerization reaction is favored in polar solvents; hence, aliphatic, aromatic, and halogenated hydrocarbons are widely employed as suitable solvents. However, alcohols, water, and other basic solvents (*e.g.*, esters, ethers, *etc.*) should be avoided as they promote unwanted side reactions. Due to the higher sensitivity of cationic polymerization reactions, stringent reaction conditions should be employed.

ROP can also be carried out using a cationic polymerization pathway, and such processes are called cationic ring-opening polymerization or simply CROP. The few heterocyclic monomers that can be polymerized through the CROP process are listed in Fig. 37a.[494–496] As an example, the CROP mechanism of an oxetane monomer in the presence of a protic acid is also illustrated in Fig. 37b.[497] The solvent, reaction conditions, and initiators used for CROP are similar to the CAP reaction. It is worth noting that CROP generally occurs through an SN1 or SN2 mechanism,[497] and in many cases (for THF and oxetane) CROP also achieves a living character (no termination). Hence, it can also be used for producing structurally well-defined polymers.[498] The following section covers the *in situ* processing of LPB cells using cationic polymerization.

Hwang *et al.* reported the separator assisted approach for LMPB (LCO|GPE|Li) fabrication using a GPE derived from a divinyl ether oligomer by CAP.[499] The homogenous precursor solution is composed of a bi-functional oligomer [tri(ethylene glycol) divinyl ether, TEGDVE], LE (1 M LiBETI in EC:DEC), and additional $LiBF_4$ salt. The polymerization is carried out at RT, where $LiBF_4$ plays multiple roles as a cationic initiator and a conducting Li-salt. Compared to other reports using acidic initiators such as protic acids, Lewis acids, or a mixture of both, in this work, the generation of $H^+BF_4^-$ from $LiBF_4$ initiates the polymerization reaction. The general mechanism of the polymerization of a (di)vinyl ether oligomer is presented in Fig. 38a. Any harmful effects due to the addition of external acidic initiators or

2752 | *Energy Environ. Sci.*, 2021, **14**, 2708–2788

This journal is © The Royal Society of Chemistry 2021

Fig. 35 (a) Schematic representation of an LMPB cell with a poly-VC-based GPE featuring a thermal shut-down mechanism at elevated temperatures. When the operating temperature is raised to 80 °C, the complete polymerization of VC occurs, leading to the formation of an SPE, which is highly resistive. This triggers the cell shutdown. (b) The mechanism of VC to poly-VC conversion initiated by the attack of I⁻ at the double bond of VC generating lithium iodoalkoxide, which further propagates the polymerization and branching. (c) and (d) present the galvanostatic charge–discharge profile and cycling stability, respectively, as a function of the increase in temperature. The cell failure at the 22nd cycle as the temperature is increased to 80 °C is evident. (e) The change in the Nyquist plot representing the increase in resistance when raising the temperature of the cell to 80 °C compared to that of a pre-cycled cell and after 21 cycles at 25 °C (reproduced/adapted from ref. 489 with permission from The Royal Society of Chemistry[489]).

This journal is © The Royal Society of Chemistry 2021

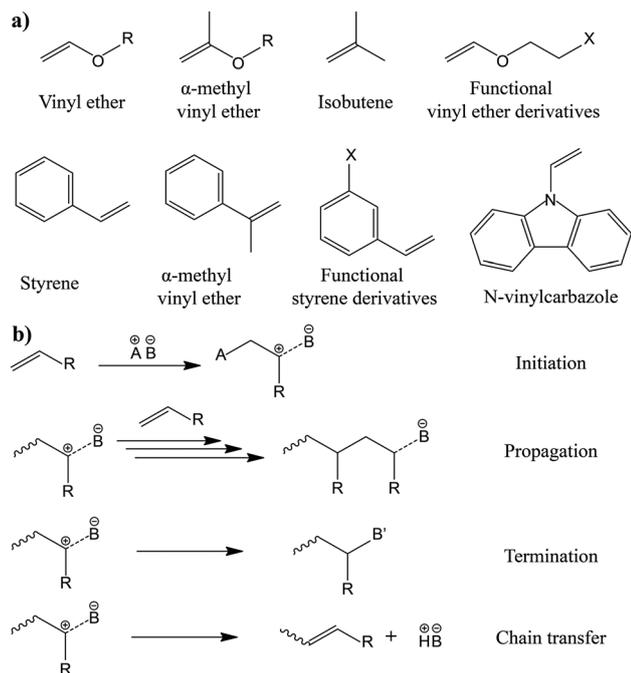*Energy Environ. Sci.*, 2021, **14**, 2708–2788 | **2753**

Fig. 36 (a) A few examples of vinyl monomers that can undergo cationic polymerization; and (b) the mechanism of polymerization of vinyl monomers in the presence of a typical protic acid (A = H).[490]

nonhomogeneous polymerization are also avoided as the LiBF$_4$ salt is homogenously dissolved in the precursor and hence called

external initiator-free polymerization. The prepared GPE possesses an ionic conductivity of ≈ 1 mS cm^{-1} (at 30 °C) with high oxidative stability (5 V *vs.* Li|Li$^+$). The assembled LMPB cell displayed a discharge capacity of 150 mA h g^{-1} (15 mA g^{-1}).

Kang *et al.* reported a separator assisted approach for preparing a cross-linked GPE and fabrication of an LIPB cell using a precursor containing a cyanoethyl polyvinyl alcohol (PVA-CN)-based functional monomer. According to the authors, even in this case, a Lewis acid-based initiator (PF$_5$) is *in situ* generated during the thermal decomposition of LiPF$_6$ salt present in the precursor.[500] The formed PF$_5$ reacts with a trace amount of water present in the precursor (2 wt% PVA-CN dissolved in 1 M LiPF$_6$ in EC:DMC:EMC), generating the protic acid H$^+$(PF$_5$OH)$^-$, which in turn initiates the cationic gelation process. However, the decomposition of LiPF$_6$ salt is a concern in LIBs. The side products formed such as PF$_5$ and POF$_3$ are hazardous, and some of these reactions in the presence of water create HF, which is unfavorable for achieving long-term cyclability. Additionally, the presence of HF can further catalyze many side reactions, including the degradation of high voltage cathodes such as NMC. Hence, a suitable salt system must be selected for initiating the polymerization reaction. A plausible polymerization mechanism for PVA-CN polymerization is provided in Fig. 38b. Herein, LIPB pouch cells (LCO|GPE|graphite) with a total capacity of 2100 mA h are assembled by two different techniques using separator assisted *in situ* processing using cationic polymerization of PVA-CN: (*technology 1*) gelation before the battery formation cycle, and (*technology 2*) gelation
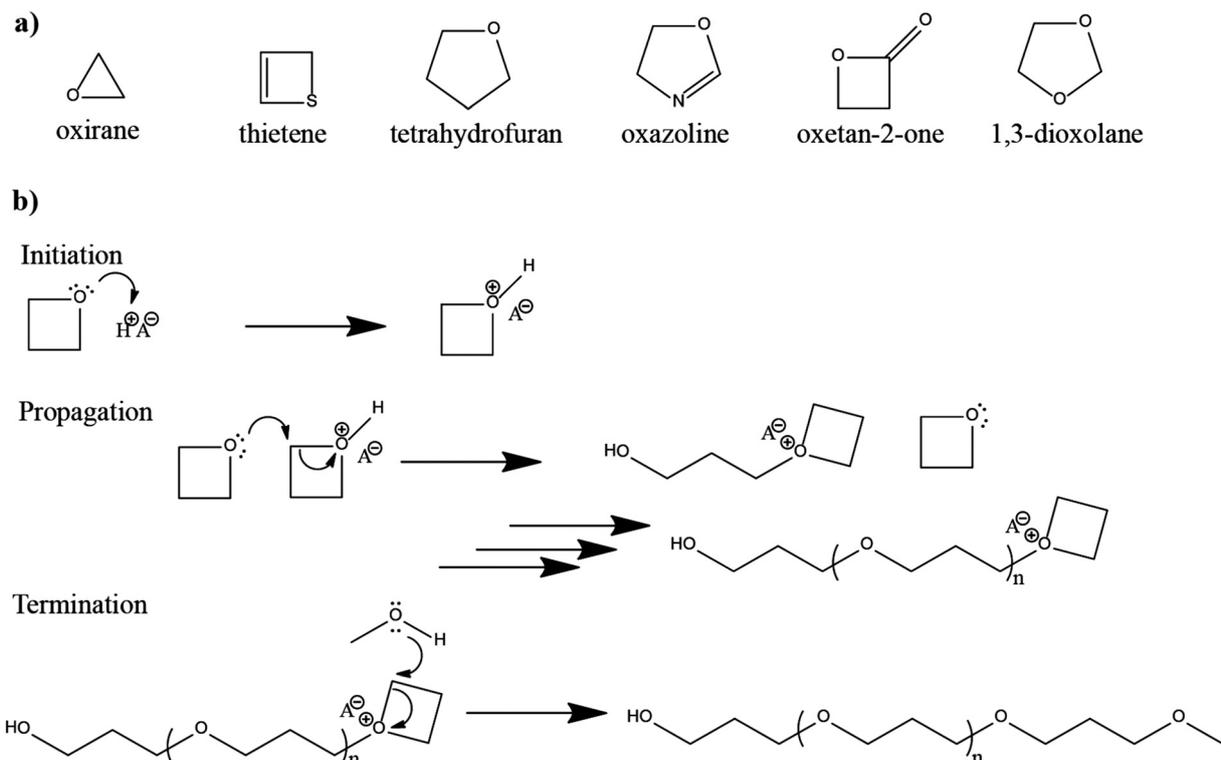

Fig. 37 (a) A few examples of the cyclic monomers that can undergo the CROP reaction; and (b) general mechanism involved in the CROP reaction of the oxetane molecule. Epoxide and tetrahydrofuran molecules can also undergo CROP reactions in a similar fashion.[497]

2754 | *Energy Environ. Sci.*, 2021, **14**, 2708–2788

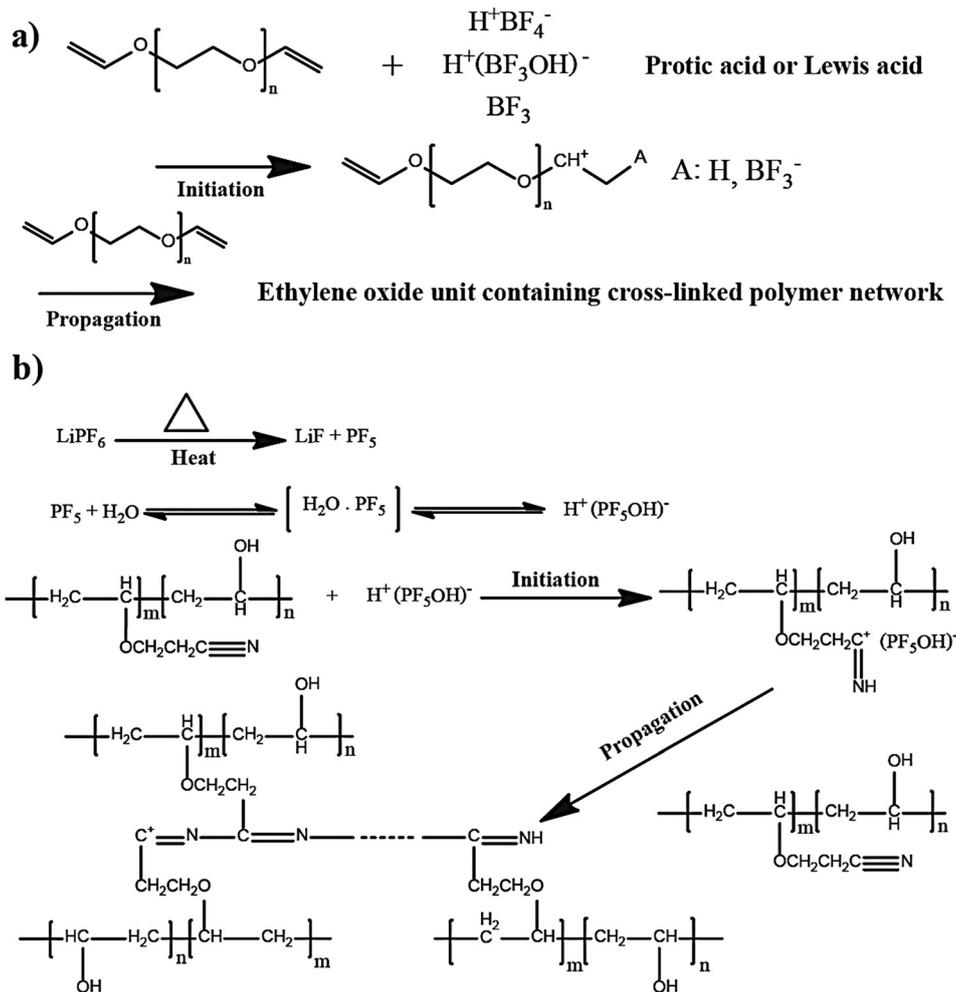This journal is © The Royal Society of Chemistry 2021

Fig. 38 (a) Mechanism of cationic polymerization of the divinyl ether monomer (reproduced/adapted from ref. 499 with permission from Elsevier, Copyright 2010[499]); and (b) polymerization mechanism of PVA-CN initiated by $H^+(PF_5OH)^-$ (reproduced/adapted from ref. 500 with permission from The Royal Society of Chemistry[500]).

after the battery formation cycle (see Fig. 39a).[500] The LIPB cell prepared using *technology 1* exhibited a low total discharge capacity of 1939 mA h (0.2C) [Fig. 39b and c] due to the poorly performing highly resistive interphase layer at the GPE|graphite interface. Besides, near to the surface of the electrode, trapped bubbles are also observed, which results in bad interfacial contact. In the LIPB cell fabricated using *technology 2*, a bubble-free electrode|electrolyte interface with a higher capacity of 2086 mA h is obtained, close to that of an LE-based LIB. In another report from the same group, plastic crystals (succinonitrile, SN) are also incorporated into the precursor along with PVA-CN and LiPF$_6$ (Fig. 40a).[501] SN is a commonly used plastic crystal in the preparation of PEs, which improves the ionic conductivity owing to its high polarity.[502,503] Herein, the GPE (PCPE) (namely, SEN) exhibits a high ionic conductivity of 2.32 mS cm^{-1} (25 °C) along with an overall broad oxidative stability value (5 V *vs.* Li|Li$^+$). Interestingly, the SEN also showed a T_{Li^+} of 0.57 and activation energy of 0.04eV, which are good values for any GPEs. Finally, the *in situ* processed LMPB cell (LFP|SEN|Li) displayed an initial discharge capacity of 154.8 mA h g^{-1} (0.1C) with a good capacity retention of 96.7% (100 cycles).

In a recent report, synthesis of a cross-linked poly(ethylene glycol) diglycidyl ether (PEGDE)-based SPE by the CROP pathway is used for LMPB cell fabrication.[504] The epoxy ring in the PEGDGE is opened by the *in situ* generated cationic initiator species $[H^+(BF_3OH)^-]$. According to the authors, disproportionation of LiDFOB salt at 80 °C produces the Lewis acid BF$_3$, which reacts with trace amounts of water to form the protic acid, $H^+(BF_3OH)^-$. A monomer to polymer conversion of 90% is achieved, and the reported polymerization mechanism is presented in Fig. 40b. According to the report, other salts such as LiClO$_4$, LiBF$_4$, and LiPF$_6$ can also undergo a similar kind of initiation process. The cellulose reinforced SPE (C-PEGDE) exhibits an ionic conductivity of 0.089 mS cm^{-1} at ambient temperature with an oxidative stability value of 4.5 V *vs.* Li|Li$^+$. The LMPB cell (LFP|C-PEGDE|Li) is prepared by a separator assisted approach in which a homogenous precursor (1.25 wt% LiDFOB and 20 wt% LiTFSI in PEGDGE) is injected into the cellulose paper inside the test cell and cured at 80 °C (4 h). The reversible capacities of the LMPB cell at RT are about 115 mA h g^{-1} (0.1C), and, after 100 cycles, 74% of the initial specific capacity is also retained. In a recent

This journal is © The Royal Society of Chemistry 2021

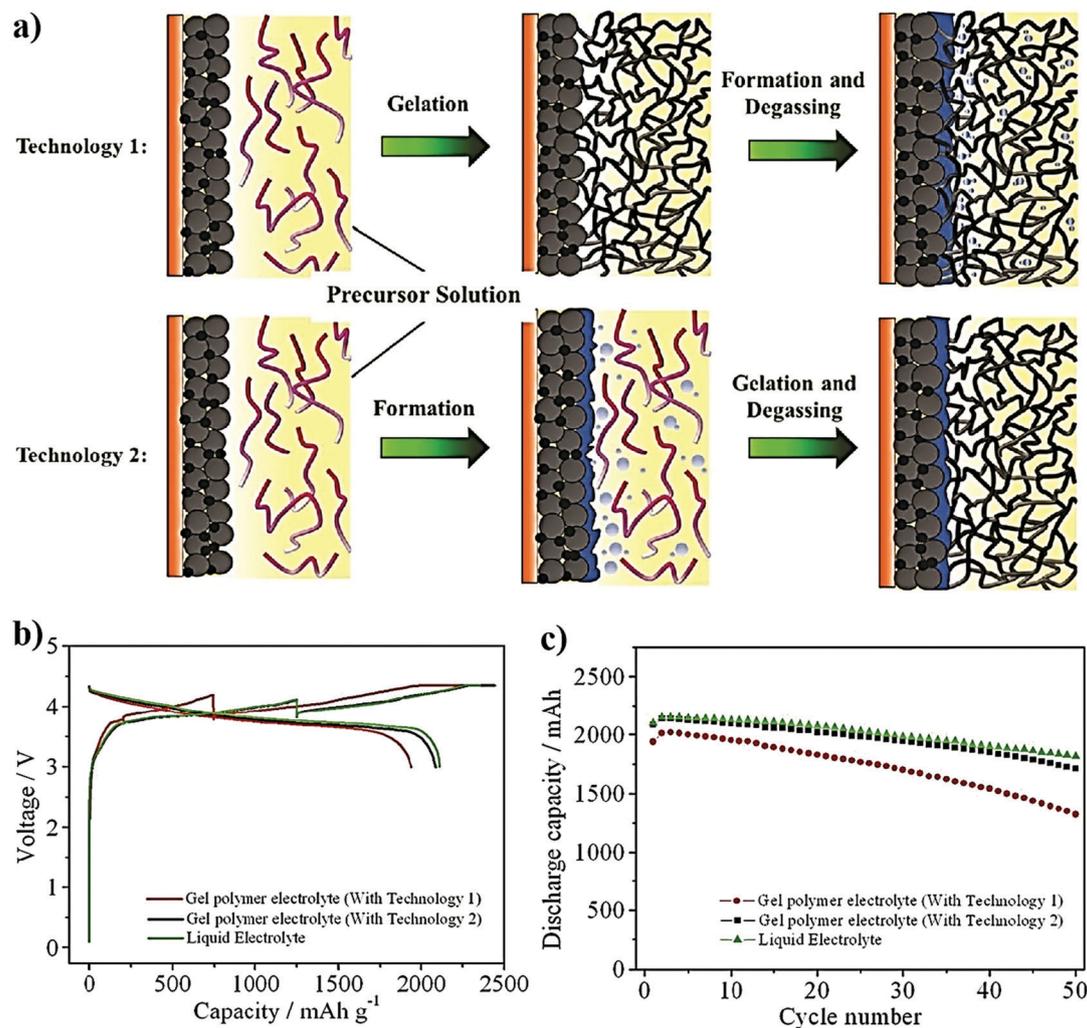*Energy Environ. Sci.*, 2021, **14**, 2708–2788 | **2755**

Fig. 39 (a) The difference between *technology 1* and *2* is schematically represented. *Technology 1* involves GPE preparation by the *in situ* process before the formation cycle of the battery cell, whereas *technology 2* is after the formation cycle. (b) and (c) present the improved electrochemical performance of the LIPB cell using *technique 2*, which is comparable to the LE-based cell (reproduced/adapted from ref. 500 with permission from The Royal Society of Chemistry[500]).

report, Nair *et al.* have proposed a different mechanism for the CROP of the diglycidyl ether oligomer that can be used for the *in situ* processing of SPE-based LPBs by a separator assisted or a separator-free approach.[505] The reported mechanism is shown in Fig. 40c, which demonstrates that the anions, in combination with a trace amount of water molecules, can initiate the CROP polymerization without decomposing into BF_3OH and HF. This mechanism can also explain the capability of other Li-salts such as $LiClO_4$ and LiFSI in initiating the CROP of cyclic ethers. The optimized SPE membrane with LiTFSI and $LiBF_4$ also showed an ionic conductivity of 0.1 mS cm^{-1} (30 °C) and oxidative stability above 4.8 V *vs.* Li|Li$^+$ due to the passivation behavior of BF_4^- anions during the oxidation process. Additionally, they have also demonstrated the electrochemical cycling performance of the cross-linked SPE in high-voltage NMC111 $(LiNi_{0.33}Mn_{0.33}Co_{0.33}O_2)$ cathode-based LMPB cells, and the resulting specific capacity of the cell at different current rates is presented in Fig. 40d.

A more ingenious method for realizing an artificial PIS-CEI is introduced by combining both free-radical and cationic polymerization processes for the fabrication of high-voltage LNMO cathode-based LPB cells.[347] Here, two precursors (A and B) are prepared in which solution A is composed of 30 wt% MMA and 10 wt% acrylic anhydride dissolved in 1 M $LiPF_6$ in EC:DEC. Solution B contains 2-methyl-acrylic acid-2-oxirane-ethyl ester (MAEOE, 3.0 wt%) and an AIBN initiator (1 wt%) with the remaining fraction being methyl ethylene carbonate (MEC). On mixing solutions A and B, both CROP of MAEOE and heat-induced free-radical polymerization (50 °C) of MMA, MAEOE, and acrylic anhydride occur concurrently (Fig. 41a). The $LiPF_6$ in the electrolyte reacts with trace amounts of water to form the cationic initiator species $H^+(PF_5OH)^-$, to initiate the CROP.[506,507] The cross-linked GPE (PAMM) is formed after 6 h, which displays good ionic conductivity (0.67 mS cm^{-1}, RT) and high oxidative stability (5 V *vs.* Li|Li$^+$). Indeed, the *in situ* processing of LPB cells is carried out by a separator assisted approach displayed an

2756 | *Energy Environ. Sci.*, 2021, **14**, 2708–2788

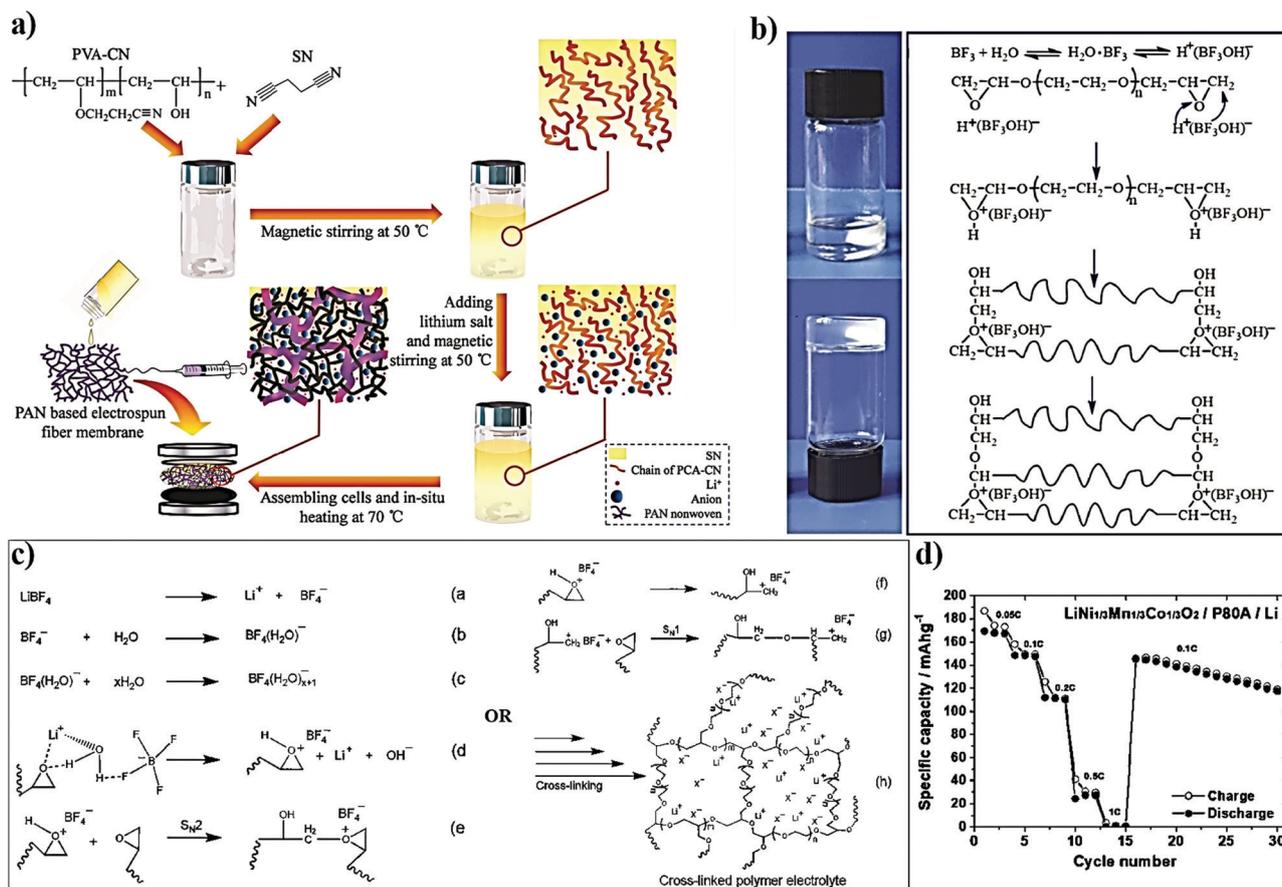This journal is © The Royal Society of Chemistry 2021

Fig. 40 (a) Scheme depicting the synthesis of SEN (PCPE) by cationic polymerization of PVA–CN followed by the *in situ* fabrication of the LMPB cell by the separator assisted approach (reproduced/adapted from ref. 501 with permission from John Wiley and Sons, Copyright 2015[501]). (b) Cationic polymerization mechanism involved in the polymerization of diglycydyl ether (PEGDE). The cationic initiator species is H$^+$(BF$_3$OH)$^-$ formed by the reaction of BF$_3$ with trace water present in the reaction mixture (reproduced/adapted from ref. 504 with permission from John Wiley and Sons, Copyright 2017[504] Distributed under a Creative Commons Attribution License International 4.0 (CC BY 4.0) (https://creativecommons.org/licenses/by/4.0/)). (c) New mechanism suggested by Nair *et al.* for the CROP of the diglycydyl ether oligomer leading to an SPE and fabrication of LMPB cells by the *in situ* process. Here, it is proven that the anions in combination with water can initiate the polymerization without decomposing into BF$_3$OH and HF. (d) presents the electrochemical performance of the *in situ* processed (direct deposition) LMPB cell (NMC111|SPE|Li) at 60 °C (reproduced/adapted from ref. 505 with permission from American Chemical Society, Copyright 2019[505]).

excellent cycling performance at RT and 55 °C due to the PAMM-based polymeric interphase (indeed, a PIS-CEI) layer formed over the LNMO cathode. The PIS-CEI created over the LNMO cathode helps minimize Mn^{2+} ion dissolution, hence increasing the lifespan of the cell.[508,509] A schematic representation of the role of PAMM in preventing Mn^{2+} dissolution compared to the PIS-CEI formed from the linear PMMA is given in Fig. 41b. The interaction of multivalent ions such as Mn^{2+} and Ni^{2+} with the anhydride group within the PAMM-based PIS-CEI layer is claimed to be the reason for the stabilization of the cathode, resulting in improved electrochemical performance. A GPE from a siloxane epoxide cross-linker and poly(2-vinylpyridine-co-styrene) (PVS) is also reported to be initiated by the *in situ* formed H$^+$(PF$_5$OH)$^-$ species.[510] Here, it is reported that the GPE with 99 wt% LE delivers an extremely high ionic conductivity value of 11 mS cm^{-1} (30 °C) with large oxidative stability (5.2 V *vs.* Li|Li$^+$). However, the extremely high LE content present in the GPE is a drawback for high-temperature applications and for achieving thinner packaging.

Finally, it has been demonstrated that the separator assisted and *in situ* processed GPE-based LIPB cell (LCO|GPE|graphite) delivers a discharge capacity of 133.2 mA h g^{-1} at 0.1C (30 °C).

The latest advancement in the cationic assisted *in situ* polymerization process is converting a traditional LE to a GPE/SPE. Liu *et al.* recently conceived this approach for the fabrication of GPE-based LMPBs. Here, an ether-based LE (1,3-dioxolane, 1,3-DOL) is *in situ* polymerized using a separator assisted approach at ambient temperature in the presence of LiPF$_6$ salt through a CROP pathway (1,2-dimethoxyethane, DME is used as a solvent).[511] The mechanism can be explained as the ROP of 1,3-DOL assisted by the *in situ* generated H$^+$(PF$_5$OH)$^-$ species (Fig. 42a). Optical images of the liquid and GPEs are also shown in Fig. 42b. The 1,3-DOL molecule undergoes fast protonation to form oxonium ions followed by a ring-opening process, which can further attack more 1,3-DOL to propagate the polymerization reaction, achieving long polymer chains. The monomer to polymer conversion rate for 1,3-DOL is as high as 91%.
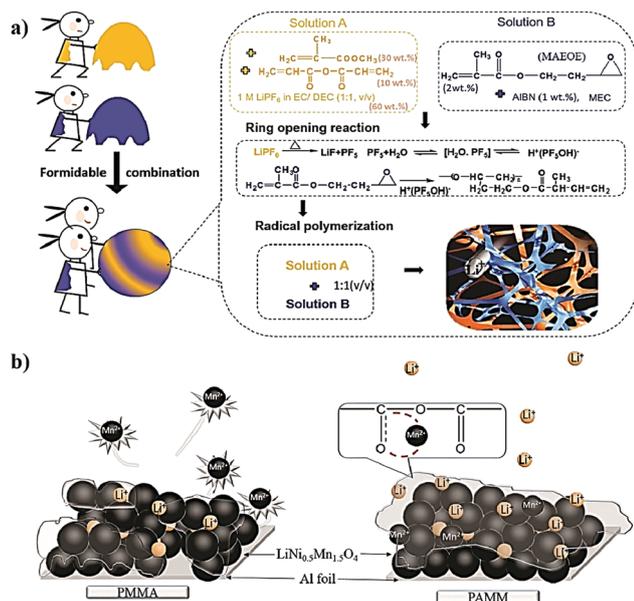
This journal is © The Royal Society of Chemistry 2021

Energy Environ. Sci., 2021, **14**, 2708–2788 | **2757**

Fig. 41 (a) Combining both free-radical and cationic pathways as a potential strategy for the *in situ* processing of LB cells; and (b) the proposed mechanism depicting the suppression of Mn^{2+} dissolution owing to the formation of $O=C-O-M$ (M = Mn, Ni) species in the PAMM-based PIS-CEI, which is absent in the PMMA-based PIS-CEI (reproduced/adapted from ref. 347 with permission from American Chemical Society, Copyright 2017[347]).

It is observed that the number average molecular weight (M_n) of the resulting polymers reaches $\approx 52\,000$ Da when the LE-mixture can react for 10 h. Indeed, the resulting GPE delivers an RT ionic conductivity of 3.8 mS cm^{-1}. Compared to LEs, this GPE in a Li‖Li symmetric cell exhibits a significantly lower overpotential for the lithium plating/stripping process for prolonged cycling. The volume-changes and HSAL formation at the Li-metal surface are also minimized with the reported GPE. The adaptability of this method for the fabrication of LMPBs with various cathode materials such as LFP, NMC622, and sulfur has been demonstrated (Fig. 42c), which illustrates the overall good cycling performance using the *in situ* fabricated GPE-based cells. The SEM image of the S cathode before and after the GPE coating is shown in Fig. 42d and e, respectively. Indeed, the *in situ* confinement of the GPE is found to restrict the free diffusion of polysulfides, thus reducing the shuttling effect. At 0.5C, the S|GPE|Li cell delivers a discharge capacity of 1010 mA h g^{-1} by retaining 50% of the initial value after 500 cycles (Fig. 42f). Hence, 1,3-DOL to poly-DOL conversion inside the LB cell is indeed an excellent approach to improve the overall cycling performance of S‖Li cells.

In the recent work by Zhao *et al.*, 1,3-DOL is converted to an SPE by CROP, followed by the separator assisted approach used for LMPB fabrication (Fig. 43a).[334] In this work, the role of aluminum triflate ($Al(OTf)_3$) salt as an electrolyte additive is proved to initiate the CROP reaction. The cationic aluminum species attacked by the oxygen atom of 1,3-DOL initiates ROP, producing poly-DOL with an M_n of 15000 Da (Fig. 43b). The ionic conductivity of the SPE is as high as 1 mS cm^{-1} (RT), which surpasses typical SPEs. However, the authors mention

that the high RT ionic conductivity could be due to the unpolymerized 1,3-DOL or oligomers entangled within the poly-DOL matrix, which is clear from the lower ionic conductivity of 0.1 mS cm^{-1} obtained for the SPEs with a higher concentration of $Al(OTf)_3$. Therefore, the poly-DOL formation should be judiciously controlled so that an optimum molecular weight of the polymer is obtained. The optimized poly-DOL-based SPE displays oxidative stability over 5 V *vs.* $Li|Li^+$ and stable lithium plating/stripping over 200 h (areal capacity = 1 mA h cm^{-2}). The morphology of the Li-metal anode after plating/stripping analysis in the case of the LE and SPE is presented in Fig. 43c and d, respectively. The smooth surface morphology of the plated Li for an SPE underlines the better interfacial properties achieved by the SPE over the LE. The authors reported three types of LMPB cells (S|SPE|Li, NMC622|SPE|Li, and LFP|SPE|Li) that are prepared and fully characterized at RT. In the case of the S|SPE|Li cell, the polysulfide shuttling is reduced, and the cell displays 98% Coulombic efficiency even after 100 cycles (at 0.1C), which is indicating the role of the *in situ* process in suppressing the side reactions. The charge–discharge profile of the S|SPE|Li cell at different current rates is provided in Fig. 43e. Similarly, the LFP and NMC622 cathode-based separator assisted *in situ* fabricated LMPB cells also show superior performance to their respective LE counterparts. Hence, from these examples, it can be summarized that the *in situ* processing of LPBs using the CROP reaction is an important approach for producing pure and long-lasting PEs, and more focused research in this direction will increase further opportunities.

6.3 Condensation polymerization

Condensation polymerization is a type of step-growth polymerization between bi-functional or multi-functional monomers to form larger polymeric chains by releasing byproducts, such as water or alcohol.[512] Contrary to chain-growth (addition) polymerization, in a condensation polymerization or step-growth polymerization, most of the monomers are consumed in the early stages of the reaction to form low molecular weight chains (short), which after a large number of steps react further to form a high molecular weight chain by the end of the reaction. When both reagents are bi-functional, the obtained polymer is linear, whereas, if at least one of the reactants or monomers is tri- or tetra-functional, then a cross-linked polymer is obtained. Esterification of carboxylic acids with alcohol is a suitable example of a condensation polymerization reaction. The industrially known polymers produced by condensation polymerization are polyesters (polyethylene terephthalate, PET), urethanes, and polyamides (Nylon 6). The type of monomers, number of functionalities per molecule, polymerization temperature, solvent type, side product formed, *etc.* largely influence the condensation polymerization reaction and the resulting characteristics of the polymer. In fact, the final molecular weight of the synthesized polymer is regulated by maintaining an equilibrium concentration between the reactants and byproducts.[512] Indeed, the polymerization termination reaction can be carried out by adding one of the reactants in excess or by adding a mono-functional molecule bearing one of the functionalities that are used to produce the polymer. This way, the
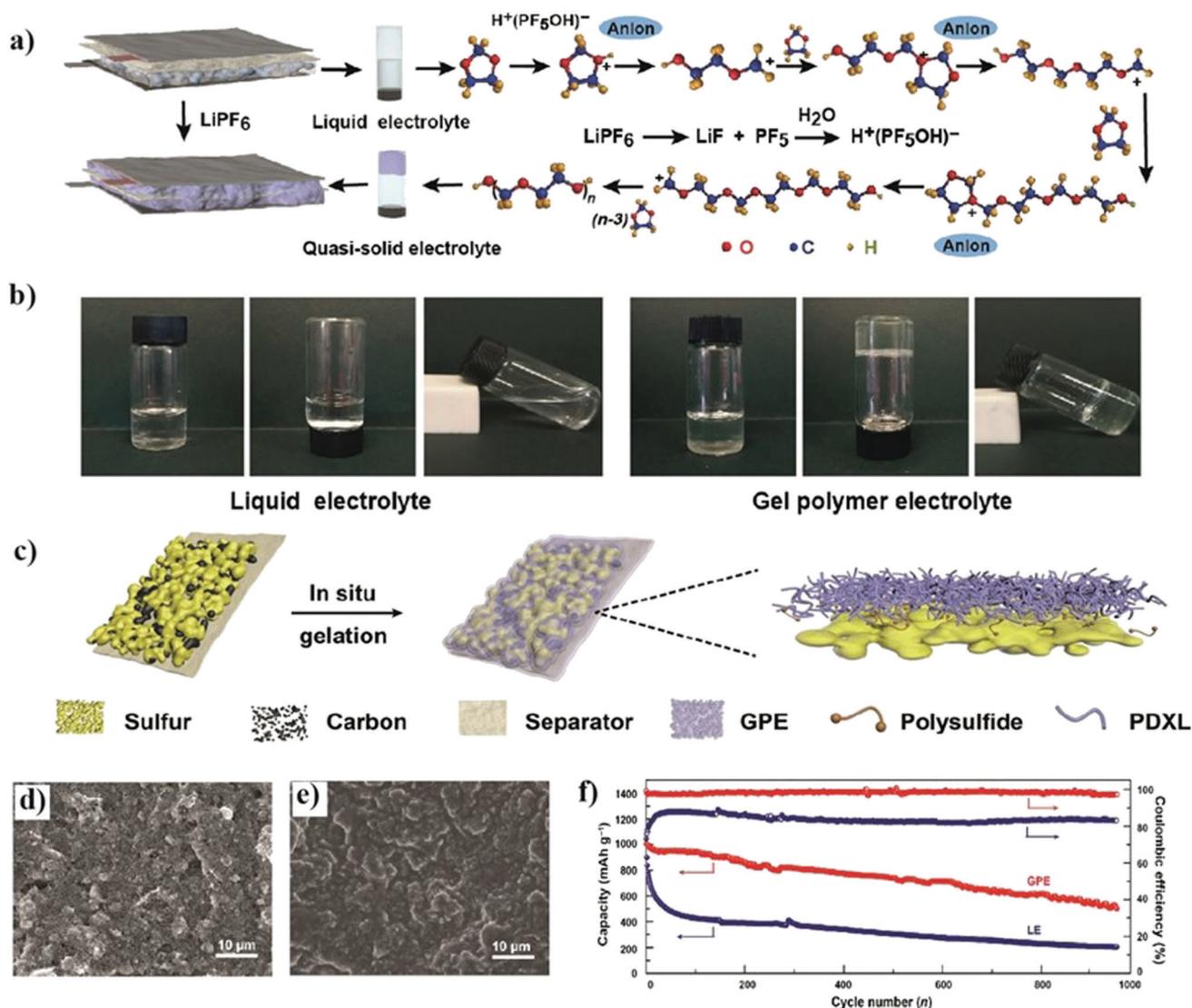
Fig. 42 (a) The mechanism of cationic polymerization of the 1,3-DOL solvent to a GPE initiated by $H^+(PF_5OH)^-$ species at ambient temperature; (b) the photographs presenting the 1,3-DOL-based LE before and after polymerization; (c) the schematic representation of the *in situ* processed 1,3-DOL-based GPE supported by a porous separator over the S cathode inside the LB cell; the SEM images of the surface of the S cathode (d) before and (e) after GPE coating; and (f) cycling performance and Coulombic efficiency comparison of the *in situ* processed S|GPE|Li and S|LE|Li battery cells. The GPE performs better than the LE due to the reduced polysulfide shuttling between the anode and cathode.[511] (Reprinted/Adapted from Reference 511. © The Authors, some rights reserved; exclusive licensee AAAS. Distributed under a Creative Commons Attribution NonCommercial License 4.0 (CC BY-NC) http:// creativecommons.org/licenses/by-nc/4.0/.)

average molecular weight and the cross-linking density can be controlled by selecting the reactant with appropriate type and number of functionalities of each monomer and their concentration. Due to the formation of side products such as water and alcohol, a direct deposition approach or *in situ* cell fabrication inside the cell pack of an LMPB/LIPB is a real challenge. However, there have been recent and encouraging reports, which demonstrate the improved performance of LB cells that employ PIS layers produced using the condensation polymerization process. For example, in the context of the *in situ* process, condensation polymerization has been adopted for the surface protection of cathode films by an artificial PIS-interphase in several reports.[513] Recent advancements in polymer systems

such as covalent organic frameworks (COFs) heavily depend on the condensation reaction, which can have potential applications in PEs as well as *in situ* cell fabrication process.[209,514–516]

Polymer-based artificial surface coatings (PIS-interphases) realized by condensation polymerization over high voltage cathodes are found to improve the cycling performance of LIBs.[348,349,517,518] In many reports, a polyimide (PI)-based surface layer is prepared by thermally assisted condensation polymerization from a precursor of a four component polyamic acid solution. The polyamic acid solution consists of pyromellitic dianhydride, biphenyl dianhydride, phenylenediamine, and oxydianiline. This solution is first introduced into the electrode slurry and then subjected to a five-step thermal curing process to initiate the imidization
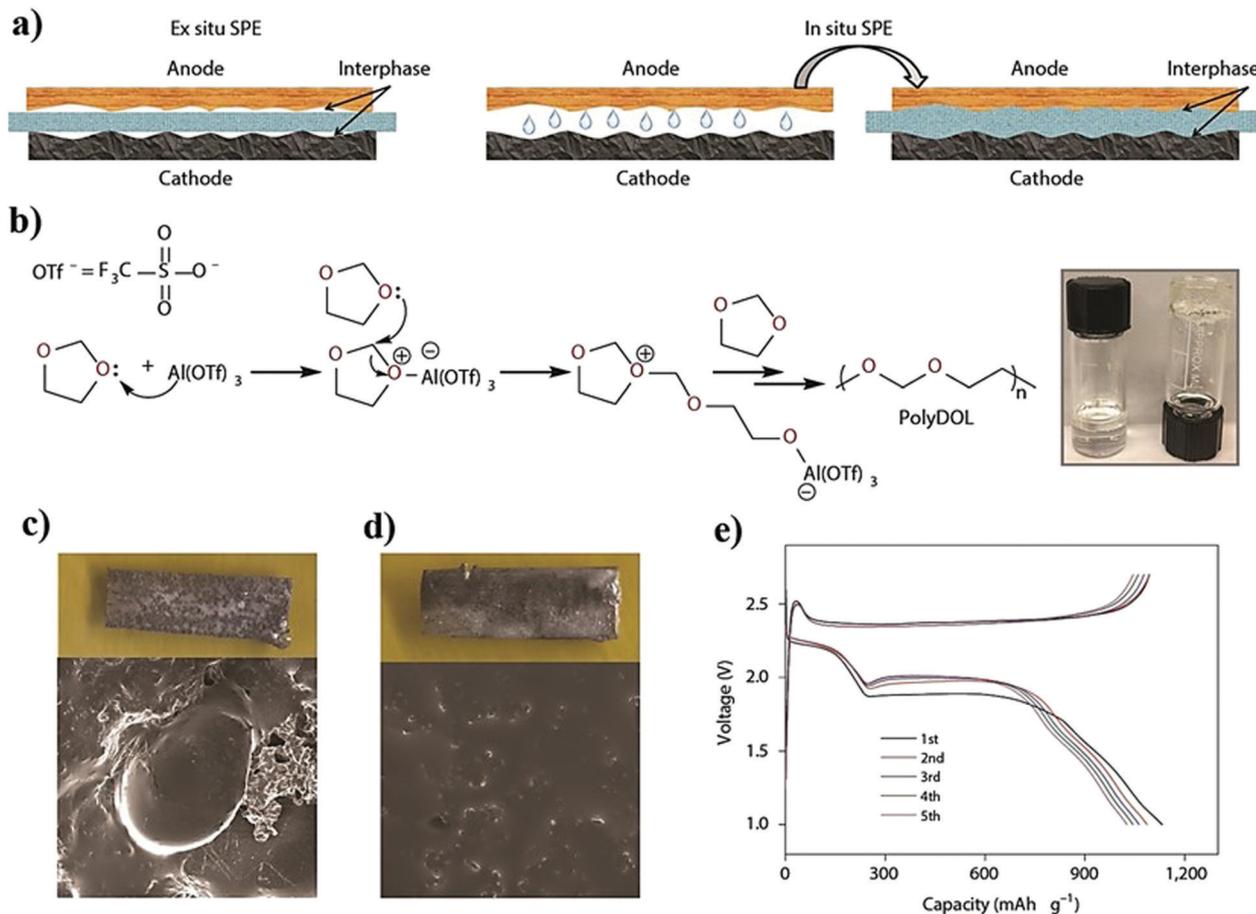
This journal is © The Royal Society of Chemistry 2021

Energy Environ. Sci., 2021, **14**, 2708–2788 | **2759**

Fig. 43 (a) Self-explanatory scheme illustrating the electrode|electrolyte interface in the *ex situ* and *in situ* processed SPE-based LB. (b) CROP mechanism for 1,3-DOL initiated by Al(OTf)$_3$. The optical photographs of 1,3-DOL LE and the formed SPE are also presented. The SEM images showing the morphology of the plated Li in the case of the (c) LE and (d) SPE. (e) The galvanostatic charge−discharge profile of the S|SPE|Li cell at RT (reproduced/adapted from ref. 334 with permission from Springer Nature, Copyright 2019[334]).

process (Fig. 44a).[518] During the operation of the battery cell, when the cathode is in contact with the LE, the PI-layer functions as an artificial PIS-CEI by protecting the cathode particles from any direct attack by the LE components, thus suppressing the undesired interfacial side reactions. This method was later successfully extended to several other high-voltage cathodes such as LCO, NMC111, and LNMO, and improved overall performance has been demonstrated.

In a report, a 10 nm thick layer of a PI-based PIS-CEI was *in situ* generated over an LCO cathode for LIB fabrication by a similar condensation polymerization reaction. The performance of the LIB cell is compared against a pristine LCO counterpart.[348,349] The separately prepared self-standing PI film swollen in the LE (1 M LiPF$_6$ in EC: EMC) exhibited an ionic conductivity of 0.15 mS cm^{-1} (RT). When the PI-coated LIB (LCO|LE|graphite) cell is cycled between 3 and 4.4 V, the cell delivered a specific capacity of 160 mA h g^{-1} (at 0.5C) with a capacity retention of 76% even after 100 cycles. In contrast, the specific capacity of PI-free cells dropped to 38% under the same conditions. It is observed that the PI coating with an average thickness of 10 nm imparts a well-balanced enhancement of the cell performance

and related thermal stability of the final LIB cell. However, as the coating thickness of PI is increased, the discharge capability (C-rate) of the cells is compromised due to an undesired rise in the overall ionic and electronic resistance at the interphase. The PI-based PIS-CEI layer is reported to reduce exothermic side reactions, which underlines the efficacy of the thermally stabilized electrode|electrolyte interface and interphase (Fig. 44b).[518] Fig. 44c and d present the SEM images of the pristine and PI-coated NMC-111 electrodes, respectively. The 10 nm thick conformal surface coating of PI over NMC111 is evident from Fig. 44e; additionally, Fig. 44f confirms the superiority of the electrochemical performance of the PI-coated LIB (NMC111|LE|graphite) cell against a PI non-coated NMC111 electrode-based LIB cell. The authors have also attempted to produce a composite of PI and carbon black to modify the LCO surface, which results in improved electrical conductivity of the surface coating by providing high rate capability during the long-term galvanostatic charge–discharge cycling.[519] Similarly, PI coated (10 nm thick) high-voltage spinel LNMO cathodes are used for the fabrication of LIB cells and cycled at RT (3.5–5 V) and 55 °C (3.5–4.9 V).[520] At RT, both the pristine and PI-LNMO based cells

2760 | *Energy Environ. Sci.*, 2021, **14**, 2708–2788

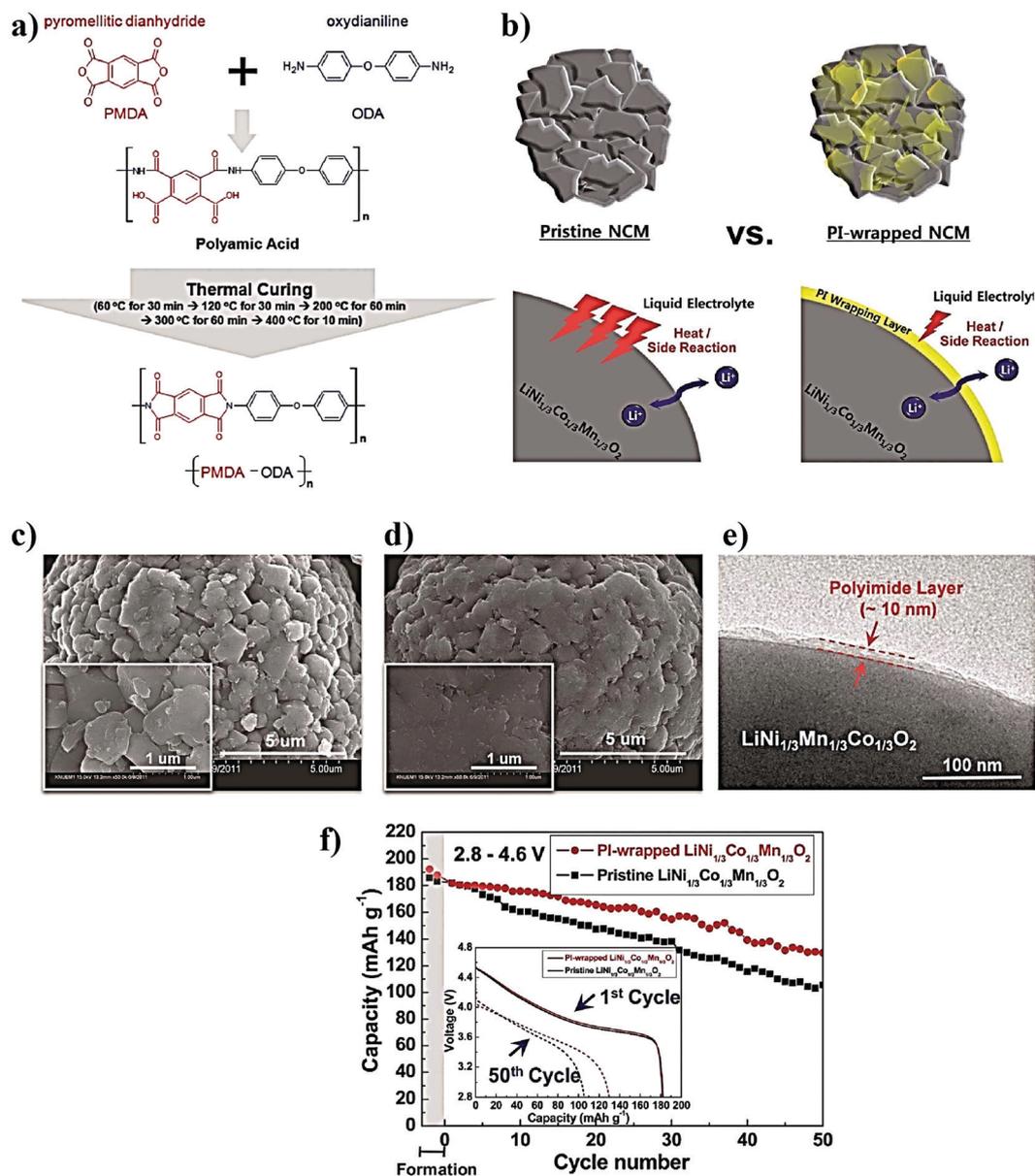This journal is © The Royal Society of Chemistry 2021

Fig. 44   (a) Chemical structures of the four components in the precursor solution used for the *in situ* processing of the polyimide (PI)-based artificial PIS-CEI over the cathode by condensation polymerization. (b) Schematic illustration of a PI-wrapped NMC111 cathode. The role of the PI coating in suppressing the unwanted side reactions as well as heat generation is also depicted. SEM images of the (c) pristine and (d) PI-coated NMC111 cathode. (e) The 10 nm thick coating of a PIS-CEI layer over NMC111. (f) The superior electrochemical performance of the PI-coated NMC111-based cell over the non-coated counterpart (reproduced/adapted from ref. 518 with permission from The Royal Society of Chemistry[518]).

exhibited almost similar cycling performance. However, at 55 °C, the cycling behavior of PI-LNMO (98% retention, 50 cycles) is far superior to the pristine-uncoated (83% retention, 50 cycles) counterpart. Apart from reducing interfacial exothermic reactions between the charged LNMO and the LE, the PI coating prevents Mn^{2+} dissolution from LNMO. The same method is adopted for high-voltage vanadium doped LNMO cathodes, and exciting characteristics similar to the above materials are also demonstrated.[521] In conclusion, all the aforementioned reports suggest that the PI-based PIS-CEI layer synergistically contributes to enhanced cycling performance. It can also be elucidated that the coating of electrode

particles by judiciously selected monomers by condensation polymerization can be an alternative approach over the existing costly and difficult to upscale processes such as pyrolysis, atomic layer coating, or even sputtering techniques.

6.4   Electropolymerization

A polymerization process in which a thin polymer film is formed from a monomer solution onto an electronically conducting substrate is called electropolymerization. It is usually employed in applications such as surface protection, electrode coating, electrocatalysis, electrogenerated chemiluminescence (ECL),

electrochemical sensors, and electrode material preparation for energy storage and conversion devices (*e.g.*, batteries, super-capacitors, solar cells, fuel cells, *etc.*).[522–525] Dall'Olio *et al.*, in 1968, reported the first example of an oxidative electropolymerization process to produce polypyrrole in water.[526,527] Later in the 1980s, the reductive electropolymerization of vinyl-substituted molecules was pioneered by Abruna and co-workers.[528] Currently, electropolymerization is a well-established process for the *in situ* deposition of polymeric films on various types of conducting surfaces.

Electropolymerization is often carried out in a precursor solution supported by a three-electrode electrochemical cell (Fig. 45a),[529,530] where the characteristics of the electropolymerized film depend on the type of monomer, electrolyte, electrodes, viscosity of the medium, applied potential/current, scan rate, and ultimately the electrochemical method used. A three-electrode system is generally used to control the respective electrode potential;[531] however, the polymerization can also be carried out in a two-electrode assembly. Electropolymerization can be developed into a sustainable polymerization process where the energy for the polymerization can come from renewable resources. Moreover, the surface coverage and thickness of the electropolymerized films can be easily fine-tuned by selecting a suitable polymerization duration, monomer type and concentration, and applied current or potential. The general drawbacks of electropolymerization include the inability to produce large molecular weight polymers as well as thick films due to the diffusion limitation of the monomers to reach the substrate electrode surface. If the electronic conductivity of the electropolymerized polymer layer is relatively low, it can affect the kinetics and continuity of the subsequent polymerization process.

Galvanostatic, potentiodynamic, or potentiostatic techniques can be used for the electrochemical polymerization process.[529,532,533] The galvanostatic approach uses a constant current, hence allowing greater control over the thickness of the electropolymerized film in addition to maintaining a constant polymerization rate. In the potentiostatic method, a constant potential is applied, where the control over the rate of polymerization is often lost. However, if the applied potential is controlled precisely, optimum morphological features of the polymer film can be achieved even with the potentiostatic technique.[494] In the case of the potentiodynamic approach, the potential of the electrode is varied at a selected scan-rate over a wide potential window, which is often used for the detailed investigation of the polymerization mechanism.[494] Generally, electropolymerization can progress through oxidation (anodic) or reduction (cathodic) pathways.[533,534] In the case of oxidative electropolymerization, the monomer unit turns into a radical cation, whereas, in the case of reductive polymerization, a radical anion is formed. Such a chain initiation process occurring through an electrochemical event is often called electro-initiation. The formation of these radical anions and cations is followed by polymer chain propagation, which can occur through an ionic or free-radical pathway. But the exact mechanism of such a propagation reaction is yet to be well-defined.[535–537] Conducting polymers (important as electrode materials in EESs) are usually prepared using oxidative electropolymerization of monomers such
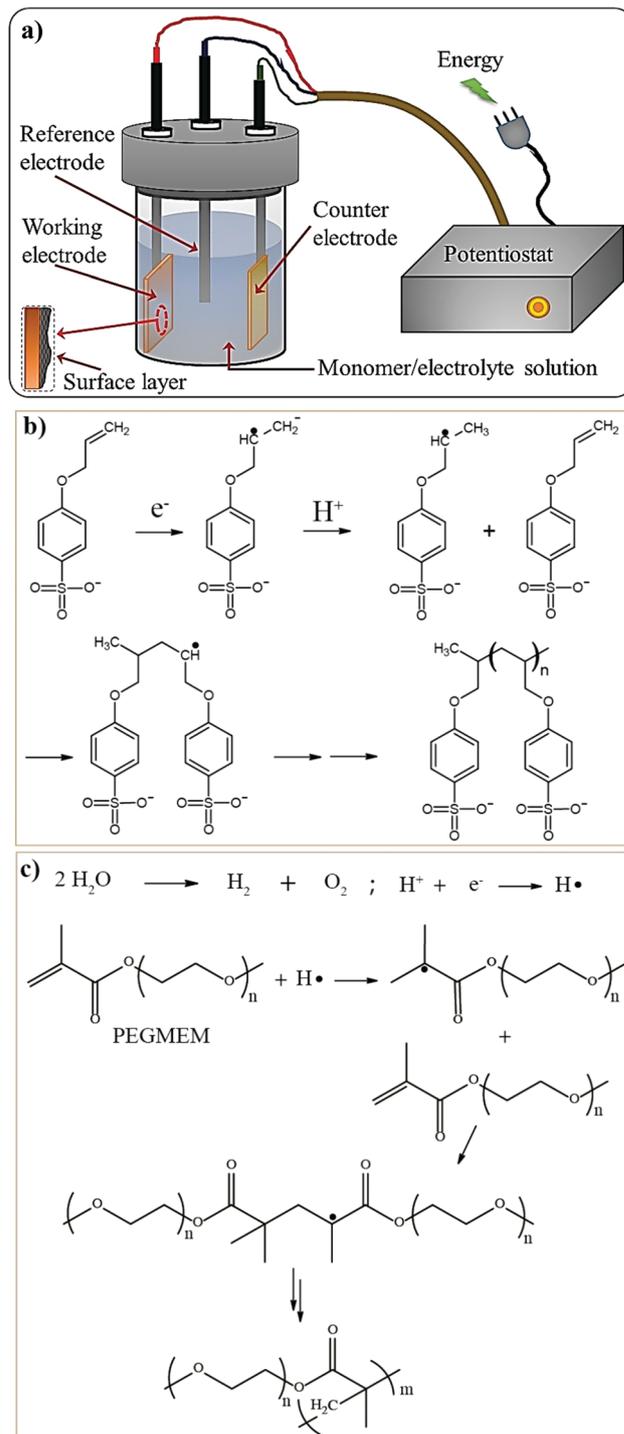
Fig. 45 (a) Schematic representation of electropolymerization of an artificial or sacrificial protection layer over the working electrode in a standard three-electrode assembly; and the mechanism of the reductive electropolymerization of (b) a *para*-sulfonated allyl phenyl ether monomer in DMSO medium (reproduced/adapted from ref. 540 with permission from Elsevier, Copyright 2017[540]) and (c) PEGMEM in an aqueous medium.[545]

as aniline, pyrrole, and so on. In contrast, vinyl- and allyl-functional monomers (important as PEs) are mostly polymerized using the reductive approach.[538,539]

2762 | *Energy Environ. Sci.*, 2021, **14**, 2708–2788

This journal is © The Royal Society of Chemistry 2021

For example, reductive electropolymerization of the *p*-sulfonated (allyl phenyl ether) monomer from a nonaqueous LE (0.5 M LiTFSI/DMSO) is presented in Fig. 45b.[540,541] Here, the first step is the formation of a radical anion followed by the addition of H^+ from the reaction medium (or a trace amount of water) to form a more stable secondary free-radical. The polymerization is propagated by the reaction between the freshly generated free-radical and monomers present at the electrode surface. Vinyl monomers can also be polymerized in a similar fashion.[542] However, in an aqueous medium, such an initiation step is not possible as the radical anion formed is terminated by the ionic end of the water.[543,544] Therefore, the electropolymerization mechanism of PEGMEM from an aqueous medium is reported to be initiated by an electrochemically generated hydrogen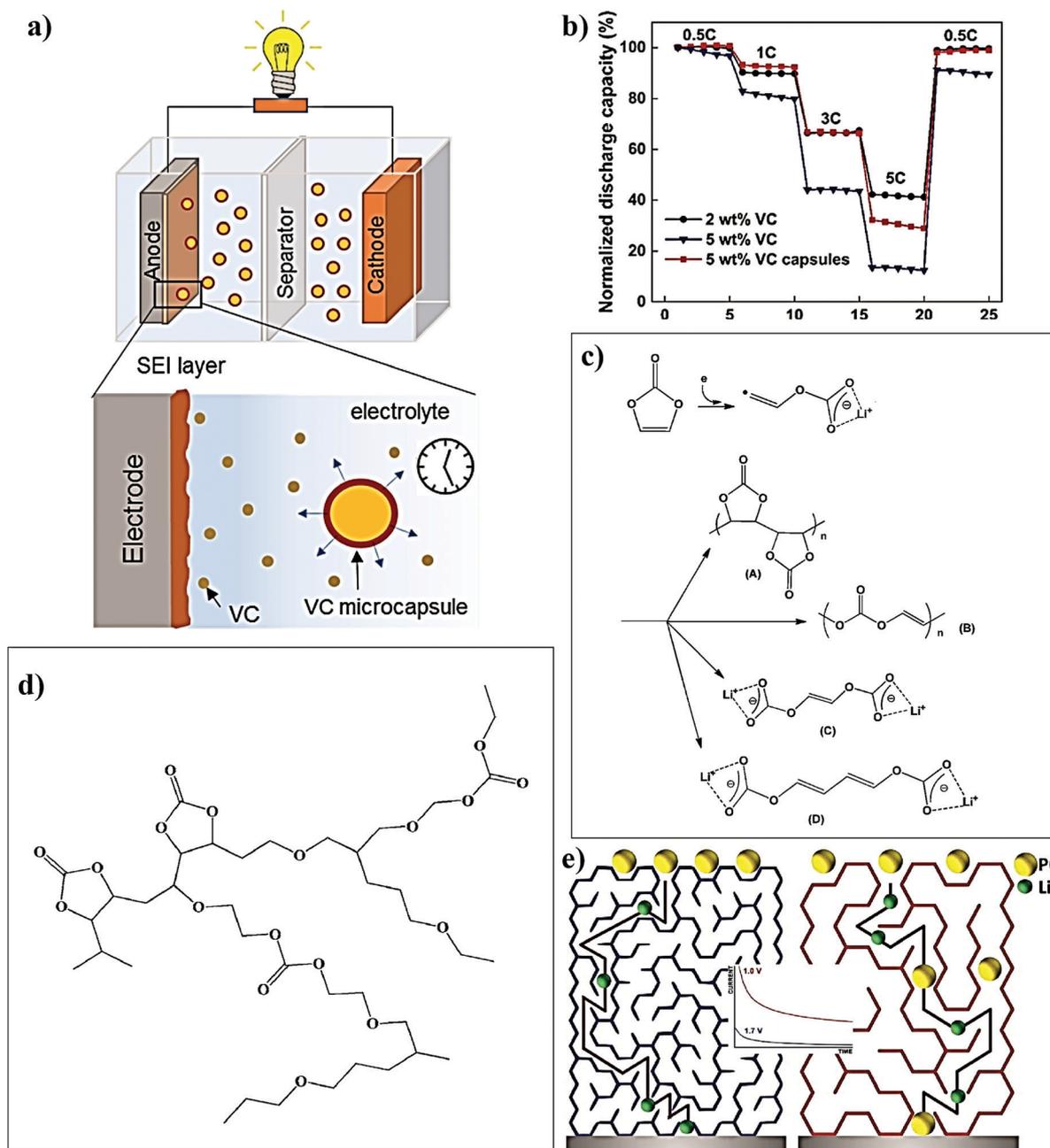 free-radical ($H^•$).[545] The $H^•$ species is formed during the reduction of H^+ to H_2 (Fig. 45c). In the past, reductive electropolymerization has been explored for the preparation of several types of polymer films (PAN, PMMA, polybutadiene, polystyrene, *etc.*) in aqueous and non-aqueous media.[544,546–548] Ultimately, the *in situ* process using the electropolymerization technique can be important in the context of surface protected electrodes, especially for PIS-SEI and PIS-CEI layers having desired properties. Even the direct conversion of an LE in an LB cell to a PE for the fabrication of LIPBs/LMPBs can also be envisaged.[549,550] Even though the electropolymerization method is not used widely in LPBs, it has the potential to be developed into a robust tool for producing well-defined polymers integrated into LPBs during the device fabrication process.

Electrochemical reduction of unsaturated organic carbonates such as VC and vinyl ethylene carbonate (VEC) is known to form an effective polymeric SEI layer in LIBs.[551] Due to the polymeric nature of the SEIs derived from VC and VEC, they can also be identified in the category of PIS-SEIs. In the conventional method, the reduction reaction that occurs during the formation cycle of the battery cell is often tricky to control externally.[407,550,552] To overcome the afore-noted difficulty, poly-VC-based PIS-SEI layers are prepared on the anode surface by a novel method involving the controlled and timely release of VC into the electrolyte solution and the diffusion of these VC molecules to the anode surface using VC-microcapsules.[553] Fig. 46a presents the scheme of the process in which the VC-microcapsules release a small amount of VC into the LE in the first charging cycle, which subsequently takes part in forming PIS-SEI layers by the reductive electropolymerization process. During successive cycles, the VC-microcapsules continue with the slow release of VC by maintaining an optimum VC concentration corresponding to 5 wt% VC. The VC-microcapsule technique is an autonomous strategy involving the temperature- and concentration-controlled diffusion of VC to the electrode surface. As compared to the conventional method of simply adding VC in the electrolyte as an additive, the VC-microcapsule technique can be controlled externally, enhancing the durability and rate performance of the LIB (NCA|LE|graphite) full cells (Fig. 46b). The scheme depicting the general pathway and electro-reduction of VC is presented in Fig. 46c, where poly-VC (product A) is generally accepted to be a major component in the interphases at both the graphite anode and LCO cathode.[88,409,554]

Apart from electrolyte additives like VC or VEC, state-of-the-art carbonate solvents such as PC can also undergo electrochemical reduction so that polycarbonate-based PIS-SEI layers can be expected. However, the compositions of the SEI formed by the electro-reduction of PC and other organic carbonate solvents are highly debated.[88] Several early reports related to SEIs suggest that the PC reduction leads to the formation of a semicarbonate known as lithium ethylene dicarbonate (($CH_2OCO_2Li)_2$, LEDC) by ROP of PC without oligomeric or polymeric products. However, several recent studies using advanced mass-spectrometry techniques (thermogravimetric mass-spectrometry (TG-MS), MALDI, *etc.*) have convincingly proved (*m/z* ratio of 3000 and 1500 from PC and EC/DMC, respectively) the polymeric nature of the electrochemical reduction products of organic carbonate solvents.[356,555–557] It is even claimed that the polymeric components evolved from the organic carbonates are 3D branched network polymers (see Fig. 46d).[88] To understand the fundamental characteristics of the PIS-SEI formed by the reduction of PC solvent in an LE-LMB, Kasmaee *et al.* conducted chronoamperometry studies at different applied potentials of 1, 1.1, and 1.7 V *vs.* Li|Li$^+$.[357] The underpotential electropolymerization (UPE is electropolymerization happening at a lower negative potential than the equilibrium reduction potential of the monomer) of PC occurring at 1.7 V *vs.* Li|Li$^+$ can ensure the formation of an efficient PIS-SEI layer, which is PC impermeable, compact, electrically insulating, and Li$^+$-ion conducting. Besides, the UPE processed PIS-SEI constitutes interconnected long polymer chains extended over the electrode surface. This study concludes that the polymerization kinetics play a critical role in controlling the properties of the PIS-SEI. The slow polymerization initiation rate under UPE conditions provides sufficient time for the formation of longer polymer chains. However, close to the equilibrium reduction potential (1 and 1.1 V *vs.* Li|Li$^+$), the PC reduction rate prevails, leading to an inferior SEI composed of short and disjointed polymer domains with high PC permeability. Since the diffusion coefficient of PC within the UPE processed PIS-SEI is very low, it can provide superior Li-metal protection compared to the PIS-SEI formed at the equilibrium reduction potential having a high PC diffusion coefficient. The schematic illustration of the PC permeable and impermeable polymer chains formed over the Li-metal electrode surface at different electrode potentials (red-colored chains indicate the equilibrium reduction of PC at 1.0 V *vs.* Li|Li$^+$ and blue under UPE conditions of 1.7 V *vs.* Li|Li$^+$) is presented in Fig. 46e.

Like in the case of LBs, the SEI is an essential component in other battery chemistries as well, especially in sodium metal anode-based Li-free alternative batteries. Even though slightly out of context considering the focus of the review, the work by Wei *et al.* regarding Na-metal batteries is interesting as it can find application in LMBs as well. They proposed the *in situ* reductive electropolymerization of allyl-/vinyl-functionalized ionic liquid monomers to realize an artificial PIS-SEI layer over a Na-metal anode.[558] Here, the unsaturated ionic liquid undergoes reductive electro-initiation to generate a radical anion (Fig. 47a), which can propagate the growth of the polymer chain. Three different ionic liquid monomers are investigated for electropolymerization and

This journal is © The Royal Society of Chemistry 2021

Energy Environ. Sci., 2021, **14**, 2708–2788 | 2763

Fig. 46 (a) Schematic of the microcapsule-based release of the VC additive in an LIB and the *in situ* electroreduction to the PIS-SEI surface protection layer at the anode electrode surface; (b) the improved rate-capability of an LIB achieved through the microcapsule technique over the conventional approach of adding VC as an additive in an LE (reproduced/adapted from ref. 553 with permission from American Chemical Society, Copyright 2017[553]); (c) the possible reaction products of the electro-reduction of VC molecules;[88,409,554] (d) the plausible 3D branched polymeric product formed by the electro-reduction of organic carbonate solvents (EC, PC, *etc.*), which becomes part of the SEI (reproduced/adapted from ref. 88 with permission from American Chemical Society, Copyright 2014[88]); and (e) representation of PC non-permeable (left side) and permeable (right side) polymeric components formed by the electro-reduction of PC at 1.0 V (equilibrium reduction potential) and 1.7 V (UPE) *vs.* Li|Li^{+} (reproduced/adapted from ref. 357 with permission from Elsevier, Copyright 2016.[357] Distributed under a Creative Commons Attribution License International 4.0 (CC BY 4.0) (https://creativecommons.org/licenses/by/4.0/)).

it is reported that the PIS-SEI formed over the anode is influenced by the molecular structure of the ionic liquid monomer used. For instance, the mono-functional 1-allyl-3-methylimidazolium perchlorate (AMIM) monomer results in an oligomeric PIS-SEI, whereas the bi-functional monomers 1,3-diallyl imidazolium

perchlorate (DAIM) and 1-allyl-3-vinyl imidazolium perchlorate (AVIM) produce high molecular weight polymers. Among the AVIM and DAIM molecules, the former is a highly reactive species due to the presence of an sp[2] hybridized vinyl group, which leads to a denser polymer layer. However, the allyl carbon in DAIM

2764 | *Energy Environ. Sci.*, 2021, **14**, 2708–2788

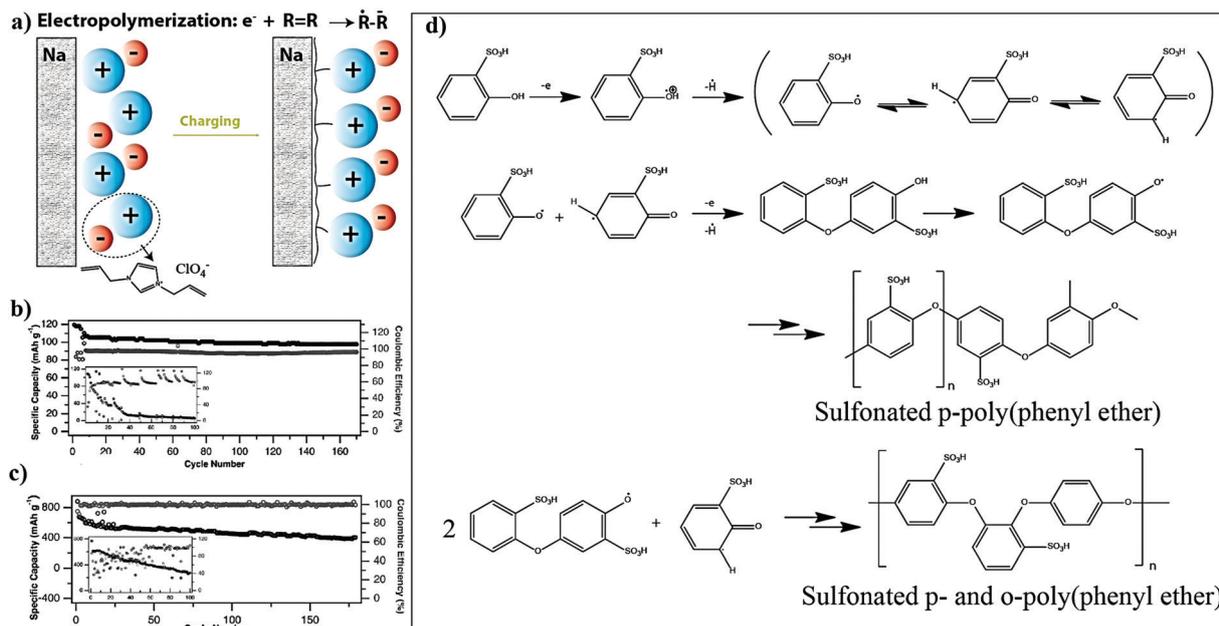This journal is © The Royal Society of Chemistry 2021

Fig. 47 (a) Schematic representation of the formation of a DAIM ionic liquid-derived PIS–SEI over Na–metal by reductive electropolymerization. Cycling performance of the PIS-layer protected (b) $Na_3V_2(PO_4)_3$|LE|Na and (c) S|LE|Na cells. In the inset (b and c), the cycling stability of the unprotected cells is also displayed (reproduced/adapted from ref. 558 with permission from John Wiley and Sons, Copyright 2017[558]). (d) Mechanism of oxidative electropolymerization of the phenyl monomer, namely o-hydroxybenzenesulfonate (o-HBS) (reproduced/adapted from ref. 567 with permission from John Wiley and Sons, Copyright 2016[567]).

imparts internal plasticization, and the formed polymer layer is soft and rubbery. Therefore, the DAIM-based PIS-SEI is employed for further investigation. Both $Na_3V_2(PO_4)_3$|LE|Na and S|LE|Na cells are fabricated using the *in situ* electropolymerized DAIM-based PIS-SEI over the metallic anode from an LE (20 wt% DAIM in 1 M $NaClO_4$ in EC:PC). In the case of the $Na_3V_2(PO_4)_3$|LE|Na cell, the PIS-SEI protection helps in retaining above 90% of the initial specific capacity (≈ 105 mA h g^{-1}) over 160 cycles, whereas, in the cell without the PIS-SEI coating, the capacity drastically dropped below 50% in just 20 cycles (Fig. 47b). Additionally, similar performance improvement is also observed in PIS-SEI-protected S|LE|Na cells over the non-protected counterpart (Fig. 47c).

Electropolymerization as a tool for the direct conversion of 1,3-DOL present in an LE to a poly-DOL-based artificial PIS-CEI that can protect the high-voltage LNMO cathode and the high-capacity sulfur cathode was demonstrated by Monaca *et al.*[559] The polymerization is carried out through chronoamperometry cycles above 4 V *vs.* Li|Li$^+$ without the use of any additional initiator so that a thin PIS-CEI layer is formed over the LNMO or sulfur working electrode. The precursor used for the electropolymerization is composed of 5 m LiTFSI in 1,3-DOL (dimethyl ether as a solvent is optional). Later, the protected working electrodes are used for LE-LMB fabrication. The LNMO|LE|Li cell displayed a specific capacity of 100 mA h g^{-1} (1C, 26 °C, 3.5–4.8 V) with 90% capacity retention over 200 cycles. The surface protected S|LE|Li cell is found to inhibit polysulfide shuttling and displayed around 100% capacity retention over 50 cycles, which is convincingly better than the non-protected cell. In a report from Kong *et al.*, the GPE formed from 1,3-DOL

by electropolymerization is found to improve the cycling life of the LMPB (LCO|GPE|Li) cell compared to that of a test cell without 1,3-DOL.[560–562] In a later published report from the same group, factors such as the cut-off voltage, current rate, and temperature influencing the electropolymerization of 1,3-DOL are emphasized.[563] On fixing the cut-off potential of electropolymerization between 3 and 4.1 V *vs.* Li|Li$^+$, the capacity retention is improved irrespective of the current rate, provided that the cell is kept below the onset temperature for the thermal polymerization of 1,3-DOL. However, the complete understanding of the electropolymerization mechanism of 1,3-DOL is still lacking.[564]

Several reports are available in the literature on the reductive electropolymerization of monomers (mainly monomers with vinyl- and allyl-functionalities) as a tool for realizing PEs, and PIS-SEI and PIS-CEI layers. However, oxidative electropolymerization for the same purpose is not very well explored. Although the oxidative polymerization of vinyl- and allyl-functional monomers governed by the formation of a radical cation is also known,[542] oxidative electropolymerization reactions of phenolic monomers are mostly employed in the context of surface protection or PEs. A report by Rhodes *et al.* demonstrated the oxidative electropolymerization of a co-monomer solution composed of two phenolic monomers p-hydroxybenzenesulfonate (p-HBS) and 2,6-dimethylphenol (DMP) in the presence of a supporting electrolyte made of 0.3 M NaOH in methanol.[565,566] As a proof of concept, oxidative electropolymerization is carried out over an indium-tin-oxide (ITO) working electrode in a three-electrode assembly [potentiostatic method, 1.5 V *vs.* sodium saturated calomel electrode (SSCE)]. The formed SPE can be considered

This journal is © The Royal Society of Chemistry 2021

Energy Environ. Sci., 2021, **14**, 2708–2788 | **2765**

as a blend electrolyte, where the poly-4-sulfonic acid-1,2-phenylene oxide (PSPO) derived from *p*-HBS with a sulfonate group is integrated into the poly-2,6-dimethyl-1,4-phenylene oxide (PDPO) from DMP. However, the possible formation of a covalently linked PSPO-*co*-PDPO copolymer is also suggested. The charge compensating Na^+-ion present in the blend SPE can be easily ion-exchanged by Li^+-ions to form an SIC-PE exhibiting an ionic conductivity in the order of 10^{-8} to 10^{-9} S cm^{-1} (RT). Considering the SPE film thickness of ≈ 100 nm, it can be employed as a PIS-based surface protection layer for LBs. In a recent work, the difference between the structure of polymers synthesized by electrochemical oxidative polymerization of *p*-HBS and its isomer *o*-hydroxybenzenesulfonate (*o*-HBS) was explained with mechanistic details by Braglia *et al.*[567] It is observed that *o*-HBS leads to a linear polymer with faster kinetics. In contrast, *p*-HBS follows slower polymerization kinetics with the formation of a sterically hindered polymer network. The detailed oxidative polymerization mechanism of *o*-HBS is presented in Fig. 47d. However, the applicability of any of these polymers is yet to be demonstrated in *ex situ* or *in situ* processed LB full cells.

In summary, Sections 6.1 to 6.4 primarily discuss the anionic, cationic, condensation, and electropolymerization methods adopted for the *in situ* processing of LIPB/LMPB cells and surface protection of electrodes. Depending on the type of

monomers and available reaction conditions, one of these methods can be used to fabricate LB cells. All these methods are suitable for producing GPEs, SPEs, and PIS-interphases. Anionic and cationic polymerization can occur even in the absence of any additional initiators, as the Li-metal or even salt can initiate the polymerization reaction. For instance, the Li-metal induced anionic polymerization of cyanoacrylate monomers is suitable for the surface protection of the Li-metal anode in LE-LMBs and LMPBs. The temperature dependency of anionic polymerization of VC can be ingenuously used for the *in situ* fabrication of smart LMPB cells, which possess a self-shutdown mechanism. Cationic polymerization is suitable for ROP reactions. For instance, the CROP of 1,3-DOL provides the opportunity for direct conversion of an LE to a PE or even a conformal electrode protection layer-based on poly-DOL. Other types of cyclic monomers, such as epoxides, are also suitable candidates for CROP. In Tables 6 and 7, the reports on anionic and cationic *in situ* polymerization processes used for LB applications are compiled and summarized.

Besides ionic polymerization methods, a few reports address the *in situ* processing of PIS-interphase layers using condensation polymerization and electropolymerization methods. These two techniques are mainly employed for surface protection, either at the anode or cathode. Condensation polymerization is adopted

Table 6 Summary of the *in situ* processing of LPBs and PIS-interphases using the anionic-polymerization method

Monomer/ oligomer	Electrolyte/ salt	Initiation	Ionic conductivity	Cell	Operating voltage range	Capacity	Capacity retention	Ref.
ECA#	4 M LiClO$_4$ in EC:DMC	Electron transfer from Li-metal	2.7 mS cm^{-1} at RT	LFP|GPE|Li	2.5–4 V	140 mA h g^{-1} (1C, RT)	90%, 100 cycles, 1C	481
ECA&	1 M LiPF$_6$ in EC:DMC	Moisture	—	LNMO|LE|Li	3.5–5 V	$\approx$122 mA h g^{-1} (1C, RT)	92%, 100 cycles, 1C	346
ECA&	1 M LiPF$_6$ EC:DMC	Hydroxyl group on Li-metal surface	—	LFP|LE|Li	2.5–4 V	150 mA h g^{-1} (2C, RT)	100%, 500 cycles, 2C	488
VC*	LiI	Lithium iodoalkoxide	1.8 mS cm^{-1} at 25 °C	LTO|GPE|Li	1–2 V	$\approx$150 mA h g^{-1} (1C, RT)	50%, 700 cycles, 1C	489

* Separator assisted. # Direct deposition. & PIS-interphase.

Table 7 Summary of the *in situ* processing of LPBs using the cationic polymerization method

Monomer/ oligomer	Electrolyte/salt/ plasticizer	Initiator species	Ionic conductivity	Cell	Operating voltage range	Capacity	Capacity retention	Ref.
TEGDVE$	1 M LiBETI in EC:DEC	H$^+$BF$_4^-$	1 mS cm^{-1} at 30 °C	LCO|GPE|Li	3–4.3 V	150 mA h g^{-1} (15 mA g^{-1}, 30 °C)	—	499
PVA-CN*	1 M LiPF$_6$ in EC:DMC:EMC	H$^+$(PF$_5$OH)$^-$	—	LCO|GPE| graphite	2–4.4 V	>1900 mA h (0.2C, 25 °C)	>80%, 50 cycles, 0.2C	500
PVA-CN*	LiTFSI, SN	H$^+$(PF$_5$OH)$^-$	2.37 mS cm^{-1} at 25 °C	LFP|GPE|Li	2.4–4.2 V	155 mA h g^{-1} (0.1C, 25 °C)	96.7%, 100 cycles, 0.1C	501
PEGDE*	LiTFSI	H$^+$(BF$_3$OH)$^-$	0.09 mS cm^{-1} at RT	LFP|SPE|Li	2.5–4 V	$\approx$115 mA h g^{-1} (0.1C, 25 °C)	74%, 100 cycles, 0.1C	504
Siloxane epoxide with PVS*	1 M LiPF$_6$ in EC:DMC	H$^+$(PF$_5$OH)$^-$	11 mS cm^{-1} at 30 °C	LCO|GPE|graphite	2.8–4.2 V	133 mA h g^{-1} (0.1C, 30 °C)	$\approx$98%, 200 cycles, 0.1C	510
1,3-DOL*	LiPF$_6$, LiTFSI	H$^+$(PF$_5$OH)$^-$	3.8 mS cm^{-1} at RT	S|GPE|Li	1.8–3 V	1010 mA h g^{-1} (0.5C, RT)	50%, 500 cycles	511
1.3-DOL*	LiTFSI	Al(OTf)$_3$	1 mS cm^{-1} at RT	LFP|SPE|Li	2.5–4 V	100 mA h g^{-1} (1C, RT)	$\approx$75%, 700 cycles, 1C	334

* Separator assisted. $ Multi-layer approach.

primarily for forming artificial protective coatings at the cathode, which act as a PIS-CEI layer. In contrast, electropolymerization reactions have been employed for the preparation of both PIS-SEI and PIS-CEI coatings. Therefore, these two methods are suitable and should be further explored for developing polymeric interphases with excellent physicochemical and electrochemical characteristics. Indeed, such judiciously prepared layers will enable the use of high-voltage cathodes for LBs and avoid some of the disadvantages related to oxidation or reduction stability of commonly used polymer hosts. The thin layer coating on high-voltage cathodes such as LCO, LMNO, and NMC111 is proven to reduce the exothermic reactions and Mn^{2+}-dissolution in the interface between the LE and electrode, improving the cycling stability. Hence, by using these polymerization techniques, safer LIBs can be built. Like ionic polymerization, electropolymerization can be carried out without the presence of additional initiators. However, fully-fledged utilization of the electropolymerization method for the *in situ* processing is rarely attempted for conventional LMPB/LIPB cell fabrication. Electropolymerization requires special attention as polymeric SEI/CEI (PIS-SEI/PIS-CEI) layer formation is an inherent and essential phenomenon in all types of LBs. In recent times, electropolymerization has evolved as an exciting method for customized LB (*e.g.* microbatteries) fabrication, as discussed in the following sections. In the case of microbatteries, their small size is an added advantage that allows electrochemically polymerized conformal coatings of PIS itself to effectively act as a separator and prevent individual electrodes from coming into contact.

7. Potential scope of the *in situ* process in customized LPB fabrication

In the previous sections, the adoption of the *in situ* process for the fabrication of conventional LPB cells is thoroughly covered. The potential of the *in situ* process is envisaged to have an imminent impact on other customized cell designs such as lithium microbatteries (mLBs), flexible and wire-shaped LBs, and even those LBs with complex geometries. Such customized battery designs are significant in micro, flexible, and portable electronics to be integrated with miniature devices such as medical aids, sensors, actuators, and other internet-connected devices, which constitute the futuristic Internet of Things (IoTs).[568–571] In this context, the following section provides an overview of several attempts for fabricating customized LBs making use of the *in situ* polymerization process.

7.1 Microbattery fabrication using the *in situ* process

The working principles of mLBs and conventional LBs are the same. Still, the size of an mLB is extremely small and generally accepted to be ≤ 0.1 cm^3.[572] Reduction in the size of state-of-the-art LBs demands updated manufacturing methods with alternative electrolyte designs to overcome the risks related to LE leakage and other safety issues. SSEs are ideal for such devices, where PEs are expected to make a huge impact. To cope with the architectural flexibility of such devices, shape deformable PEs are
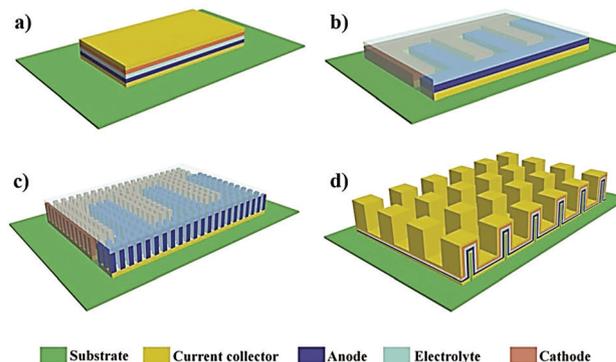

Fig. 48 Schematic representation of the four commonly used mLB configurations: (a) 2D stacked, (b) 2D in-plane, (c) 3D in-plane, and (d) 3D stacked (reproduced/adapted from ref. 281 with permission from John Wiley and Sons, Copyright 2019[281]).

indeed inevitable.[279,573,574] Despite significant advancement in physical and chemical methods for mLB fabrication such as 3D-printing, thin-film lithography, physical and chemical vapor deposition, thermal evaporation, atomic layer deposition, laser printing, and sol–gel methods, the limited areal/volumetric capacity, energy density, and power density offered by mLBs remain a considerable challenge.[368,574,575] A summary of the different types of commonly used mLB designs is presented in Fig. 48a–d.[281] Generally, the architecture of the microelectrode in mLBs can be either 2D or 3D. Using 2D- and 3D-microelectrodes, mLBs can be fabricated in both in-plane and stacked geometries.[281] The recent trend in mLB fabrication is the patterning of interdigitated microelectrodes on a single plane and these are called interdigitated in-plane mLBs. Detailed descriptions of the type of mLBs and the different electrode configurations are available elsewhere.[281,574,576,577] In the case of an interdigitated cell architecture, the specific capacity, energy/power density, *etc.* can be improved by increasing the height of the deposited electrodes, which facilitates an increased mass-loading of the active materials.[578]

Like conventional LBs, the electrode|electrolyte interface/interphase significantly influences the performance metrics of mLBs. For instance, the infiltration of an LE and wetting of the interiors in 3D-microelectrodes is relatively easy and efficient. However, LEs are not a suitable choice for mLBs due to the risk of leakage and the requirement of stringent packaging norms. Therefore, the adoption of the *in situ* process, which can ensure efficient electrode|electrolyte interface/interphase, and maximum active material utilization, will be beneficial while fabricating mLBs. Since the integration of different components (electrode and electrolyte) of mLB cells in the micron-dimension is challenging, the direct generation of conformal and ultra-thin PE layers (can be considered as PIS layers due to the sleek nature of the PE in mLBs) over microelectrode arrays by the *in situ* process can leverage certain manufacturing/fabrication advantages. In the case of conventional LBs, the role of PIS layers is to protect the electrode surface, where the luxury of an additional separator soaked in an LE or a PE film provides the physical separation between the anode and cathode. However, in mLBs, the PIS should be ideally capable enough to

simultaneously play the role of a separator and an electrolyte since the use of an external separator or PE film is not feasible due to the small dimension and the interdigitated configuration of most mLBs.

Brandell et al. have synthesized and explored several UV polymerized electrolytes for mLB applications. In one of the reports, a thin SPE is in situ processed (direct deposition) over the LFP electrode during mLB fabrication.[580,583,584] They prepared a precursor consisting of a cross-linker (poly(propylene oxide) diacrylate (PPOD)), a surfactant polyetheramine (glyceryl poly(oxypropylene) (PEA), LiTFSI (Li : O ratio of 1 : 20), and a photoinitiator (Irgacure 2022) in ethanol (ethanol is evaporated during SPE processing step). PEA is a molecule with surfactant properties, which can be considered an additive/plasticizer capable of inducing hydrogen bonding interactions with the oxygen moieties present in the electrode particles. These interactions help in ensuring the effective wetting of the electrode by the precursor. Although not mentioned, it is possible that the PEA molecule can become part of the polymer host by an aza-Michael addition reaction.[579,585] An example of the aza-Michael addition reaction between amine and acrylate in the mixture is presented in Fig. 49a.[579] This is a multi-step process, which involves the formation of an aza-Michael network that can undergo subsequent cross-linking polymerization on UV-irradiation.
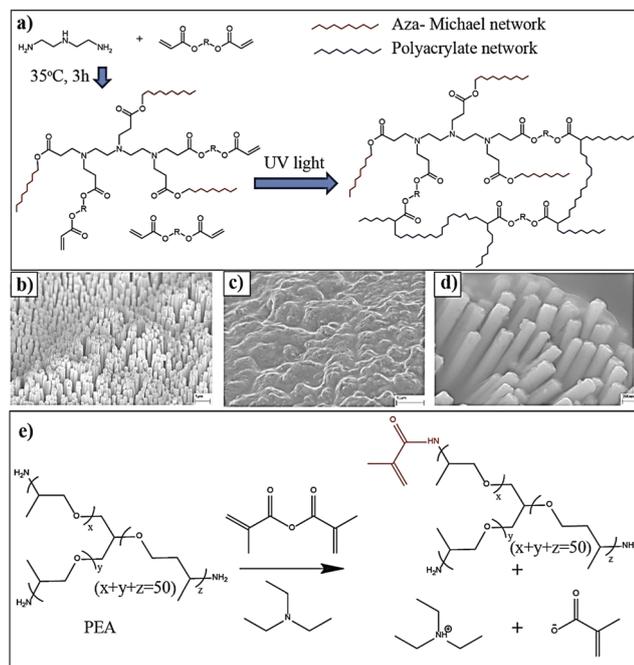
Fig. 49 (a) Thermally triggered aza-Michael addition reaction occurring between amine and acrylate molecules. The aza-Michael product on UV curing produces a cross-linked polymer network (reproduced/adapted from ref. 579 with permission from The Royal Society of Chemistry[579]). SEM image of the (b) 3D Cu-pillar microelectrodes and (c and d) the 3D Cu-pillar microelectrode surface after the in situ polymerization process at two different magnifications (reproduced/adapted from ref. 580 with permission from Elsevier, Copyright 2011[580]). (e) Synthetic modification of PEA to PEA-methacrylate (reproduced/adapted from ref. 581 with permission from Elsevier, Copyright 2013[581]).

The heat generated during the UV irradiation would be sufficient to catalyze the aza-Michael reaction. This method of cross-linking polymerization is industrially important and is generally used to prepare thermosets. The UV-cured SPE prepared by Brandell et al. comprises a conformal coating (1–3 μm thick) over the LFP surface. The SPE film exhibits an ionic conductivity and oxidative stability of 0.00345 mS cm^{-1} and 5.2 V vs. Li|Li$^+$, respectively (30 °C). It is worth noting that due to the short transport distances in mLBs, the low ionic conductivity value compared to conventional PEs does not significantly influence the internal cell resistance.[327] At 60 °C, a specific capacity of 120 mA h g^{-1} is obtained with stable cycling over 30 cycles for the LFP|SPE|Li cell. The same SPE prepared over 3D-Cu$_2$Sb microelectrodes is also illustrated in Fig. 49b–d, demonstrating the possibility of obtaining a conformal coating essential for mLB applications.[580] The 3D-Cu$_2$Sb-based mLB displays a higher discharge capacity than the 2D-Cu$_2$Sb counterpart due to the availability of more surface area within the 3D microelectrode architecture, which is accessible by the in situ generated SPE. The bi-functional oligomer species synthesized by modification of the PEA molecule by substituting the methacrylate monomer is also reported as a potential candidate for the in situ processing of mLBs.[581] The PEA-methacrylate monomer is prepared by the simple Michael-addition reaction, unlike the aza-Michael reaction in the earlier case. The reaction between PEA and methacrylic anhydride (MAA) in the presence of triethylamine (TEA), leading to the formation of methacrylate substituted PEA, is displayed in Fig. 49e. Due to the possible presence of more than one methacrylate end group in the substituted PEA, the use of additional cross-linker monomers such as PPOD is avoided here. Ultimately, the authors claim that the substituted PEA performs better than the unsubstituted counterpart combined with LFP electrodes.

In situ electropolymerization is also used to generate a conformal PIS layer on the microelectrodes that can be used for mLB applications. The direct electropolymerization of PEG-MEM onto nano-structured TiO$_2$ was reported by Djenizian et al.[545,586,587] To achieve this, the electropolymerization of PEGMEM in the presence of LiTFSI salt is carried out by CV onto a 3D-TiO$_2$ nanotube electrode in an aqueous medium (three-electrode assembly where TiO$_2$ is employed as the working electrode). The polymerization mechanism of PEGMEM is already presented in Fig. 45c. Later, an mLB is fabricated by the generation of a PE layer onto the TiO$_2$ nanotube anode and LNMO cathode by the in situ electropolymerization process. The schematic representation of the mLB and the cross-sectional SEM images are displayed in Fig. 50a.[582,588] With a prolonged number of CV cycles, it is observed that the electrodes are covered with a smooth layer of PE [Fig. 50b and c]. However, for safety reasons, an additional thin PE layer is used apart from the electropolymerized PIS layer during the full cell fabrication. Interestingly, the use of an LE is avoided here so that it can be considered as the in situ processing of an SPE-based mLB by a multi-layer approach. The in situ processed mLB is cycled in a voltage window of 1 to 3.3 V at 0.1C for 10 cycles. In the first cycle, a discharge capacity of 169 mA h g^{-1} (82 mA h cm^{-2} μm^{-1}) is obtained, and 88% of the capacity is retained after 10 cycles. The C-rate performance of

2768 | Energy Environ. Sci., 2021, **14**, 2708–2788

This journal is © The Royal Society of Chemistry 2021

the mLB is also presented in Fig. 50d, where the mLB with pristine electrodes is found to show far inferior performance to the *in situ* electropolymerized counterpart.

Ferrari and Braglia *et al.* extended the *in situ* electro-polymerization strategies for realizing SIC-PEs for potential application in mLBs.[540,589] The electro-polymerization of *p*-sulfonated allyl phenyl ether is achieved by both CV and chronoamperometry techniques. A precursor consisting of the monomer and 0.5 M LiTFSI salt is prepared in DMSO solvent. TiO_2 nanotubes, platinum, and Ag|AgCl are used as the working, counter and reference electrodes, respectively, in a standard three-electrode cell assembly. The mechanism of electropolymerization of the *p*-sulfonated allyl phenyl ether is already presented in Fig. 45b,[540] and the SEM images confirmed that the thickness of the PE layer is 300 nm. Here also, an additional separator is used during the cell fabrication to avoid any possible cell failure due to short-circuit. The cycling of the TiO_2|SIC-PE|Li mLB half-cell is carried out at 25 °C (1–3 V) (Fig. 50e), which exhibited a high areal energy density (65 μW h cm^{-2} $μm^{-1}$) and power density (90 μW h cm^{-2} $μm^{-1}$). Therefore, from the electrochemical performance point of view, these results are claimed to be the best among the results reported in the recent literature on mLBs.

7.2 Printable LBs

User-tailored devices such as shape-conformable portable devices, wireless gadgets, and roll up displays are growing in demand day by day. To bring them to fully-fledged utilization, shape conformable and miniaturized energy storage devices are equally important. To fabricate such energy storage devices, flexible and readily deformable PEs are inevitable.[570,590–593]
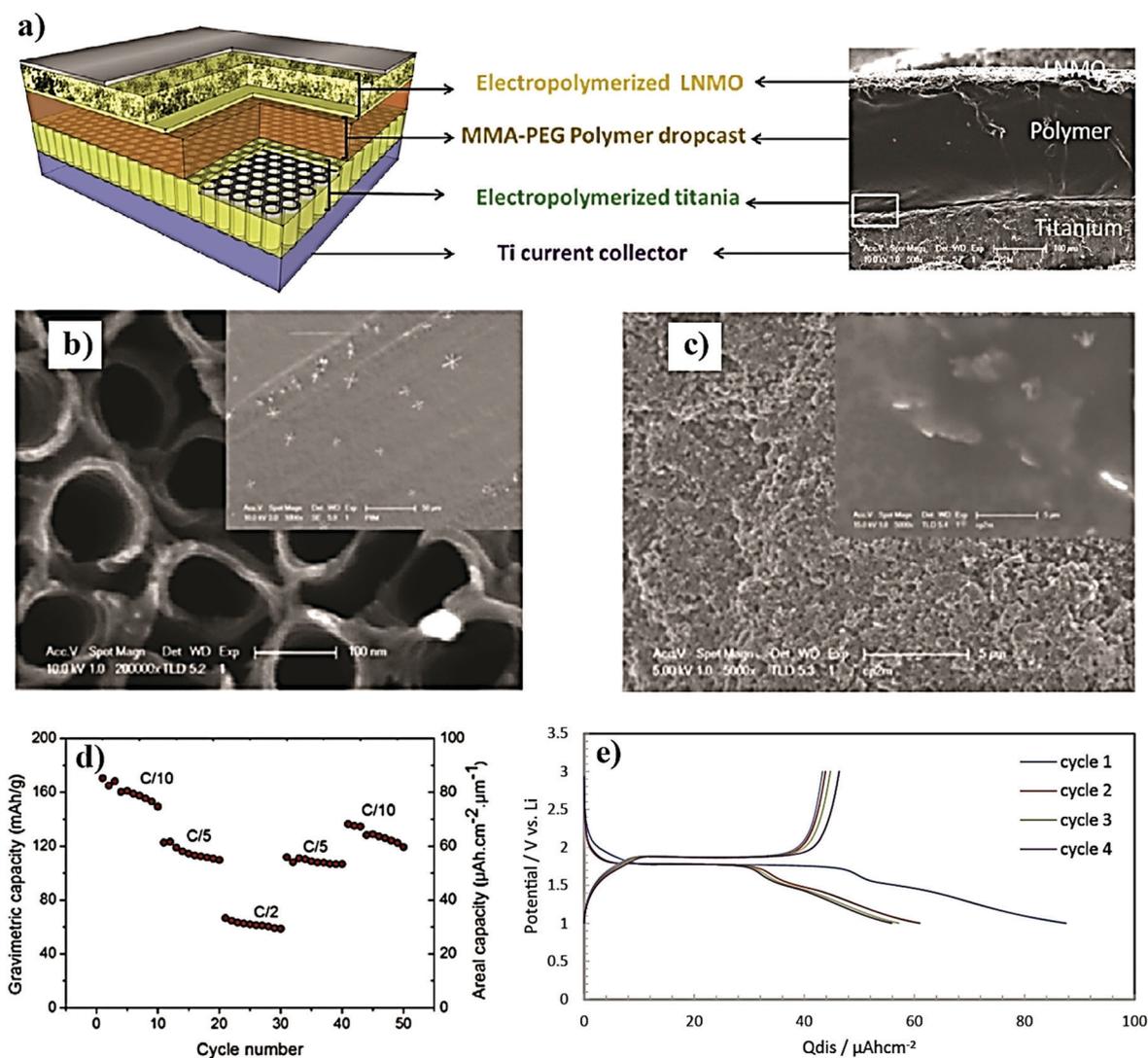
Fig. 50 (a) Schematic representation of the mLB (LNMO|SPE|TiO$_2$) cell fabricated by the *in situ* electropolymerization process. An SEM image of the cross-sectional view of the battery cell showing the various cell components is also presented. SEM images of the (b) TiO$_2$ nanotube electrode and (c) LNMO electrode before and after (inset) the electropolymerization process. (d) C-rate performance of the LNMO|SPE|TiO$_2$ mLB full cell (reproduced/adapted from ref. 582 with permission from Elsevier, Copyright 2017[582]). (e) Electrochemical performance of the *in situ* processed TiO$_2$ microelectrode in the TiO$_2$|SIC–PE|Li cell. (reproduced/adapted from ref. 540 with permission from Elsevier, Copyright 2017[540]).

This journal is © The Royal Society of Chemistry 2021

Energy Environ. Sci., 2021, **14**, 2708–2788 | 2769

The *in situ* process has the potential to be integrated with sophisticated printing techniques for the fabrication of both conventional and customizable LBs. In any printing technique, a digitally designed pattern is inscribed on a substrate of interest. The most important prerequisite for successful printing is a suitable ink with reasonable viscosity characteristics. Depending on the end-user application, tailor-made inks with desirable properties can be prepared and used for the printing process. Once suitable inks are available with electrode and electrolyte components, sophisticated printing techniques such as 3D-printing, inkjet printing, laser printing, screen-printing (stencil printing), spray printing, and so on can be employed for LB fabrication.[594] In this section, a few reports in which the free-radical polymerization assisted *in situ* process combined with advanced printing techniques is used for the fabrication of customized LBs are included.[463,481,595,596] Considering the industrial importance, more emphasis is given to 3D-printed LBs, with few reports on screen-printed and stencil printed LBs. Soon, more studies on printable LBs are expected to be evolved by employing suitable printing techniques due to the increased interest in wearable, portable, and flexible electronics, IoT, *etc.*

7.2.1 3D-printing and other printing methods integrated with the *in situ* process. Low-cost and high-throughput methods such as 3D-printing can be integrated with the *in situ* process to fabricate both conventional and mLBs.[387,414,597,598] 3D-printing (introduced in the 1980s), also called additive manufacturing, is considered an engineering revolution due to the possibility of building highly intricate and precise designs and structures, which is otherwise not possible using conventional techniques such as casting, molding, machining, *etc.*[599–601] In simple words, one can design 3D rendered images using computer-aided design (CAD) or other customized software applications, which are digitally sliced into 2D cross-sections, and later the

respective physical objects are fabricated by printing in a layer-by-layer, point by point, or line by line approach.[600] The major advantages of 3D-printing include high precision while building complex objects and architectures, even in ultrathin configurations. These features are rather important in both microbattery and microsupercapacitor fabrication processes as the high precision patterning of interdigitated microelectrodes is often a challenging task when conventional physical and chemical methods are used. Besides, 3D-printing is characterized by advantages of low cost, easy and fast prototyping, accuracy, a wide choice of materials, and robust opportunities for customized product design such as 3D scaffolds and fibers.[578]

In the case of 3D-printing, inks and their components are very important. Different types of inks can be used depending on the end application, which is often a solution of polymer, fillers, and additives in a suitable solvent or solvent mixture. In the context of LPBs, the fillers in the polymeric ink can be electrode materials and binders, which eventually form a 3D-printable electrode slurry, which can be used for electrode patterning. A polymeric ink devoid of any electrode components can be used for the 3D-printing of polymeric scaffolds and battery cell components. For the *in situ* processing of LPBs with a 3D-printing step, a polymerizable precursor, which is composed of reactive monomers with the electrolyte components, such as the salt, solvent, and plasticizers, can be used as the ink. Similarly, a polymerizable precursor slurry containing reactive monomers and electrode materials is useful for the patterning of battery electrodes bound by the formed polymer host. LPBs that are essentially fabricated by a 3D-printing step involving the *in situ* processing of a PE using a precursor (by heat/photo-polymerization) within the cell assembly can be included in the category of '*in situ-processed-3D-printed*' LPBs. The general representation of the 3D-printing of the electrode and the PE
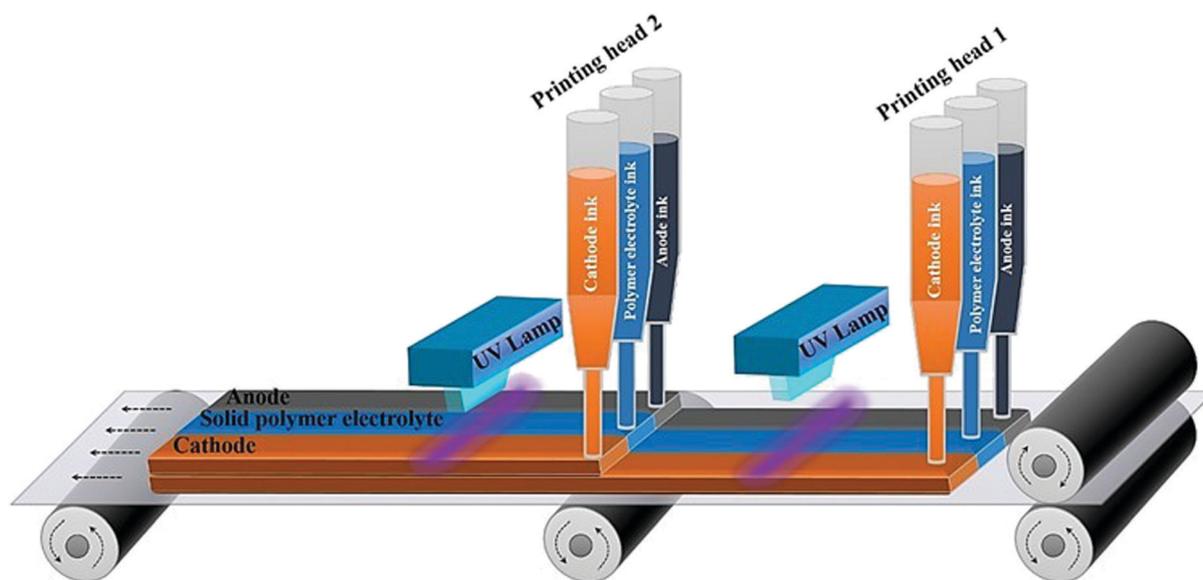

Fig. 51 Scheme depicting the throughput 3D-printing of the anode, cathode, and PE by the extrusion process through a nozzle followed by subsequent UV-irradiation in authors imagination for the *in situ-processed-3D-printed* LPBs.

2770 | *Energy Environ. Sci.*, 2021, **14**, 2708–2788

This journal is © The Royal Society of Chemistry 2021

from a UV-curable electrode slurry and electrolyte ink followed by concomitant UV irradiation to realize all-3D-printed LPBs is shown in Fig. 51. Such a method is applicable for the 3D-printing of mLBs as well as conventional LPBs or even flexible LPBs with complex architectures. Direct ink writing (DIW), fused deposition modeling (FDM), stereolithography (SLA), and selective laser sintering (SLS) are a few of the commonly used 3D-printing techniques employed for both research and industrial purposes.[578]

For example, in a report from Sun *et al.*, an interdigitated LFP|LE|LTO mLB is fabricated by precise patterning of polymeric inks made of electrode materials dispersed in a solution composed of ethylene glycol, glycerol, hydroxyethyl cellulose, and hydroxypropyl cellulose by 3D-printing.[597] However, this work cannot be considered as an example of *in situ-processed-3D-printed* LPBs as an LE is used without the involvement of the *in situ* polymerization processing step for the full cell fabrication. Still, this work opens up the possibility of employing an additional 3D-printing step for the patterning of a PE in the space between the already 3D-printed anode and cathode scaffolds so that an *in situ-processed-3D-printed* LPB can be realized. Herein, the polymeric electrode slurry is used for the patterning of battery electrodes by 3D-printing. The viscosity of the ink is tuned such that it can be extruded through a nozzle. Once the 3D-scaffolds of LTO and LFP are patterned by 3D-printing, the space between the interdigitated electrodes is filled with an LE (1 M LiClO$_4$ in EC:DMC) followed by PMMA-based cell packaging. The schematic illustration of the patterning of the 3D-microelectrodes (Fig. 52a–d) using the extrusion of polymeric inks through a 30 μm nozzle, the optical microscopy image of the nozzle (Fig. 52e), and the SEM image of the patterned interdigitated architecture (Fig. 52f) are all displayed. The charge–discharge profiles and the cycling performance of the LFP|LE|LTO full cell are also presented in Fig. 52g and h, which exhibited an areal capacity close to 1.5 mA h cm^{-2} (1C) while retaining more than 90% of the initial capacity over 30 cycles.

The 3D-printing of a PE can improve the prospects of mLBs as reported in the work of Fu *et al.*[602] Herein, the anode and cathode inks are made by dispersing LTO and LFP nanoparticles, respectively, in a highly concentrated aqueous solution of graphene oxide (GO). The photographs of the LTO/GO and LFP/GO inks loaded in syringes are displayed in Fig. 53a, and the 3D-printed microelectrode and the interdigitated electrode assembly are presented in Fig. 53b and c, respectively. Once the 3D-printing of the anode and cathode microelectrodes and their post-processing for the conversion of GO to reduced GO (rGO) are carried out, the 3D-printing of the PE in the space between the interdigitated electrodes can be completed. For this purpose, a polymeric ink is made, which is composed of PVdF-HFP and Al$_2$O$_3$ nanoparticles in the NMP solvent. The sequential steps involved in the 3D-printing of the anode, cathode, and polymer electrolyte are shown in Fig. 53d. Once the polymer host is 3D-printed between the anode and cathode fingers, it can be activated by the injection of a conventional LE so that the LFP-rGO|GPE|LTO-rGO mLB full cell is ready for cycling. Fig. 53e and f present the cycling stability and charge–discharge
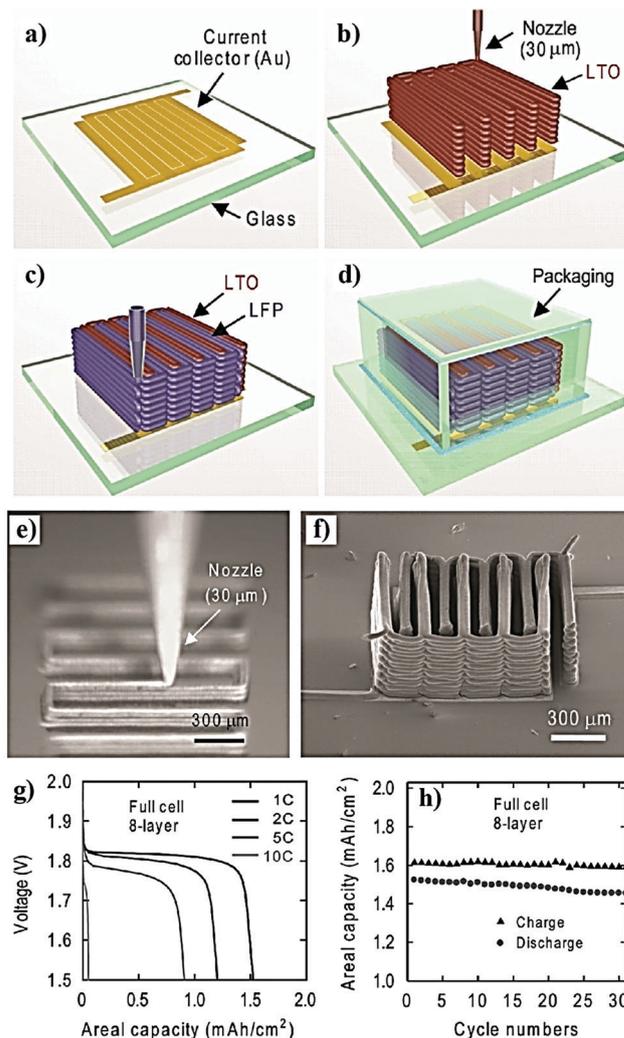
Fig. 52 (a) Glass substrate and the current collector patterned in the interdigitated configuration; 3D-printing of the (b) LTO anode, (c) LFP cathode, and (d) PMMA-based cell package; (e) optical microscopy image of the extrusion of 3D-printable ink through the nozzle; (f) SEM image of the 3D-printed interdigitated mLB microelectrodes; (g) galvanostatic charge–discharge profiles of the 3D-printed mLB as a function of C-rate; and (h) cycling stability profile of the 3D-printed mLB (reproduced/adapted from ref. 597 with permission from John Wiley and Sons, Copyright 2013[597]).

profiles of the 3D-printed full cells, respectively. A digital image of the 3D-printed microelectrode arrays is also displayed (see Fig. 53g). Although this work demonstrates the processing of PE-based mLB cells by 3D-printing of a polymeric solution, the *in situ* polymerization process involving the generation of a PE from a precursor is still missing during the full cell fabrication; hence, it cannot be considered as a typical example of an *in situ-processed-3D-printed* LPB.

In a recent report by Chen *et al.*, the patterning of a UV-curable electrode slurry and electrolyte inks and fabrication of an mLB by microstereolithography (μSLA) are reported, which is a perfect example of an *in situ-processed-3D-printed* LPB.[387] μSLA is a 3D-printing method in which the desired structure is fabricated layer-by-layer using a photo-polymerization process. In this work,
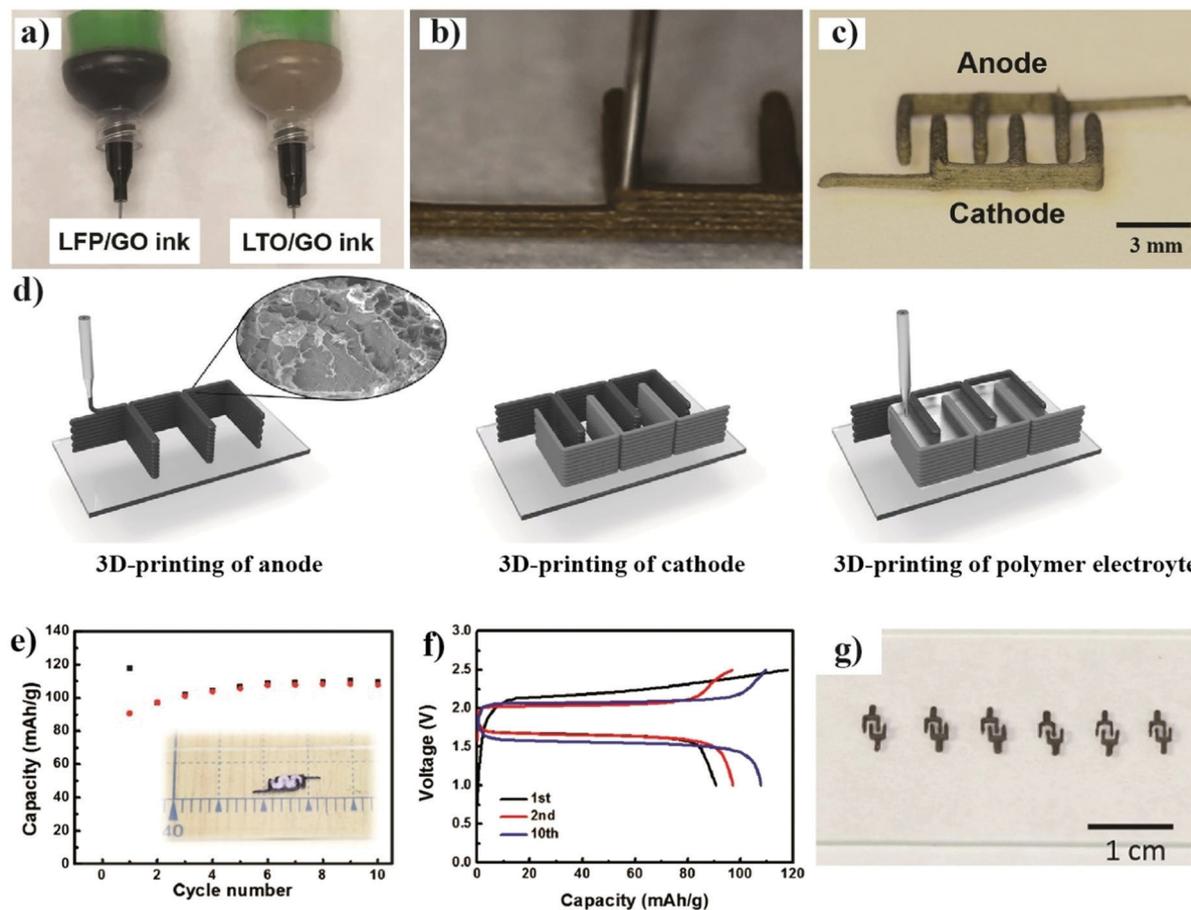
Fig. 53 (a) LTO/GO (anode) and LFP/GO (cathode) inks loaded in syringes used for the 3D-printing of mLBs; patterning of the microelectrode (b) and the interdigitated electrode assembly (c); (d) step-wise 3D-printing of the anode, cathode, and the PE in the space between the anode and cathode fingers; (e) cycling stability and (f) galvanostatic charge–discharge profiles of the 3D-printed full cell as a function of the number of cycles; and (g) digital image of the 3D-printed interdigitated microelectrode arrays (reproduced/adapted from ref. 602 with permission from John Wiley and Sons, Copyright 2016[602]).
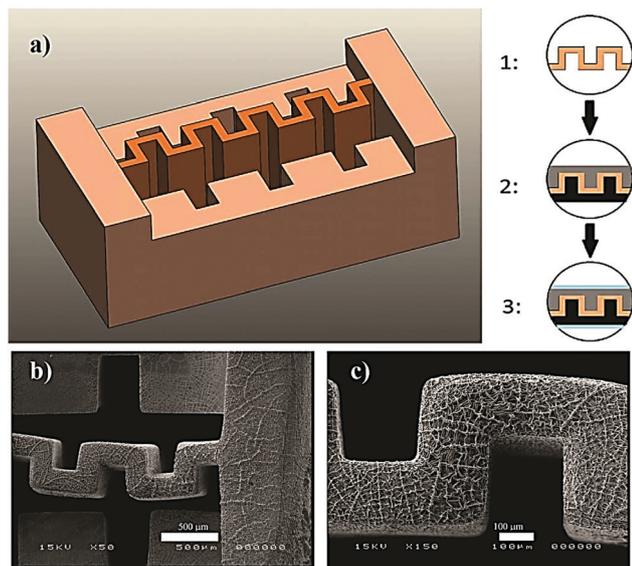
a UV-curable resin is prepared in a bulk quantity, which is composed of PEGDA (97 wt%), Irgacure 819 (1 wt%, photo-initiator), and a photo-absorber Sudan I (2 wt%) dye. The bulk solution is later mixed with an LE (20 wt%, 1 M LiClO$_4$ in EC:PC) to form the precursor for the GPE. Here, the photo-absorber is used for tuning the curing depth. The presence of the photo-absorber is crucial as it can avoid stray light from polymerizing the precursor providing a maximum resolution for the μSLA process. Also, the photo-absorber can absorb a certain quantity of photons and thereby control the polymerization rate, which is essential in μSLA for achieving ideal patterning.[603] The schematic representation of the mLB assembly is given in Fig. 54a. The two trenches separated by the GPE is filled with the anode (LTO) and cathode (LCO) inks (a slurry made of the respective active materials dispersed in the UV-curable resin) on UV irradiation solidify by the cross-linking polymerization process. The SEM image of the GPE 3D-structure is shown in Fig. 54b and c. The specific areal discharge capacity of the cell (1.5–4.5 V) is 1.4 μA h cm^{-2}.

Wei *et al.* also reported an *in situ-processed-3D-printed* LIPB cell,[414] and demonstrated that 3D-printing in combination with the *in situ* process could be extended for the production of LBs

beyond mLBs. The LTO and LFP inks used in this work are made in PC solvent in the presence of LiTFSI salt and PVP binder. The presence of LiTFSI salt in the electrode ink can help in improving the inter-particle ion diffusion. A UV curable precursor containing the monomer ETPTA, PC, LiTFSI, Al$_2$O$_3$ nanoparticles, and HMPP is used as the ink for the preparation of a PCE by the *in situ* process. For the cell encapsulation, a packaging ink made of a UV-curable epoxy resin and SiO$_2$ is used. The cell components and the steps involved in layer-by-layer 3D-printing of the customized LIPB cell are demonstrated in Fig. 55a and b, respectively. In the first step, the packaging ink is 3D-printed onto a glassy carbon substrate to form packaging walls, followed by the UV curing step. Later, the anode is 3D-printed over the glassy carbon substrate in the space between the packaging walls. Subsequently, the 3D-printing of the PCE layer over the anode is achieved by the *in situ* process. Later, the cathode ink is 3D-printed over the PCE layer, and the cell is closed with another glassy carbon lid. In the final step, the cell encapsulation is completed by the 3D-printing of another layer of packaging ink over the glassy carbon lid, making the cell ready to be cycled. The charge–discharge profile of the 3D-printed LIPB full cell is presented in Fig. 55c, which exhibits an areal

2772 | *Energy Environ. Sci.*, 2021, **14**, 2708–2788

This journal is © The Royal Society of Chemistry 2021

Fig. 54 3D-printing of an mLB using the μSLA technique. (a) On the left side, the 3D-mLB architecture is presented where the anode and cathode trenches are separated by a GPE. The liquid resin used for μSLA patterning of the GPE contains the methacrylate monomer, electrolyte components, and an initiator. The assembly process for the mLB (top view) is also provided. (1) Zig-zag GPE membrane in the center, (2) filling of the UV-curable anode and cathode slurry in respective trenches, and (3) insertion of the aluminum current collector. (b) and (c) are the SEM images (top-view) of the GPE zig-zag structure (reproduced/adapted from ref. 387 with permission from IOP Publishing, Copyright 2017[387]).
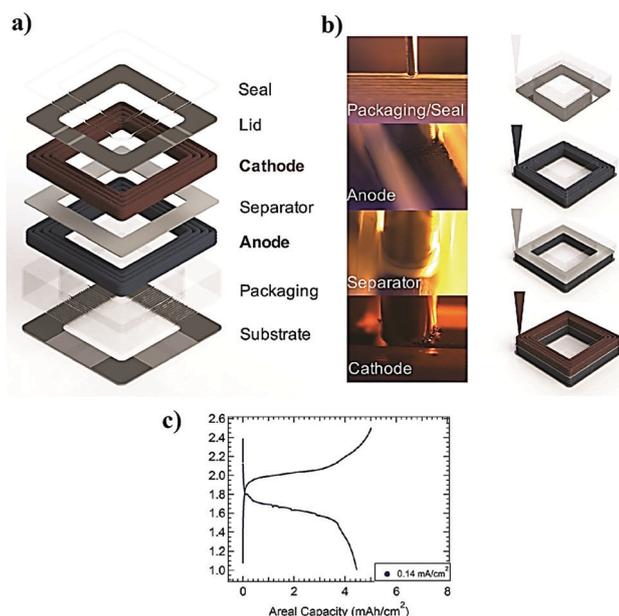
Fig. 55 (a) The components of the fully 3D-printed customized LIPB. (b) The illustration of the 3D-printing (direct writing method) of the cell packaging, anode, PE (denoted as the separator), and cathode inks. For packaging and PE preparation, followed by the writing step, a UV curing step is used. (c) Galvanostatic charge–discharge profile of a 3D-printed LIPB full cell (reproduced/adapted from ref. 414 with permission from John Wiley and Sons, Copyright 2018[414]).

specific capacity of 4.4 mA h cm^{-2} (at 0.14 mA cm^{-2}). In the work of Yoshima *et al.*, the *in situ* thermal polymerization approach is extended to the fabrication of mLB cells with LTO (anode) and LCO (cathode) electrodes in an interdigitated configuration.[368] The authors are not claiming this work as an example of 3D-printed mLB fabrication anywhere in the report. However, the microinjection system with a glass-capillary used for patterning the microelectrodes is similar to the already discussed 3D-printing approaches. Once the anode and cathode are assembled in an interdigitated fashion over the substrate, the precursor consisting of 1 M LiClO$_4$ in EC:DEC in the presence of MMA, EGDMA, and AIBN is filled in the vacancies and gaps between the anode and cathode. This is followed by a thermal curing process, which completes the *in situ* processing of the mLB. At 25 °C, the cell is operated between 1.5 and 2.5 V at 2C, and a discharge capacity of 270 μA h cm^{-2} is achieved. All the above-discussed studies are interesting as they systematically demonstrate the possible integration of 3D-printing technologies and *in situ* processes, which opens up new avenues for developing customized LB designs.

Other than 3D-printing, in several reports of Lee *et al.*, the screen-printing combined with the UV-light assisted *in situ* process is used for the fabrication of flexible LPB assemblies. Herein, one of the screen-printing techniques known as *stencil printing* is used, and the new class of printable LIPBs is referred to as PRISS batteries.[415] Here, the PE layer and the PE embedded electrode materials are printed on substrates having complex geometries. Owing to the use of an LE (1 M LiPF$_6$ in EC:PC) and ETPTA monomer, a cross-linked GPE can be derived by the UV curing process. The PRISS cell fabrication method is presented in Fig. 56a. In a typical procedure, a UV-curable slurry of LTO is first prepared in the precursor of the GPE. This slurry is coated over an aluminum current-collector, and a GPE embedded LTO anode is formed on UV curing. Over the anode layer, a PCE (called SCE) layer containing an Al$_2$O$_3$ nanofiller is formed by the *in situ* process from an electrolyte precursor. Subsequently, an LFP cathode layer is formed over the SCE layer by UV curing of a cathode slurry. Finally, another aluminum current-collector is placed over the LFP, and the formed LIPB cells (LFP|SCE|LTO) are hence called PRISS batteries. This work can be considered as an example of flexible LB fabrication by a multi-layer approach. The cross-sectional SEM image of the PRISS cell is presented in Fig. 56b, which clearly depicts the different cell components. At RT, the PRISS cell displayed a discharge capacity close to 160 mA h g^{-1} (0.05C) with cycling stability over 30 cycles (90% retention) (Fig. 56c). Similarly, photo-rechargeable portable power sources based on PRISS batteries integrated with miniaturized crystalline Si photovoltaics are also reported.[604]

Very recently, a screen-printing technique that is similar to the fabrication of PRISS battery cells is extended to bipolar-stacked LIPB packs (Fig. 57a).[416] Two types of bipolar-stacked LIPBs possessing in-series and in-plane configurations are designed (Fig. 57a). The anode (LTO), cathode (LCO), and PE are stencil printed in a layer-by-layer manner by using the UV-curing process. The precursor for the GPE (denoted as GCE) contains ETPTA and PVdF-*co*-HFP in the presence of
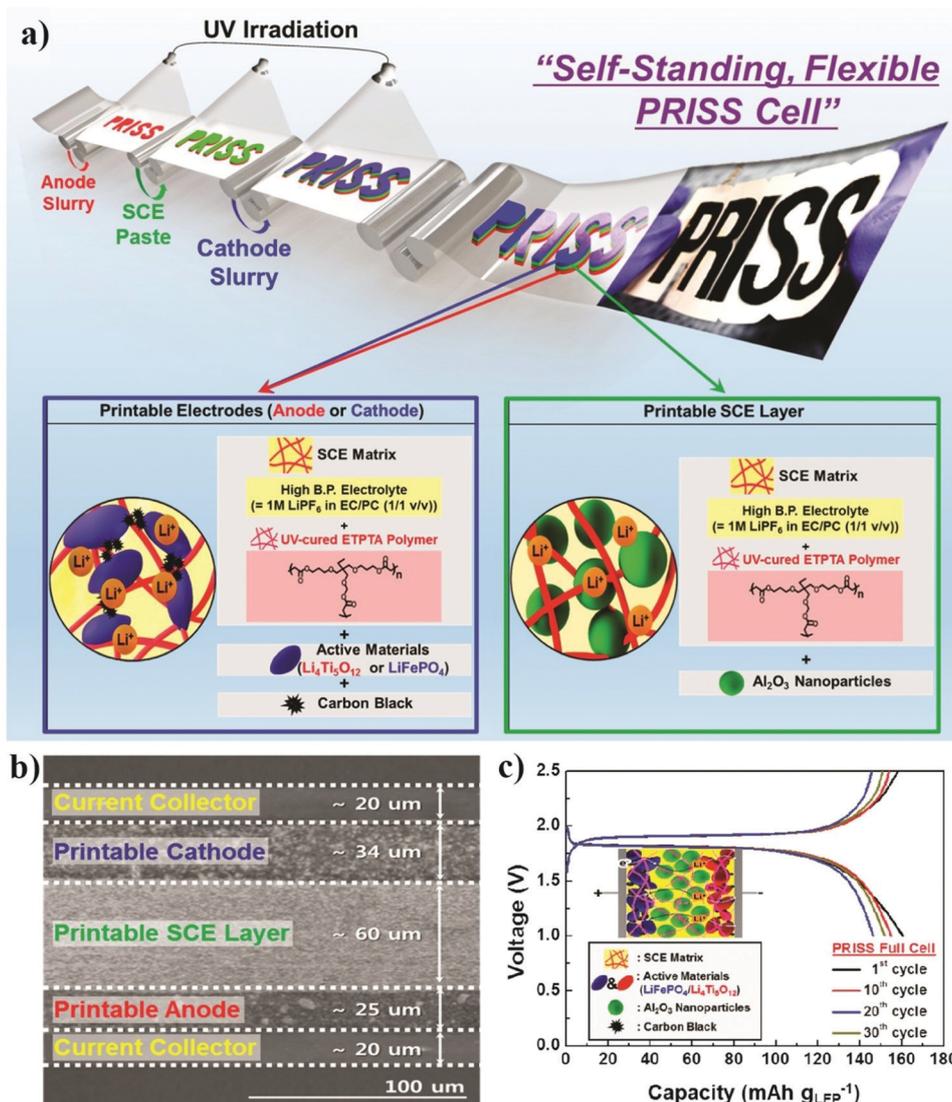
Fig. 56 (a) Design architecture and fabrication of the PRISS battery cell by the stencil printing technique in combination with the *in situ* process, and the composition of the printed electrodes and SCE; (b) the SEM image of the PRISS battery cell (cross-sectional view) depicting the various components such as the printed anode, cathode, SCE, and current collectors, and their thickness; and (c) the electrochemical performance (galvanostatic charge–discharge profiles) of the PRISS battery full cell as a function of cycle number (reproduced/adapted from ref. 415 with permission from American Chemical Society, Copyright 2015[415]).

HMPP and $LiPF_6$ in a non-flammable solvent called sebaconitrile (SBN). Depending on the number of cells connected, the bipolar-stacked LIPBs can have different voltages that vary from 2.4 V (mono cell) to 4.8 V (two cells), 7.2 V (three cells), and so on. The galvanostatic charge–discharge profiles of the printed mono cell and the bipolar-stacked LIPBs that exhibit a specific capacity close to 120 mA h g^{-1} (0.05C, 25 °C) are shown in Fig. 57b. Finally, the comparison of the electrochemical performance of the in-series and in-plane cells is also presented in Fig. 57c. Along with 3D-printing, screen-printing technology is also envisaged to be important for customized LB fabrication.

In summary, Section 7 provides an overview of the potential of the *in situ* process as a tool to simplify the fabrication of customized LB designs with tunable electrode|electrolyte interfaces and interphases. In the case of mLBs, a conformal coating

of the PIS that can ensure effective separation between the anode and cathode electrodes is indeed necessary. The UV curing process can ensure very thin PEs possessing thicknesses between 1 and 3 μm, suitable for mLB fabrication. The *in situ* electropolymerization reactions are useful for realizing a thin PIS-interphase layer protecting the electrodes and for preparing thin PEs compatible with mLBs. Additionally, 3D-printing is also emerging as a unique tool to fabricate customized and geometrically complex LBs, which can be integrated with the *in situ* process. The technique is slowly emerging for simplifying the conventional LB processing, and, in the coming years, it can play a vital role in futuristic EES device fabrication. Apart from 3D-printing, other printing techniques such as screen-printing and stencil printing, combined with the *in situ* process, are also employed for flexible and customized LPB fabrication.

2774 | *Energy Environ. Sci.*, 2021, **14**, 2708–2788

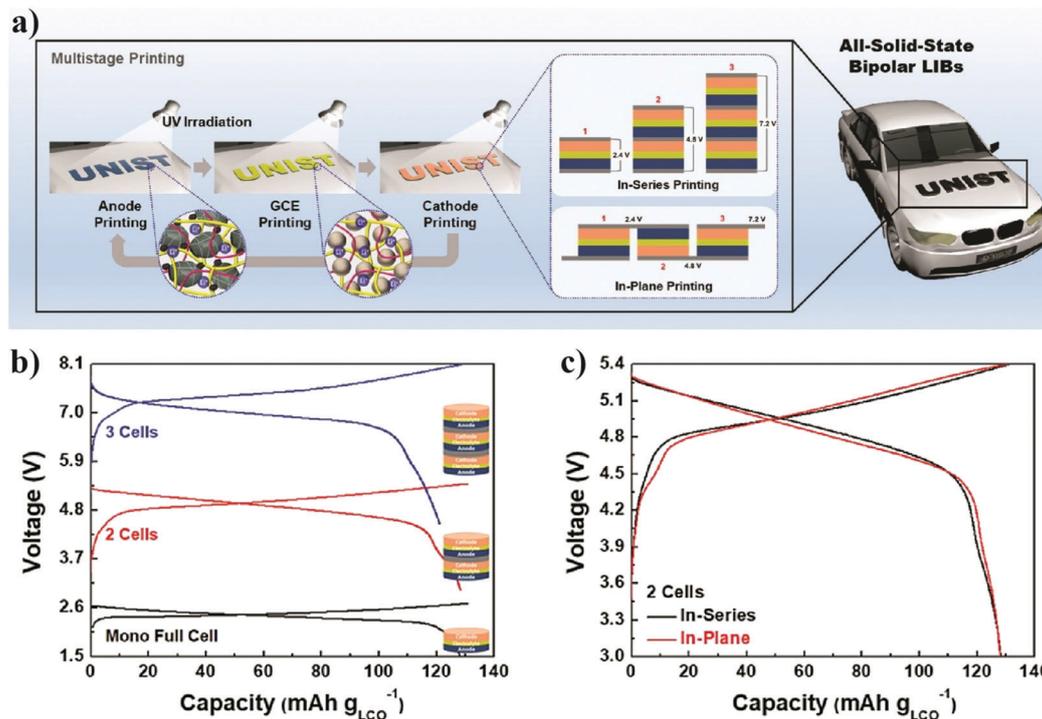This journal is © The Royal Society of Chemistry 2021

Fig. 57 (a) Schematic illustration of the fabrication of a bipolar-stacked LIPB by the stencil printing technique in combination with the *in situ* process and the in-series and in-plane configurations; (b) galvanostatic charge–discharge profiles of the single-cell and the bipolar-stacked LIPBs; and (c) comparison of the electrochemical performance of the in-series and in-plane bipolar-stacked LIPB cells (reproduced/adapted from ref. 416 with permission from The Royal Society of Chemistry[416]).

As explained in PRISS battery cells, the integration of the *in situ* process with screen-printing technology can simplify flexible LIPB and LMPB processing.

8. Conclusion and future perspectives

In this review, we have overviewed the LMPB and LIPB fabrication methods based on the *ex situ* or *in situ* polymerization processes. The conventional approach of LMPB and LIPB fabrication using the *ex situ* processed PE film is tenuous compared to the *in situ* process for achieving efficient and conformal electrode|electrolyte interfaces and interphases (SEIs and CEIs). Unlike the *ex situ* process, the *in situ* process involves the generation of a PE directly within the cell assembly or over the composite electrode in line with LPB cell fabrication. The interfaces and interphases in LPBs can be modified or engineered through the *in situ* process by several methods such as free-radical polymerization, electropolymerization, condensation polymerization, or ionic polymerization. Until now, the *in situ* process has been used in LPBs to achieve enhancements such as (i) lowering the charge transfer resistance at the interface, (ii) reducing volume expansion and pulverization of metal oxide-based electrode particles during charge–discharge cycling, (iii) improving active material utilization, (iv) decreasing transition metal dissolution, (v) thin and separator free electrolyte fabrication for micro-batteries, (vi) single-step 3D-printing of LPBs, (vii) protection

of the electrode by artificially and sacrificially created conformal interphase layers, and (viii) multi-layer processing of LIPB and LMPB cells. Most of the literature reports regarding the *in situ* processing of LPBs are focused on GPEs, where the presence of a liquid constituent may compromise their mechanical stability and non-flammability, and such shortcomings can only be addressed through all-solid-state systems, in particular using SPEs. Hence a more focused approach towards developing superior SPEs that are *in situ* processable is necessary for the realization of industrial-scale production of futuristic LPBs.

Most of the work in the field of LPBs using the *in situ* polymerization process is carried out on LFP-based electrodes, and the voltage range in which these electrolytes are working is mostly below 4 V. Besides, most of the reported cells have an areal capacity below 1.0 mA h cm^{-2}. However, futuristic battery systems are focused on high-voltage cathode materials due to the demand for high energy and power. Indeed, the recent trend is to employ nickel- and Li-rich cathode materials (*e.g.*, NMC622, NMC 811, NCA, *etc.*). In all these cases, the critical factor that limits the compatibility of PEs with high-voltage cathodes is their low oxidative stability and dendrite resistance capabilities. In general, high oxidative stability values are claimed in many literature reports for PEs (≥ 4.5 V *vs.* Li|Li^{+}) in electrodes such as Pt, stainless steel, and Al. However, when Ni-, Mn-, or Co-based cathode materials are used, accelerated oxidative degradation or inferior long-term cyclability is witnessed. Additionally, the undesirable side reactions at the interfaces

should be appropriately addressed to achieve the best performance in high-voltage battery systems. Hence, a real understanding of the oxidative stability values along with new characterization methods is required for the further development of PEs that are *in situ* processable for high power and energy-dense LMPBs/LIPBs.

To further improve the *in situ* polymerization process, the know-how of organic chemistry, polymer chemistry, physical chemistry, and electrochemistry should contribute equally. This multi- and inter-disciplinary approach can help in designing new polymerizable monomers and oligomers, which can ensure a better chemical and electrochemical stability in their pristine form and post-polymerized form. Along with the plethora of available studies on acrylate and methacrylate monomers/oligomers, other functionalities such as allyl and vinyl should also be investigated in the *in situ* free-radical polymerization process. Modification of acrylate and other monomers with hetero-functionalities (P, Si, F, *etc.*) is rarely explored for the *in situ* process and should be considered in future works. Besides, recent reports on *in situ* ionic polymerization suggest that it can evolve as a competitor to the free-radical methods. The potential of electropolymerization to ensure conformal coating of PE layers and artificial interphases should be exploited well for LIPBs and LMPBs. Especially in microbatteries, the electropolymerization method can have an imminent impact since it can effectively control the thickness of the PE in the nano-structured microelectrodes.

The future of PE-based energy storage is challenging, and we must address essential concerns such as:

1. Lack of fundamental studies on electrochemical reduction and oxidation of polymers, salts, and plasticizers to understand the stability and durability of LMPBs/LIPBs.

a. Investigating LPB cells with areal capacity above 1.0 mA h cm^{-2} and exploring their practicality in high energy and high power applications.

b. PE-based battery cells need to be investigated using accelerated testing models to understand the degradation processes *via* post-mortem analysis; however, present cycling studies are performed at low C-rates and are time-consuming.

c. The role of conductive carbon as an electrode additive in PE degradation during long-term cycling must be clarified. *In situ* and *ex situ* analytical tools need to be adapted/developed to elucidate the degradation mechanism in addition to exploring alternate conductivity enhancing additives and binders that are often polymer-based.

2. The behaviors of PEs against thin Li-metal (<50 μm) and the native oxide layers on Li-metal, which play a vital role during the charge–discharge cycles or in dendrite resistance, must be understood. Hence the fundamental understanding of the interface and interphase with Li-metal will be crucial for the development of true solid-state LPBs. Besides, the scope of *in situ* processing in the context of advanced anode-free LPBs should also be addressed in future works.

3. The significant concerns related to SPEs are also valid for GPEs, even though the performance of a GPE in a Li-ion/Li-metal cell is primarily dominated by the added plasticizer. Hence, the role of the polymer host and its peculiarities in the electrochemical performance are least investigated; however, a detailed study is necessary to understand the role of individual polymer hosts that have been employed in GPEs until now.

4. The interface engineering against thick electrodes, particularly at the cathode of an LMPB (both the anode and the cathode in the case of an LIPB), might be extensively influenced by the *in situ* and *ex situ* process; hence, a detailed investigation is necessary to understand the reactions taking place at the interface as the maximum surface of the active materials is exposed to the PEs due to the *in situ* process. Thus, new approaches and engineering strategies must be developed.

5. Controlling the electrical and ionic conduction in composite electrodes, and the ion and current flux at the Li-metal anode of an LMPB is required to avoid HSAL growth.

6. The approaches that are yet to be widely incorporated in PE research are:

a. Design and use of new polymer architectures and plasticizer chemistries to stabilize the PE during the continuous redox processes occurring at the electrodes.

b. A tailor-made passivation layer at the anode and cathode, and the engineering of artificial SEIs and CEIs should be encouraged in LPBs. The use of separately engineered and integrated passivation layers, followed by multi-layer cell assembly processes, should be adopted. The *in situ* polymerization process is a suitable candidate for the fabrication of such LPBs with enhanced safety, design flexibility, easy and fast cell fabrication, targeted interphase tuning, *etc.*

c. *In situ* processing should be integrated with other physical and chemical techniques for electrode protection. For instance, either coated metal oxide particles as active materials (*e.g.*, Al$_2$O$_3$ coated NMC) or composite electrode films with a protection layer (by AlP$_x$O$_y$, ZnO, Al$_2$O$_3$, *etc.*) made of atomic layer deposition (ALD), chemical vapor deposition (CVD), or other physical or chemical methods must be investigated.

Hence the challenges are enormous even if the *in situ* polymerization process is successfully implemented in the lab-scale for LPB fabrication. A broad spectrum of materials, processing methods, and engineering adaptations should be developed so that large-scale LPBs can be realized by using the *in situ* process. Apart from LPBs, in recent times, the *in situ* process has found applications in the fabrication of other electrochemical energy devices such as supercapacitors, solar cells, fuel cells, and Li-free alternate batteries. All the limitations regarding the electrode|electrolyte interfaces and interphases in LBs also recur for most of these devices. In this aspect, the applicability of the *in situ* process is vast and further optimization and focus are necessary to adopt an industrial-scale strategy for large-scale battery manufacturing. Hence, the realization of the *in situ* processable PEs with the requisite characteristics will enable upcoming energy storage devices to be affordable, upscalable, energy-dense, durable, and safe, which will revolutionize the global energy landscape.

Conflicts of interest

There are no conflicts to declare.

2776 | *Energy Environ. Sci.*, 2021, **14**, 2708–2788

This journal is © The Royal Society of Chemistry 2021

Acknowledgements

References

1 M. Winter and R. J. Brodd, *Chem. Rev.*, 2004, **104**, 4245–4270.

2 J. Betz, G. Bieker, P. Meister, T. Placke, M. Winter and R. Schmuch, *Adv. Energy Mater.*, 2019, **9**, 1803170.

3 Q. Zhao, J. Zheng and L. Archer, *ACS Energy Lett.*, 2018, **3**, 2104–2113.

4 M. A. Rahman, X. Wang and C. Wen, *J. Appl. Electrochem.*, 2014, **44**, 5–22.

5 J. Liu, Z. Bao, Y. Cui, E. J. Dufek, J. B. Goodenough, P. Khalifah, Q. Li, B. Y. Liaw, P. Liu, A. Manthiram, Y. S. Meng, V. R. Subramanian, M. F. Toney, V. V. Viswanathan, M. S. Whittingham, J. Xiao, W. Xu, J. Yang, X.-Q. Yang and J.-G. Zhang, *Nat. Energy*, 2019, **4**, 180–186.

6 D. Larcher and J. M. Tarascon, *Nat. Chem.*, 2014, **7**, 19.

7 D. Di Lecce, R. Verrelli and J. Hassoun, *Green Chem.*, 2017, **19**, 3442–3467.

8 Y. Lavoie, F. Danet and B. Lombard, in 2017 Petroleum and Chemical Industry Technical Conference (PCIC), IEEE, 2017, pp. 283–290.

9 T. Nagaura and K. Tozawa, *JEC Press*, 1990, **9**, 209.

10 W. N. Association, Heat values of various fuels, https://www.world-nuclear.org/informationlibrary/facts-and-figures/heat-values-of-various-fuels.aspx, Accessed 29/10, 2020.

11 Tesla, https://www.tesla.com/en_EU/support/european-union-energy-label, Accessed 29/10, 2020.

12 P. V. Kamat, *ACS Energy Lett.*, 2019, **4**, 2757–2759.

13 M. Winter, K.-C. Moeller and J. Besenhard, in *Lithium Batteries*, Springer, 2009, pp. 145–194.

14 M. Winter and J. Besenhard, *Handbook of Battery Materials*, 2007, pp. 383–418.

15 M. Winter, J. Besenhard, J. Albering, J. Yang and M. Wachtler, *Prog. Batteries Battery Mater.*, 1998, **17**, 208–213.

16 W.-R. Liu, Y.-C. Yen, H.-C. Wu, M. Winter and N.-L. Wu, *J. Appl. Electrochem.*, 2009, **39**, 1643–1649.

17 J. O. Besenhard and M. Winter, *ChemPhysChem*, 2002, **3**, 155–159.

18 Y. Arinicheva, M. Wolff, S. Lobe, C. Dellen, D. Fattakhova-Rohlfing, O. Guillon, D. Böhm, F. Zoller, R. Schmuch and J. Li, in *Advanced Ceramics for Energy Conversion and Storage*, Elsevier, 2020, pp. 549–709.

19 J. Kasnatscheew, M. Evertz, R. Kloepsch, B. Streipert, R. Wagner, I. Cekic Laskovic and M. Winter, *Energy Technol.*, 2017, **5**, 1670–1679.

20 I. Cekic-Laskovic, N. von Aspern, L. Imholt, S. Kaymaksiz, K. Oldiges, B. R. Rad and M. Winter, *Top. Curr. Chem.*, 2017, **375**, 37.

21 P. Arora and Z. Zhang, *Chem. Rev.*, 2004, **104**, 4419–4462.

22 J. Holtmann, M. Schäfer, A. Niemöller, M. Winter, A. Lex-Balducci and S. Obeidi, *J. Appl. Electrochem.*, 2016, **46**, 69–76.

23 S. Lux, F. Schappacher, A. Balducci, S. Passerini and M. Winter, *J. Electrochem. Soc.*, 2010, **157**, A320–A325.

24 X. Qi, B. Blizanac, A. DuPasquier, A. Lal, P. Niehoff, T. Placke, M. Oljaca, J. Li and M. Winter, *J. Electrochem. Soc.*, 2014, **162**, A339.

25 X. Qi, B. Blizanac, A. DuPasquier, P. Meister, T. Placke, M. Oljaca, J. Li and M. Winter, *Phys. Chem. Chem. Phys.*, 2014, **16**, 25306–25313.

26 X. Qi, B. Blizanac, A. DuPasquier, M. Oljaca, J. Li and M. Winter, *Carbon*, 2013, **64**, 334–340.

27 E. Krämer, S. Passerini and M. Winter, *ECS Electrochem. Lett.*, 2012, **1**, C9–C11.

28 J. Kasnatscheew, M. Börner, B. Streipert, P. Meister, R. Wagner, I. C. Laskovic and M. Winter, *J. Power Sources*, 2017, **362**, 278–282.

29 M. Wachtler, M. R. Wagner, M. Schmied, M. Winter and J. O. Besenhard, *J. Electroanal. Chem.*, 2001, **510**, 12–19.

30 E. M. Erickson, E. Markevich, G. Salitra, D. Sharon, D. Hirshberg, E. de la Llave, I. Shterenberg, A. Rosenman, A. Frimer and D. Aurbach, *J. Electrochem. Soc.*, 2015, **162**, A2424–A2438.

31 K. Xu, *Chem. Rev.*, 2004, **104**, 4303–4418.

32 M. Amereller, T. Schedlbauer, D. Moosbauer, C. Schreiner, C. Stock, F. Wudy, S. Zugmann, H. Hammer, A. Maurer, R. M. Gschwind, H. D. Wiemhöfer, M. Winter and H. J. Gores, *Prog. Solid State Chem.*, 2014, **42**, 39–56.

33 J. Kasnatscheew, R. Wagner, M. Winter and I. Cekic-Laskovic, *Modeling Electrochemical Energy Storage at the Atomic Scale*, Springer, 2018, pp. 23–51.

34 H. Schranzhofer, J. Bugajski, H. Santner, C. Korepp, J. Besenhard, M. Winter and W. Sitte, *J. Power Sources*, 2006, **153**, 391–395.

35 S. Röser, A. Lerchen, L. Ibing, X. Cao, J. Kasnatscheew, F. Glorius, M. Winter and R. Wagner, *Chem. Mater.*, 2017, **29**, 7733–7739.

36 Y.-M. Liu, B. G. Nicolau, J. L. Esbenshade and A. A. Gewirth, *Anal. Chem.*, 2016, **88**, 7171–7177.

37 R. W. Schmitz, P. Murmann, R. Schmitz, R. Müller, L. Krämer, J. Kasnatscheew, P. Isken, P. Niehoff, S. Nowak, G.-V. Röschenthaler, N. Ignatiev, P. Sartori, S. Passerini, M. Kunze, A. Lex-Balducci, C. Schreiner, I. Cekic-Laskovic and M. Winter, *Prog. Solid State Chem.*, 2014, **42**, 65–84.

38 G. Bieker, M. Winter and P. Bieker, *Phys. Chem. Chem. Phys.*, 2015, **17**, 8670–8679.

39 S. Krueger, R. Kloepsch, J. Li, S. Nowak, S. Passerini and M. Winter, *J. Electrochem. Soc.*, 2013, **160**, A542–A548.

40 P. Meister, X. Qi, R. Kloepsch, E. Krämer, B. Streipert, M. Winter and T. Placke, *ChemSusChem*, 2017, **10**, 804–814.

41 H. Q. Pham, H.-Y. Lee, E.-H. Hwang, Y.-G. Kwon and S.-W. Song, *J. Power Sources*, 2018, **404**, 13–19.

42 N. von Aspern, S. Röser, B. Rezaei Rad, P. Murmann, B. Streipert, X. Mönnighoff, S. D. Tillmann, M. Shevchuk, O. Stubbmann-Kazakova, G.-V. Röschenthaler, S. Nowak, M. Winter and I. Cekic-Laskovic, *J. Fluorine Chem.*, 2017, **198**, 24–33.

43 K. Liu, Y. Liu, D. Lin, A. Pei and Y. Cui, *Sci. Adv.*, 2018, **4**, eaas9820.

44 Q. Li, J. Chen, L. Fan, X. Kong and Y. Lu, *Exergy Its Appl.*, 2016, **1**, 18–42.

45 L. Xia, L. Yu, D. Hu and G. Z. Chen, *Mater. Chem. Front.*, 2017, **1**, 584–618.

46 L. Suo, F. Han, X. Fan, H. Liu, K. Xu and C. Wang, *J. Mater. Chem. A*, 2016, **4**, 6639–6644.

47 C. Yang, J. Chen, T. Qing, X. Fan, W. Sun, A. von Cresce, M. S. Ding, O. Borodin, J. Vatamanu, M. A. Schroeder, N. Eidson, C. Wang and K. Xu, *Joule*, 2017, **1**, 122–132.

48 J. M. Tarascon, *Philos. Trans. R. Soc., A*, 2010, **368**, 3227–3241.

49 M. Armand and J. M. Tarascon, *Nature*, 2008, **451**, 652–657.

50 J. Janek and W. G. Zeier, *Nat. Energy*, 2016, **1**, 1–4.

51 A. Eftekhari, *ACS Sustainable Chem. Eng.*, 2019, **7**, 3684–3687.

52 M. H. Ryou, Y. M. Lee, Y. Lee, M. Winter and P. Bieker, *Adv. Funct. Mater.*, 2015, **25**, 834–841.

53 J. Heine, S. Krüger, C. Hartnig, U. Wietelmann, M. Winter and P. Bieker, *Adv. Energy Mater.*, 2014, **4**, 1300815.

54 J. Heine, P. Hilbig, X. Qi, P. Niehoff, M. Winter and P. Bieker, *J. Electrochem. Soc.*, 2015, **162**, A1094–A1101.

55 Y. Liu, Q. Liu, L. Xin, Y. Liu, F. Yang, E. A. Stach and J. Xie, *Nat. Energy*, 2017, **2**, 17083.

56 P. Barai, K. Higa and V. Srinivasan, *Phys. Chem. Chem. Phys.*, 2017, **19**, 20493–20505.

57 R. Khurana, J. L. Schaefer, L. A. Archer and G. W. Coates, *J. Am. Chem. Soc.*, 2014, **136**, 7395–7402.

58 C. Monroe and J. Newman, *J. Electrochem. Soc.*, 2005, **152**, A396–A404.

59 G. Stone, S. Mullin, A. Teran, D. Hallinan, A. Minor, A. Hexemer and N. Balsara, *J. Electrochem. Soc.*, 2012, **159**, A222–A227.

60 S. Yu, R. D. Schmidt, R. Garcia-Mendez, E. Herbert, N. J. Dudney, J. B. Wolfenstine, J. Sakamoto and D. J. Siegel, *Chem. Mater.*, 2016, **28**, 197–206.

61 A. Sakuda, A. Hayashi and M. Tatsumisago, *Sci. Rep.*, 2013, **3**, 2261.

62 S. Liang, W. Yan, X. Wu, Y. Zhang, Y. Zhu, H. Wang and Y. Wu, *Solid State Ionics*, 2018, **318**, 2–18.

63 J. Y. Song, Y. Y. Wang and C. C. Wan, *J. Power Sources*, 1999, **77**, 183–197.

64 H. Zhang, C. Li, M. Piszcz, E. Coya, T. Rojo, L. M. Rodriguez-Martinez, M. Armand and Z. Zhou, *Chem. Soc. Rev.*, 2017, **46**, 797–815.

65 W. H. Meyer, *Adv. Mater.*, 1998, **10**, 439–448.

66 Q. Zhang, K. Liu, F. Ding and X. Liu, *Nano Res.*, 2017, **10**, 4139–4174.

67 N. Boaretto, L. Meabe, M. Martinez-Ibañez, M. Armand and H. Zhang, *J. Electrochem. Soc.*, 2020, **167**, 070524.

68 Q. Zhao, S. Stalin, C.-Z. Zhao and L. A. Archer, *Nat. Rev. Mater.*, 2020, **5**, 229–252.

69 A. Manuel Stephan and K. S. Nahm, *Polymer*, 2006, **47**, 5952–5964.

70 A. Manuel Stephan, *Eur. Polym. J.*, 2006, **42**, 21–42.

71 R. C. Agrawal and G. P. Pandey, *J. Phys. D: Appl. Phys.*, 2008, **41**, 223001.

72 Z. Xue, D. He and X. Xie, *J. Mater. Chem. A*, 2015, **3**, 19218–19253.

73 L. Long, S. Wang, M. Xiao and Y. Meng, *J. Mater. Chem. A*, 2016, **4**, 10038–10069.

74 J. Mindemark, M. J. Lacey, T. Bowden and D. Brandell, *Prog. Polym. Sci.*, 2018, **81**, 114–143.

75 D. Golodnitsky, E. Strauss, E. Peled and S. Greenbaum, *J. Electrochem. Soc.*, 2015, **162**, A2551–A2566.

76 S. B. Aziz, T. J. Woo, M. F. Z. Kadir and H. M. Ahmed, *J. Sci.: Adv. Mater. Devices*, 2018, **3**, 1–17.

77 M. Winter, B. Barnett and K. Xu, *Chem. Rev.*, 2018, **118**, 11433–11456.

78 Y.-F. Y. Yao and J. Kummer, *J. Inorg. Nucl. Chem.*, 1967, **29**, 2453–2475.

79 M. S. Whittingham, *Proc. IEEE*, 2012, **100**, 1518–1534.

80 W. Nernst, *Z. Electrochem.*, 1899, **6**, 41–43.

81 M. Faraday, *Philos. Trans. R. Soc. London*, 1833, 23–54.

82 A. Manthiram, X. Yu and S. Wang, *Nat. Rev. Mater.*, 2017, **2**, 16103.

83 C. Gassner, *US Pat.*, 373064. US Patent and Trademark Office, Washington, DC, 1887.

84 C. J. Coleman, *US Pat.*, 495306. US Patent and Trademark Office, Washington, DC, 1893.

85 W. L. F. Hellesen, *US Pat.*, 439151. US Patent and Trademark Office, Washington, DC, 1890.

86 C. Hambuechen, *US Pat.*, 1292764, US Patent and Trademark Office, Washington, DC, 1919.

87 J. R. Nair, L. Imholt, G. Brunklaus and M. Winter, *Electrochem. Soc. Interface*, 2019, **28**, 55–61.

88 K. Xu, *Chem. Rev.*, 2014, **114**, 11503–11618.

89 K. Kanamura, in *Encyclopedia of Electrochemical Power Sources*, ed. J. Garche, Elsevier, Amsterdam, 2009, pp. 27–39.

90 W. S. Harris, *Electrochemical studies in cyclic esters*, University of California Radiation Laboratory, 1958.

91 X. Yu and A. Manthiram, *Energy Environ. Sci.*, 2018, **11**, 527–543.

92 E. Peled, *J. Electrochem. Soc.*, 1979, **126**, 2047–2051.

93 X.-B. Cheng, R. Zhang, C.-Z. Zhao, F. Wei, J.-G. Zhang and Q. Zhang, *Adv. Sci.*, 2016, **3**, 1500213.

94 E. Peled and S. Menkin, *J. Electrochem. Soc.*, 2017, **164**, A1703.

95 D. Aurbach, M. Daroux, P. Faguy and E. Yeager, *J. Electrochem. Soc.*, 1987, **134**, 1611.

96 H. Bauman, J. Chilton, W. Conner and G. Cook, *New Cathode-Anode Couples using Nonaqueous Electrolyte*, Technical Documentary Report No. RTD-TDR-63-4083, Lockheed Missiles and Space Co Inc, 1963.

97 N. Gupta, R. Radkey, A. Remanick and M. Shaw, *Electrochemical Characterization of Systems for Secondary Battery Application*, NASA CR-72138, NASA, 1966.

98 W. F. Meyers and J. W. Simmons, *US Pat.*, 3423242, U.S. Patent and Trademark Office, Washington, DC, 1969.

99 M. V. Reddy, A. Mauger, C. M. Julien, A. Paolella and K. Zaghib, *Materials*, 2020, **13**, 1884.

2778 | *Energy Environ. Sci.*, 2021, **14**, 2708–2788

This journal is © The Royal Society of Chemistry 2021

100 T. Placke, R. Kloepsch, S. Dühnen and M. Winter, *J. Solid State Electrochem.*, 2017, **21**, 1939–1964.

101 R. Somoano, V. Hadek, A. Rembaum, S. Samson and J. Woollam, *J. Chem. Phys.*, 1975, **62**, 1068–1073.

102 D. Murphy, P. Christian, F. DiSalvo and J. Carides, *J. Electrochem. Soc.*, 1979, **126**, 497–499.

103 M. S. Whittingham, *Prog. Solid State Chem.*, 1978, **12**, 41–99.

104 R. Selim and P. Bro, *J. Electrochem. Soc.*, 1974, **121**, 1457–1459.

105 M. S. Whittingham, *Chem. Rev.*, 2014, **114**, 11414–11443.

106 M. S. Whittingham, *Science*, 1976, **192**, 1126–1127.

107 K. Mizushima, P. C. Jones, P. J. Wiseman and J. B. Goodenough, *Mater. Res. Bull.*, 1980, **15**, 783–789.

108 N. Nitta, F. Wu, J. T. Lee and G. Yushin, *Mater. Today*, 2015, **18**, 252–264.

109 O. V. Bushkova, T. V. Yaroslavtseva and Y. A. Dobrovolsky, *Russ. J. Electrochem.*, 2017, **53**, 677–699.

110 M. S. Whittingham, *Chem. Rev.*, 2004, **104**, 4271–4302.

111 W. Qi, J. G. Shapter, Q. Wu, T. Yin, G. Gao and D. Cui, *J. Mater. Chem. A*, 2017, **5**, 19521–19540.

112 P. Roy and S. K. Srivastava, *J. Mater. Chem. A*, 2015, **3**, 2454–2484.

113 A. Mishra, A. Mehta, S. Basu, S. J. Malode, N. P. Shetti, S. S. Shukla, M. N. Nadagouda and T. M. Aminabhavi, *Mater. Sci. Energy Technol.*, 2018, **1**, 182–187.

114 J. B. Goodenough, *Nat. Electron.*, 2018, **1**, 204.

115 K. J. Stevenson, *J. Solid State Electrochem.*, 2012, **16**, 2017–2018.

116 Y. Yamada and A. Yamada, *J. Electrochem. Soc.*, 2015, **162**, A2406–A2423.

117 V. Aravindan, J. Gnanaraj, S. Madhavi and H.-K. Liu, *Chem. – Eur. J.*, 2011, **17**, 14326–14346.

118 D. Puthusseri, M. Wahid and S. Ogale, *ACS Omega*, 2018, **3**, 4591–4601.

119 I. Yoshimatsu, T. Hirai and J. I. Yamaki, *J. Electrochem. Soc.*, 1988, **135**, 2422–2427.

120 L. Li, S. Li and Y. Lu, *Chem. Commun.*, 2018, **54**, 6648–6661.

121 S. Xia, X. Wu, Z. Zhang, Y. Cui and W. Liu, *Chem*, 2019, **5**, 753–785.

122 D. A. Scherson, in *Nonaqueous Electrochemistry*, ed. D. Aurbach, Marcel Dekker, 1999, pp. 213–288.

123 K. Brandt, *Solid State Ionics*, 1994, **69**, 173–183.

124 J. O. Besenhard and H. P. Fritz, *J. Electroanal. Chem. Interfacial Electrochem.*, 1974, **53**, 329–333.

125 J. O. Besenhard, *Carbon*, 1976, **14**, 111–115.

126 J. O. Besenhard and H. P. Fritz, *Angew. Chem., Int. Ed. Engl.*, 1983, **22**, 950–975.

127 M. Wachtler, M. Winter and J. O. Besenhard, *J. Power Sources*, 2002, **105**, 151–160.

128 M. Winter, J. O. Besenhard, M. E. Spahr and P. Novák, *Adv. Mater.*, 1998, **10**, 725–763.

129 J. R. Dahn, T. Zheng, Y. Liu and J. S. Xue, *Science*, 1995, **270**, 590–593.

130 R. Fong, U. Von Sacken and J. R. Dahn, *J. Electrochem. Soc.*, 1990, **137**, 2009–2013.

131 Z. Ogumi and H. Wang, in *Lithium-Ion Batteries: Science and Technologies*, ed. M. Yoshio, R. J. Brodd and A. Kozawa, Springer New York, New York, NY, 2009, pp. 49–73.

132 Y. P. Wu, E. Rahm and R. Holze, *J. Power Sources*, 2003, **114**, 228–236.

133 M. Winter, K. C. Moeller and J. O. Besenhard, in *Lithium Batteries: Science and Technology*, ed. G.-A. Nazri and G. Pistoia, Springer US, Boston, MA, 2003, pp. 145–194.

134 T. P. Kumar, T. S. D. Kumari and M. A. Stephan, *J. Indian Inst. Sci.*, 2012, **89**, 393–424.

135 R. Yazami and P. Touzain, *J. Power Sources*, 1983, **9**, 365–371.

136 S. Basu, C. Zeller, P. J. Flanders, C. D. Fuerst, W. D. Johnson and J. E. Fischer, *Mater. Sci. Eng.*, 1979, **38**, 275–283.

137 M. Zanini, S. Basu and J. E. Fischer, *Carbon*, 1978, **16**, 211–212.

138 S. Basu, *US Pat.*, 4423125, U.S. Patent and Trademark Office, Washington, DC, 1983.

139 S. Basu, *US Pat.*, 4304825, U.S. Patent and Trademark Office, Washington, DC, 1981.

140 R. Fong, U. Von Sacken and J. R. Dahn, *J. Electrochem. Soc.*, 1990, **137**, 2009.

141 J. Asenbauer, T. Eisenmann, M. Kuenzel, A. Kazzazi, Z. Chen and D. Bresser, *Sustainable Energy Fuels*, 2020, **4**, 5387–5416.

142 A. Yoshino, *Angew. Chem., Int. Ed.*, 2012, **51**, 5798–5800.

143 X. Li, S. Guo, H. Deng, K. Jiang, Y. Qiao, M. Ishida and H. Zhou, *J. Mater. Chem. A*, 2018, **6**, 15517–15522.

144 B. Liu, J.-G. Zhang and W. Xu, *Joule*, 2018, **2**, 833–845.

145 C. Liang, M. Gao, H. Pan, Y. Liu and M. Yan, *J. Alloys Compd.*, 2013, **575**, 246–256.

146 K. Cao, T. Jin, L. Yang and L. Jiao, *Mater. Chem. Front.*, 2017, **1**, 2213–2242.

147 P. V. Wright, *Br. Polym. J.*, 1975, **7**, 319–327.

148 D. E. Fenton, J. M. Parker and P. V. Wright, *Polymer*, 1973, **14**, 589.

149 M. Armand, *Solid State Ionics*, 1994, **69**, 309–319.

150 M. Armand, J. Chabagno and M. Duclot, *St Andrews, Scotland*, 1978, 20–22.

151 M. Armand, *Solid State Ionics*, 1983, **9-10**, 745–754.

152 H. Zhang and M. Armand, *Isr. J. Chem.*, 2020, DOI: 10.1002/ijch.202000066.

153 O. Borodin and G. D. Smith, *Macromolecules*, 2006, **39**, 1620–1629.

154 H. Kataoka, Y. Saito, M. Tabuchi, Y. Wada and T. Sakai, *Macromolecules*, 2002, **35**, 6239–6244.

155 T. Morioka, K. Nakano and Y. Tominaga, *Macromol. Rapid Commun.*, 2017, **38**, 1600652.

156 J. W. Fergus, *J. Power Sources*, 2010, **195**, 4554–4569.

157 J. B. Goodenough and P. Singh, *J. Electrochem. Soc.*, 2015, **162**, A2387–A2392.

158 C. Cao, Z.-B. Li, X.-L. Wang, X.-B. Zhao and W.-Q. Han, *Front. Energy Res.*, 2014, **2**, 25.

159 F. Han, A. S. Westover, J. Yue, X. Fan, F. Wang, M. Chi, D. N. Leonard, N. J. Dudney, H. Wang and C. Wang, *Nat. Energy*, 2019, **4**, 187–196.

160 S. Wenzel, S. J. Sedlmaier, C. Dietrich, W. G. Zeier and J. Janek, *Solid State Ionics*, 2018, **318**, 102–112.

161 V. Thangadurai, H. Kaack and W. J. F. Weppner, *J. Am. Ceram. Soc.*, 2003, **86**, 437–440.

This journal is © The Royal Society of Chemistry 2021

Energy Environ. Sci., 2021, **14**, 2708–2788 | 2779

162 Z. Gao, H. Sun, L. Fu, F. Ye, Y. Zhang, W. Luo and Y. Huang, *Adv. Mater.*, 2018, **30**, 1705702.

163 C. R. Mariappan, M. Gellert, C. Yada, F. Rosciano and B. Roling, *Electrochem. Commun.*, 2012, **14**, 25–28.

164 H. Yamane, M. Shibata, Y. Shimane, T. Junke, Y. Seino, S. Adams, K. Minami, A. Hayashi and M. Tatsumisago, *Solid State Ionics*, 2007, **178**, 1163–1167.

165 J. Lau, R. H. DeBlock, D. M. Butts, D. S. Ashby, C. S. Choi and B. S. Dunn, *Adv. Energy Mater.*, 2018, **8**, 1800933.

166 F. Mizuno, A. Hayashi, K. Tadanaga and M. Tatsumisago, *Solid State Ionics*, 2006, **177**, 2721–2725.

167 J. C. Bachman, S. Muy, A. Grimaud, H.-H. Chang, N. Pour, S. F. Lux, O. Paschos, F. Maglia, S. Lupart, P. Lamp, L. Giordano and Y. Shao-Horn, *Chem. Rev.*, 2016, **116**, 140–162.

168 A. Banerjee, X. Wang, C. Fang, E. A. Wu and Y. S. Meng, *Chem. Rev.*, 2020, **120**, 6878–6933.

169 D. Lin, Y. Liu and Y. Cui, *Nat. Nanotechnol.*, 2017, **12**, 194.

170 R. Koerver, W. Zhang, L. de Biasi, S. Schweidler, A. O. Kondrakov, S. Kolling, T. Brezesinski, P. Hartmann, W. G. Zeier and J. Janek, *Energy Environ. Sci.*, 2018, **11**, 2142–2158.

171 J. Hu, J. Tian and C. Li, *ACS Appl. Mater. Interfaces*, 2017, **9**, 11615–11625.

172 X. Cheng, J. Pan, Y. Zhao, M. Liao and H. Peng, *Adv. Energy Mater.*, 2018, **8**, 1702184.

173 H. Wu, Y. Cao, H. Su and C. Wang, *Angew. Chem., Int. Ed.*, 2018, **57**, 1361–1365.

174 M. Winter, *Z. Phys. Chem.*, 2009, **223**, 1395–1406.

175 W. A. Henderson, in *Electrolytes for Lithium and Lithium-Ion Batteries*, ed. T. R. Jow, K. Xu, O. Borodin and M. Ue, Springer, New York, New York, NY, 2014, pp. 1–92.

176 Q. Pan, Y. Zheng, S. Kota, W. Huang, S. Wang, H. Qi, S. Kim, Y. Tu, M. W. Barsoum and C. Y. Li, *Nanoscale Adv.*, 2019, **1**, 395–402.

177 Y. Inaguma, C. Liquan, M. Itoh, T. Nakamura, T. Uchida, H. Ikuta and M. Wakihara, *Solid State Commun.*, 1993, **86**, 689–693.

178 R. Murugan, V. Thangadurai and W. Weppner, *Angew. Chem., Int. Ed.*, 2007, **46**, 7778–7781.

179 A. Dumon, M. Huang, Y. Shen and C.-W. Nan, *Solid State Ionics*, 2013, **243**, 36–41.

180 B. V. Lotsch and J. Maier, *J. Electroceram.*, 2017, **38**, 128–141.

181 H. Y. P. Hong, *Mater. Res. Bull.*, 1978, **13**, 117–124.

182 H. Aono, E. Sugimoto, Y. Sadaoka, N. Imanaka and G. Y. Adachi, *J. Electrochem. Soc.*, 1990, **137**, 1023–1027.

183 N. V. Kosova, E. T. Devyatkina, A. P. Stepanov and A. L. Buzlukov, *Ionics*, 2008, **14**, 303–311.

184 M. A. Kraft, S. P. Culver, M. Calderon, F. Böcher, T. Krauskopf, A. Senyshyn, C. Dietrich, A. Zevalkink, J. Janek and W. G. Zeier, *J. Am. Chem. Soc.*, 2017, **139**, 10909–10918.

185 H.-J. Deiseroth, S.-T. Kong, H. Eckert, J. Vannahme, C. Reiner, T. Zaiß and M. Schlosser, *Angew. Chem., Int. Ed.*, 2008, **47**, 755–758.

186 C. Yu, J. Hageman, S. Ganapathy, L. van Eijck, L. Zhang, K. R. Adair, X. Sun and M. Wagemaker, *J. Mater. Chem. A*, 2019, **7**, 10412–10421.

187 Y. Seino, T. Ota, K. Takada, A. Hayashi and M. Tatsumisago, *Energy Environ. Sci.*, 2014, **7**, 627–631.

188 C. Dietrich, D. A. Weber, S. Culver, A. Senyshyn, S. J. Sedlmaier, S. Indris, J. Janek and W. G. Zeier, *Inorg. Chem.*, 2017, **56**, 6681–6687.

189 N. Kamaya, K. Homma, Y. Yamakawa, M. Hirayama, R. Kanno, M. Yonemura, T. Kamiyama, Y. Kato, S. Hama, K. Kawamoto and A. Mitsui, *Nat. Mater.*, 2011, **10**, 682.

190 D. T. Hallinan Jr and N. P. Balsara, *Ann. Rev. Mater. Res.*, 2013, **43**, 503–525.

191 K. S. Ngai, S. Ramesh, K. Ramesh and J. C. Juan, *Ionics*, 2016, **22**, 1259–1279.

192 D. R. MacFarlane and M. Forsyth, *Adv. Mater.*, 2001, **13**, 957–966.

193 S. Wang, X. Liu, A. Wang, Z. Wang, J. Chen, Q. Zeng, X. Wang and L. Zhang, *Polym. Chem.*, 2018, **9**, 4674–4682.

194 P.-L. Champagne, D. Ester, A. Bhattacharya, K. Hofstetter, C. Zellman, S. Bag, H. Yu, S. Trudel, V. K. Michaelis, V. E. Williams, V. Thangadurai and C.-C. Ling, *J. Mater. Chem. A*, 2019, **7**, 12201–12213.

195 Y. Zhou, F. Zhang, P. He, Y. Zhang, Y. Sun, J. Xu, J. Hu, H. Zhang and X. Wu, *J. Energy Chem.*, 2020, **46**, 87–93.

196 V. Di Noto, S. Lavina, G. A. Giffin, E. Negro and B. Scrosati, *Electrochim. Acta*, 2011, **57**, 4–13.

197 A. Arya and A. L. Sharma, *Ionics*, 2017, **23**, 497–540.

198 S. Chen, K. Wen, J. Fan, Y. Bando and D. Golberg, *J. Mater. Chem. A*, 2018, **6**, 11631–11663.

199 A. Varzi, R. Raccichini, S. Passerini and B. Scrosati, *J. Mater. Chem. A*, 2016, **4**, 17251–17259.

200 Z. Gadjourova, Y. G. Andreev, D. P. Tunstall and P. G. Bruce, *Nature*, 2001, **412**, 520–523.

201 Z. Stoeva, I. Martin-Litas, E. Staunton, Y. G. Andreev and P. G. Bruce, *J. Am. Chem. Soc.*, 2003, **125**, 4619–4626.

202 N. A. Stolwijk, C. Heddier, M. Reschke, M. Wiencierz, J. Bokeloh and G. Wilde, *Macromolecules*, 2013, **46**, 8580–8588.

203 Z. Gadjourova, Y. G. Andreev, D. P. Tunstall and P. G. Bruce, *Nature*, 2001, **412**, 520.

204 D. Bresser, S. Lyonnard, C. Iojoiu, L. Picard and S. Passerini, *Mol. Syst. Des. Eng.*, 2019, **4**, 779–792.

205 T. Morioka, K. Ota and Y. Tominaga, *Polymer*, 2016, **84**, 21–26.

206 Y. Tominaga, T. Shimomura and M. Nakamura, *Polymer*, 2010, **51**, 4295–4298.

207 Y. Jiang, X. Yan, Z. Ma, P. Mei, W. Xiao, Q. You and Y. Zhang, *Polymers*, 2018, **10**, 1237.

208 B. Kim, C.-G. Chae, Y. Satoh, T. Isono, M.-K. Ahn, C.-M. Min, J.-H. Hong, C. F. Ramirez, T. Satoh and J.-S. Lee, *Macromolecules*, 2018, **51**, 2293–2301.

209 G. Zhang, Y.-l. Hong, Y. Nishiyama, S. Bai, S. Kitagawa and S. Horike, *J. Am. Chem. Soc.*, 2019, **141**, 1227–1234.

210 S.-K. Kim, D.-G. Kim, A. Lee, H.-S. Sohn, J. J. Wie, N. A. Nguyen, M. E. Mackay and J.-C. Lee, *Macromolecules*, 2012, **45**, 9347–9356.

211 A. Ghosh, C. Wang and P. Kofinas, *J. Electrochem. Soc.*, 2010, **157**, A846–A849.

212 Y. Tong, H. Lyu, Y. Xu, B. Prasad Thapaliya, P. Li, X.-G. Sun and S. Dai, *J. Mater. Chem. A*, 2018, **6**, 14847–14855.

2780 | *Energy Environ. Sci.*, 2021, **14**, 2708–2788

This journal is © The Royal Society of Chemistry 2021

213 J. Hu, W. Wang, B. Zhou, Y. Feng, X. Xie and Z. Xue, *J. Membr. Sci.*, 2019, **575**, 200–208.

214 J.-C. Daigle, A. Vijh, P. Hovington, C. Gagnon, J. Hamel-Pâquet, S. Verreault, N. Turcotte, D. Clément, A. Guerfi and K. Zaghib, *J. Power Sources*, 2015, **279**, 372–383.

215 P. E. Trapa, B. Huang, Y.-Y. Won, D. R. Sadoway and A. M. Mayes, *Electrochem. Solid-State Lett.*, 2002, **5**, A85–A88.

216 J. Herzberger, K. Niederer, H. Pohlit, J. Seiwert, M. Worm, F. R. Wurm and H. Frey, *Chem. Rev.*, 2016, **116**, 2170–2243.

217 H. R. Allcock, R. Prange and T. J. Hartle, *Macromolecules*, 2001, **34**, 5463–5470.

218 C. Michot, A. Vallée, P. É. Harvey, M. Gauthier and M. Armand, *US Pat.*, 6492449, U.S. Patent and Trademark Office, Washington, DC, 2002.

219 C. A. Angell, C. Liu and E. Sanchez, *Nature*, 1993, **362**, 137–139.

220 C. A. Angell, K. Xu, S. S. Zhang and M. Videa, *Solid State Ionics*, 1996, **86-88**, 17–28.

221 Y. Tominaga, V. Nanthana and D. Tohyama, *Polym. J.*, 2012, **44**, 1155.

222 H. Gao and K. Lian, *ACS Appl. Mater. Interfaces*, 2014, **6**, 464–472.

223 M. Berman and S. Greenbaum, *Membranes*, 2015, **5**, 915–923.

224 E. M. Masoud, A. A. El-Bellihi, W. A. Bayoumy and E. A. Mohamed, *J. Mol. Liq.*, 2018, **260**, 237–244.

225 R. Chen, W. Qu, X. Guo, L. Li and F. Wu, *Mater. Horiz.*, 2016, **3**, 487–516.

226 N. Angulakshmi, K. S. Nahm, J. R. Nair, C. Gerbaldi, R. Bongiovanni, N. Penazzi and A. M. Stephan, *Electrochim. Acta*, 2013, **90**, 179–185.

227 C. Gerbaldi, J. R. Nair, M. A. Kulandainathan, R. S. Kumar, C. Ferrara, P. Mustarelli and A. M. Stephan, *J. Mater. Chem. A*, 2014, **2**, 9948–9954.

228 Y. Mussa, A. Fathima, M. Arsalan and E. Alsharaeh, *Mater. Res. Express*, 2019, **6**, 092003.

229 N. Zhang, J. He, W. Han and Y. Wang, *J. Mater. Sci.*, 2019, **54**, 9603–9612.

230 M. Falco, L. Castro, J. R. Nair, F. Bella, F. Bardé, G. Meligrana and C. Gerbaldi, *ACS Appl. Energy Mater.*, 2019, **2**, 1600–1607.

231 S. Skaarup, K. West and B. Zachau-Christiansen, *Solid State Ionics*, 1988, **28-30**, 975–978.

232 L. Chen, Y. Li, S.-P. Li, L.-Z. Fan, C.-W. Nan and J. B. Goodenough, *Nano Energy*, 2018, **46**, 176–184.

233 Q. Guo, Y. Han, H. Wang, S. Xiong, Y. Li, S. Liu and K. Xie, *ACS Appl. Mater. Interfaces*, 2017, **9**, 41837–41844.

234 S. H. Siyal, M. Li, H. Li, J.-L. Lan, Y. Yu and X. Yang, *Appl. Surf. Sci.*, 2019, **494**, 1119–1126.

235 X. Ban, W. Zhang, N. Chen and C. Sun, *J. Phys. Chem. C*, 2018, **122**, 9852–9858.

236 L. Porcarelli, M. A. Aboudzadeh, L. Rubatat, J. R. Nair, A. S. Shaplov, C. Gerbaldi and D. Mecerreyes, *J. Power Sources*, 2017, **364**, 191–199.

237 S. Li, A. I. Mohamed, V. Pande, H. Wang, J. Cuthbert, X. Pan, H. He, Z. Wang, V. Viswanathan, J. F. Whitacre and K. Matyjaszewski, *ACS Energy Lett.*, 2018, **3**, 20–27.

238 D. J. Bannister, G. R. Davies, I. M. Ward and J. E. McIntyre, *Polymer*, 1984, **25**, 1291–1296.

239 N. Lago, O. Garcia-Calvo, J. M. Lopez del Amo, T. Rojo and M. Armand, *ChemSusChem*, 2015, **8**, 3039–3043.

240 A. Blazejczyk, M. Szczupak, W. Wieczorek, P. Cmoch, G. Appetecchi, B. Scrosati, R. Kovarsky, D. Golodnitsky and E. Peled, *Chem. Mater.*, 2005, **17**, 1535–1547.

241 A. Plewa, F. Chyliński, M. Kalita, M. Bukat, P. Parzuchowski, R. Borkowska, M. Siekierski, G. Żukowska and W. Wieczorek, *J. Power Sources*, 2006, **159**, 431–437.

242 M. Kalita, M. Bukat, M. Ciosek, M. Siekierski, S. H. Chung, T. Rodríguez, S. G. Greenbaum, R. Kovarsky, D. Golodnitsky, E. Peled, D. Zane, B. Scrosati and W. Wieczorek, *Electrochim. Acta*, 2005, **50**, 3942–3948.

243 L. Imholt, T. S. Dörr, P. Zhang, L. Ibing, I. Cekic-Laskovic, M. Winter and G. Brunklaus, *J. Power Sources*, 2019, **409**, 148–158.

244 L. Imholt, D. Dong, D. Bedrov, I. Cekic-Laskovic, M. Winter and G. Brunklaus, *ACS Macro Lett.*, 2018, **7**, 881–885.

245 H. Zhang, F. Chen, O. Lakuntza, U. Oteo, L. Qiao, M. Martinez-Ibañez, H. Zhu, J. Carrasco, M. Forsyth and M. Armand, *Angew. Chem., Int. Ed.*, 2019, **58**, 12070–12075.

246 N. Goujon, T.-V. Huynh, K. J. Barlow, R. Kerr, K. Vezzù, V. Di Noto, L. A. O'Dell, J. Chiefari, P. C. Howlett and M. Forsyth, *Batteries Supercaps*, 2019, **2**, 132–138.

247 J. Yuan, D. Mecerreyes and M. Antonietti, *Prog. Polym. Sci.*, 2013, **38**, 1009–1036.

248 W. Qian, J. Texter and F. Yan, *Chem. Soc. Rev.*, 2017, **46**, 1124–1159.

249 P. Prabakaran, R. P. Manimuthu, S. Gurusamy and E. Sebasthiyan, *Chin. J. Polym. Sci.*, 2017, **35**, 407–421.

250 G. Feuillade and P. Perche, *J. Appl. Electrochem.*, 1975, **5**, 63–69.

251 M. Ghosh, V. Vijayakumar, R. Soni and S. Kurungot, *Nanoscale*, 2018, **10**, 8741–8751.

252 V. Vijayakumar, M. Ghosh, A. Torris AT, N. Chandran, S. B. Nair, M. V. Badiger and S. Kurungot, *ACS Sustainable Chem. Eng.*, 2018, **6**, 12630–12640.

253 A. Chiappone, F. Bella, J. R. Nair, G. Meligrana, R. Bongiovanni and C. Gerbaldi, *ChemElectroChem*, 2014, **1**, 1350–1358.

254 A. Natarajan, A. M. Stephan, C. H. Chan, N. Kalarikkal and S. Thomas, *J. Appl. Polym. Sci.*, 2017, **134**, 44594.

255 W. Li, Z. Zhu, W. Shen, J. Tang, G. Yang and Z. Xu, *RSC Adv.*, 2016, **6**, 97338–97345.

256 A. M. Stephan, K. S. Nahm, M. Anbu Kulandainathan, G. Ravi and J. Wilson, *Eur. Polym. J.*, 2006, **42**, 1728–1734.

257 W. Liu, X. K. Zhang, F. Wu and Y. Xiang, *IOP Conf. Ser.: Mater. Sci. Eng.*, 2017, **213**, 012036.

258 S.-H. Wang, P.-L. Kuo, C.-T. Hsieh and H. Teng, *ACS Appl. Mater. Interfaces*, 2014, **6**, 19360–19370.

259 M. Ulaganathan and S. Rajendran, *J. Appl. Electrochem.*, 2011, **41**, 83–88.

260 S. Chintapalli and R. Frech, *Macromolecules*, 1996, **29**, 3499–3506.

261 S. Ramesh and O. P. Ling, *Polym. Chem.*, 2010, **1**, 702–707.

262 O. E. Geiculescu, B. B. Hallac, R. V. Rajagopal, S. E. Creager, D. D. DesMarteau, O. Borodin and G. D. Smith, *J. Phys. Chem. B*, 2014, **118**, 5135–5143.

This journal is © The Royal Society of Chemistry 2021

Energy Environ. Sci., 2021, **14**, 2708–2788 | **2781**

263 B. Singh and S. S. Sekhon, *J. Phys. Chem. B*, 2005, **109**, 16539–16543.

264 K. Elamin, M. Shojaatalhosseini, O. Danyliv, A. Martinelli and J. Swenson, *Electrochim. Acta*, 2019, **299**, 979–986.

265 J. Tang, R. Muchakayala, S. Song, M. Wang and K. N. Kumar, *Polym. Test.*, 2016, **50**, 247–254.

266 S. K. Chaurasia, R. K. Singh and S. Chandra, *CrystEngComm*, 2013, **15**, 6022–6034.

267 Y.-S. Ye, J. Rick and B.-J. Hwang, *J. Mater. Chem. A*, 2013, **1**, 2719–2743.

268 Y. Yang, Q. Wu, D. Wang, C. Ma, Z. Chen, C. Zhu, Y. Gao and C. Li, *J. Membr. Sci.*, 2020, **595**, 117549.

269 D. Aidoud, A. Etiemble, D. Guy-Bouyssou, E. Maire, J. Le Bideau, D. Guyomard and B. Lestriez, *J. Power Sources*, 2016, **330**, 92–103.

270 M. Safa, A. Chamaani, N. Chawla and B. El-Zahab, *Electrochim. Acta*, 2016, **213**, 587–593.

271 G. G. Eshetu, D. Mecerreyes, M. Forsyth, H. Zhang and M. Armand, *Mol. Syst. Des. Eng.*, 2019, **4**, 294–309.

272 X. Wang, H. Zhu, G. M. A. Girard, R. Yunis, D. R. MacFarlane, D. Mecerreyes, A. J. Bhattacharyya, P. C. Howlett and M. Forsyth, *J. Mater. Chem. A*, 2017, **5**, 23844–23852.

273 C. Yang, X. Ji, X. Fan, T. Gao, L. Suo, F. Wang, W. Sun, J. Chen, L. Chen, F. Han, L. Miao, K. Xu, K. Gerasopoulos and C. Wang, *Adv. Mater.*, 2017, **29**, 1701972.

274 P. C. Sekhar, P. N. Kumar, U. Sasikala and A. K. Sharma, *AIP Conf. Proc.*, 2013, **1536**, 859–860.

275 L. Tian, M. Wang, L. Xiong, H. Guo, C. Huang, H. Zhang and X. Chen, *Appl. Sci.*, 2018, **8**, 2587.

276 K. Man Gu, P. Nam-Gyu, P. Kwang-Man, R. Kwang Sun, C. Soon Ho and K. Kang-Jin, in 3rd World Conference onPhotovoltaic Energy Conversion, 2003. Proceedings of, 2003, vol. 201, pp. 204–207.

277 S. Venkatesan, S.-C. Su, S.-C. Kao, H. Teng and Y.-L. Lee, *J. Power Sources*, 2015, **274**, 506–511.

278 V. Zadin and D. Brandell, *Electrochim. Acta*, 2011, **57**, 237–243.

279 B. Sun, H. D. Asfaw, D. Rehnlund, J. Mindemark, L. Nyholm, K. Edström and D. Brandell, *ACS Appl. Mater. Interfaces*, 2018, **10**, 2407–2413.

280 E. Strauss, S. Menkin and D. Golodnitsky, *Printed Batteries*, 2018, pp. 80–111.

281 S. Zheng, X. Shi, P. Das, Z.-S. Wu and X. Bao, *Adv. Mater.*, 2019, **31**, 1900583.

282 H. Li, C. Han, Y. Huang, Y. Huang, M. Zhu, Z. Pei, Q. Xue, Z. Wang, Z. Liu, Z. Tang, Y. Wang, F. Kang, B. Li and C. Zhi, *Energy Environ. Sci.*, 2018, **11**, 941–951.

283 S. A. Hashmi and S. Chandra, *Mater. Sci. Eng., B*, 1995, **34**, 18–26.

284 J. J. Xu, H. Ye and J. Huang, *Electrochem. Commun.*, 2005, **7**, 1309–1317.

285 G. P. Pandey, R. C. Agrawal and S. A. Hashmi, *J. Power Sources*, 2009, **190**, 563–572.

286 Y. Q. Yang, Z. Chang, M. X. Li, X. W. Wang and Y. P. Wu, *Solid State Ionics*, 2015, **269**, 1–7.

287 M. Ghosh, V. Vijayakumar and S. Kurungot, *Energy Technol.*, 2019, **7**, 1900442.

288 M. Ghosh, V. Vijayakumar, B. Anothumakkool and S. Kurungot, *ACS Sustainable Chem. Eng.*, 2020, **8**, 5040–5049.

289 V. Vijayakumar, M. Ghosh, M. Kurian, A. Torris, S. Dilwale, M. V. Badiger, M. Winter, J. R. Nair and S. Kurungot, *Small*, 2020, **16**, 2002528.

290 Ionic Materials, https://ionicmaterials.com/, Accessed 16/09, 2019.

291 DNK Power COMPANY LIMITED, https://www.dnkpower.com/, Accessed 17/09, 2019.

292 J. Motavalli, *Nature*, 2015, **526**, S96–S97.

293 M. S. Reisch, *Chem. Eng. News*, 2017, **95**, 3.

294 B. Halford, *Chem. Eng. News*, 2018, **96**, 3.

295 K. Nie, Y. Hong, J. Qiu, Q. Li, X. Yu, H. Li and L. Chen, *Front. Chem.*, 2018, **6**, 616.

296 A. Chiappone, J. Nair, C. Gerbaldi, E. Zeno and R. Bongiovanni, *RSC Adv.*, 2014, **4**, 40873–40881.

297 Y. Zhu, F. Wang, L. Liu, S. Xiao, Y. Yang and Y. Wu, *Sci. Rep.*, 2013, **3**, 3187.

298 H. Kim, B. Oh and Y. Kang, *Polym. Bull.*, 2000, **44**, 509–515.

299 C. Gerbaldi, J. R. Nair, G. Meligrana, R. Bongiovanni, S. Bodoardo and N. Penazzi, *Electrochim. Acta*, 2010, **55**, 1460–1467.

300 J. R. Nair, C. Gerbaldi, G. Meligrana, R. Bongiovanni, S. Bodoardo, N. Penazzi, P. Reale and V. Gentili, *J. Power Sources*, 2008, **178**, 751–757.

301 C. Tao, M.-H. Gao, B.-H. Yin, B. Li, Y.-P. Huang, G. Xu and J.-J. Bao, *Electrochim. Acta*, 2017, **257**, 31–39.

302 R. He, M. Echeverri, D. Ward, Y. Zhu and T. Kyu, *J. Membr. Sci.*, 2016, **498**, 208–217.

303 W. He, Z. Cui, X. Liu, Y. Cui, J. Chai, X. Zhou, Z. Liu and G. Cui, *Electrochim. Acta*, 2017, **225**, 151–159.

304 C. Gerbaldi, J. R. Nair, G. Meligrana, R. Bongiovanni, S. Bodoardo and N. Penazzi, *J. Appl. Electrochem.*, 2009, **39**, 2199.

305 B.-K. Oh, W.-I. Jung, D.-W. Kim and H.-W. Rhee, *Bull. Korean Chem. Soc.*, 2002, **23**, 683–687.

306 W. Li, Y. Pang, J. Liu, G. Liu, Y. Wang and Y. Xia, *RSC Adv.*, 2017, **7**, 23494–23501.

307 F. Colò, F. Bella, J. R. Nair and C. Gerbaldi, *J. Power Sources*, 2017, **365**, 293–302.

308 K. M. Abraham, M. Alamgir and D. K. Hoffman, *J. Electrochem. Soc.*, 1995, **142**, 683–687.

309 S. Ikeda, Y. Mori, Y. Furuhashi, H. Masuda and O. Yamamoto, *J. Power Sources*, 1999, **81-82**, 720–723.

310 D.-W. Kim, B. Oh, J.-H. Park and Y.-K. Sun, *Solid State Ionics*, 2000, **138**, 41–49.

311 J. Wang, W. Yang and J. Lei, *J. Electrost.*, 2008, **66**, 627–629.

312 T. Eriksson, A. Mace, Y. Manabe, M. Yoshizawa-Fujita, Y. Inokuma, D. Brandell and J. Mindemark, *J. Electrochem. Soc.*, 2020, **167**, 070537.

313 S. N. F. Yusuf, S. Z. Yusof, M. Z. Kufian and L. P. Teo, *Mater. Today: Proc.*, 2019, **17**, 446–458.

314 H. Jia, H. Onishi, R. Wagner, M. Winter and I. Cekic-Laskovic, *ACS Appl. Mater. Interfaces*, 2018, **10**, 42348–42355.

315 N. Sugihara, K. Nishimura, H. Nishino, S. Kanehashi, K. Mayumi, Y. Tominaga, T. Shimomura and K. Ito, *Electrochim. Acta*, 2017, **229**, 166–172.

2782 | *Energy Environ. Sci.*, 2021, **14**, 2708–2788

This journal is © The Royal Society of Chemistry 2021

316 Y. Saito, A. M. Stephan and H. Kataoka, *Solid State Ionics*, 2003, **160**, 149–153.

317 K. Kezuka, T. Hatazawa and K. Nakajima, *J. Power Sources*, 2001, **97-98**, 755–757.

318 A. Hosseinioun and E. Paillard, *J. Membr. Sci.*, 2020, **594**, 117456.

319 J. M. Tarascon, A. S. Gozdz, C. Schmutz, F. Shokoohi and P. C. Warren, *Solid State Ionics*, 1996, **86-88**, 49–54.

320 Y. J. Hwang, K. S. Nahm, T. P. Kumar and A. M. Stephan, *J. Membr. Sci.*, 2008, **310**, 349–355.

321 J. Kim, S. Choi, S. Jo, W. Lee and B. C. Kim, *J. Electrochem. Soc.*, 2005, **152**, A295–A300.

322 H. Wang, H. Huang and S. L. Wunder, *J. Electrochem. Soc.*, 2000, **147**, 2853–2861.

323 J. M. Tarascon and M. Armand, *Nature*, 2001, **414**, 359.

324 B. Anothumakkool, A. Torris AT, S. N. Bhange, S. M. Unni, M. V. Badiger and S. Kurungot, *ACS Appl. Mater. Interfaces*, 2013, **5**, 13397–13404.

325 B. Anothumakkool, A. Torris AT, S. Veeliyath, V. Vijayakumar, M. V. Badiger and S. Kurungot, *ACS Appl. Mater. Interfaces*, 2016, **8**, 1233–1241.

326 V. Vijayakumar, B. Anothumakkool, A. Torris AT, S. B. Nair, M. V. Badiger and S. Kurungot, *J. Mater. Chem. A*, 2017, **5**, 8461–8476.

327 N. Kazemi, D. L. Danilov, L. Haverkate, N. J. Dudney, S. Unnikrishnan and P. H. L. Notten, *Solid State Ionics*, 2019, **334**, 111–116.

328 Z. Wang, D. Santhanagopalan, W. Zhang, F. Wang, H. L. Xin, K. He, J. Li, N. Dudney and Y. S. Meng, *Nano Lett.*, 2016, **16**, 3760–3767.

329 J. R. Nair, M. Destro, C. Gerbaldi, R. Bongiovanni and N. Penazzi, *J. Appl. Electrochem.*, 2013, **43**, 137–145.

330 Y. G. Cho, C. Hwang, D. S. Cheong, Y. S. Kim and H. K. Song, *Adv. Mater.*, 2019, **31**, 1804909.

331 Y. F. Zhou, S. Xie, X. W. Ge, C. H. Chen and K. Amine, *J. Appl. Electrochem.*, 2004, **34**, 1119–1125.

332 S. Z. Zhang, X. H. Xia, D. Xie, R. C. Xu, Y. J. Xu, Y. Xia, J. B. Wu, Z. J. Yao, X. L. Wang and J. P. Tu, *J. Power Sources*, 2019, **409**, 31–37.

333 J. J. Xu and H. Ye, *Electrochem. Commun.*, 2005, **7**, 829–835.

334 Q. Zhao, X. Liu, S. Stalin, K. Khan and L. A. Archer, *Nat. Energy*, 2019, **4**, 365–373.

335 R. Soni, V. Vijayakumar and S. Kurungot, *ACS Appl. Nano Mater.*, 2018, **1**, 4576–4586.

336 M.-K. Song, J.-Y. Cho, B. W. Cho and H.-W. Rhee, *J. Power Sources*, 2002, **110**, 209–215.

337 X. Zuo, X.-M. Liu, F. Cai, H. Yang, X.-D. Shen and G. Liu, *J. Power Sources*, 2013, **239**, 111–121.

338 M.-H. Ryou, Y. M. Lee, K. Y. Cho, G.-B. Han, J.-N. Lee, D. J. Lee, J. W. Choi and J.-K. Park, *Electrochim. Acta*, 2012, **60**, 23–30.

339 S.-H. Kim, K.-H. Choi, S.-J. Cho, J.-S. Park, K. Y. Cho, C. K. Lee, S. B. Lee, J. K. Shim and S.-Y. Lee, *J. Mater. Chem. A*, 2014, **2**, 10854–10861.

340 J. Suk, Y. H. Lee, D. Y. Kim, D. W. Kim, S. Y. Cho, J. M. Kim and Y. Kang, *J. Power Sources*, 2016, **334**, 154–161.

341 A. J. D'Angelo and M. J. Panzer, *J. Phys. Chem. B*, 2017, **121**, 890–895.

342 J. R. Nair, M. Destro, F. Bella, G. B. Appetecchi and C. Gerbaldi, *J. Power Sources*, 2016, **306**, 258–267.

343 H.-S. Kim, J.-H. Shin, C.-H. Doh, S.-I. Moon and S.-P. Kim, *J. Power Sources*, 2002, **112**, 469–476.

344 M. Chen, M. Zhong and J. A. Johnson, *Chem. Rev.*, 2016, **116**, 10167–10211.

345 S. Huang, Z. Cui, L. Qiao, G. Xu, J. Zhang, K. Tang, X. Liu, Q. Wang, X. Zhou, B. Zhang and G. Cui, *Electrochim. Acta*, 2019, **299**, 820–827.

346 Z. Liu, P. Hu, J. Ma, B. Qin, Z. Zhang, C. Mou, Y. Yao and G. Cui, *Electrochim. Acta*, 2017, **236**, 221–227.

347 Y. Ma, J. Ma, J. Chai, Z. Liu, G. Ding, G. Xu, H. Liu, B. Chen, X. Zhou, G. Cui and L. Chen, *ACS Appl. Mater. Interfaces*, 2017, **9**, 41462–41472.

348 J.-H. Park, J.-S. Kim, E.-G. Shim, K.-W. Park, Y. T. Hong, Y.-S. Lee and S.-Y. Lee, *Electrochem. Commun.*, 2010, **12**, 1099–1102.

349 J.-H. Park, J.-H. Cho, J.-S. Kim, E.-G. Shim, Y.-S. Lee and S.-Y. Lee, *J. Korean Electrochem. Soc.*, 2011, **14**, 117–124.

350 K. Kojio, M. Furukawa, S. Matsumura, S. Motokucho, T. Osajima and K. Yoshinaga, *Polym. Chem.*, 2012, **3**, 2287–2292.

351 M. L. Lehmann, G. Yang, J. Nanda and T. Saito, *J. Electrochem. Soc.*, 2020, **167**, 070539.

352 Y. Nishi, in *Advances in Lithium-Ion Batteries*, ed. W. A. van Schalkwijk and B. Scrosati, Springer US, Boston, MA, 2002, pp. 233–249.

353 S. Abbrent, S. Greenbaum, E. Peled and D. Golodnitsky, *Handbook of Solid State Batteries*, World Scientific, 2016, pp. 523–589.

354 C. Gerbaldi, M. Destro, J. R. Nair, S. Ferrari, I. Quinzeni and E. Quartarone, *Nano Energy*, 2013, **2**, 1279–1286.

355 N.-S. Choi, J.-G. Han, S.-Y. Ha, I. Park and C.-K. Back, *RSC Adv.*, 2015, **5**, 2732–2748.

356 I. A. Shkrob, Y. Zhu, T. W. Marin and D. Abraham, *J. Phys. Chem. C*, 2013, **117**, 19270–19279.

357 L. M. Kasmaee, A. Aryanfar, Z. Chikneyan, M. R. Hoffmann and A. J. Colussi, *Chem. Phys. Lett.*, 2016, **661**, 65–69.

358 G. Moad and E. Rizzardo, *Nitroxide Mediated Polymerization: From Fundamentals to Applications in Materials Science*, The Royal Society of Chemistry, 2016, pp. 1–44.

359 M. A. Tasdelen, N. Moszner and Y. Yagci, *Polym. Bull.*, 2009, **63**, 173–183.

360 S. P. S. Koo, M. M. Stamenović, R. A. Prasath, A. J. Inglis, F. E. Du Prez, C. Barner-Kowollik, W. Van Camp and T. Junkers, *J. Polym. Sci., Part A: Polym. Chem.*, 2010, **48**, 1699–1713.

361 S. Li, Y.-M. Chen, W. Liang, Y. Shao, K. Liu, Z. Nikolov and Y. Zhu, *Joule*, 2018, **2**, 1838–1856.

362 M. Falco, S. Palumbo, G. Lingua, L. Silvestri, M. Winter, R. Lin, V. Pellegrini, F. Bonaccorso, J. R. Nair and C. Gerbaldi, *Electrochem. Commun.*, 2020, **118**, 106807.

363 H.-S. Kim, S.-I. Kim, C.-W. Lee and S.-I. Moon, *J. Electroceram.*, 2006, **17**, 673–677.

364 C. Niu, M. Zhang, G. Chen, B. Cao, J. Shi, J. Du and Y. Chen, *Electrochim. Acta*, 2018, **283**, 349–356.

This journal is © The Royal Society of Chemistry 2021

Energy Environ. Sci., 2021, **14**, 2708–2788 | **2783**

365 H. Fan, H. Li, L.-Z. Fan and Q. Shi, *J. Power Sources*, 2014, **249**, 392–396.

366 K. Dai, C. Ma, Y. Feng, L. Zhou, G. Kuang, Y. Zhang, Y. Lai, X. Cui and W. Wei, *J. Mater. Chem. A*, 2019, **7**, 18547–18557.

367 Y. F. Zhou, S. Xie and C. H. Chen, *J. Mater. Sci.*, 2006, **41**, 7492–7497.

368 K. Yoshima, H. Munakata and K. Kanamura, *J. Power Sources*, 2012, **208**, 404–408.

369 C. Gerbaldi, J. R. Nair, S. Ferrari, A. Chiappone, G. Meligrana, S. Zanarini, P. Mustarelli, N. Penazzi and R. Bongiovanni, *J. Membr. Sci.*, 2012, **423-424**, 459–467.

370 L. Porcarelli, A. S. Shaplov, F. Bella, J. R. Nair, D. Mecerreyes and C. Gerbaldi, *ACS Energy Lett.*, 2016, **1**, 678–682.

371 A.-H. Bonardi, F. Bonardi, G. Noirbent, F. Dumur, D. Gigmes, C. Dietlin and J. Lalevée, *J. Polym. Sci.*, 2020, **58**, 300–308.

372 S. Chatani, C. J. Kloxin and C. N. Bowman, *Polym. Chem.*, 2014, **5**, 2187–2201.

373 T. B. Stachowiak, F. Svec and J. M. Fréchet, *Chem. Mater.*, 2006, **18**, 5950–5957.

374 G. T. Kim, G. B. Appetecchi, M. Carewska, M. Joost, A. Balducci, M. Winter and S. Passerini, *J. Power Sources*, 2010, **195**, 6130–6137.

375 L. Porcarelli, C. Gerbaldi, F. Bella and J. R. Nair, *Sci. Rep.*, 2016, **6**, 19892.

376 A. K. Sinha and D. Equbal, *Asian J. Org. Chem.*, 2019, **8**, 32–47.

377 C. E. Hoyle and C. N. Bowman, *Angew. Chem., Int. Ed.*, 2010, **49**, 1540–1573.

378 N. B. Cramer, S. K. Reddy, A. K. O'Brien and C. N. Bowman, *Macromolecules*, 2003, **36**, 7964–7969.

379 H. C. Kolb, M. G. Finn and K. B. Sharpless, *Angew. Chem., Int. Ed.*, 2001, **40**, 2004–2021.

380 B. D. Fairbanks, D. M. Love and C. N. Bowman, *Macromol. Chem. Phys.*, 2017, **218**, 1700073.

381 N. B. Cramer, J. P. Scott and C. N. Bowman, *Macromolecules*, 2002, **35**, 5361–5365.

382 M. Uygun, M. A. Tasdelen and Y. Yagci, *Macromol. Chem. Phys.*, 2010, **211**, 103–110.

383 S. V. Radl, C. Schipfer, S. Kaiser, A. Moser, B. Kaynak, W. Kern and S. Schlögl, *Polym. Chem.*, 2017, **8**, 1562–1572.

384 Y. Jian, Y. He, Y. Sun, H. Yang, W. Yang and J. Nie, *J. Mater. Chem. C*, 2013, **1**, 4481–4489.

385 H.-S. Kim, J.-H. Shin, S.-I. Moon and M.-S. Yun, *J. Power Sources*, 2003, **119-121**, 482–486.

386 E.-H. Lee, J.-H. Park, J.-M. Kim and S.-Y. Lee, *Electrochim. Acta*, 2013, **104**, 249–254.

387 Q. Chen, R. Xu, Z. He, K. Zhao and L. Pan, *J. Electrochem. Soc.*, 2017, **164**, A1852–A1857.

388 Z. Wei, S. Chen, J. Wang, Z. Wang, Z. Zhang, X. Yao, Y. Deng and X. Xu, *J. Power Sources*, 2018, **394**, 57–66.

389 J. Alemán, A. V. Chadwick, J. He, M. Hess, K. Horie, R. G. Jones, P. Kratochvíl, I. Meisel, I. Mita and G. Moad, *Pure Appl. Chem.*, 2007, **79**, 1801–1829.

390 D. Zhou, R. Liu, Y.-B. He, F. Li, M. Liu, B. Li, Q.-H. Yang, Q. Cai and F. Kang, *Adv. Energy Mater.*, 2016, **6**, 1502214.

391 N.-S. Choi, Y. M. Lee, J. H. Park and J.-K. Park, *J. Power Sources*, 2003, **119-121**, 610–616.

392 L. X. Yuan, J. D. Piao, Y. L. Cao, H. X. Yang and X. P. Ai, *J. Solid State Electrochem.*, 2005, **9**, 183–189.

393 X. Liu, G. Ding, X. Zhou, S. Li, W. He, J. Chai, C. Pang, Z. Liu and G. Cui, *J. Mater. Chem. A*, 2017, **5**, 11124–11130.

394 G. Homann, L. Stolz, M. Winter and J. Kasnatscheew, *iScience*, 2020, **23**, 101225.

395 J.-A. Choi, J.-H. Yoo, W. Y. Yoon and D.-W. Kim, *Electrochim. Acta*, 2014, **132**, 1–6.

396 J. R. Nair, D. Cíntora-Juárez, C. Pérez-Vicente, J. L. Tirado, S. Ahmad and C. Gerbaldi, *Electrochim. Acta*, 2016, **199**, 172–179.

397 L. Sun, K. Higaki and R. C. McDonald, *J. Power Sources*, 1997, **68**, 352–356.

398 H. Yang, G. V. Zhuang and P. N. Ross, *J. Power Sources*, 2006, **161**, 573–579.

399 C. L. Campion, W. Li and B. L. Lucht, *J. Electrochem. Soc.*, 2005, **152**, A2327.

400 M. Tochihara, H. Nara, D. Mukoyama, T. Yokoshima, T. Momma and T. Osaka, *J. Electrochem. Soc.*, 2015, **162**, A2008.

401 R. Younesi, G. M. Veith, P. Johansson, K. Edström and T. Vegge, *Energy Environ. Sci.*, 2015, **8**, 1905–1922.

402 M. Grünebaum, A. Buchheit, C. Lürenbaum, M. Winter and H.-D. Wiemhöfer, *J. Phys. Chem. C*, 2019, **123**, 7033–7044.

403 S. Raghu, K. Archana, C. Sharanappa, S. Ganesh and H. Devendrappa, *J. Radiat. Res. Appl. Sci.*, 2016, **9**, 117–124.

404 P. Nanda, S. K. De, S. Manna, U. De and S. Tarafdar, *Nucl. Instrum. Methods Phys. Res., Sect. B*, 2010, **268**, 73–78.

405 M. H. Abdul Rahaman, M. U. Khandaker, Z. R. Khan, M. Z. Kufian, I. S. M. Noor and A. K. Arof, *Phys. Chem. Chem. Phys.*, 2014, **16**, 11527–11537.

406 Y.-C. Jung, M.-S. Park, D.-H. Kim, M. Ue, A. Eftekhari and D.-W. Kim, *Sci. Rep.*, 2017, **7**, 17482.

407 Y. Qian, C. Schultz, P. Niehoff, T. Schwieters, S. Nowak, F. M. Schappacher and M. Winter, *J. Power Sources*, 2016, **332**, 60–71.

408 T. Dagger, M. Grützke, M. Reichert, J. Haetge, S. Nowak, M. Winter and F. M. Schappacher, *J. Power Sources*, 2017, **372**, 276–285.

409 A. L. Michan, B. S. Parimalam, M. Leskes, R. N. Kerber, T. Yoon, C. P. Grey and B. L. Lucht, *Chem. Mater.*, 2016, **28**, 8149–8159.

410 Q. Lu, Y.-B. He, Q. Yu, B. Li, Y. V. Kaneti, Y. Yao, F. Kang and Q.-H. Yang, *Adv. Mater.*, 2017, **29**, 1604460.

411 J. Jeong, H. Lee, J. Choi, M.-H. Ryou and Y. M. Lee, *Electrochim. Acta*, 2015, **154**, 149–156.

412 D. Zhou, L.-Z. Fan, H. Fan and Q. Shi, *Electrochim. Acta*, 2013, **89**, 334–338.

413 T. Bok, S.-J. Cho, S. Choi, K.-H. Choi, H. Park, S.-Y. Lee and S. Park, *RSC Adv.*, 2016, **6**, 6960–6966.

414 T.-S. Wei, B. Y. Ahn, J. Grotto and J. A. Lewis, *Adv. Mater.*, 2018, **30**, 1703027.

415 S.-H. Kim, K.-H. Choi, S.-J. Cho, S. Choi, S. Park and S.-Y. Lee, *Nano Lett.*, 2015, **15**, 5168–5177.

2784 | *Energy Environ. Sci.*, 2021, **14**, 2708–2788

This journal is © The Royal Society of Chemistry 2021

416 S.-H. Kim, K.-H. Choi, S.-J. Cho, J. Yoo, S.-S. Lee and S.-Y. Lee, *Energy Environ. Sci.*, 2018, **11**, 321–330.

417 X. Li, K. Qian, Y.-B. He, C. Liu, D. An, Y. Li, D. Zhou, Z. Lin, B. Li, Q.-H. Yang and F. Kang, *J. Mater. Chem. A*, 2017, **5**, 18888–18895.

418 M. Liu, D. Zhou, Y.-B. He, Y. Fu, X. Qin, C. Miao, H. Du, B. Li, Q.-H. Yang, Z. Lin, T. S. Zhao and F. Kang, *Nano Energy*, 2016, **22**, 278–289.

419 M. Liu, H. R. Jiang, Y. X. Ren, D. Zhou, F. Y. Kang and T. S. Zhao, *Electrochim. Acta*, 2016, **213**, 871–878.

420 J. Zhang, Y. Bai, X.-G. Sun, Y. Li, B. Guo, J. Chen, G. M. Veith, D. K. Hensley, M. P. Paranthaman, J. B. Goodenough and S. Dai, *Nano Lett.*, 2015, **15**, 3398–3402.

421 Q. Huang, J. Song, Y. Gao, D. Wang, S. Liu, S. Peng, C. Usher, A. Goliaszewski and D. Wang, *Nat. Commun.*, 2019, **10**, 5586.

422 M. Liu, Y. Ren, D. Zhou, H. Jiang, F. Kang and T. Zhao, *ACS Appl. Mater. Interfaces*, 2017, **9**, 2526–2534.

423 A. Manthiram, Y. Fu, S.-H. Chung, C. Zu and Y.-S. Su, *Chem. Rev.*, 2014, **114**, 11751–11787.

424 A. Manthiram, Y. Fu and Y.-S. Su, *Acc. Chem. Res.*, 2013, **46**, 1125–1134.

425 S. Jeong, D. Bresser, D. Buchholz, M. Winter and S. Passerini, *J. Power Sources*, 2013, **235**, 220–225.

426 M. Liu, D. Zhou, H. R. Jiang, Y. X. Ren, F. Y. Kang and T. S. Zhao, *Nano Energy*, 2016, **28**, 97–105.

427 B. Wu, Z.-W. Zhang, M.-H. Huang and Y. Peng, *RSC Adv.*, 2017, **7**, 5394–5401.

428 Y.-S. Lee and D.-W. Kim, *Electrochim. Acta*, 2013, **106**, 460–464.

429 B. Huang, Y. Zhang, M. Que, Y. Xiao, Y. Jiang, K. Yuan and Y. Chen, *RSC Adv.*, 2017, **7**, 54391–54398.

430 E. A. Campo, in *Selection of Polymeric Materials*, ed. E. A. Campo, William Andrew Publishing, Norwich, NY, 2008, pp. 205–225.

431 Y. E. Hyung, D. R. Vissers and K. Amine, *J. Power Sources*, 2003, **119–121**, 383–387.

432 T. Dagger, B. R. Rad, F. M. Schappacher and M. Winter, *Energy Technol.*, 2018, **6**, 2011–2022.

433 R. Shibutani and H. Tsutsumi, *J. Power Sources*, 2012, **202**, 369–373.

434 R. Hooper, L. J. Lyons, M. K. Mapes, D. Schumacher, D. A. Moline and R. West, *Macromolecules*, 2001, **34**, 931–936.

435 J. Máca, M. Sedlarikova, J. Vondrák and M. Frk, *ECS Trans.*, 2014, **63**, 81–84.

436 S. Tian, Y. Pak and G. Xu, *J. Polym. Sci., Part B: Polym. Phys.*, 1994, **32**, 2019–2023.

437 W. Kim, J.-J. Cho, Y. Kang and D.-W. Kim, *J. Power Sources*, 2008, **178**, 837–841.

438 J.-A. Choi, Y. Kang, H. Shim, D. W. Kim, H.-K. Song and D.-W. Kim, *J. Power Sources*, 2009, **189**, 809–813.

439 J.-A. Choi, Y. Kang, H. Shim, D. W. Kim, E. Cha and D.-W. Kim, *J. Power Sources*, 2010, **195**, 6177–6181.

440 F. Ye, X. Zhang, K. Liao, Q. Lu, X. Zou, R. Ran, W. Zhou, Y. Zhong and Z. Shao, *J. Mater. Chem. A*, 2020, **8**, 9733–9742.

441 C. Korepp, H. Santner, T. Fujii, M. Ue, J. Besenhard, K.-C. Möller and M. Winter, *J. Power Sources*, 2006, **158**, 578–582.

442 H. Santner, C. Korepp, M. Winter, J. Besenhard and K.-C. Möller, *Anal. Bioanal. Chem.*, 2004, **379**, 266–271.

443 J. Chai, Z. Liu, J. Ma, J. Wang, X. Liu, H. Liu, J. Zhang, G. Cui and L. Chen, *Adv. Sci.*, 2017, **4**, 1600377.

444 J. Chai, Z. Liu, J. Zhang, J. Sun, Z. Tian, Y. Ji, K. Tang, X. Zhou and G. Cui, *ACS Appl. Mater. Interfaces*, 2017, **9**, 17897–17905.

445 J. Mindemark, L. Imholt, J. Montero and D. Brandell, *J. Polym. Sci., Part A: Polym. Chem.*, 2016, **54**, 2128–2135.

446 K. M. Diederichsen, E. J. McShane and B. D. McCloskey, *ACS Energy Lett.*, 2017, **2**, 2563–2575.

447 G. C. Rawsky, T. Fujinami and D. F. Shriver, *Chem. Mater.*, 1994, **6**, 2208–2209.

448 R. Bouchet, S. Maria, R. Meziane, A. Aboulaich, L. Lienafa, J.-P. Bonnet, T. N. T. Phan, D. Bertin, D. Gigmes, D. Devaux, R. Denoyel and M. Armand, *Nat. Mater.*, 2013, **12**, 452.

449 K. Borzutzki, J. Thienenkamp, M. Diehl, M. Winter and G. Brunklaus, *J. Mater. Chem. A*, 2019, **7**, 188–201.

450 I. Osada, H. de Vries, B. Scrosati and S. Passerini, *Angew. Chem., Int. Ed.*, 2016, **55**, 500–513.

451 V. Vijayakumar, D. Diddens, A. Heuer, S. Kurungot, M. Winter and J. R. Nair, *ACS Appl. Mater. Interfaces*, 2020, **12**, 567–579.

452 M. S. Grewal, M. Tanaka and H. Kawakami, *Polym. Int.*, 2019, **68**, 684–693.

453 J. Shim, L. Kim, H. J. Kim, D. Jeong, J. H. Lee and J.-C. Lee, *Polymer*, 2017, **122**, 222–231.

454 A. Matsumoto, T. Kumagai, H. Aota, H. Kawasaki and R. Arakawa, *Polym. J.*, 2009, **41**, 26–33.

455 J. R. Nair, L. Porcarelli, F. Bella and C. Gerbaldi, *ACS Appl. Mater. Interfaces*, 2015, **7**, 12961–12971.

456 E. A. Baroncini and J. F. Stanzione, *Int. J. Biol. Macromol.*, 2018, **113**, 1041–1051.

457 M. S. Grewal, M. Tanaka and H. Kawakami, *Electrochim. Acta*, 2019, **307**, 148–156.

458 N.-S. Choi, Y. M. Lee, W. Seol, J. A. Lee and J.-K. Park, *Solid State Ionics*, 2004, **172**, 19–24.

459 N.-S. Choi, Y. M. Lee, K. Y. Cho, D.-H. Ko and J.-K. Park, *Electrochem. Commun.*, 2004, **6**, 1238–1242.

460 E.-H. Lee, J.-H. Park, J.-H. Cho, S.-J. Cho, D. W. Kim, H. Dan, Y. Kang and S.-Y. Lee, *J. Power Sources*, 2013, **244**, 389–394.

461 H. Li and H. Zhou, *Chem. Commun.*, 2012, **48**, 1201–1217.

462 Y. Abu-Lebdeh and I. Davidson, *J. Power Sources*, 2009, **189**, 576–579.

463 K.-H. Choi, S.-J. Cho, S.-H. Kim, Y. H. Kwon, J. Y. Kim and S.-Y. Lee, *Adv. Funct. Mater.*, 2014, **24**, 44–52.

464 D. R. MacFarlane, J. Huang and M. Forsyth, *Nature*, 1999, **402**, 792.

465 K.-H. Choi, S.-H. Kim, H.-J. Ha, E.-H. Kil, C. K. Lee, S. B. Lee, J. K. Shim and S.-Y. Lee, *J. Mater. Chem. A*, 2013, **1**, 5224–5231.

This journal is © The Royal Society of Chemistry 2021

Energy Environ. Sci., 2021, **14**, 2708–2788 | **2785**

466 Y. Lu, K.-W. He, S.-J. Zhang, Y.-X. Zhou and Z.-B. Wang, *Ionics*, 2019, **25**, 1607–1615.

467 W. Liang, Y. Shao, Y.-M. Chen and Y. Zhu, *ACS Appl. Energy Mater.*, 2018, **1**, 6064–6071.

468 J. Cao, R. He and T. Kyu, *Curr. Opin. Chem. Eng.*, 2017, **15**, 68–75.

469 T. Ishizone and R. Goseki, in *Encyclopedia of Polymeric Nanomaterials*, ed. S. Kobayashi and K. Müllen, Springer Berlin Heidelberg, Berlin, Heidelberg, 2021, pp. 1–11.

470 J. Paulsdorf, M. Burjanadze, K. Hagelschur and H. D. Wiemhöfer, *Solid State Ionics*, 2004, **169**, 25–33.

471 J. Paulsdorf, N. Kaskhedikar, M. Burjanadze, S. Obeidi, N. A. Stolwijk, D. Wilmer and H. D. Wiemhöfer, *Chem. Mater.*, 2006, **18**, 1281–1288.

472 B.-A. Feit and B. Halak, *J. Polym. Sci., Part A: Polym. Chem.*, 2002, **40**, 2171–2183.

473 A. Pazat, E. Beyou, C. Barrès, F. Bruno and C. Janin, *Appl. Surf. Sci.*, 2017, **396**, 902–911.

474 A.-L. Brocas, C. Mantzaridis, D. Tunc and S. Carlotti, *Prog. Polym. Sci.*, 2013, **38**, 845–873.

475 B. M. Mandal, *Fundamentals of polymerization*, World Scientific, 2013, pp. 213–257.

476 C. E. Carraher Jr, *Seymour/Carraher's Polymer Chememistry*, CRC press, 2003, pp. 249–290.

477 A. Rudin and P. Choi, in *The Elements of Polymer Science & Engineering*, ed. A. Rudin and P. Choi, Academic Press, Boston, 3rd edn, 2013, pp. 449–493.

478 A. Sudo, in *Encyclopedia of Polymeric Nanomaterials*, ed. S. Kobayashi and K. Müllen, Springer Berlin Heidelberg, Berlin, Heidelberg, 2021, pp. 1–11.

479 J. Penelle, *J. Am. Chem. Soc.*, 1999, **121**, 5102.

480 R. P. Quirk, Q. Zhuo, S. H. Jang, Y. Lee and G. Lizarraga, *Applications of Anionic Polymerization Research*, American Chemical Society, 1998, pp. 2–27.

481 Y. Cui, J. Chai, H. Du, Y. Duan, G. Xie, Z. Liu and G. Cui, *ACS Appl. Mater. Interfaces*, 2017, **9**, 8737–8741.

482 C. Limouzin, A. Caviggia, F. Ganachaud and P. Hémery, *Macromolecules*, 2003, **36**, 667–674.

483 K. Ficht and C. D. Eisenbach, *Die Makromolekulare Chemie, Rapid Commun.*, 1993, **14**, 669–676.

484 P. Hu, J. Chai, Y. Duan, Z. Liu, G. Cui and L. Chen, *J. Mater. Chem. A*, 2016, **4**, 10070–10083.

485 R. Sáez, C. McArdle, F. Salhi, J. Marquet and R. M. Sebastián, *Chem. Sci.*, 2019, **10**, 3295–3299.

486 P. Hu, Y. Duan, D. Hu, B. Qin, J. Zhang, Q. Wang, Z. Liu, G. Cui and L. Chen, *ACS Appl. Mater. Interfaces*, 2015, **7**, 4720–4727.

487 C. Duffy, P. Zetterlund and F. Aldabbagh, *Molecules*, 2018, **23**, 465.

488 Z. Hu, S. Zhang, S. Dong, W. Li, H. Li, G. Cui and L. Chen, *Chem. Mater.*, 2017, **29**, 4682–4689.

489 H. Zhou, H. Liu, Y. Li, X. Yue, X. Wang, M. Gonzalez, Y. S. Meng and P. Liu, *J. Mater. Chem. A*, 2019, **7**, 16984–16991.

490 S. Aoshima and S. Kanaoka, *Chem. Rev.*, 2009, **109**, 5245–5287.

491 M. Sawamoto and M. Ouchi, in *Encyclopedia of Polymeric Nanomaterials*, ed. S. Kobayashi and K. Müllen, Springer Berlin Heidelberg, Berlin, Heidelberg, 2015, pp. 320–324.

492 A. Lyapkov, E. Ionova, V. Bondaletov and A. Pestryakov, in *Polymerization*, ed. A. D. S. Gomes, IntechOpen, 2012, pp. 245–260.

493 S. G. Roy, S. Banerjee and P. De, in *Reference Module in Materials Science and Materials Engineering*, Elsevier, 2016, DOI: 10.1016/B978-0-12-803581-8.01357-6.

494 S. Penczek, P. Kubisa and K. Matyjaszewski, in *Cationic Ring-Opening Polymerization of Heterocyclic Monomers*, ed. S. Penczek, P. Kubisa and K. Matyjaszewski, Springer Berlin Heidelberg, Berlin, Heidelberg, 1980, pp. 3–7.

495 P. Kubisa and S. Penczek, *Prog. Polym. Sci.*, 1999, **24**, 1409–1437.

496 L. C. Reibel, C. P. Durand and E. Franta, *Can. J. Chem.*, 1985, **63**, 264–269.

497 O. Nuyken and S. D. Pask, *Polymers*, 2013, **5**, 361–403.

498 M. E. Piotti, in *Encyclopedia of Materials: Science and Technology*, ed. K. H. J. Buschow, R. W. Cahn, M. C. Flemings, B. Ilschner, E. J. Kramer, S. Mahajan and P. Veyssière, Elsevier, Oxford, 2001, pp. 4610–4613.

499 S. S. Hwang, C. G. Cho and H. Kim, *Electrochem. Commun.*, 2010, **12**, 916–919.

500 D. Zhou, Y.-B. He, Q. Cai, X. Qin, B. Li, H. Du, Q.-H. Yang and F. Kang, *J. Mater. Chem. A*, 2014, **2**, 20059–20066.

501 D. Zhou, Y.-B. He, R. Liu, M. Liu, H. Du, B. Li, Q. Cai, Q.-H. Yang and F. Kang, *Adv. Energy Mater.*, 2015, **5**, 1500353.

502 H. Gao, L. Xue, S. Xin, K. Park and J. B. Goodenough, *Angew. Chem.*, 2017, **129**, 5633–5637.

503 D. Zhang, L. Zhang, K. Yang, H. Wang, C. Yu, D. Xu, B. Xu and L.-M. Wang, *ACS Appl. Mater. Interfaces*, 2017, **9**, 36886–36896.

504 Y. Cui, X. Liang, J. Chai, Z. Cui, Q. Wang, W. He, X. Liu, Z. Liu, G. Cui and J. Feng, *Adv. Sci.*, 2017, **4**, 1700174.

505 J. R. Nair, I. Shaji, N. Ehteshami, A. Thum, D. Diddens, A. Heuer and M. Winter, *Chem. Mater.*, 2019, **31**, 3118–3133.

506 S. Nowak and M. Winter, *J. Electrochem. Soc.*, 2015, **162**, A2500.

507 L. Terborg, S. Weber, F. Blaske, S. Passerini, M. Winter, U. Karst and S. Nowak, *J. Power Sources*, 2013, **242**, 832–837.

508 D. R. Gallus, R. Schmitz, R. Wagner, B. Hoffmann, S. Nowak, I. Cekic-Laskovic, R. W. Schmitz and M. Winter, *Electrochim. Acta*, 2014, **134**, 393–398.

509 M. Evertz, F. Horsthemke, J. Kasnatscheew, M. Börner, M. Winter and S. Nowak, *J. Power Sources*, 2016, **329**, 364–371.

510 S. Oh, D. W. Kim, C. Lee, M.-H. Lee and Y. Kang, *Electrochim. Acta*, 2011, **57**, 46–51.

511 F.-Q. Liu, W.-P. Wang, Y.-X. Yin, S.-F. Zhang, J.-L. Shi, L. Wang, X.-D. Zhang, Y. Zheng, J.-J. Zhou, L. Li and Y.-G. Guo, *Sci. Adv.*, 2018, **4**, eaat5383.

512 W. H. Carothers, *Chem. Rev.*, 1931, **8**, 353–426.

513 S. Ramakrishnan, *Resonance*, 2017, **22**, 355–368.

514 D. Dong, H. Zhang, B. Zhou, Y. Sun, H. Zhang, M. Cao, J. Li, H. Zhou, H. Qian, Z. Lin and H. Chen, *Chem. Commun.*, 2019, **55**, 1458–1461.

515 S. Kim, H. Lim, J. Lee and H. C. Choi, *Langmuir*, 2018, **34**, 8731–8738.

2786 | *Energy Environ. Sci.*, 2021, **14**, 2708–2788

This journal is © The Royal Society of Chemistry 2021

516 Z. Li, Z.-W. Liu, Z.-J. Mu, C. Cao, Z. Li, T.-X. Wang, Y. Li, X. Ding, B.-H. Han and W. Feng, *Mater. Chem. Front.*, 2020, **4**, 1164–1173.

517 M. Kim, S. Kim, V. Aravindan, W. Kim, S.-Y. Lee and Y. Lee, *J. Electrochem. Soc.*, 2013, **160**, A1003–A1008.

518 J.-H. Park, J.-H. Cho, S.-B. Kim, W.-S. Kim, S.-Y. Lee and S.-Y. Lee, *J. Mater. Chem.*, 2012, **22**, 12574–12581.

519 J.-H. Park, J.-M. Kim, J.-S. Kim, E.-G. Shim and S.-Y. Lee, *J. Mater. Chem. A*, 2013, **1**, 12441–12447.

520 J.-H. Cho, J.-H. Park, M.-H. Lee, H.-K. Song and S.-Y. Lee, *Energy Environ. Sci.*, 2012, **5**, 7124–7131.

521 G. Lee, H. Kim, S. Baek, H. Choi, K. Chung, B. Cho, S. Lee and Y.-S. Lee, *J. Power Sources*, 2015, **298**, 379–384.

522 J. Oravec, K. Mori, Y. Oishi and Z. Kang, *IEEE Trans. Appl. Supercond.*, 2004, **14**, 1592–1595.

523 M. Shabani-Nooshabadi, M. Mollahoseiny and Y. Jafari, *Surf. Interface Anal.*, 2014, **46**, 472–479.

524 S. Ben Jadi, A. El Jaouhari, Z. Aouzal, A. El Guerraf, M. Bouabdallaoui, R. Wang, E. A. Bazzaoui and M. Bazzaoui, *Mater. Today: Proc.*, 2020, **22**, 52–56.

525 B. Anothumakkool, A. Torris AT, S. N. Bhange, M. V. Badiger and S. Kurungot, *Nanoscale*, 2014, **6**, 5944–5952.

526 A. Dall'Olio, G. Dascola, V. Vacara and V. Bocchi, *C. R. Acad. Sci.*, 1968, **267**, 433–435.

527 G. Bidan, in *Electropolymerization: Concepts, Materials and Applications*, ed. S. Cosnier and A. Karyakin, Wiley, 2010, pp. 1–26.

528 H. D. Abruna, P. Denisevich, M. Umana, T. J. Meyer and R. W. Murray, *J. Am. Chem. Soc.*, 1981, **103**, 1–5.

529 M. D. Imisides, R. John, P. J. Riley and G. G. Wallace, *Electroanalysis*, 1991, **3**, 879–889.

530 A. C. Pereira, A. E. F. Oliveira and G. B. Bettio, *Chem. Pap.*, 2019, **73**, 1795–1804.

531 R. Nölle, K. Beltrop, F. Holtstiege, J. Kasnatscheew, T. Placke and M. Winter, *Mater. Today*, 2020, **32**, 131–146.

532 V. Ruiz, Á. Colina, A. Heras and J. López-Palacios, *Electrochim. Acta*, 2004, **50**, 59–67.

533 G. Fomo, T. Waryo, U. Feleni, P. Baker and E. Iwuoha, in *Functional Polymers*, ed. M. A. Jafar Mazumder, H. Sheardown and A. Al-Ahmed, Springer International Publishing, Cham, 2019, pp. 105–131.

534 Y.-W. Zhong, C.-J. Yao and H.-J. Nie, *Coord. Chem. Rev.*, 2013, **257**, 1357–1372.

535 S. Gabriel, R. Jérôme and C. Jérôme, *Prog. Polym. Sci.*, 2010, **35**, 113–140.

536 R. Waltman and J. Bargon, *Can. J. Chem.*, 1986, **64**, 76–95.

537 S. Sadki, P. Schottland, N. Brodie and G. Sabouraud, *Chem. Soc. Rev.*, 2000, **29**, 283–293.

538 E. De Giglio, S. Cometa, L. Sabbatini, P. G. Zambonin and G. Spoto, *Anal. Bioanal. Chem.*, 2005, **381**, 626–633.

539 D. P. Harrison, L. S. Carpenter and J. T. Hyde, *J. Visualized Exp.*, 2015, e52035.

540 I. V. Ferrari, M. Braglia, T. Djenizian, P. Knauth and M. L. Di Vona, *J. Power Sources*, 2017, **353**, 95–103.

541 V. A. Sugiawati, F. Vacandio, Y. Ein-Eli and T. Djenizian, *APL Mater.*, 2019, **7**, 031506.

542 M. Braglia, I. V. Ferrari, L. Pasquini, T. Djenizian, M. Sette, M. L. Di Vona and P. Knauth, *Electrochim. Acta*, 2018, **265**, 78–88.

543 S. L. Cram, G. M. Spinks, G. G. Wallace and H. R. Brown, *Electrochim. Acta*, 2002, **47**, 1935–1948.

544 J. Breitenbach and C. Srna, *Pure Appl. Chem.*, 1962, **4**, 245–254.

545 N. A. Kyeremateng, F. Dumur, P. Knauth, B. Pecquenard and T. Djenizian, *C. R. Chim.*, 2013, **16**, 80–88.

546 S. N. Bhadani, Q. Ansari and S. K. S. Gupta, *J. Appl. Polym. Sci.*, 1992, **44**, 121–126.

547 B. L. Funt and S. N. Bhadani, *J. Polym. Sci., Part A: Gen. Pap.*, 1965, **3**, 4191–4199.

548 B. Sun, D. Rehnlund, M. J. Lacey and D. Brandell, *Electrochim. Acta*, 2014, **137**, 320–327.

549 G. Chen, G. V. Zhuang, T. J. Richardson, G. Liu and P. N. Ross, *Electrochem. Solid-State Lett.*, 2005, **8**, A344–A347.

550 A. M. Haregewoin, A. S. Wotango and B.-J. Hwang, *Energy Environ. Sci.*, 2016, **9**, 1955–1988.

551 D. C. Johnson, A. L. Prieto, M. Rawls, D. J. Bates and C. M. Elliott, *US Pat.*, 9337514, U.S. Patent and Trademark Office, Washington, DC, 2016.

552 X. Zhang, R. Kostecki, T. J. Richardson, J. K. Pugh and P. N. Ross, *J. Electrochem. Soc.*, 2001, **148**, A1341–A1345.

553 T.-W. Lim, C. W. Park, S. R. White and N. R. Sottos, *ACS Appl. Mater. Interfaces*, 2017, **9**, 40244–40251.

554 L. El Ouatani, R. Dedryvère, C. Siret, P. Biensan, S. Reynaud, P. Iratçabal and D. Gonbeau, *J. Electrochem. Soc.*, 2009, **156**, A103.

555 I. A. Shkrob, Y. Zhu, T. W. Marin and D. Abraham, *J. Phys. Chem. C*, 2013, **117**, 19255–19269.

556 H. Tavassol, M. K. Y. Chan, M. G. Catarello, J. Greeley, D. G. Cahill and A. A. Gewirth, *J. Electrochem. Soc.*, 2013, **160**, A888–A896.

557 H. Tavassol, J. W. Buthker, G. A. Ferguson, L. A. Curtiss and A. A. Gewirth, *J. Electrochem. Soc.*, 2012, **159**, A730–A738.

558 S. Wei, S. Choudhury, J. Xu, P. Nath, Z. Tu and L. A. Archer, *Adv. Mater.*, 2017, **29**, 1605512.

559 A. La Monaca, F. De Giorgio, F. Soavi, G. Tarquini, M. Di Carli, P. Paolo Prosini and C. Arbizzani, *ChemElectroChem*, 2018, **5**, 1272–1278.

560 D. Aurbach, O. Youngman and P. Dan, *Electrochim. Acta*, 1990, **35**, 639–655.

561 G. Newman, R. Francis, L. Gaines and B. Rao, *J. Electrochem. Soc.*, 1980, **127**, 2025–2027.

562 L. Kong, H. Zhan, Y. Li and Y. Zhou, *Electrochem. Commun.*, 2007, **9**, 2557–2563.

563 L. Kong, H. Zhan, Y. Li and Y. Zhou, *Electrochim. Acta*, 2008, **53**, 5373–5378.

564 Q. Lan, Y. Yang, Z. Song, N. Liu, J. Qin, F. Men and H. Zhan, *ACS Appl. Energy Mater.*, 2020, **3**, 3586–3595.

565 C. P. Rhodes, J. W. Long and D. R. Rolison, *Electrochem. Solid-State Lett.*, 2005, **8**, A579.

566 D. R. Rolison, J. W. Long, J. C. Lytle, A. E. Fischer, C. P. Rhodes, T. M. McEvoy, M. E. Bourg and A. M. Lubers, *Chem. Soc. Rev.*, 2009, **38**, 226–252.

567 M. Braglia, I. V. Ferrari, F. Vacandio, P. Knauth and M. L. Di Vona, *ChemistrySelect*, 2016, **1**, 3114–3119.

This journal is © The Royal Society of Chemistry 2021

Energy Environ. Sci., 2021, **14**, 2708–2788 | **2787**

568 A. Vlad, N. Singh, C. Galande and P. M. Ajayan, *Adv. Energy Mater.*, 2015, **5**, 1402115.

569 S. Ferrari, M. Loveridge, S. D. Beattie, M. Jahn, R. J. Dashwood and R. Bhagat, *J. Power Sources*, 2015, **286**, 25–46.

570 T. Tao, S. Lu and Y. Chen, *Adv. Mater. Technol.*, 2018, **3**, 1700375.

571 H. Gwon, J. Hong, H. Kim, D.-H. Seo, S. Jeon and K. Kang, *Energy Environ. Sci.*, 2014, **7**, 538–551.

572 N. A. Kyeremateng and R. Hahn, *ACS Energy Lett.*, 2018, **3**, 1172–1175.

573 T. S. Arthur, D. J. Bates, N. Cirigliano, D. C. Johnson, P. Malati, J. M. Mosby, E. Perre, M. T. Rawls, A. L. Prieto and B. Dunn, *MRS Bull.*, 2011, **36**, 523–531.

574 J. F. M. Oudenhoven, L. Baggetto and P. H. L. Notten, *Adv. Energy Mater.*, 2011, **1**, 10–33.

575 M. Roberts, P. Johns, J. Owen, D. Brandell, K. Edstrom, G. El Enany, C. Guery, D. Golodnitsky, M. Lacey, C. Lecoeur, H. Mazor, E. Peled, E. Perre, M. M. Shaijumon, P. Simon and P.-L. Taberna, *J. Mater. Chem.*, 2011, **21**, 9876–9890.

576 C. Lethien, J. Le Bideau and T. Brousse, *Energy Environ. Sci.*, 2019, **12**, 96–115.

577 Z. Qu, M. Zhu, H. Tang, L. Liu, Y. Li and O. G. Schmidt, *Energy Storage Mater.*, 2020, **29**, 17–41.

578 M. Cheng, R. Deivanayagam and R. Shahbazian-Yassar, *Batteries Supercaps*, 2020, **3**, 130–146.

579 G. González, X. Fernández-Francos, À. Serra, M. Sangermano and X. Ramis, *Polym. Chem.*, 2015, **6**, 6987–6997.

580 S. Tan, S. Walus, T. Gustafsson and D. Brandell, *Solid State Ionics*, 2011, **198**, 26–31.

581 B. Sun, I. Y. Liao, S. Tan, T. Bowden and D. Brandell, *J. Power Sources*, 2013, **238**, 435–441.

582 G. D. Salian, C. Lebouin, A. Demoulin, M. S. Lepihin, S. Maria, A. K. Galeyeva, A. P. Kurbatov and T. Djenizian, *J. Power Sources*, 2017, **340**, 242–246.

583 S. Tan, S. Walus, J. Hilborn, T. Gustafsson and D. Brandell, *Electrochem. Commun.*, 2010, **12**, 1498–1500.

584 S. Tan, E. Perre, T. Gustafsson and D. Brandell, *Solid State Ionics*, 2012, **225**, 510–512.

585 M. Retailleau, A. Ibrahim, C. Croutxé-Barghorn, X. Allonas, C. Ley and D. Le Nouen, *ACS Macro Lett.*, 2015, **4**, 1327–1331.

586 N. Plylahan, N. A. Kyeremateng, M. Eyraud, F. Dumur, H. Martinez, L. Santinacci, P. Knauth and T. Djenizian, *Nanoscale Res. Lett.*, 2012, **7**, 349.

587 V. A. Sugiawati, F. Vacandio and T. Djenizian, *Molecules*, 2020, **25**, 2121.

588 G. D. Salian, C. Lebouin, A. Galeyeva, A. P. Kurbatov and T. Djenizian, *Front. Chem.*, 2019, **6**, 675.

589 M. Braglia, I. V. Ferrari, T. Djenizian, S. Kaciulis, P. Soltani, M. L. Di Vona and P. Knauth, *ACS Appl. Mater. Interfaces*, 2017, **9**, 22902–22910.

590 L. Li, Z. Wu, S. Yuan and X.-B. Zhang, *Energy Environ. Sci.*, 2014, **7**, 2101–2122.

591 X. Wang, X. Lu, B. Liu, D. Chen, Y. Tong and G. Shen, *Adv. Mater.*, 2014, **26**, 4763–4782.

592 H. Sun, J. Zhu, D. Baumann, L. Peng, Y. Xu, I. Shakir, Y. Huang and X. Duan, *Nat. Rev. Mater.*, 2019, **4**, 45–60.

593 Z. Zhao and H. Wu, *Nano Res.*, 2019, **12**, 2477–2484.

594 C.-F. Du, Q. Liang, Y. Luo, Y. Zheng and Q. Yan, *J. Mater. Chem. A*, 2017, **5**, 22442–22458.

595 C. Reyes, R. Somogyi, S. Niu, M. A. Cruz, F. Yang, M. J. Catenacci, C. P. Rhodes and B. J. Wiley, *ACS Appl. Energy Mater.*, 2018, **1**, 5268–5279.

596 S.-H. Kim, J.-H. Kim, S.-J. Cho and S.-Y. Lee, *Adv. Energy Mater.*, 2019, **9**, 1901841.

597 K. Sun, T.-S. Wei, B. Y. Ahn, J. Y. Seo, S. J. Dillon and J. A. Lewis, *Adv. Mater.*, 2013, **25**, 4539–4543.

598 Y. Yang, W. Yuan, X. Zhang, Y. Yuan, C. Wang, Y. Ye, Y. Huang, Z. Qiu and Y. Tang, *Appl. Energy*, 2020, **257**, 114002.

599 J.-Y. Lee, J. An and C. K. Chua, *Appl. Mater. Today*, 2017, **7**, 120–133.

600 Z. Chen, Z. Li, J. Li, C. Liu, C. Lao, Y. Fu, C. Liu, Y. Li, P. Wang and Y. He, *J. Eur. Ceram. Soc.*, 2019, **39**, 661–687.

601 J. Edgar and S. Tint, *Johnson Matthey Technol. Rev.*, 2015, **59**, 193–198.

602 K. Fu, Y. Wang, C. Yan, Y. Yao, Y. Chen, J. Dai, S. Lacey, Y. Wang, J. Wan, T. Li, Z. Wang, Y. Xu and L. Hu, *Adv. Mater.*, 2016, **28**, 2587–2594.

603 X. Zheng, J. Deotte, M. P. Alonso, G. R. Farquar, T. H. Weisgraber, S. Gemberling, H. Lee, N. Fang and C. M. Spadaccini, *Rev. Sci. Instrum.*, 2012, **83**, 125001.

604 H.-D. Um, K.-H. Choi, I. Hwang, S.-H. Kim, K. Seo and S.-Y. Lee, *Energy Environ. Sci.*, 2017, **10**, 931–940.

2788 | *Energy Environ. Sci.*, 2021, **14**, 2708–2788

This journal is © The Royal Society of Chemistry 2021